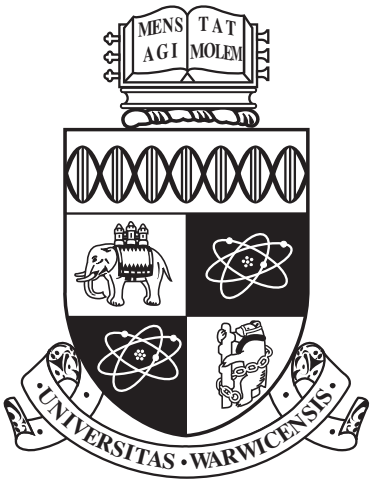

Exploring the role of histone marks and chromatin remodelling ATPases in plant immunity

by

Alonso Javier Pardal Bermejo

Thesis

Submitted to the University of Warwick

for the degree of

Doctor of Philosophy

School of Life Sciences

September 2017

THE UNIVERSITY OF
WARWICK

To my friends, source of inspiration,
To my teachers and mentors for their guidance,
And to my family, for their unconditional support

Table of Contents

Results

List of Figures

List of Tables

Acknowledgements

I would like to express my gratitude to the University of Warwick and the BBSRC for the funding of this PhD project through the MIBTP program.

I am extremely grateful to Dr. Vardis Ntoukakis for the supervision of this thesis. He supported me through and through from the very application, during three years of heterogeneous results, towards two successful collaborations, sent me to national and international conferences and not least at the final writing.

I am much obliged to Dr. Roberto Solano and Dr Selena Gimenéz-Ibáñez in CNB-CSIC, Madrid, Dr Moussa Benhamed in IPS2, Paris-Saclay, Paris, and their teams for the opportunity to work in their labs and share their science and their time.

I would like to acknowledge Prof. Katherine Denby and Maura di Martino for providing with a *Botrytis* line and the knowledge to use it. I would like to thank to Dr Daniel Hebenstreit, and Prof. Lorenzo Frigerio for all of their honest advice. Dr Julia Engelhorn, for teaching me how to do ChIP and sharing so much chromatin wisdom. The computational community: Dr Sascha Ott, for his support and considering me a part of the team, Dr Krzysztof Polanski, Dr Mark Walsh, Daniel Cooper, Charlotte Rich and Jon Price for sharing bits and pieces of code and advice on RNA-seq analysis.

Last but not least, it would not be so exaggerated to say that if I can call myself a plant pathologist it is thanks to Dr Sophie Piquerez. I also have to thank Dr Ruth Shafer, Dr Silke Lehmann, Dr Ana Dominguez, Dr Arsheed Seikh, and the rest of the postdoc office people, the people in the lab and in SLS, the “oldies” and the “newbies”, all of the “Ntoukakinis”, to Manos Mastorakis, Xrysa Sergaki, Jim Skinner, Gurdaman Singh, Quentin Santain and Joana Furtado, for pushing and pulling of this thesis and keeping me well-fed, and very, very specially to Steph Kancy and to my family, with their support they made possible this work.

Declarations

This thesis is presented in accordance with the regulations for the degree of Doctor of Philosophy. It has been composed by myself and has not been submitted in any previous application for any degree except where otherwise stated. The work in this thesis has been undertaken by myself except where otherwise stated.

Abstract

Plant cells require considerable transcriptional reprograming to mount an effective response to pathogens. Plant responses to pathogens have to be finely balanced with other vital biological processes such as development and growth. A major mechanism controlling the modulation of gene expression is chromatin remodelling. Chromatin remodelling requires histone covalent modifications and/or the action of ATP-dependent remodelling complexes. The combined action of these determine the accessibility of transcription factors and the basal transcription machinery to DNA and therefore greatly impact gene expression. There are several examples of histone modifying and chromatin remodelling enzymes previously shown to regulate plant development and immunity.

This thesis explored the role of chromatin in plant defences, and how chromatin remodelling forms an integral part of the defence response. Chapter 1 aimed to discover a "hidden" signal of chromatin marks in plant defence-responsive genes using an array of bioinformatics techniques. Subsequently, histone H3K27 tri-methylation (H3K27me3) was identified as a mark associated with gene repression at defence-related loci. The role of histone H3K27me3 and its associated histone demethylase enzymes REF6 and ELF6 were empirically characterised. Chapter 2 is dedicated to a reverse genetics screening investigating the role of the chromatin remodelling ATPases *Arabidopsis* family in plant defences, and describes the most prominent phenotypes. And lastly, Chapter 3 dissects in greater detail the role of the chromatin remodelling ATPase EDA16 in plant defence. Pathogen assays, RNA-seq and other molecular techniques suggest that EDA16 is a negative regulator of immunity induced upon pathogen perception to regulate the amplitude of defence responses.

Abbreviations

35S	Cauliflower mosaic virus promoter
5mC	5-methylcytosine
ABA	Abscisic acid
ATP	Adenosine tri-phosphate
Avr	Avirulence
Bp	Base pair
BRM	*Arabidopsis thaliana* BRAHMA
SYD	*Arabidopsis thaliana* SPLAYED
$CaCl_2$	Calcium chloride
CC	Coiled-coil
cDNA	Complementary DNA
CDPK/CPK	Calcium-dependent protein kinase
CDS	Coding DNA sequence
ChIP	Chromatin immuno-precipitation
Col-0	Colombia-0
CRA	Chromatin Remodelling ATPases
CTD	C-terminal domain
CYP82C2	Cytochrome P450 family 82 subfamily C2
DNA	Deoxyribonucleic acid
DTT	Dithiothreitol
ECDF	Empirical cumulative density function
ECL	Enhanced chemiluminescence
EDA16	Embryo sac development arrest 16
EDTA	Ethylenediaminetetraacetic acid
EF-Tu	Elongation factor-Tu
EGTA	Egtazic acid
ELF6	Early flowering 6
ETI	Effector-triggered immunity
EtOH	Ethanol

ETS	Effector-triggered susceptibility
EV	Empty vector
EYFP	Enhanced yellow fluorescent protein
FDR	False discovery rate
flg22	Flagellin 22
FLS2	Flagellin-senstive 2
FRAP	Fluorescence recovery after photobleaching
FRG1/2	SNF2- RING-HELICASE–LIKE1 and -2, CHR27 and CHR28
FRK1	flg22-induced receptor-like kinase
GA	Gibberellic acid
GEO	Gene expression omnibus
GFP	Green fluorescent protein
GO	Gene ontology
HA	Haemagglutinin
HCl	Hydrochloric acid
HR	Hypersenstive response
HRP	Horseradish peroxidase
Hz	Hertz
IP	Immuno-precipitation
JA	Jasmonic acid
ET	Ethylene
JAZ	Jasmonate ZIM domain
K_2HPO_4	Potassium phosphate
KB	King's broth
KO	Knock out
KOH	Potassium hydroxide
LB	Lysogeny broth
LecRK	L-type lectin rector kinase
LP	Left primer
M	Moles
MAPK/MPK	Mitogen-activated protein kinases
MeJA	Methyl jasmonate
MES	2-(N-morpholino)ethanesulfonic acid
$MgCl_2$	Magnesium chloride

MNase	Micrococcal nuclease
MNase-seq	Micrococcal nuclease sequencing
mRNA	Messenger RNA
MS	Murashige and Skoog
NaCl	Sodium chloride
NB-LRR	Nucleotide-binding leucine-rich repeat
NHL10	NDR1/HIN1-like 10
OD	Optical density
OE	Overexpressor
PAMP	Pathogen-associated molecular pattern
PCA	Principle component analysis
PCR	Polymerase chain reaction
PDA	Potato dextrose agar
PDB	Protein data bank
PHI-1	Phosphate-induced 1
PIE1	Photoperiod-independent early flowering 1
PMSF	Phenylmethylsulfonyl fluoride
Pol II	RNA Polymerase II
PR	Pathogenesis-related
PRR	PAMP recognition receptor
PTI	Pattern-triggered immunity
Pst	*Pseudomonas syringae* pv. tomato
qPCR	Quantitative PCR
RdDM	RNA-directed DNA methylation
REF6	Arabidopsis thaliana Relative of early flowering 6
RNA	Ribonucleic acid
RNA-seq	Ribonucleic acid sequencing
RNAi	Ribonucleic acid interference
ROS	Reactive oxygen species
RP	Right primer
SAR	Systemic acquired resistance
SA	Salicylic acid
SDS-PAGE	Sodium dodecyl sulfate polyacrylamide gel electrophoresis
SNF2	*Arabidopsis thaliana* Sucrose non-fermentable 2

SYD	SPLAYED
T-DNA	Transfer-DNA
TBS	Tris-buffered saline
TE	Tris-EDTA
TES	Transcription end site
TF	Transcription factor
TIR	Toll/interleukin-1 receptor
TPL	Topless
TSS	Transcription start site
WT	Wild type
Zeo	Zeocin

Introduction

1. Chromatin and gene regulation

1.1 Chromatin

Chromatin is the histone-DNA nucleoprotein complex that serves for both structure and organisation of the DNA in eukaryotes (Kornberg, 1974; Kornberg and Lorch, 1999; Rando and Chang, 2009). 146 base pairs of DNA helix are wrapped around a histone octamer, which is known as a nucleosome (Luger et al., 1997). Each nucleosome contains 8 core histones, a tetramer with two histone H3 and two histone H4 and two H2A/H2B dimers (Dyer et al., 2004). Nucleosomes are then further compacted into higher structures. Chromatin structure retains a highly functional role. For example, centromeric and pericentromeric regions have a very regular nucleosome spacing which is related to DNA methylation (Chodavarapu et al., 2010). These characteristics of chromatin are conserved across eukaryotes and also in plants (See Supplementary figure **SI.1**). The degree of compaction impacts on the accessibility of transcription factors and the basal transcription machinery to the DNA thus affecting gene expression (Li et al., 2007).

1.2 Chromatin marks

Chromatin is meticulously marked with histone post-transcriptional modifications and DNA methylation. In animals and plants, each of these marks occurs in specific environments: transposable elements, gene transcription start sites, actively transcribed genes and so forth (Barth and Imhof, 2010; Roudier et al., 2011). Different chromatin marks are associated with different gene expression levels, influence DNA replication and act as beacons for DNA-repair (Table **I.1**). Histone acetylation and histone di and tri-methylation at histone H3 lysine 4 (H3K4me3 and H3K4me2) are strongly linked with active transcription (Bannister and Kouzarides, 2011; Oh et al., 2008; Shilatifard, 2012; Zhang et al., 2009). Maintenance of transcription and transcriptional elongation is associated with histone H2B ubiquitination (H2Bub) and the methylation mark H3K36me3, which generally accumulates along the first half of the gene body in *Arabidopsis* active genes (Roudier et al., 2011). Gene repression is associated with DNA methylation and H3K27me3. DNA methylation anti-correlates with H2A.Z deposition at the transcription start site (TSS) of genes (Zilberman et al., 2008). However, DNA methylation tends to increase together with H3K9me2 along heterochromatic regions, whereas H3K27me3 is an euchromatin mark restricted to gene bodies (Table I.1; Roudier et al., 2011).

Table I.1 Effect of chromatin marks on gene expression and distribution. The outcome column refers to the most commonly associated gene expression: active gene transcription (green letters) or gene repression (red letters). The shape column represents the expected distribution around an average gene body delimited by the transcription start site (TSS) and the transcription end site (TES). Adapted from multiple sources (Alvarez et al., 2010; Kouzarides, 2007; Roudier et al., 2011).

Chromatin mark	Symbol	Outcome	Shape
Acetylation	H3K9 ac/ H3K14 ac	Gene transcription	
Methylation	H3K4me2 me3	Gene transcription	
	H3K9me2	Heterochromatin	
	H3K27me1	Heterochromatin / gene repression	
	H3K27me3	Gene repression	
	H3K36me3	Gene transcription	
Ubiquitination	H2Bub	Gene transcription	
DNA methylation			
	CG CHG CHH	Gene repression Mixed outcomes	
Histone variants			
	H2A.Z	Gene transcription	
	H2A.X	DNA repair	
	H3.3	Centromere	TSS TES

Histone-modifying enzymes regulate the deposition or removal of the chromatin marks. Histone modifying enzymes, together with chromatin remodelling complexes, determine the chromatin configuration (Figure **I.2**), degree of compaction and therefore the accessibility of DNA during transcription, replication and repair (Tang et al., 2010).

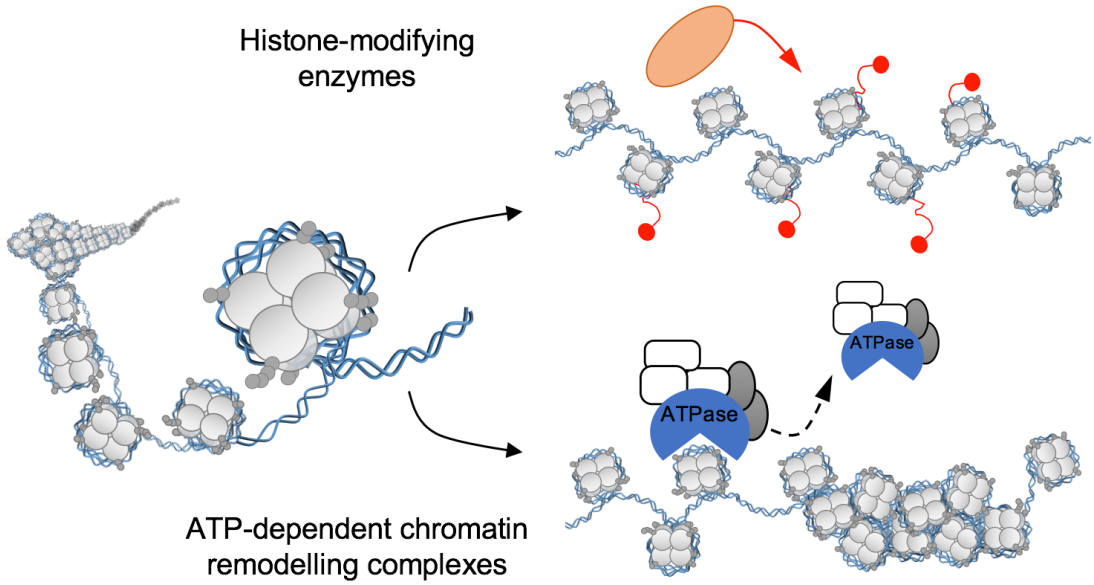

Figure I.1. Histone modifying enzymes and chromatin remodelling complexes. Histone modifying enzymes (top) deposit or remove post-translational modifications usually on histone N-terminal tails (red).. The most common modifications are acetylation, methylation, ubiquitination, sumoylation and phosphorylation. These covalent modifications influence the histone-DNA affinity directly affecting the chromatin stability and accessibility of RNA/DNA polymerases (Kouzarides, 2007) or they can act indirectly as recognisable signatures for chromatin remodelling complexes. Chromatin remodelling complexes (bottom) bind to the nucleosomes (see Supplementary figure **SI.2**) and slide or replace them utilising energy derived from ATP hydrolysis. Their activity affects nucleosome position, spacing (affecting regulatory DNA elements by exposing them in nucleosome-free regions (such as gene promoters) or burying them within the densely packed and highly inaccessible heterochromatin (Clapier and Cairns, 2009).

1.3 Chromatin remodelling and chromatin remodelling ATPases

Some histone post-translational modifications, such as lysine acetylation, have a direct impact on the histone-DNA interaction, since the acetyl moiety changes the charge of the amino group at the end of the lysine residue from positive to neutral when forming the amide bond. This charge change affects the histone tail affinity towards the DNA backbone, which is negatively charged due to the phosphate groups. The result is a

looser histone-DNA interaction that is correlated with increased DNA accessibility and gene expression (Kouzarides, 2007). However, this is not the case with other modifications such as histone methylation. Lysine methylation does not change the charge of the residue and therefore the structural implications of these marks are deployed by other interactors or "reader" domains that further change the chromatin conformation. There is a variety of reader domains that are capable of interacting with histone marks and conferring selectivity to the proteins and complexes that carry them.

Chromatin remodelling complexes interact through their reader domain subunits with nucleosomes to re-structure chromatin compaction (Clapier and Cairns, 2009). The central subunits, chromatin remodelling ATPases, are the motor domains that utilise ATP hydrolysis to move, destabilize, eject, or restructure nucleosomes (Flaus and Owen-Hughes, 2011). Recent advances in protein imaging have allowed a closer understanding of remodelling mechanisms of action. The DNA translocation event is estimated to move 1-3 bp per single step, accumulating up to 35 bp before disengaging (Blosser et al., 2009; Sirinakis et al., 2011) and using the hydrolysis of one ATP molecule per bp (Singleton et al., 2007) (Figure **I.1** and Supplementary figure **SI.2**). As energetically taxing as it may seem, they are not rare enzymes in the cell; in yeast, there is one SNF2 ATPase for every 25 genes, and up to one ATPase for each gene for some other subunits (Flaus and Owen-Hughes, 2011). The conserved active core suggests that the different ATPases within the family have a similar mechanism of action, but the specificity is brought by the different adjacent domains specific to each of them (Liu et al., 2017).

1.3.1 Chromatin remodelling ATPases in plants

Chromatin remodelling ATPases are highly conserved across eukaryotes with great conservation of the motor domains, SNF2_N (from the yeast Sucrose non-fermenting, SNF2; Nasmyth et al., 1987; Stern et al., 1984) and Helicase C (Flaus et al., 2006). *Arabidopsis* has 41 genes with the identified catalytic core domains (SNF2, Helicase C), with members in each of the conserved subfamilies (Flaus et al., 2006; Knizewski et al., 2008). Only a few of them have been functionally characterised: the first ATPases described in *Arabidopsis* were the homologues of yeast SNF2 and

Drosophila BRAHMA, named AtBRM (BRM) and SPLAYED (SYD). BRM conserves the SNF2 ability to interact with histone H3 and histone H4 (Farrona, 2004; Farrona et al., 2007). SYD was found to be related to reproductive development and hormonal signalling (Wagner and Meyerowitz, 2002).

Micrococcal nuclease digestion paired with deep sequencing provided an insight into the imitation switch subfamily (ISWI) CHR11 and CHR17 proteins as redundant in the nucleosome distribution patterning over the gene body (Li et al., 2014b). To date, tested *Arabidopsis* chromatin remodelling ATPases have been shown to influence gene expression in the case of BRM and SYD (Bezhani et al., 2007; Walley et al., 2008; Wu et al., 2012a), gene silencing and DNA methylation in the case of DEFICIENT IN DNA METHYLATION 1 (DDM1), RING-HELICASE–LIKE 1 and -2 (hereafter referred to as FRG1 and FRG2, also known as CHROMATIN REMODELING 27 and 28 or CHR27 and CHR28) and ENHANCER TRAP LOCUS 1 (hereafter referred to as ETL1, CHROMATIN REMODELING 19 or CHR19) (Groth et al., 2014; Han et al., 2014; Vongs et al., 1993) and DNA repair in the case of RAD54 (Klutstein et al., 2008; Osakabe et al., 2002). PHOTOPERIOD-INDEPENDENT EARLY FLOWERING 1 (PIE1) and SYD have been involved in development and flowering (Deal et al., 2007; Wagner and Meyerowitz, 2002) but also, along with BRM, are involved in other processes such as abiotic and biotic stresses (Han et al., 2012; March-Díaz et al., 2008; Walley et al., 2008).

2. Plant defences

2.1 Microbe perception and subsequent triggered immunity

Plants are protected from biotic stresses by structural barriers such as the cell wall, the waxy cuticle on the leaf surface and a myriad of volatile secondary metabolites (Sollars et al., 2016). In addition, plants possess an innate immune system divided in two layers (Jones and Dangl, 2006). The first layer of plant defences consists of membrane receptors (often referred to as pattern recognition receptors; PRRs) with extracellular domains capable of recognising conserved molecular patterns. The term pathogen-associated molecular pattern (PAMP) was coined for these epitopes (Janeway, 1989). In plants, well-studied examples are the flagellin protein from the flagellum of the bacterium *Pseudomonas syringae* detected by the receptor kinase FLS2 (Chinchilla et al., 2006), the elongation factor Tu also from *P. syringae* recognised by the receptor kinase ERF (Zipfel et al., 2006), or the polysaccharide chitin from the fungi cell wall detected by the receptor kinase CHITIN ELICITOR RECEPTOR KINASE 1 (CERK1) (Miya et al., 2007). These three receptors possess intracellular kinase domains that, together with other membrane co-receptors (i.e. BRASSINOSTEROID INSENSITIVE1-ASSOCIATED RECEPTOR KINASE 1 i.e. BAK1, BOTRYTIS-INDUCED KINASE1 i.e. BIK1 or BRASSINOSTEROID-SIGNALING KINASE 1 i.e. BSK1), trigger the transduction of the signal.

The immediate consequences of PAMP-triggered immunity (PTI) are the production of reactive oxygen species (ROS) and calcium influx (Macho and Zipfel, 2014). Calcium-dependent protein kinases (CDPKs) and Mitogen-activated Protein kinases (MAPK) cascades transduce the PAMP signal towards the nucleus. Regardless of the triggering PAMP, there is a considerable overlap between the genes upregulated downstream; flagellin, elongation factor-Tu (EF-Tu), chitin or oligogalacturonides derived during cell wall degradation generate a similar response (Denoux et al., 2008; Wan et al., 2008; Zipfel et al., 2006). However, some genes respond preferentially to certain signalling cascades. For example, *FLG22-INDUCED RECEPTOR-LIKE*

KINASE 1 (*FRK1*) responds to the MAP kinase pathway, with little input from CDPKs. Conversely, *PHOSPHATE-INDUCED 1* (*PHI-1*) expression is almost exclusively mediated by the CDPK signalling cascade. Between these extreme examples there is a wide range of partial and synergistic inducible genes such as *NDR1/HIN1-LIKE 10* (*NHL10*) or *Cytochrome P450 82C2* (*CYP82C2*) that require both the MAP kinases and CDPKs (Boudsocq et al., 2010). The mechanisms for specificity may rely on the activation of the transcriptional machinery through phosphorylation. For example, MITOGEN-ACTIVATED PROTEIN KINASE 4 (MPK4) indirectly interacts with transcription factor (TF) WRKY33 through the kinase MKS1. Upon flagellin peptide flg22 treatment, WRKY33 is released from this complex to associate with the promoter of the camalexin biosynthetic gene *PAD3* (Qiu et al., 2008). Other TF such as ETHYLENE RESPONSE FACTOR 104 (ERF104), are similarly phosphorylated by MPK3/6 following activation of immunity (Bethke et al., 2009). The basal transcription machinery is also directly targeted by multiple kinases: RNA polymerase II CTD subunit is phosphorylated downstream of the MPK3/6 kinase cascade (Li et al., 2014a).

PAMP perception leads to a rapid and substantial gene reprograming culminating in callose deposition, stomatal closure and the production of small molecules such as ethylene (Wu et al., 2014). These responses are often sufficient to deter non-specific or opportunistic microbes (Xin and He, 2013). On the contrary, aggressive pathogens have evolved to manipulate the host defences through the secretion of toxins that can for instance mimic plant hormones and the releasing into the host cytoplasm or apoplast of proteins called effectors. One illustrative example is the secondary metabolite coronatine produced by certain strains of *P. syringae*. Coronatine is a structural analogue of jasmonoyl isoleucine (Krumm et al., 1995), the active isoform of the phytohormone family of jasmonate metabolites (JA) (Fonseca et al., 2009). Coronatine mediates pathogenesis in processes such as overcoming stomatal defences, mediating disease symptoms or inducing susceptibility in systemic tissues (Bender et al., 1999; Xin and He, 2013). Interestingly, early research on coronatine led to the discovery of *coronatine insensitive 1* (*coi1*) mutant (Feys et al., 1994). Later on *COI1* gene was characterised as a the F-box subunit of the SCF^{COI1} ubiquitin ligase and the JA receptor (Xu et al., 2002). Protein effectors similarly target and deactivate the PTI

signalling and response, leading to susceptibility, often called effector-triggered susceptibility (ETS, see Figure **I.2**; Xin and He, 2013; Jones and Dangl, 2006).

2.2 Effector recognition and plant counter-attack

In turn, plants have adapted to detect effectors with cytosolic receptors encoded by resistance (R). R proteins either interact directly with the effectors or indirectly by guarding the targets (or even sometimes decoy targets) of the effectors (van der Hoorn and Kamoun, 2008; Jones and Dangl, 2006; Figure **I.2**) Typically, the R proteins possess a central Nuclear Binding (NB) and a C-terminal leucine-Rich repeat domain (LRR) therefore known as NB-LRR proteins. The N-terminal domain can be a coil-coil (CC) domain, and belong to the CC NB-LRR subfamily, like the well-characterised R protein RPM1, that recognises alterations caused by the *Pseudomonas maculicula* effector AvrRpm1 in the immunity hub RIN4 protein (Kim et al., 2005). Other R proteins contain an N-terminal domain with a Toll/interleukin-1 receptor (TIR), composing the TIR-NB-LRR subfamily (Cui et al., 2015), like the R gene RPS4 that recognises the *P. syringae* AvrRps4 effector (Gassmann et al., 1999). This effector-triggered immunity (ETI) leads to a somewhat similar gene reprograming to PTI, but with a stronger response (Tsuda et al., 2009). PTI induced by flg22 and ETI induced by the *P. syringae* effector AvrRpt2 extensively share mechanisms for the transduction of the signal (Qi et al., 2011). However, ETI leads to an intense oxidative burst followed by localised cell death at the infection site known as the hyper-sensitive response (HR; Coll et al., 2011; Mur et al., 2008). ETI is commonly followed by systemic acquired resistance (SAR) mediated by small molecules and hormones moving across tissues, for which the hormone salicylic acid (SA) is required (Fu and Dong, 2013).

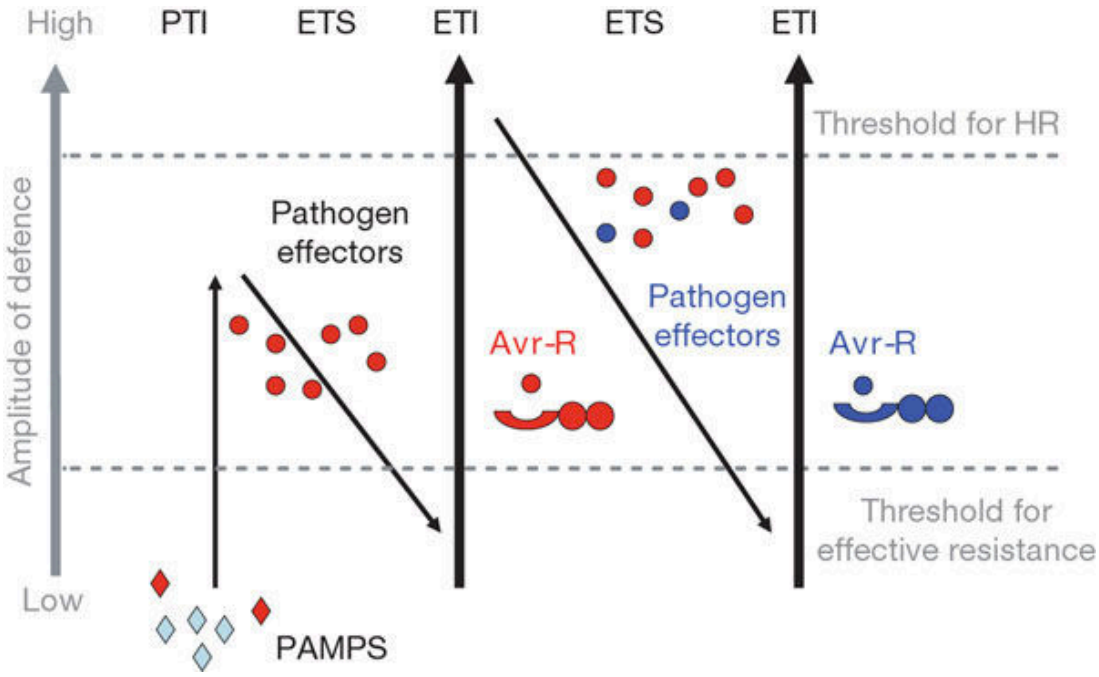

Figure I.2 Co-evolutionary model of the plant immune system versus the defence evasion pathogen strategies. The ”zig-zag” model describes qualitative outputs of plant-pathogen interactions. On the “x” axis (left to right) the different defence responses: PTI, ETI and effector triggered susceptibility (ETS). The “y” axis represents the intensity of the response. In the first phase, plasma membrane receptors detect pathogen (or microbe)-associated molecular patterns (PAMPs or MAMPs) triggering PTI. In the next phase, successfully adapted pathogens utilise effector proteins to overcome PTI and contributing to pathogen nutrition and dispersal, resulting in ETS. Subsequent phases are based on the evolutionary arms race between the pathogen and the plant intracellular receptors (Resistance proteins, or R proteins) recognising certain effectors (avirulence effectors, or Avr) in an interaction triggering a stronger response characterised by cell death (hypersensitive response or HR), conferring immunity ETI. Figure taken from Jones and Dangl (2006).

2.3 The role of plant hormones in defence

Plant hormones are small molecules derived from secondary metabolism. They are characterised by a strong regulatory activity at the cellular level, acting normally at low concentrations. Plant hormones are involved in controlling biotic and abiotic stresses as well as several physiological processes such as development, growth or flowering.

SAR is established by an important gene reprograming dependent on the transcription cofactor NONEXPRESSER OF PR GENES 1 (NPR1) (Fu and Dong, 2013), that eventually leads to the systemic expression of the antimicrobial pathogenesis-related (*PR*) genes, such as *PR1*. PRs confer protection in uninfected tissue against a broad spectrum of pathogens (Durrant and Dong, 2004). It is unclear how NPR1 is regulated upon SA perception. Either NPR1 itself, or its paralogue proteins NPR3 and NPR4, bind to SA to mediate NPR1-dependent transcription co-activation of the *PR* loci (Fu et al., 2012; Maier et al., 2011; Wu et al., 2012b). Additionally, at the local level, SA is an important hormone in defence against pathogens with biotrophic or hemibiotrophic lifestyles, such as rusts, mildews or the bacterium *P. syringae* (Glazebrook, 2005). NPR1 also plays a role in the cytosol, where it inhibits the jasmonic acid (JA) pathway (Spoel et al., 2003).

The JA and closely related ethylene (ET) pathway are associated with defences against necrotrophic pathogens and insects (Gfeller et al., 2010; Glauser et al., 2008). The JA and ET mechanism of action consists of degradation of the JASMONATE-ZIM-DOMAIN PROTEIN (JAZ) family of transcriptional repressors by joining JAZ to its co-receptor CORONATINE-INSENSITIVE PROTEIN 1 (COI1) E3 ligase adaptor protein (Chini et al., 2007; Thines et al., 2007; Yan et al., 2007). JAZ proteins exert gene repression by means of linking TFs, such as MYC2, to the general transcription repressor TOPLESS (TPL) (Pauwels and Goossens, 2011). In response to wounding and infection by necrotrophic pathogens, plants induce JA biosynthesis promoting de-repression of well characterised TFs such as MYC2 or the related MYC3 and MYC4 (Fernández-Calvo et al., 2011).

The abscisic acid (ABA) has a major role in developmental processes such as seed germination ripening but it also mediates the responses to abiotic stresses (Atkinson and Urwin, 2012; Lee and Luan, 2012; Rajjou et al., 2012). In biotic stresses, ABA can be either an activator of defences at an early infection stage, or it can repress defences through a negative interaction with JA and SA hormones in latter stages (Asselbergh et al., 2008; Ton et al., 2009). Other hormones such as auxins, gibberelins cytokinins and brassinosteroids also play a part in regulating the complex plant hormonal interaction network (Robert-Seilaniantz et al., 2011).

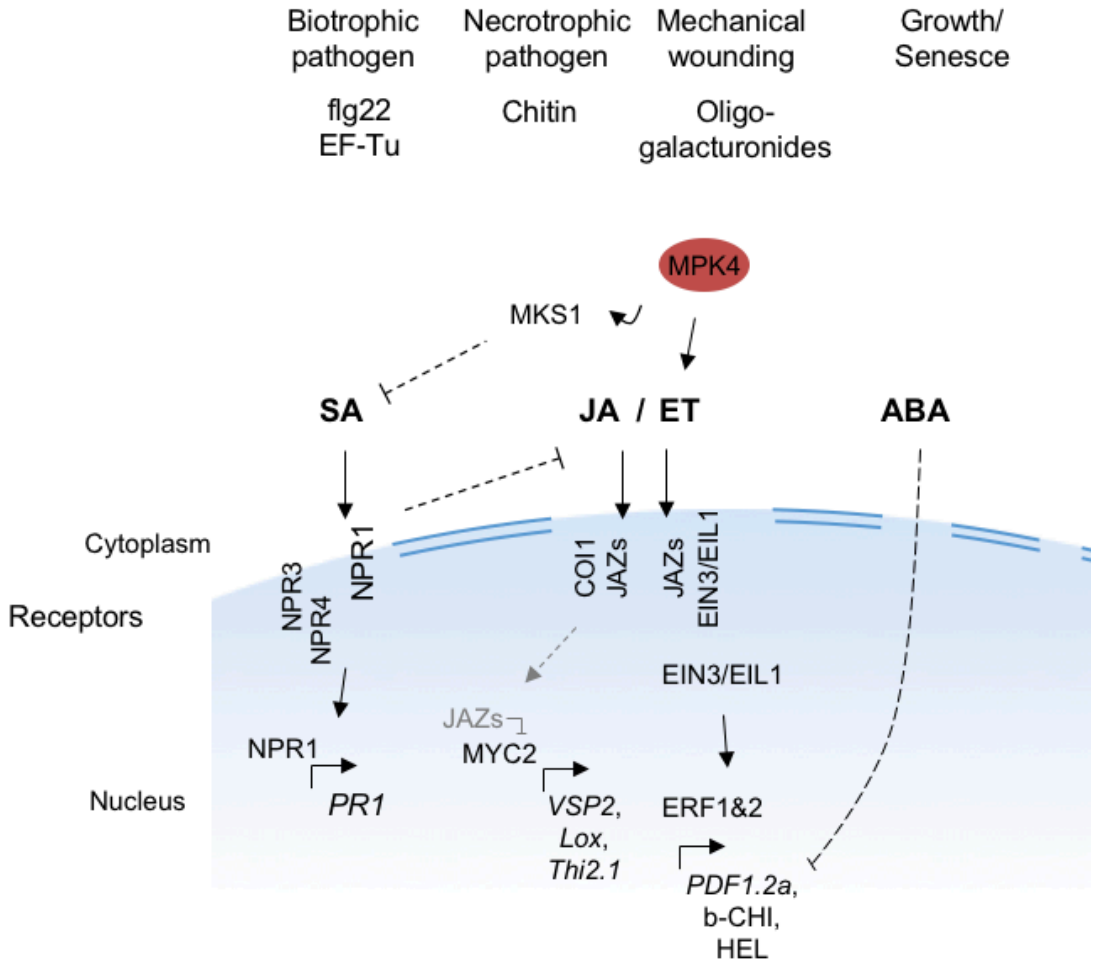

Figure I.3. Plant hormonal pathways cross-over. Different biotic and abiotic cues trigger the hormonal pathways. Biotrophic pathogens elicit the hormone salicylic acid (SA), interacts with TF NPR1, NPR3 and NPR4 strongly promoting defence responses through the transcription of genes encoding pathogen related proteins such as PR1 (gene transcription represented with a bended arrow). Necrothrophic pathogens, herbivores and mechanical wounding stimulate the ethylene (ET) and jasmonates (JA) pathways. JA and ET hormonal signalling crosstalk occurs through receptor-mediated protein ubiquitination. JA receptor COI1 can ubiquitinate JAZ proteins for degradation. In absence of ET, receptors ETHYLENE-INSENSITIVE3 (EIN3) and EIN3 LIKE 1 (EIL1) are ubiquitinated and targeted to proteasome degradation. ET stabilises EIN3/EIL1 that sequestrate JAZ proteins fine-tuning a broad range of inputs. Abscisic acid (ABA) is related to growth, senescence and defences de-activation through a negative interaction with downstream components.

2.4 Chromatin and gene expression modulation during plant immunity

As it has been introduced previously, pathogen detection induces an intense and dynamic reprogramming of plant gene expression, which coordinates an effective defence response (Buscaill and Rivas, 2014; Tsuda and Somssich, 2015). In addition to local responses, pathogen perception also induces some distal (and sometimes whole plant) defensive processes such as SAR.

Chromatin can influence both processes. Downstream of kinase cascades impacting on TF and the basal transcription machinery, the chromatin component of transcription also has an impact on plant defences. In addition, some chromatin modifications are quite stable and can be passed from one generation to another (as epigenetic mechanisms), so is not surprising that chromatin has been studied with great interest.

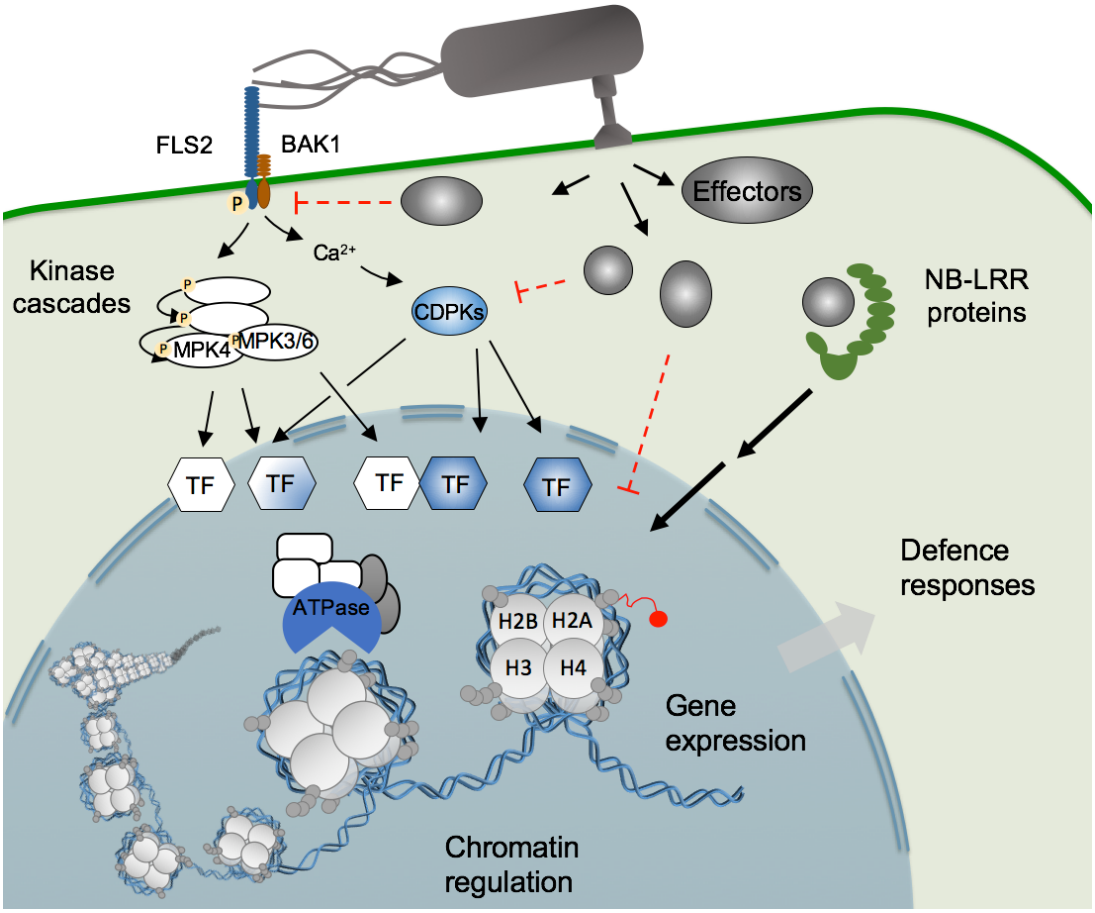

Figure I.4. Plant/pathogen interaction and signalling cascade. During pathogen infection (such as that of certain bacterial species of the *Pseudomonas* genus), plants rapidly respond through the activation of membrane PRRs such as the flagellin receptor FLS2, that hetero-dimerizes with the general co-receptor kinase BAK1 in order to transduce the signal. Kinase cascades MAPK (MPK4, MPK3 and MPK6) and CDPKs are phosphorylated during rapid PTI responses and relay the signal to TF (such as WRKY family) in a specific, cumulative or synergistic manner. Immune responses to pathogens require reprogramming of gene expression. An important mechanism controlling the modulation of gene expression is chromatin remodelling. Chromatin remodelling requires histone covalent modifications (such as histone H3 lysine 27 methylation, depicted as a red circle on top of the nucleosome) and/or the action of ATP-dependent remodelling complexes to mount an appropriate response. In an additional layer of immunity, pathogens deploy an array of effectors (in black) to counteract the plant defences and facilitate the infection, ETS (see Figure **I.2**). If these effectors are detected by NB-LRR resistance proteins, strong defence responses will be built through gene reprograming culminating in the hypersensitive response and cell death (Figure **I.2**).

2.4.1 Chromatin mark changes during plant immunity

As previously described, acetylation is one of the histone marks positively linked with gene expression. Environmental stresses lead to histone acetylation at defence-related loci such as *WRKY53*, *FRK1* or *NHL10* and also to histone methylation at H3K4 in a histone acetyltransferase HAC1-dependent manner, suggesting the strong interrelation between different histone marks co-occurring on the same locus (Singh et al., 2014).

Both, histone acetylation and deacetylation have been observed on the onset of PTI. Furthermore, upon flagellin perception HISTONE DEACETYLASE 2B (HD2B) is directly phosphorylated by MPK3, causing HD2B to translocate from the nucleolus to the nucleus, where it regulates gene expression (Latrasse et al., 2017). Other histone deacetylates have been associated with plant immunity. JAZ proteins require HISTONE DEACETYLASE 6 (HDA6), a RPD3-class histone deacetylase, for the repression of ET-dependent genes *ETHYLENE-INSENSITIVE3* (*EIN3*) and *ETHYLENE-INSENSITIVE3-LIKE 1* (*EIL1*), (Zhu et al., 2011). In fact, HDA6 and the closely related HDA19, had been previously associated with the regulation of JA/ET-dependent genes such as *ETHYLENE RESPONSE FACTOR 1* (*ERF1*) or *VEGETATIVE STORAGE PROTEIN 2* (*VSP2*) (Wu et al., 2008; Zhou et al., 2005). Interestingly, TPL-mediated repression is also linked with histone deacetylation by the same histone deacetylase class: RPD3 and with HDA6 (Davie, 2003; Wang et al., 2013).

The histone methyl transferases SET DOMAIN GROUP 8 and 25 (SDG8 and SDG25) regulate PAMP signalling (flg22, PEP1) and ETI, as well as SAR. They affect H3K4 and H3K36 methylations in two specific loci involved in the biosynthesis of cuticule wax and biosynthesis of carotenoids (Lee et al., 2016). In rice, the jumojiC (jmjC) family of histone demethylases contains two members (JMJ04 and JMJ05) related to innate immunity. JMJ704 positively regulates rice defence response against *Xanthomonas oryzae* infection reducing H3K4 di and tri-methylation on negative regulators of immunity loci, decreasing this way their gene expression (Hou et al., 2015). Rice JMJ05 is a histone H3K27 demethylase and affects defence loci in a JA-responsive manner. JMJ05 de-repress gene expression of defensive loci by removing the negative mark (Li et al., 2013).

2.4.2 Chromatin remodelling ATPases in plant immunity

The first study looking into the impact of the canonical chromatin remodelling ATPases BRM and SYD (homologues of SNF2 in yeast) focused on alteration of gene expression in the corresponding mutants. Disappointingly, mutations in single ATPase genes did not produce a generalised effect in gene expression, but only impacted few genes many of which were shared between the two mutants (Bezhani et al., 2007). It later emerged that some of the genes affected by *brm* were involved in immune responses such as *PR1*. SYD was shown to be directly recruited for the expression of genes in the JA-pathway such as *MYC2* or *VSP2* (Walley et al., 2008). These genes were not identified in the previous transcriptional analysis work since it was performed only on uninfected plants, where the expression of defence-induced genes had remained at basal levels. Therefore, if BRM and SYD functions overlap and given the antagonistic nature of the JA and SA pathways, is not surprising that *PR1* is overexpressed in the *brm* mutant background. Further supporting the relevance of chromatin remodelling within the hormonal pathway corss-talk, BRM is regulated by protein phosphorylation downstream of the ABA signalling pathway (Han et al., 2012; Peirats-Llobet et al., 2016).

How exactly BRM or SYD exert their remodelling activity remains unknown, especially as nucleosome deposition data on *brm* and *syd* mutants are lacking. However, recent data showed that BRM location is concerted with the histone-modifying enzyme Relative of Early Flowering 6 (REF6; Li et al., 2016). REF6 DNA-binding ability through its C-terminal zing-finger domains constituted a mechanism to recruit BRM to specific DNA loci (Li et al., 2016). REF6 is a histone H3K27 demethylase from the jmjC family (Lu et al., 2011). REF6 and Early Flowering 6 (ELF6), another jmjC histone H3K27 demethylase, are involved in regulating a number of developmental responses such as flowering and vernalisation (Crevillén et al., 2014; Noh et al., 2004). This connects the REF6/ELF6 functional overlap with SYD and BRM, also involved in overcoming H3K27me3 gene repression over flowering loci (Li et al., 2015a; Wu et al., 2012a). Despite REF6 and ELF6 having a role in brassinosteroid hormone gene regulation (Yu et al., 2008) and the involvement of the rice H3K27me3 demethylase JMJ05 in JA-induced resistance to *X. oryzae* (Li

et al., 2013), to date, *Arabidopsis* histone demethylases REF6 and ELF6 have not been directly linked to defence responses.

The PIE1 chromatin remodelling ATPase is the central subunit of the chromatin remodelling complex SWR1-like in *Arabidopsis*. This complex conserves its nucleosome replacing activity as first described in yeast (Deal et al., 2007; Krogan et al., 2003). *Arabidopsis* SWR1 complex replaces canonical histone H2A with the histone variant H2A.Z, important function for the regulation of the flowering locus *FLC* (Deal et al., 2007). In addition, similar to *brm* mutant, *pie1* mutant showed constitutive increased expression in defence-related genes within the SA pathway (such as *PR1*, *PR4* or *EDS5*), and the *pie1* mutations resulted in increased resistance to the bacterial pathogen *P. syringae* pathovar *tomato* (*Pst*) strain, DC3000 (March-Díaz et al., 2008). Again, H2A.Z deposition is highly anti-correlated with DNA methylation and occurs at the TSS of actively transcribed genes (Zilberman et al., 2008), but little is known about the PIE1-dependent histone dynamics at the genome level during immunity, or the regulatory processes upstream (Berriri et al., 2016). A recent phosphoproteomics study revealed that PIE1 (as well as REF6) are phosphorylated upon radiation treatment dependent on protein kinases ATM and ATR, crucial in the coordination of DNA repair mechanisms (Roitinger et al., 2015).

Arabidopsis chromatin remodelling ATPase RAD54 has been extensively characterised as a conserved DNA repair component through the homologous recombination pathway (Hirakawa et al., 2017; Klutstein et al., 2008; Osakabe et al., 2006). Despite the oxidative burst generated during biotic stresses that could lead to DNA damage, little is known about the role of RAD54 in plant defences. Two conflicting reports associate its function with geminivirus infection, where it may play a role, but it is not essential in viral replication (Kaliappan et al., 2012; Richter et al., 2015). However, closely related proteins working within the homologous recombination pathway, or even directly interacting with RAD54, have been linked with defence responses through SA-dependent gene de-repression. RAD51D interacts with RAD51 (Tambini et al., 2010) which in turn works closely with RAD54 (Klutstein et al., 2008; Osakabe et al., 2002). Upon defence activation, SUPPRESSOR OF SNI1 2 (SSN2) (a protein containing a SWIM, SWI2/SNF2 and MuDR, domain) together with RAD51D are recruited to *PR1* promoter, possibly mediating

SUPPRESSOR OF NPR1 INDUCIBLE 1 (SNI1) repressor removal (Durrant et al., 2007; Song et al., 2011). SNI1 acts as a negative regulator of the TF NPR1, which promotes *PR1* expression upon SA perception (Li et al., 1999; Pape et al., 2010; Spoel et al., 2003). In addition, RAD54 direct interactor RAD51 (Klutstein et al., 2008) is also recruited to the *PR1* promoter (Wang et al., 2010).

DDM1, another chromatin remodelling ATPase, has been associated with indirect repression of the *PR1* locus. DDM1 is involved in *de novo* DNA methylation (Vongs et al., 1993). The *ddm1* single mutant did not show different susceptibility to the biotrophic oomycete *Hyaloperonospora arabidopsidis* (Li et al., 2010), but had increased resistance against *P. syringae* (Dowen et al., 2012). In addition, DNA methylation affects the expression of *SUPPRESSOR OF NPR1-1, CONSTITUTIVE 1* (*SNC1*), a constitutive repressor of *PR1* (Li et al., 2010). Furthermore, DDM1 and another chromatin remodelling ATPase MOM1, are associated with the removal of the epigenetic marks across transgenerational stresses (Iwasaki and Paszkowski, 2014). The chromatin remodelling ATPases FRG1, FRG2 and ETL1 are involved in the *de novo* RNA-directed DNA methylation as well as in gene silencing through interactions with the histone methyltransferase SUVR2 (Groth et al., 2014; Han et al., 2014). None of these ATPases have been related to stress responses in *Arabidopsis*, but the closest protein to FRG2 in rice, 1,2-benzisothiazol-3(2h)-one,1,1-dioxide (BIT)-responsive Histone-interacting SNF2 ATPase 1 (BRHIS1), represses defences in a SA-independent manner, through association with H2A and H2B monoubiquitinated histone variants. Upon defences activation, the expression of *BRHIS1* drops and BRHIS1 is removed from defence-related gene loci (Li et al., 2015b).

Scope of the Thesis

Chromatin remodelling is still a world to explore in genome-wide terms. Chromatin remodelling ATPases, as the central subunits of the chromatin remodelling complexes, bind with other histone-modifying enzymes and are recruited by DNA-interacting factors. Furthermore, they present direct phosphorylation target sites upon stimuli. All of these make them ideal hubs for regulating complex and dynamic processes such as development and defence at the chromatin level. In this work, a bioinformatics approach exploring histone marks present over defence-related loci revealed that H3K27me3 is overrepresented in genes lowly expressed in the basal state prior to flg22 elicitation, specially, for CDPK-responsive genes. Further investigation demonstrated that REF6 histone H3K27 demethylase is important for a prompt defence activation. A reverse genetic screen for altered defence responses with mutants of the *Arabidopsis* chromatin remodelling ATPase family revealed new defence-related genes with functions at the chromatin level. This screen revealed that, from the Ris-1 subfamily, *FRG2* and *EDA16* act as negative regulators of immunity. In the case of *FRG2* mutant *frg2-1*, an increase size was also observed making it an ideal candidate for future research in an agricultural context.

Methods

1 Plant and Microbe materials and growth conditions

1.1 Plant lines

1.1.1 Arabidopsis thaliana

Arabidopsis thaliana ecotype Columbia (Col-0), was used along this work. *Arabidopsis* seeds were sowed on Arabidopsis mix with Intercept and stratified for 2 to 3 days at 4 °C in darkness. Seeds were germinated and grown in an Aralab growth chamber set at a short photoperiod of 10 h light, 21 °C, 60% humidity. Two weeks after germination, seedlings were carefully transferred to individual pots. When necessary, plants were moved to a growth chamber with 16 h light period in order to obtain seeds.

For *in vitro* work, *Arabidopsis* seeds were surface-sterilised by chlorine gas exposure. Seeds in a seed storage (glassine) bag were kept for 4 h inside a sealed desiccator. To generate the chlorine gas inside the desiccator, to a beaker containing 100 mL 10% sodium hypochlorite 3 mL hydrochloric acid 37% were added. Seedlings were grown in sterile half (2.15 g/L) Murashige and Skoog medium (1/2 MS, Duchefa Biochemie), with 1% sucrose if indicated, pH adjusted with KOH 1 M at 5.80 ± 0.02 and 0.5% Phytagel (Sigma) if solid medium required. Glufosinate at a final concentration of 20 µg/mL or nystatin 25 µg/mL, were added, if required, once the medium was autoclaved and cooled below 65 °C.

The T-DNA insertion lines for *Arabidopsis* were purchased from the Nottingham Arabidopsis Stock Centre (NASC). SALK lines (Alonso et al., 2003), SAIL lines from Syngenta (Sessions et al., 2002), Wisconsin DsLox T-DNA lines (Woody et al., 2007) and one JIC Gene Traps line (Sundaresan et al., 1995) were used (Table **A.1,** Appendix, for Chromatin remodelling ATPase family and Table **A.2**, Appendix, for

other lines and crosses). *Arabidopsis* crosses were generated by emasculating closed flowers and pollinating the pistil with stamens of the desired line the next day.

1.1.2 *Nicotiana benthamiana*

N. benthamiana plants were sowed on F2 compost soil, and grown under short photoperiod conditions; 10 h light, 21 °C, 60% humidity. Plantlets were transferred to individual pots after two weeks. Fully extended leaves were used for transient protein expression (see **4.8** *A.tumefaciens*-mediated transient protein expression in *N. benthamiana*). *N. benthamiana* wild type and DICER2/DICER3 double mutant (Dadami et al., 2013; Katsarou et al., 2016) were used in this work.

1.2 Bacterial and fungal strains

Bacteria were kept as glycerol stocks (20% glycerol) at -80 °C. Stocks were streaked onto solid plates for single colony isolation prior to liquid medium inoculation. *Escherichia coli* strains and *Agrobacterium tumefaciens* (*Rhizobium radiobacter*) were grown on Luria Broth (LB) medium (1% tryptone, 0.5% yeast extract, 1% NaCl liquid, or solid, with the addition of 1.5% agar Bertani, 1951) adding the required selective antibiotics once the medium was autoclaved and cooled below 65 °C. *P. syringae* strains were grown in King's Broth medium (20g/L proteose peptone, 8.6 mM K_2HPO_4, 163 mM glycerol, pH adjusted to 7.0 with HCl before autoclaving; liquid, or solid, with the addition of 1.5% agar King et al., 1954) adding the required selective antibiotics (Table **M.1**), after the medium was autoclaved and cooled below 65 °C. *E. coli* strains were grown at 37 °C. *A. tumefaciens* and *P. syringae* strains were grown at 28 °C. Liquid cultures were grown with 220 rpm shaking. The different microbe strains used in this project are detailed in Table **M.1**.

Table M.1. Different Microbe strains and selective antibiotics

Species	Strain	Construct	Selection	Citation
E. coli	TOP10	-	-	Thermo Fisher, C404010
A. tumefaciens	GV3101	-	Rifampicin 100 µg/mL Gentamycin 100 µg/mL	(Holsters et al., 1980)
P. syringae	pv *tomato* DC3000	(Wild type)	Rifampicin 100 µg/mL	(Cuppels, 1986)
"	"	Δ*avrPto* Δ*avrPtoB*	Rifampicin 100 µg/mL Kanamycin 25 µg/mL Spectinomycin 50 µg/mL	(Lin and Martin, 2005)
"	"	*hrcC*	Rifampicin 100 µg/mL	(Penaloza-Vazquez et al., 2000)
"	"	LUX	Rifampicin 100 µg/mL Kanamycin 25 µg/mL	(Fan et al., 2008)
"	"	LUX *hrcC*	Rifampicin 100 µg/mL Kanamycin 25 µg/mL	(Fabro et al., 2011)
"	"	EV (pVSP61)	Rifampicin 100 µg/mL Kanamycin 25 µg/mL	(Chen et al., 2000)
"	"	AvrRpt2 (pV288)	Rifampicin 100 µg/mL Kanamycin 25 µg/mL	(Whalen et al., 1991)

The fungus *Botrytis cinerea* var *pepper* (Denby et al., 2004) was stored as a 5 x 10^5 spores/mL solution in 20% glycerol at -80 °C. It was cultured in potato dextrose agar (PDA) plates. In order to maintain full virulence, spores were transferred to sterile apricots and grown there for two weeks prior to infection assays.

2 Biotic stress assays

2.1 Bacterial assays

2.1.1 Bacterial inoculation

P. syringae strains were grown overnight in liquid cultures to obtain an optical density at 600 nm (OD_{600}) equal or greater than 1.0. A bacterial suspension of OD_{600} 0.1 (equivalent to 10^7 colony-forming units/mL) was prepared in 10 mM $MgCl_2$, 0.04% Silwet L-77 (Lehle Seeds, USA) for spray inoculation. A 0.001 OD_{600} bacterial suspension (equivalent to 10^5 colony-forming units/mL) was prepared in 10 mM $MgCl_2$ for syringe-infiltration inoculations (unless otherwise stated). Six 4-5 week-old plants per line were inoculated. Plants were preferably infected before midday (~11 am). Before spray inoculation, plants were labelled and randomly reallocated intermixing lines to avoid position bias. Spray inoculation was performed with a Sparmax TC-620X spray paintbrush (The AirbrushCompany, UK), at a pressure of 1 bar until the whole leaf surface was completely wet. Infected plants were then sealed in the infection tray and kept for the required infection time (0 to 3 days).

After the desired period of time, 0.5 cm^2 leaf discs were collected with a disc borer. Two leaf discs were collected per plant, amounting to twelve leaf discs per line. To add a confounding factor to account for inherent variability, leaf discs from the same line and treatment were combined by pairs avoiding pairing discs from the same plant and avoiding repeating the same pair combinations. 2 leaf discs (corresponding to a leaf surface area of 1 cm^2) were ground in 2 mL tubes containing two metallic beads (3 mm diameter) and 200 µL 10 mM $MgCl_2$. To grind the plant tissue, two pulses of 28 Hz for 30 seconds were applied with a mixer mill (Tissue Lyser MM300, Retsch). Plant and bacterial suspension was then diluted up to 1 mL with 800 µL 10 mM $MgCl_2$ and serial dilutions were plated on KB plates containing the selective antibiotics. 24 h later the bacterial colonies were counted at the pertinent dilution.

Each experiment, as described, was repeated 3 times on different days, or otherwise as stated.

2.1.2 Elicitor infiltration

4 to 5 week-old plants were pre-treated 24 h before bacterial infection. Plants were infiltrated with of 100 nM flg22 and water (mock) in three leaves choosing from leaves 7 to 10. *P. syringae* strains were cultured, used for syringe-infiltration infection, and harvested in the same way as described in section 2.1.1.

2.1.3 Ion leakage experiment

P. syringae strains were cultured in the same way as above described (2.1.1). A 0.1 OD_{600} bacterial suspension (equivalent to 10^7 colony-forming units/mL) was prepared in 10 mM $MgCl_2$ and syringe-infiltrated into 4-5 week-old plants. Immediately after infiltration, 0.5 cm^2 leaf surface was collected from each infected leaf. Six plants per line were infected, with 2 leaves per plant, choosing between leaves number 7 to 10 (counting from the first true leaves). Leaf discs were collected in sterile water and kept with mild agitation for 1 h. Then, the leaf discs were transferred to wells containing 1 mL of sterile water placing two discs per well. 50 µL of solution were taken to measure conductivity with a conductivity-meter Horiba B-173 Twin Cond (Horiba, Japan), every 2 h.

2.2 *Botrytis* detached leaf assay

In order to maintain full virulence, *B. cinerea* var *pepper* spores were harvested from 2 week-old apricot cultures as previously described (Windram et al., 2012). Briefly, the mycelium growing on the apricots was washed with 5 mL sterile water and the spore suspension filtered with glass wool or two layers of Miracloth (Merck Millipore). Spores were quantified with a haemocytometer chamber and diluted to 400 000 spores / mL in sterile water. Before infection, an equal volume of filter-sterilised grape juice (Purple Grape Juice from concentrate, Welch's; www.welchsjuice.co.uk) was added to the spore suspension. 5 µL of 200 000 spores/mL suspension in grape juice was added to each detached leaf. ~20 leaves from 4 to 5 weeks old plants were used for each line, using leaves 7 to 10 and avoiding taking more than two leaves per plant. Pictures were taken 0, 24, 48, 72 and 96 h after infection. Leaf lesion areas were measured and analysed on the pictures using ImageJ software (

https://imagej.nih.gov/ij/). The lesion areas were used to calculate means and standard errors and to perform Two-tailed Student T-test assuming equal variance.

2.3 Flagellin peptide treatment

Seedlings grown in sterile conditions were treated with the small peptide flg22 from flagellin (Bartels et al., 2013), sequence: QRLSTGSRINSAKDDAAGLQIA (EZBiolabs, USA). Seedlings were germinated and allowed to grow for 7 days in solid ½ MS, 1% sucrose. Then, seedlings were transferred to liquid ½ MS, 1% sucrose. Two seedlings were transferred to each well containing 1 mL medium, and were allowed to grow for another 7 days. After this adaptation period to the liquid medium, the remaining liquid was carefully removed from each well. Immediately, 1.5 mL of 100 nM flg22, ½ MS, 1 % sucrose was added to the treatment wells, and fresh ½ MS, 1% sucrose was added to the mock wells. Then, seedlings were harvested after desired period of time (e.g. 1 h) and if required, flash frozen in liquid nitrogen for RNA or protein extraction.

2.4 Reactive oxygen species (ROS) assay

Adult leaves (4 to 5 week-old plants) number 7 to 10 were used to harvest a leaf disc with a cork borer of 4 mm diameter (Kai Medical, Japan), avoiding the central vasculature. 24 leaf discs were collected for each line. Leaf discs were kept individually in a white 96-well plate, flat bottom, Lumitrac 200 (Greiner Bio-One), with 150 µL of sterile water, in the dark for 8 h. Then, the water was removed and 100 µL of luminescent solution (100 nM flg22, 100 µM luminol, Sigma, 10 µg/mL horseradish peroxidase, 9003-99-0, Sigma) was added. Immediately, the plate was placed in a Photek dark box and imaged with a photon-sensitive camera HRPCS218 (Photek) for 1 h using the software Image32 (Photek) to integrate photon capture. Images were processed with the Image32 software binning the photons captured for each minute into a time resolved image (TRI). Then, for each well total intensity values were extracted on a 1 min time resolution. Wells containing leaves for the same line were averaged and standard error of the mean calculated.

2.5 Seedling growth inhibition assay

In vitro grown seedlings were transferred 7 days after germination in ½ MS solid, 1% sucrose to either ½ MS liquid, 1% sucrose (mock) or same medium with different concentrations of flg22 (1, 10 and 100 nM flg22). Two seedlings were transferred to a well in a 24-well plate containing 1 mL of medium, using at least 6 wells per treatment (using preferably the same plate for different genotypes and different plates for different treatments). Then, 7 days after (seedlings were 14 days old) seedlings were removed from the media, gently dried on paper towel and weighted in pairs (every well containing two seedlings) as fresh weigh. *fls2* line was used as a control.

3 Abiotic stress assays

3.1 Salt stress assay

Seeds (sterilised for *in vitro* work as described in section 1.1.1) were germinated and allowed to grow in ½ MS solid, 1% sucrose with 0, 50, 100 or 150 mM NaCl. Then, pictures were taken 4 to 7 days after germination.

3.2 JA assays

In vitro grown seedlings were germinated and allowed to grow in Johnson, 1% sucrose with 0 and 50 µM meJA. Then, pictures were taken 7 days after germination. Treated and untreated seedlings were used for anthocyanin extraction overnight. Anthocyanin extraction was performed as described by (Boter et al., 2015; Swain and Hillis, 1959). Anthocyanin concentration was measured by spectrophotometry. Anthocyanin content is expressed as A_{530}/g of fresh weight.

4 Molecular Biology

4.1 Plant DNA extraction for genotyping PCR

DNA from *Arabidopsis* was extracted from leaf issue (an amount of tissue equivalent to 0.5 cm^2) with 100 µL 5% Chelex (Biorad), (HwangBo et al., 2010). The samples were ground manually at room temperature. Samples were further mixed with a vortex machine and then boiled at 95 °C for five minutes. To remove the resin and the tissue debris, the samples were spun at maximum speed on a benchtop centrifuge for two minutes. 30 µL of supernatant were collected and stored at 4 °C for further DNA testing.

Genotyping PCR

Two PCR reactions were used per sample to amplify DNA fragments from T-DNA insertion lines. LP – RP primers, flanking the T-DNA insertion, in wild type plants produced a PCR fragment of 1000 ± 200 base pairs. LBb1.3 – RP primers in homozygous lines produced a band of an expected size of 500 ± 200 base pairs. Heterozygous lines produced bands in both PCR reactions. The primer sequences were obtained through the software provided by the Salk institute, http://signal.salk.edu/tdnaprimers.2.html (see Table of primers used for PCR characterization together with T-DNA insertion lines Table 1, Appendix). Primers were synthesised by IDT Integrated DNA Technologies, Inc. (IDT).

4.2 RNA extraction, cDNA synthesis and qPCR

RNA extraction

Plant tissue for RNA extraction was frozen in liquid nitrogen immediately after harvesting and kept at -80 °C until processing. Plant tissue was ground in liquid nitrogen with a drill borer fitting a 2 mL micro-centrifuge tube. Immediately after, 1 mL of TRIzol® Reagent (Thermo Fisher Scientific) was added to the powder, mixed well by vortexing, and incubated at room temperature for 5 min. 200 µL of chloroform

was added to the sample, mixed gently and incubated for another further 5 minutes at room temperature. Samples were spun at 12,500 g for 20 minutes at 4 °C. The aqueous supernatant was carefully transferred to RNase-free tubes avoiding carrying over contamination from the aqueous/organic interface. RNA were precipitated adding an equal volume of isopropanol, mixing gently and incubating for 3 h at -20 °C. Samples were spun at 16,800 g for 20 minutes at 4 °C. The supernatant was removed and the RNA pellet was rinsed twice with 1 mL 70% ethanol in DEPC water. Dried RNA pellets were re-suspended in 50 µL nuclease-free water by incubating at 65 °C for 5 minutes.

DNase treatment and RNA quality assessment

RNA samples were treated with TURBO™ DNase (AM1907, Ambion, Thermo Fisher Scientific) following manufacturer's instructions. 5 µL of buffer and 1 µL of DNase enzyme were added to each RNA sample and incubated at 37 °C for 30 minutes. Then, 5 µL of the Inactivation Reagent were added, incubated at room temperature for 5 minutes and gently mixed by hand. After precipitating inactivating resin by centrifugation at 10,000 g for 1.5 minutes, 35 µL of clean RNA were transferred to a RNase-free tube. RNA quality was determined on a 1% agarose gel electrophoresis, and the concentration and purity were measured with a NanoDrop ND-1000 (Thermo Fisher Scientific). RNAs were stored at -20 °C for short-term use and at -80 °C for long-term storage.

Complementary DNA (cDNA) synthesis

For cDNA synthesis 2 µg of RNA were reverse-trancribed with the SuperScript™ II Reverse Transcriptase (18064, Thermo Fisher Scientific), following manufacturer's specifications, using a primer for polyA tails (TTTTTTTTTTTTTTTTTTVN). Final cDNAs were diluted with 40 µL nuclease free water for a final volume of 60 µL. cDNAs were stored at -20 °C.

Quantitative PCR (qPCR) conditions

qPCR was performed with SYBR® Green JumpStart™ Taq ReadyMix™ (S4438, Sigma), following manufacturer's recommendations; see Table qPCR primers Appendix for primers used, Table **M.2** for mix and Table **M.3** for PCR conditions. Three technical replicates were used for each sample. A 384-well plate CFX384 Touch™ Real-Time PCR Detection System (Bio-Rad Laboratories), and a 96-well plate Mx3005P qPCR System (Agilent Technologies) were used.

Table M.2. Components used for qPCR with SYBR® Green JumpStart™ polymerase .

Component	**Volume per triplicate**	
	66 µL (96-well)	**30 µL (384-well)**
2 x JumpStart Taq ReadyMix	33 µl	15 µL
10 µM Forward Primer	2.96 µl	1.35 µL
10 µM Reverse Primer	2.96 µl	1.35 µL
Template DNA	5 µL	2.3 µL
Water	22.66 µL	10 µL

Table M.3. Thermal cycling conditions used in qPCR with SYBR® Green JumpStart™ polymerase.

Step	**Temperature**	**Time**	**Cycles**
Initial Denaturation	94 °C	2 minutes	1
Denaturation	94 °C	15 seconds	40 Cycles
Annealing, elongation & fluorescence reading	*60/62 °C	60 seconds	
Dissociation curve	40 – 98 °C	10 seconds / 0.5 °C	1

* See annealing temperature for primer pair in Supplementary table **S.2**, Primers for qPCR, Appendix. Primers used for transcript (cDNA) quantification were designed for an elongation temperature of 62 °C and primers for ChIP DNA quantification were designed for an elongation temperature of 60 °C.

qPCR analysis

qPCR data was extracted for C_T values (theoretical cycle to overcome a threshold) accepting automatically calculated thresholds and imported into an excel file. Data was analysed with the $\Delta\Delta C_T$ method (Livak and Schmittgen, 2001). As controls, several genes with highly consistent expression levels at the studied conditions were used as a reference for the total messenger RNA concentration. Different primer pairs were tested and used: *ATCTIN 8* (ACT8), α-TUBULIN (*α-TUB*), *TIP41-like family protein* (*TIP41*) (see Supplementary table **S.2**, Primers for qPCR). All qPCR primers were tested for efficiency on a standard curve with at least 6 template concentrations diluted 10-fold, accepting only efficiencies between 90 and 105%.

4.3 Gateway cloning

To add the *att* sites to the DNA inserts required for Gateway® Technology cloning, a two-step PCR was used. Specific primers containing overhangs of half of the *att* sites, an adaptor sequence (underlined, below) and 16-18 nucleotides on targeted DNA sequences were designed (Table Cloning primers Appendix).

Forward: AAAAAGCAGGCTCCACC $n^1 – n^{16\text{-}18}$
Reverse: AGAAAGCTGGGTC $n^1 – n^{16\text{-}18}$
$n^1 – n^{16\text{-}18}$: Nucleotides specific to targeted sequence

Required DNA fragments were amplified from their corresponding DNA template (genomic DNA or cDNA) with Q5® High-Fidelity DNA Polymerase (M0491S, New England Biolabs), following manufacturer's instructions (Table **M.4** for PCR mix and table **M.5** relates the PCR settings).

Table M.4. PCR Components used for amplification with Q5 Polymerase.

Component	Volume
Q5 High-Fidelity 2X Master Mix	12.5 µL
10 µM Forward Primer	1.25 µL
10 µM Reverse Primer	1.25 µL
Template DNA	1 ng
Nuclease-Free Water	to 25 µL

Table M.5. Thermal Cycling Conditions used in PCR amplifications with Q5 polymerase.

Step	Temperature	Time	Cycles
Initial Denaturation	98 °C	30 seconds	1
Denaturation	98 °C	10 seconds	5 Cycles
Annealing	*50–72 °C	20 seconds	
Elongation	72 °C	50 seconds/kb	
Denaturation	98 °C	10 seconds	25 Cycles
Annealing & elongation	72 °C	3:20	
Final Extension	72 °C	2 minutes	1
Hold	4 °C		

* See annealing temperature for primer pair in qPCR Primer Table Appendix.

After checking amplification size and quality on a 1% agarose gel electrophoresis, PCR products were cleaned with a QIAquick PCR Purification Kit (Qiagen). A second PCR was performed with 1µL 0.1 ng/µL of DNA template and universal primers

corresponding to the full *att* sites (Cloning primers Table Apppendix); conditions as above (Table **M.4** and Table **M.5**).

attB1: GGGGACAAGTTTGTACAAAAAAGCAGGCT
attB2: GGGGACCACTTTGTACAAGAAAGCTGGGT

BP recombination

PCR fragments containing the full *att*B sites were cloned into the entry vector pDONR™/Zeo with Gateway™ BP Clonase™ II Enzyme mix (Invitrogen™, Thermo Fisher Scientific) following manufacturer's instructions (Table **M.6**). The DNA insert, entry plasmid and BP clonase were incubated at 25 °C overnight and treated with 0.4 µL Proteinase K at 37 °C for 15 minutes to stop the reaction.

Table M.6. Conditions used for BP clonase recombination.

Component	Volume
BP Clonase™ Enzyme Mix	0.5 µL
pDONR/zeo (75 ng/µL)	0.5 µL
Template DNA (12 ng/µL)	1.5 µL

E. coli transformation and plasmid DNA extraction

2.5 µL of plasmid were transformed into 50 µL *E. coli* TOP10 electro-competent cells (Bio-Rad, program Ec1). Transformed cells were allowed to recover in 500 µL LB medium free of antibiotics for 1 h at 37 °C and 210 rpm. Positively transformed cells were selected in 50 µg/mL Zeocin LB solid plates at 37 °C, overnight. Individual colonies were re-cultured in 50 µg/mL Zeocin liquid LB medium. *E. coli* bacterial

cultures were grown over night up to an OD_{600} of 1. Plasmid DNA was extracted with a mini-prep kit NucleoSpin® Plasmid (Macherey-Nagel), following manufacturer's specifications. DNA quality and concentration was determined with a NanoDrop ND-1000 (Thermo Fisher Scientific). Plasmid sequence was verified by Sanger sequencing LIGHTRUN (GATC Biotech), following supplier's instructions (400 ng of DNA and 1 µM plasmid in 10 µL were sent to supplier). Primers used for sequencing are detailed in Table **A.2**, Primers for cloning, Appendix.

LR recombination

Plasmids containing the insert were subjected to the second recombination into the binary vectors; Gateway™ LR Clonase™ II Enzyme Mix (11791, Invitrogen™, Thermo Fisher Scientific), following manufacturer's instructions. Binary vectors pEG101, containing a 35S promoter and a C-terminal EYFP-HA tag (Earley et al., 2006) and pBAV154, containing a dexamethasone-inducible promoter and a C-terminal HA tag (Vinatzer et al., 2006) were used as final destination vectors for the inserts (Table **M.7**). The DNA insert, entry plasmid and LR clonase™ were incubated at 25 °C overnight and treated with 0.4 µL Proteinase K at 37 °C for 15 minutes to stop the reaction. Plasmids were transformed into *E. coli*, purified and sequenced as above described.

Table M.7. Conditions used for LR clonase recombination.

Component	Volume
LP Clonase™ Enzyme Mix	0.8 µL
Entry vector pDONR (60 ng/µL)	1 µL
Destination vector (150 ng/µL)	0.4 µL
Water	1.8 µL

A. tumefaciens heat-shock transformation

To obtain competent cells, *A. tumefaciens* GV3101 were sub-cultured overnight in 50 mL LB liquid medium. Span at 3000 g for 10 min at 21 °C and re-suspended in 20 mL 10 mM $CaCl_2$. These cells were alliqouted and kept at -80 °C until needed. 1 µg of plasmid DNA was added to 50 µL of *A. tumefaciens* GV3101 competent cells and incubated on ice for 30 minutes. Then, cells were incubated in liquid nitrogen for 5 minutes, followed by an incubation at 37 °C for 5 minutes, and on ice for another 5 minutes. Then 1 mL LB (without antibiotics) was added and cells were incubated 2 h and a half at 28 °C, 210 rpm. Colonies were selected on 100 µg/mL rifampicin, 100 µg/mL gentamicin (GV3101 strain-selective), 25 µg/mL kanamycin (plasmid-selective) resistant LB solid plates. Plasmid sequence was verified by Sanger sequencing LIGHTRUN (GATC Biotech), following supplier's instructions (400 ng of DNA and 1 µM plasmid in 10 µL were sent to supplier). Primers used for sequencing are detailed in Table **A.2**, Other genotyping primers, Appendix.

4.4 *A.tumefaciens*-mediated stable transformation of *A. thaliana*

Flowering plants were trimmed 4-5 days before transformation. Successfully transformed *A. tumefaciens* lines were pre-cultured in 100 µg/mL rifampicin, 100 µg/mL gentamicin, 25 µg/mL kanamycin liquid LB overnight 2 days before transformation. Stable transformation was performed by paintbrush application of *A. tumefaciens* (carrying required cassette on a binary vector) on the surface of meristematic tissue and flowering buds (Chang et al., 1994; Katavic et al., 1994).

4.5 *A.tumefaciens*-mediated transient protein expression in *N. benthamiana*

Successfully transformed *A. tumefaciens* lines were grown in 100 µg/mL rifampicin, 100 µg/mL gentamicin, 25 µg/mL kanamycin liquid LB overnight. A bacterial suspension of OD_{600} 0.6 was prepared in infiltration buffer (10 mM MES, 10 mM

$MgCl_2$ pH 5.70). *N. benthamiana* fully expanded leaves were infiltrated and tissue was harvested and frozen in liquid nitrogen 2 days after infection.

4.6 Crude protein extraction, Bradford protein quantification assay and SDS-PAGE immuno-blot protein detection (western blot)

Arabidopsis frozen tissue was ground in liquid nitrogen and re-suspended in SDS Protein Loading Buffer (50 mM Tris-HCl pH 6.8, 2% SDS, 10 % Glycerol, 0.03 % bromophenol blue, and 10 mM dithiothreitol added before use) 1:2 weight/volume. Homogenised was boiled at 95 °C for 5 minutes and samples were spun at 14,000 g for 5 min. The soluble fraction was kept further quantification and blotting. Bradford protein quantification assay was performed with BradfordUltra (Expedeon), following manufacturer's specifications. Protein concentration was quantified against calibrated bovine serum albumin, BioRad, (500-0202) at 595 nm. Protein SDS-PAGE, transfer and Western blot was performed following Sambrook and Maniatis (1989). Briefly, 15 % polyacrylamide gels[1] were run with Running Buffer (25 mM Tris, 200 mM Glycine, 0.1% (w/v) SDS) during 2 h at 80 V. Gels were transferred to a methanol pre-activated Amersham™ Hybond 0.45µm PVDF (10600023) membrane using the Criterion System (BioRad) in Transfer Buffer (25 mM Tris, 192 mM glycine, 20% (v/v) methanol) for 1.5 h at 100 V. Membranes were block with 5% milk TBS-T for 1 h at room temperature.

Membrane blots were developed using secondary, or in some cases primary anti-bodies, fused to Horseradish Peroxidase (HRP). After two washes with TBS-T (50 mM Tris-Cl, pH 7.6, 150 mM NaCl, 0.1 % Tween 20) and another wash with TBS (50 mM Tris-Cl, pH 7.6, 150 mM NaCl), each wash for 10 min at room temperature, membranes were incubated for 2 minutes with a mix of 1:1 Amersham enhanced chemical luminescence (ECL) Prime Western Blotting Detection Reagent solution A and B, pre-mixed for 2 minutes (GE Healthcare). X-ray film (Thermo Fisher Scientific) was exposed to the blot in a dark room for between 10 seconds and 3 h to

[1] Discontinuous gel: Stacking (125 mM Tris-HCl pH 6.8, 0.1% SDS, 4 % polyacrylamide) and resolving (400 mM Tris-HCl pH 8.8, 0.1% SDS, 15% polyacrylamide), (Laemmli, 1970).

obtain sufficient signal, depending on protein sample and antibody. Films were developed with a CuriX 60 (Agfa).

Table M.8. Antibodies used for Western blot

Target	Reference number	Dilution (µL / mL)
Rabbit polyclonal to Histone H3	ab1791 Abcam	1 / 20
Rabbit polyclonal to H3K27me3	07-449 Millipore	1 / 5
Goat polyclonal anti-rabbit IgG - HRP	A0545 Sigma Aldrich	1 /20

4.7 Chromatin immuno-precipitation (ChIP) and qPCR

Plant tissue treated with flagellin (as described in section **2.3** Flagellin peptide treatment) was cross-linked and processed for chromatin immuno-precipitation (ChIP) following Engelhorn et al., (personal communication). Plant tissue was cross-linked by adding 25 mL of cross-linking buffer (40 mM sucrose, 1 mM PMSF, 10 mM Tris/HCl pH 8.00, 1 mM EDTA and 1% formaldehyde) and vacuum-infiltration on ice for three rounds of 10 minutes. Excess of formaldehyde was quenched by the addition of 1 mL 2 M glycine solution and vacuum-infiltration for 5 more minutes. Cross-linked tissue was rinsed twice in sterile water and dried with tissue paper before freezing it in liquid nitrogen. Frozen tissue was stored at -80 °C.

Nuclei extraction and chromatin sonication

Cross-linked tissue was thoroughly ground to fine powder in liquid nitrogen using a chilled pestle and mortar. Approximately, 1 g worth of powder was used for chromatin

extraction. Nuclei extraction was performed in 25 mL of Honda buffer (0.44 M sucrose, 1.25% ficoll, 2.5% dextran T40, 20 mM Hepes KOH pH 7.40, 10 mM $MgCl_2$, 0.5% Triton X-100, 5 mM DTT, 1 mM PMSF, and 0.2% Protease Inhibitor Mix P, 39103 Serva, Germany; Honda et al., 1966). Homogenised tissue was filter with two layers of miracloth (Millipore), and nuclei were concentrated by centrifuging 3000 g for 15 minutes at 4 °C. Iterative washes with Honda buffer and nuclei precipitation (1,500 g, 4 °C, 7 minutes' centrifugation) ensured chloroplast depletion.

Clean nuclei (white pellet) were lysed and sonicated in 300 µL of Nuclei Lysis buffer (50 mM Tris/HCl pH 8.00, 10 mM EDTA, 1% SDS, 1 mM PMSF and 0.2% Plant Protease Inhibitors, Serva) per 1.5 mL tube. Sonication was conducted with a Bioruptor® (Diagenode) in ice-cold water, following manufacturer's specifications. Samples were exposed to 6 cycles of 30 seconds "on", 1 minute "off" at high intensity (H). Then, the water in the sonicator bath was changed for fresh ice-cold water and another 6 more cycles with identical conditions were applied, for a total sonication of 12 cycles. Chromatin (diluted 10 times in TE buffer for measuring concentration) was quantified with a NanoDrop ND-1000 (Thermo Fisher Scientific), flash frozen in liquid nitrogen and stored at -20 °C unless immunoprecipitation was performed immediately after sonication. An aliquot from the pre-sonicated fraction as well as post sonicated were kept separate for on-gel fragment-size testing.

Chromatin IP

Sonicated chromatin samples were diluted in NLB for a final amount of 25 µg of chromatin in 50 µL per IP. A 10% sample was separated as DNA Input (e.g. for a three-antibody IP, 15 µL were taken out of 150 µL). Then, chromatin samples were diluted 10 times in 450 µL of IP dilution buffer (1.1% Triton X-100, Sigma, 1.2 mM EDTA, 16.7 mM Tris/HCl pH 8.00, 167 mM NaCl, 0.2% Plant Protease Inhibitors). The required concentration of antibody was added (Table of antibodies used for ChIP **M.9**) and samples were incubated for 10 h at 4 °C and 12 rpm on a Intelli-Mixer Rotator Mixer RM-2 (EL-RM2L).

After antibody incubation, Protein A Agarose/Salmon Sperm DNA beads (16-157, Millipore) were added to the samples and incubated at 4 °C, gentle rotation, 12 rpm, overnight. Beads were washed five times in Washing buffer (150 mM NaCl, 20 mM Tris HCl pH 8.00, 2 mM EDTA, 1% Triton X-100, 0.1% SDS, 1 mM PMSF, 0.2% Plant protease inhibitors) and eluted three times with 100 µL glycine elution buffer (0.1 M glycine, 0.5 M NaCl, 0.05% Tween-20, pH 3.80 adjusted with 37% HCl). The glycine elution buffer was made fresh every time and filter-sterilised. pH was neutralised by adding 150 µL of 1M Tris/HCl pH 9.00. Input samples were incorporated to the treatment from this point onwards, adding 300 µL of glycine elution buffer and 150 µL of Tris/HCl pH 9.00.

Samples were treated with 1.5 µL RNase A (10 mg/mL, R5125, Sigma) for 15 minutes at 37 °C, followed by 3 µL Proteinase K treatment overnight at 37 °C. Samples were de-crosslinked by incubating at 65 °C for 6 h. DNA samples were divided into two tubes and purified with a MinElute PCR Purification Kit (Qiagen), following manufacturer's instructions. Samples were eluted in 30 µL elution buffer and DNA from the same IP sample were pooled together for a final volume of ~60 µL per sample. DNA samples were stored at -20 °C.

Table M.9. Antibodies used for ChIP

Target	Reference number	Volume used per IP
Rabbit polyclonal to Histone H3	ab1791 Abcam	1 µL
Rabbit polyclonal to H3K27me3	07-449 Millipore	9 µL

qPCR quantification

ChIP DNA samples were quantified by qPCR. Relative abundance of IP DNA was compared to input. qPCR was performed with SYBR® Green JumpStart™ Taq ReadyMix™ (S4438, Sigma), following manufacturer's recommendations; see Table

A.2, Primers for ChIP, Appendix, Table **M.2** for mix and Table **M.3** for PCR conditions. Three technical replicates were used for each sample. A 384-well plate CFX384 Touch™ Real-Time PCR Detection System (Bio-Rad Laboratories), and a 96-well plate Mx3005P qPCR System (Agilent Technologies) were used.

qPCR analysis

qPCR data was extracted for C_T values (theoretical cycle to overcome a threshold) accepting automatically calculated thresholds and imported into an excel file. As controls, genes ACTIN 7 (ACT7) an actively transcribed gene depleted on H3K27me3 and SEPALLATA3 (SEP3) a transcriptionally repressed locus and enriched in H3K27me3 in the vegetative state (Engelhorn et al., personal communication; Zhang et al., 2016). All ChIP-qPCR primers were tested for efficiency on a standard curve with at least 6 template concentrations diluted 10-fold, accepting only efficiencies between 90 and 105%.

5. RNA-seq transcriptomic analysis

Sample treatment for RNA-sequencing

Arabidopsis seedlings were grown on ½ MS solid medium, long day conditions, 16 h light, 21 °C. Seedlings were transferred to ½ MS liquid medium overnight in a beaker sealed with Micropore™ Medical Tape (3M™). The next day, the liquid medium was removed and samples were treated with 100 nM flg22 ½ MS liquid or ½ MS liquid (control) for 2 h. Then, samples were removed from the liquid media, dried on tissue paper and flash frozen in liquid nitrogen. Frozen tissue was thoroughly ground to fine powder in liquid nitrogen using a chilled pestle and mortar. Ground tissue was stored at -80 °C for future RNA extraction.

RNA extraction

RNA extraction for RNA library prep was performed with the RNA extraction kit NucleoSpin® RNA (Macherey-Nagel) starting from ~500 µL worth of powder, following manufacturer's specifications. RNA quality was assessed by Nanodrop and concentrations were obtained with a Qubit™ RNA HS Assay Kit.

RNA library prep

RNA library prep was carried out with a #E7420 S/L NEBNext® Ultra™ Directional RNA Library Prep Kit for Illumina® (New England Biolabs), following manufacturer's instructions. Agencourt® AMPure® XP Beads (#A63881, Beckman Coulter, Inc.) magnetic beads (recommended by RNA library prep protocol) were used for RNA and DNA purification.

6 Microscopy

6.1 Confocal imaging

Samples were prepared from *N. benthamiana* leaf tissue. Typically, plants were infiltrated 3 days before with *A. tumefaciens* containing the desired construct (see **4.8** Transient protein expression in *N. benthamiana*). Images were obtained using a Zeiss Laser Scanning Microscope (LSM) 710 (Carl Zeiss Ltd; Cambridge, UK), and processed (including the addition of scale bars) using the Zeiss 2011 software (Zeiss). Usually, the 40x or the 63x objective lenses were used.

6.2 FRAP

Samples were prepared from 12 to 15 days *Arabidopsis* seedlings grown in sterile ½ MS 1% sucrose, square plates, kept vertical. Seedlings were treated with 100 nM flg22 medium and mock as described in section **2.3** (Flagellin peptide treatment), except that the seedlings were transfer directly from the solid ½ MS into the liquid ½ MS containing the elicitor flg22. After desired incubation period, true leaves (avoiding cotyledons), as extended and flat as possible, were harvested and placed with the adaxial surface on the slide glass. This way, the abaxial surface (which lacks big trichomes) would face the confocal objective.

Fluorescence recovery after photobleaching (FRAP) was performed with a Zeiss LSM 710 (Carl Zeiss Ltd; Cambridge, UK). After selecting a developmentally mature cell nucleus (Rosa et al., 2014), an area of 1µm in radius was bleached in the centre section of the nucleus, avoiding the nucleolus, with a three-channel laser (458, 488 and 514 nm) 100% power, and 18 iterations. Subsequently, the nucleus was imaged (Frame size: 512 x 512) every minute for 30 minutes taking a Z-stack with 14 planes separated by 1 µm. FRAP recovery curves were generated from raw images processed with ImageJ software (https://imagej.nih.gov/ij/). Relative recovery was normalised to total nucleus intensity (affected by the imaging) and background noise, according to Rosa et al., (2014).

7 Computational methods

7.1 RNA-seq Analysis

RNA libraries were checked for size quality with a Bioanalyzer, and sequenced with an Ilumina sequencer. After quality controls of raw sequencing data with FastQC (https://www.bioinformatics.babraham.ac.uk/projects/fastqc/), untrimmed data sequences were map to *Arabidopsis* TAIR10. 36, downloaded from Ensembl (http://plants.ensembl.org/info/website/ftp/index.html) with STAR (Dobin et al., 2013), followed by read counting with HTseq-count implemented with LiBiNorm

(Anders et al., 2015; Archer et al., 2016), using the following parameters: --order=pos --minaqual=10 --mode=intersection-nonempty --idattr=gene_id --type=exon --stranded=reverse. The data counts were normalised and analysed with the R package DEseq2 (Love et al., 2014). The adjusted p-values accepted for significance were < 0.01 with a fold-change > 2, unless otherwise stated. Different models where built to discover differentially expressed genes between conditions: For the discovery of batch-effect genes (those genes that showed a variation between biological replicates) a simple model "~Replicate" was used. To compare the treated and untreated samples a model accounting for a replicate effect was used: "~Treatment + replicate". Finally, to establish the differences between mutants and the distinct effect of the treatment on the mutants a model with an interaction term was built: "~genotype + treatment + genotype:treatment".

7.2 Methods in chapter 1

Denoux et al., (2008) available data (Supplementary Table 1. Fold-change, P-value, and intensity values for all ATH1 GeneChip probe sets). Stable expression across conditions and time points were selected when every fold-change for the 4 conditions (+/-OGs 1h, and 3 h, +/-flg22 1h and 3 h) were between 2 and -2. Then, in order to select highly expressed genes and lowly expressed genes, the set of stable genes was sorted according to averaged intensity signal for the 4 conditions and subdivided into 2 groups, one group of highly expressed genes, with those genes with average intensity greater than 5, and another group of lowly expressed genes, containing those genes with average intensity smaller than 0.05.

To select the random genes with similar gene expression profile of the defence genes prior to elicitation, an empirical cumulative distribution function (ECDF, Tucker, 1959) was built on the microarray intensities for the desired genes (differentially expressed genes according to Denoux et al., 2008). Then, random sampling was reversed through the ECDF to obtain a virtually identically distributed set of genes.

7.3 Computational tools and databases used

For the Principal component analysis (PCA), Hinton diagram generation, ECDF construction and random sampling, and other plotting and visualising tools, Excel, R, Matlab and C++ in-house scripts were used. For Venn diagram generation online Venny (http://bioinfogp.cnb.csic.es/tools/venny/; Oliveros, 2007) and R package VennDiagram were used. For GO term analysis Virtualplant online server (http://virtualplant.bio.nyu.edu/cgi-bin/vpweb/; Katari et al., 2010), and topGO R package were used (https://www.bioconductor.org/packages/devel/bioc/html/topGO.html). GEO (https://www.ncbi.nlm.nih.gov/gds), TAIR (http://www.arabidopsis.org/), Araport (https://www.araport.org/), SALK primer T-DNA design (http://signal.salk.edu/tdnaprimers.2.html), Epigara (http://epigara.biologie.ens.fr/cgi-bin/gbrowse/a2e/), PlantDHS (http://plantdhs.org/), String (https://string-db.org/), ArrayExpress (https://www.ebi.ac.uk/arrayexpress/) and BAR (http://bar.utoronto.ca/) databases were regularly accessed throughout this work.

Chapter 1. Immune gene activation related to Histone 3 Lysine 27 demethylation

Introduction

In contrast to vertebrates, plants lack an adaptive immune system and solely rely on the innate immunity of each cell and on systemic signals originated from the infected cells. The initial onset of plant innate immunity primarily depends on plasma-membrane localised receptors coupled with cytoplasmic kinases that upon stimulation, undertake the transduction of the signal via kinase cascades and calcium influx. For example, the pattern recognition receptor FLS2 and its co-receptor BAK1 detect flagellin and initiate multiple signalling cascades by directly or indirectly phosphorylating several receptor-like protein kinases such as the brassinosteroid signalling kinase 1 (BSK1), which is involved in ROS production (Couto and Zipfel, 2016). Other receptors, like the receptor for the bacterial elongation factor Tu (EF-Tu) (Kunze et al., 2004; Zipfel et al., 2006), and surface kinases, such as the lectin receptor-like kinases (LecRK) that bind to bacterial lipopolysaccharides, fulfil equivalent roles (Ranf et al., 2015).

Downstream, several kinase families, such as triple, double and single MAP kinases (Tena et al., 2011) or calcium-dependent protein kinases (CDPKs; Boudsocq et al., 2010), amplify and transduce the signal towards multiple intracellular responses, including regulation of transcription. In fact, there is a substantial overlap between the genes upregulated by flagellin and EF-Tu and oligogalacturonides, derived during cell wall degradation (Denoux et al., 2008; Zipfel et al., 2006). However, some genes respond preferentially to certain signalling cascades. For example, *FRK1* (encoding a kinase itself) responds to the MAP kinases MPK3/6 pathway, with little input from CDPKs. The opposite happens with *PHI-1*. Between these extreme examples there are a wide range of partial and synergistic inducible genes such as *NHL10* or *CYP82C2* that require both the MAP kinases and CDPKs (Boudsocq et al., 2010).

The mechanisms for specificity may rely on the activation of the transcriptional machinery through phosphorylation. For example, MAP kinase MPK4 interacts with transcription factor (TF) WRKY33 through the kinase MKS1. Upon flagellin peptide flg22 treatment, WRKY33 is released from complexes with MPK4 to associate with the promoter of the camalexin biosynthetic gene *PAD3* (Qiu et al., 2008). Another TF, ERF104, is similarly phosphorylated by MAPK MPK3/6 during immunity (Bethke et al., 2009), and rice TF OsEREBP1, has also been shown to be targeted by MAP kinases in rice (Cheong et al., 2003). The basal transcription machinery is also directly targeted by multiple kinases. RNA polymerase II CTD subunit is phosphorylated downstream the MPK3/6 kinase cascade (Li et al., 2014). In yeast and mammals, several MAP kinases phosphorylate histone H3 at the promoters of genes that they directly regulate (Drobic et al., 2010; Pokholok et al., 2006). In plants, histone H3 phosphorylation, either alone or in combination with other chromatin marks, has been related to the cell cycle regulation, transcription activation, DNA-damage repair and abiotic stresses (Houben et al., 1999, 2007; Wang et al., 2015b).

In addition to histone phosphorylation, chromatin is decorated with other histone and DNA modifications (chromatin marks) that regulate gene expression, DNA replication and DNA repair. Chromatin marks strongly linked with active transcription are histone acetylation (almost at any permissive lysine, the acetyl moiety decreases the histone tail basicity, decreasing its affinity with DNA; Bannister and Kouzarides, 2011) and histone di and tri-methylation at histone H3 lysine 4 (H3K4me2 and H3K4me3; Oh et al., 2008; Shilatifard, 2012; Zhang et al., 2009). Maintenance of transcription and transcriptional elongation are associated with histone H2B ubiquitination (H2Bub) and the methylation mark H3K36me3, which generally accumulates at the 3' end (or along the first half of the gene body in *Arabidopsis*; Roudier et al., 2011) of active genes and is typically associated with phosphorylated RNA polymerase (Joshi and Struhl, 2005; Wang et al., 2009). Gene repression is associated with DNA methylation and H3K27me3. DNA methylation anti-correlates with H2A.Z deposition at the transcription start site (TSS) of genes (Zilberman et al., 2008). However, DNA methylation tends to increase, together with H3K9me2, along heterochromatic regions, whereas H3K27me3 is an euchromatin mark mainly restricted to gene bodies (Roudier et al., 2011). Interestingly, fluctuations in H3K27me3 levels have been

associated with the epigenetic memory of different stresses (Liu et al., 2014; Luna et al., 2012).

Histone modifying enzymes alter the chromatin landscape impacting on gene expression. In particular, histone demethylase enzymes are recognised as important chromatin modulators, affecting plant growth and development (Noh et al., 2004). Compared to other histone-modifying enzymes, they are fairly specific in their substrate (Kooistra and Helin, 2012; Kouzarides, 2007). Within the jmjC family of histone demethylases, histone H3K27 demethylases REF6 and ELF6 have been strongly linked with the de-repression of flowering master regulators, such as *FLC* in *Arabidopsis* (Crevillén et al., 2014; Lu et al., 2011). Also, they modulate brassinosteroid-mediated gene expression by binding through their C-terminal motif to the phosphorylated TF BES1 (Yu et al., 2008). More recently, REF6 was also shown to interact with a DNA motif through its Zinc-finger C-terminal domain (Cui et al., 2016). In rice, there is evidence of a histone H3K27 demethylase role in plant defence. *JMJ705*, a putative orthologue of the *Arabidopsis REF6*, affects JA-driven gene expression. In addition, *JMJ705* overexpression resulted in increased resistance to the bacterial pathogen *Xanthomonas oryzae* (Li et al., 2013). Interestingly, in *Arabidopsis*, some jmjC domain-encoding genes, including *ELF6*, were clustered as up-regulated in the presence of effector molecules from the bacterial pathogen *P. syringae* (Lewis et al., 2015).

The aim of this chapter is to explore whether flagellin-induced gene expression changes (Denoux et al., 2008; Navarro et al., 2004; Zipfel et al., 2004) are correlated with chromatin marks. These potential chromatin signatures may act as a molecular guide for the immunity-activated TFs and ultimately control the transcription machinery. Since the development of deep sequencing techniques (Cuvier and Fierz, 2017), an ever-increasing wealth of genome-wide transcriptomic and epigenomic data sets have been published. For the initial analysis, publicly available data on flg22-induced gene expression (Denoux et al., 2008) was combined with chromatin state data (histone and DNA modifications; Roudier et al., 2011; Sequeira-Mendes et al., 2014). This allowed the identification of H3K27me3 as a mark highly correlated with defence gene loci silencing. For the tested genes, flagellin-induced gene expression was concomitant with H3K27me3 reduction. In addition, the immunity phenotypes of

the histone demethylases *REF6* and *ELF6* mutants further supported the role of a dynamic histone methylation/demethylation in plant immunity.

Results

1 Chromatin marks in defence-related loci

In order to test whether flagellin-induced gene expression is correlated with chromatin marks, publicly available data on gene expression and chromatin state data (histone and DNA modifications) were combined. Up to the date of performing these experiments, several data sets on chromatin marks had been published. In particular, Roudier et al., (2011) published an extensive effort to characterise up to 8 chromatin marks along *Arabidopsis* genome. Histone H3, lysine 4 di and tri-methylation (H3K4me2 and H3K4me3), histone H3, lysine 27 mono and tri-methylation (H3K27me1 and H3K27me3), histone H3 lysine 36 tri-methylation (H3K36me3), histone H2B ubiquitination (H2Bub), DNA methylation (5mC) and histone H3 enrichment, as a proxy of nucleosome occupancy (H3), were studied by chromatin immuno-precipitation paired with tiling microarray analysis (ChIP-chip). Other previous works have looked into genome distribution of one, two or three chromatin marks by using ChIP-chip (Oh et al., 2008; Turck et al., 2007; Zhang et al., 2007, 2009; Zilberman et al., 2008). Later on, new datasets using ChIP paired with next generation sequencing (ChIP-seq) were produced (Latrasse et al., 2017; Zhang et al., 2016). To avoid the loss of resolution due to the combination of datasets prepared with different biological conditions and different sequencing techniques (microarray versus next generation sequencing), the most comprehensive dataset from Roudier et al., (2011) was chosen for the analysis.

To render the comparison between two different datasets (chromatin data and gene expression data) more relevant, several datasets of flg22-induced gene expression were considered (Table **1.1**). The microarray data in the work by Denoux et al., 2008 used the same conditions as the ones used to generate the chromatin data by Roudier et al., (2011) (Table **1.1)**, making these datasets directly comparable.

Table 1.1. Transcriptomic and chromatin datasets considered.

Authors	**Navarro *et al.*, 2004**	**Zipfel *et al.*, 2004**	**Denoux *et al.*, 2008**	**Frei dit Frey *et al.*, 2014**	**Roudier *et al.*, 2011**
flg22 treatments	0.5 & 1 h	1 h	1 h	0.5 h	Untreated
Tissue	Protoplasts	leaf	Seedling	Seedling	Seedling
Age	7 days subculture	5-6 weeks	10 days	13 days	10 days
Photoperiod		8 h light	16 h light	16 h light	16 h light
Background	Ler	Ler	Col-0	Col-0	Col-0
Up-regulated genes	93	967	1611	1529	NA

1.1 Comparison between stable gene expression and chromatin state

Before testing defence-related genes, to add confidence to the analysis and the conclusions that could be drawn, it was important to validate that the two datasets, one with flagellin-induced gene expression data and the other with chromatin enrichment data, were comparable. For this, known results, such as the correlation of certain histone marks with gene expression levels, were confirmed (Roudier et al., 2011; Sequeira-Mendes et al., 2014). As proof of concept, chromatin modifications of genes at the extremes of gene expression were compared: highly expressed genes were compared with lowly expressed genes. To define them using the gene expression dataset (Denoux et al., 2008), first, stably expressed genes were selected by choosing genes showing less than 2-fold gene expression change in every replicate and treatment (14745 genes). Then, using average intensity across replicates and treatments, stably expressed genes were divided into highly expressed genes (more than 5 $\log_2$ intensity; top 486 genes) and lowly expressed genes (probes with less than 0.05 $\log_2$ intensity, bottom 2011 genes, see Supplementary figure **S1.1**).

Normalised data of histone modifications (H3K4me2, H3K4me3, H3K36me3, H2Bub, H3K27me3, H3K27me1 and histone H3 as control) and DNA methylation ChIP were gathered (Roudier et al., 2011, from the GEO database, https://www.ncbi.nlm.nih.gov/geo/, under the super-series accession number GSE24710) for each of the 2497 stably expressed genes. The correlation matrix showed a remarkably high co-occurrence between histone modifications associated with expressed genes (H3K4me3, H3K4me2, H3K36me3 and H2Bub) in accordance to previously described results (Roudier et al., 2011; Sequeira-Mendes et al., 2014; Figure **1.1 A & B**). In the same way, the marks anti-correlated with gene expression (H3K27me1, DNA methylation, 5mC, and histone abundance) were also co-occurring. However, the repressive mark H3K27me3 did not correlate with any other chromatin modifications, not even with other repressive marks such as H3K27 mono-methylation or DNA methylation (Figure **1.1 B**).

To test the proximity between chromatin data and gene expression a simple classification using Euclidean distances was built solely based on the histone modifications data. Most genes were successfully separated as highly or lowly expressed, suggesting a strong correlation between gene expression and certain chromatin state. While chromatin marks for actively expressed genes were found clustering closely together, marks for lowly (or non-) expressed genes differed greatly. Lowly expressed genes separated mainly in two clusters, one being much more related to that of the active genes than to the other group of repressed genes (Figure **1.1 C**). This clustering suggests that active loci require a precise set of chromatin marks but gene repression is associated with at least two independent chromatin marks: DNA methylation (5mC) and histone H3K27me3.

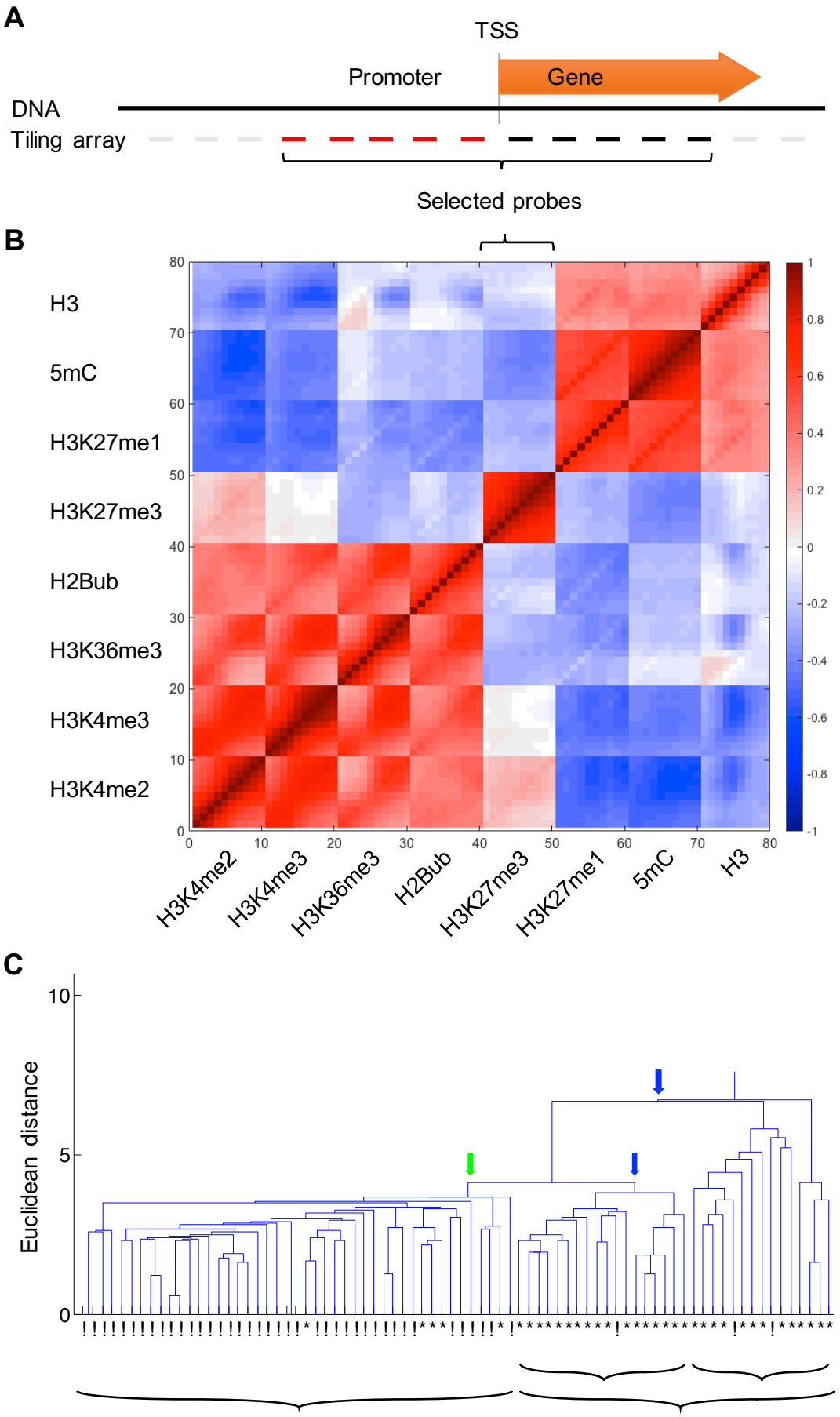
A
TSS
Promoter
Gene
DNA
Tiling array
Selected probes
B
H3
5mC
H3K27me1
H3K27me3
H2Bub
H3K36me3
H3K4me3
H3K4me2
H3K4me2
H3K4me3
H3K36me3
H2Bub
H3K27me3
H3K27me1
5mC
H3
C
Euclidean distance

Figure 1.1. Correlation between histone marks and gene expression. (A) Selected probes around the TSS. 5 probes were selected in the promoter region and 5 more after the TSS. (B) Correlation matrix heat map for histone marks and DNA methylation of 2497 stably expressed genes. Selected probes as explained in panel A: Oriented 5' to 3' left to right for the X axis and bottom to top for the Y axis. Red colours indicate high correlation, blues indicate anti-correlation and whites no correlation. (C) Small sample (40 stably expressed genes, representing ~1.6% of the 2497 stable expressed genes selected) hierarchical clustering illustrating the resolution power of chromatin data by the good separation between highly expressed genes (exclamation mark "!") and low expressed genes (asterisk "*"). Arrows point to nodes where main clusters separated.

1.2 Comparison between stably expressed genes and defence genes

A set of defence genes were selected from the selected transcriptomic experiment (Denoux et al., 2008). 1611 genes as up-regulated and 1075 as down-regulated were chosen having a fold-change > 2 and a p-value ≤ 0.01. Up-regulated defence genes were compared with the previously described set of stably expressed genes as a control. Principal Component Analysis (PCA) of histone modifications (H3K4me2, H3K4me3, H3K36me3, H3K27me1, H3K27me3 and histone H3) and DNA methylation (Roudier et al., 2011) at the TSS probe were compared. Stably expressed genes and defence genes did not show similar distributions of the variance weight over the principal components, suggesting different sources of variation for the two sets of genes. Greater variability of particular chromatin marks may indicate a role in regulating the expression of either of those particular set of genes (Figure **1.2 top**). In the stably expressed genes group, Principal Component 1 (PC1) and PC2 accumulated more than 80% of the total variability. However, in the defence genes the distribution of the variation was more evenly spread across the principal components, indicating that the variability of the two data sets is spread differently. Alternatively, the different size of the two datasets, could have also affected the contribution to the variance of each principal component (Cattell, 1966).

Considering the chromatin enrichment data as a vector space, the data relating to the abundance of each chromatin mark is an independent variable (data expands in one dimension). Principal components can be defined as combinations of the original independent variables, and therefore can be de-composed or expressed as the sum of contributions of the original chromatin mark data, making the interpretation of each principal component more accessible. To aid in the visualisation of the de-composition analysis of principal components, a Hinton diagram representing the weight of each original component (vertical axis) on each principal component (horizontal axis), using two colours to represent the sign of the magnitude (positive or negative) was created. In the stably expressed genes group, H3K4me2 and H3K4me3 were the main contributors to PC1 and H3K27me3 of PC2. However, in the defence genes group PC1 H3K27me3 has similar magnitude to H3K4me3, and PC2 is mainly driven by DNA methylation (Figure **1.2 bottom**). These results, in combination with the previous observation of H3K27me3 as an independent repressive mark, suggest that H3K27me3, either alone or with H3K4me3 (an activation mark important for gene expression) or DNA methylation on its own, contribute to gene silencing prior to flg22-induced transcriptional activation.

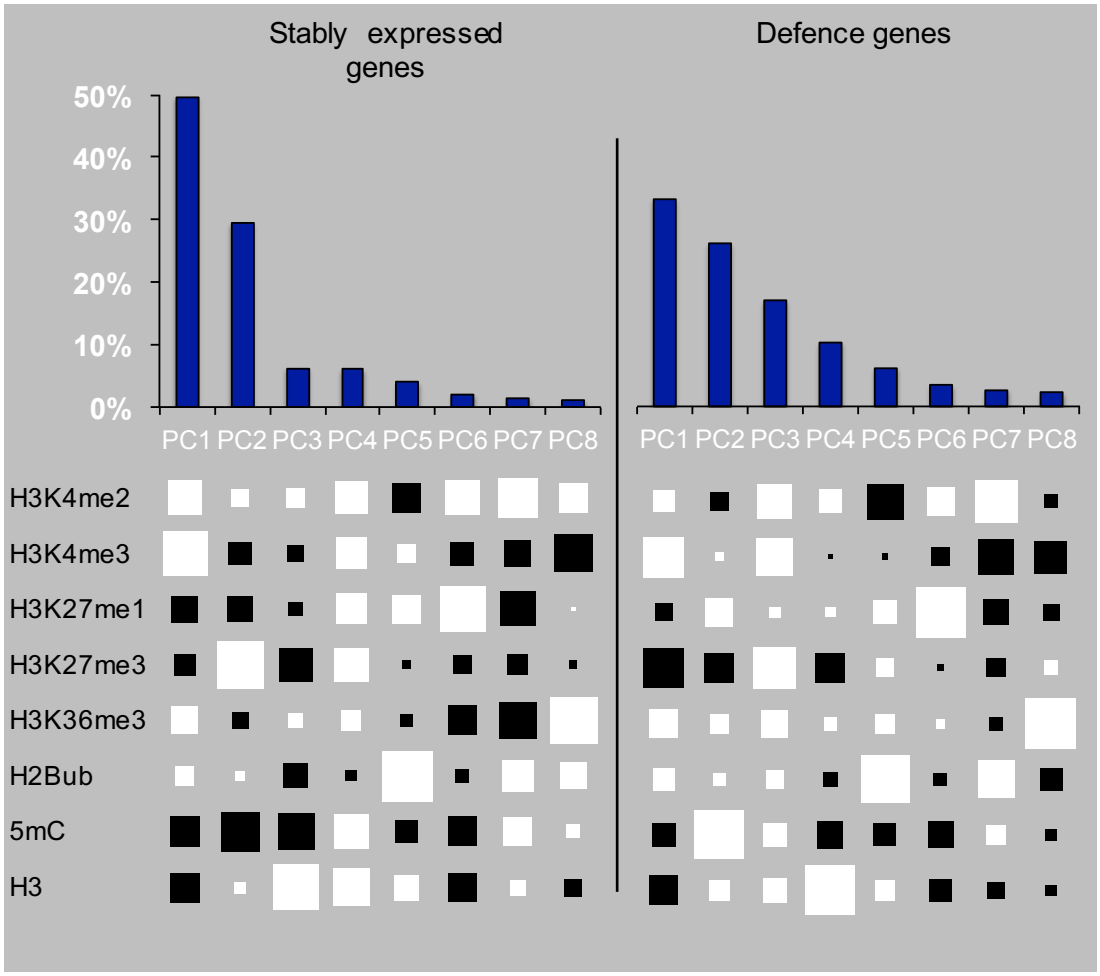

Figure 1.2. Stably expressed genes and defence genes present different sources of variance at the chromatin level. (top) Variance contribution percentage of each principal component after PCA of histone modification enrichment at TSS of constitutively expressed genes (left) and defence genes (right) and (bottom) associated Hinton diagram of the covariance matrix. The area of the square is proportional to the contribution of each element to the vector's magnitude; white positive and black negative values. Right: Principal components of stably expressed genes, active and repressed. Left: Principal components of defence genes.

Recently, Sequeira-Mendes et al., (2014) reviewed and compiled the available genome-wide chromatin data, describing 9 chromatin states according to the combination of co-occurring chromatin marks (including DNA methylation and histone variants H3.1, H3.3 and H2A.Z). To gain confidence on the observations made so far, flg22-induced genes were classified within these 9 chromatin states and compared with random gene sets. When comparing sets of genes based on their

expression levels to another set of genes chosen randomly (i.e. with no criteria regarding expression), it is highly unlikely that these two sets of genes have a similar gene expression distribution (see Supplementary figure **S1.2**). To select the random genes with similar gene expression profile of the defence genes prior to elicitation, an empirical cumulative density function (ECDF, Tucker, 1959) was built on the microarray intensities with the desired set of genes as a model for gene expression. Random sampling (uniformly distributed) was reversed through the ECDF to obtain a new set of values virtually identically distributed as the original dataset. Then, those genes closer to the values of this new dataset were chosen for further comparison at the chromatin level. This allowed the repetition of random set extractions and to learn expected distributions and deviations over the 9 chromatin states.

Overall, prior to immune activation flg22-induced genes showed a similar profile to what would be expected from a random sample of genes with very similar levels of expression (**1.3 B**). However, in comparison with the random generated sets of genes, there was a difference larger than expected in the percentage of flg22-induced genes allocated on chromatin state 2. Chromatin state 2 is enriched both in marks correlated with active gene expression (H3K4me3, H3K4me2, H2A.Z) and gene repression (H3K27me3). Interestingly, genes defined within chromatin state 2 display low levels of basal expression (Sequeira-Mendes et al., 2014). Down-regulated genes showed differences in chromatin state 2 and also chromatin state 1 compared to random generated gene sets with correction for gene expression. Chromatin state 1 is very similar to 2, except that it excludes the repressive mark H3K27me3, and includes other marks positively correlated with gene expression such as H3K36me3 and H2Bub. In line with the results from the comparison with stably expressed genes, these results indicate that flg22-induced genes are fairly similar in chromatin marks to other expressed genes, but distinctive in key histone marks such as H3K27me3 (related to low levels of transcription) or H3K4me3 (related to actively transcribed genes). This could suggest a mechanism of repression of otherwise “primed” genes, poised for the removal of H3K27me3 to initiate transcription.

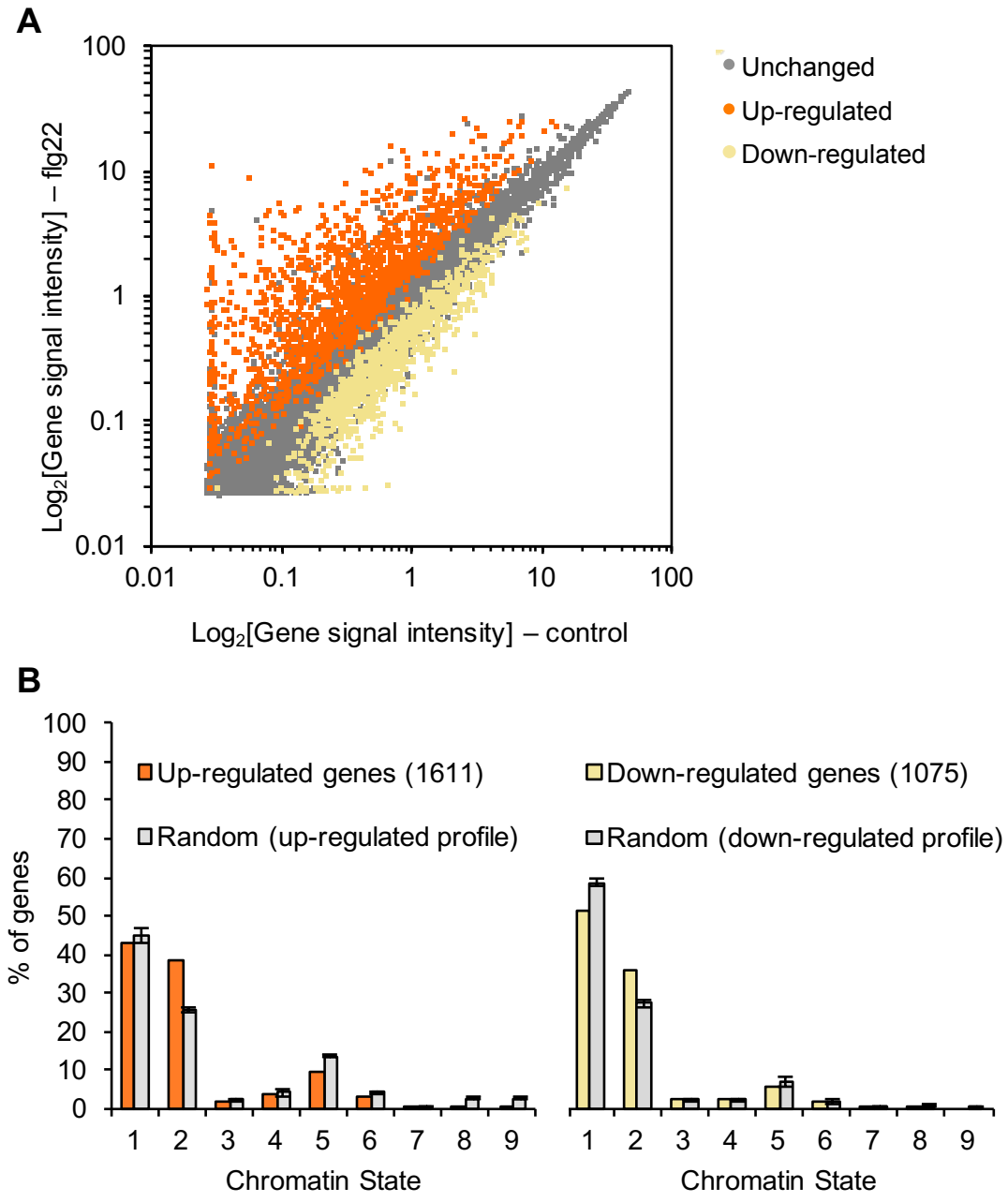

Figure 1.3. Chromatin state percentages for flg22-induced genes. (A) Differentially expressed genes between control and 1 hour after 1 µM flg22 (Denoux et al., 2008). (B) Classification of previously defined chromatin states (Sequeira-Mendes et al., 2014) for defence genes, up- (1611) and down-regulated (1075). Random gene sets were corrected for comparable levels of gene expression by means of a ECDF, and repeated 10 times to produce an estimate of chromatin state distribution and expected variability. Error bars represent standard deviations.

1.3 Comparing chromatin in kinase-relevant subgroups of defence genes

To test if signal transduction pathways may lead to a certain chromatin mark (or set of marks defined as a chromatin state), flg22-induced genes were subdivided into their defined transduction activation pathway (when known) and examined for chromatin state distribution (Sequeira-Mendes et al., 2014), and individual marks. Genes responsive to MAPK kinases MPK3, MPK4 and MPK6 (Frei dit Frey et al., 2014), and calcium-dependent protein kinases CPK5, CPK6 and CPK11 (Boudsocq et al., 2010) were compared. Initially, the genes were filtered to select those that were exclusively activated downstream of MAPKs or CDPKs (Figure **1.4 A**). Only MPK4 (264) and CDPK (140) responsive genes were selected for further analysis due to the low number of genes described as regulated by the other MAPKs. The distribution of the MPK4 responsive genes along the 9 chromatin states was comparable to the whole set of flg22-induced genes. However, CDPK-responsive genes had a different distribution compared to the whole set of flg22-induced genes (Figure **1.4 B**). In particular, CDPK-responsive genes were underrepresented in chromatin state 1 (comprised of mainly active marks, lacking H3K27me3), and overrepresented in chromatin states 2 and 5, both having in common the presence of H3K27me3.

Previous results indicated that lowly expressed genes and active genes were very different at the chromatin level (Figure **1.1 C**). Therefore, selected MPK4-responsive genes and CDPK-responsive genes were further divided between lowly expressed genes and partially expressed genes. Using the gene expression at the basal state, two set of genes were arbitrarily generated by taking the lower quartile as lowly expressed genes, and the two upper quartiles (or gene expression greater than median gene expression) as partially expressed genes. This separation evidenced that genes with some levels of expression (partially expressed genes) are overrepresented in chromatin state 2 and lowly expressed genes are overrepresented in chromatin state 5. Overall, these results highlight the abundance of H3K27me3, suggesting its role on gene repression on its own or correlated with other marks, prior to flg22-induced transcription.

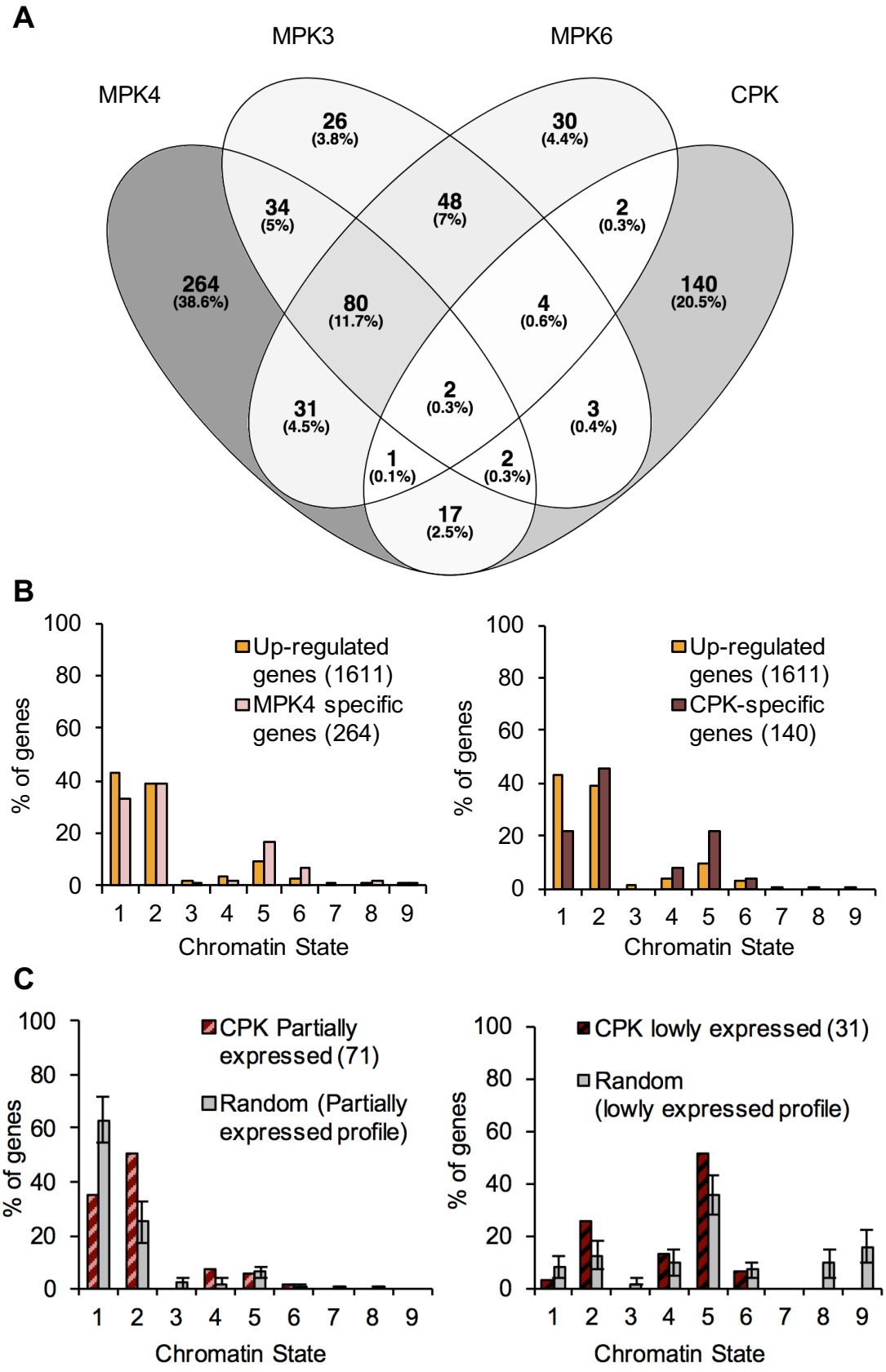
A
MPK3
MPK6
MPK4
CPK
26 (3.8%)
30 (4.4%)
34 (5%)
48 (7%)
2 (0.3%)
264 (38.6%)
80 (11.7%)
4 (0.6%)
140 (20.5%)
2 (0.3%)
31 (4.5%)
3 (0.4%)
1 (0.1%)
2 (0.3%)
17 (2.5%)
B
% of genes
Up-regulated genes (1611)
MPK4 specific genes (264)
Chromatin State
Up-regulated genes (1611)
CPK-specific genes (140)
Chromatin State
C
% of genes
CPK Partially expressed (71)
Random (Partially expressed profile)
Chromatin State
CPK lowly expressed (31)
Random (lowly expressed profile)
Chromatin State

Figure 1.4. Analysis of flg22-induced, kinase-responsive genes into 9 chromatin states. (A) Venn diagram showing overlap between different kinase responsive genes, MPK4, MPK3, MPK5 (Frei dit Frey et al., 2014) and CPK (Boudsocq et al., 2010). Percentages (in parentheses, %) are taken over the whole number of different genes compared. (B) Chromatin state classification (Sequeira-Mendes et al., 2014) of MPK4 exclusive genes (Left) and CPK exclusive genes (Right) compared to flagellin-induced defence genes (Denoux et al., 2008). (C) CPK exclusive, partially expressed genes (Left) CPK exclusive, lowly expressed genes compared with random control corrected for basal gene expression.

The role of single chromatin modifications in controlling flg22-induced gene expression was also investigated (Figure **1.5**). This confirmed H3K27me3 as the only histone mark overrepresented in the CDPK-responsive, lowly expressed genes compared to controls gene sets (Figure **1.5 B** and **C**).

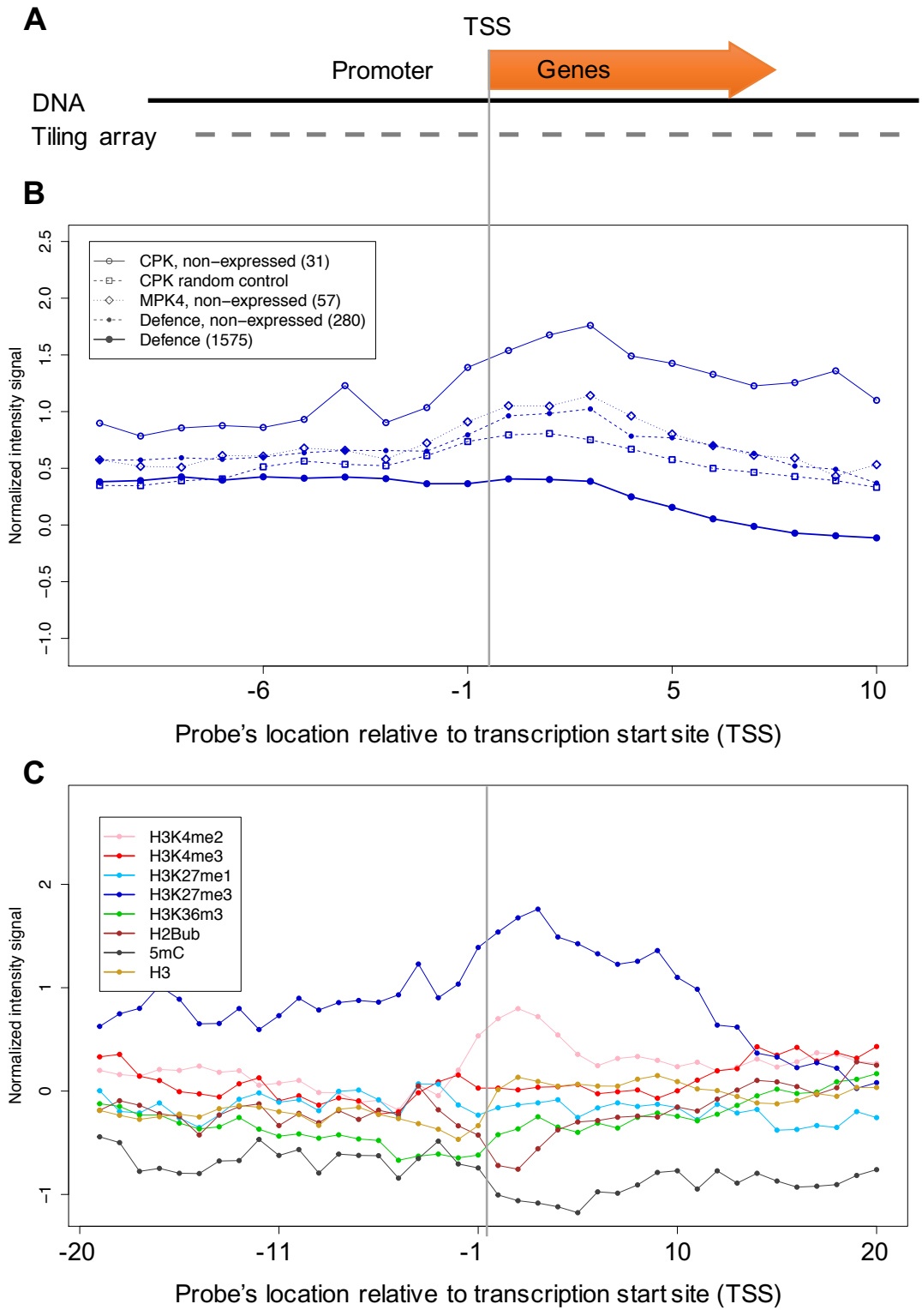

Figure 1.5. H3K27me3 histone mark is overrepresented in flg22-induced CDPK-responsive, non-expressed genes. (A) Representation of selected probes around the TSS. (B and C) Average of histone modificationa ChIP-chip signal (Roudier et al 2011) for chosen probes. (B) H3K27me3 enrichment for selected groups of genes responsive to flg22 but with non-detectable expression prior to elicitation (CPK non-expressed, MPK4 non-expressed and general non-expressed),

compared to respective controls (calculated to represent expected enrichment for the given gene expression. See Methods, 7.2 Methods in chapter 1), and (C) Average chromatin marks on the 31 CPK-responsive, non-expressed genes.

Overall, the results of this bioinformatic analysis highlights the correlation between low expressed genes and the histone mark H3K27me3. This mark was overrepresented in flg22-induced genes, suggesting a potential role in gene regulation (gene repression) perhaps similar to the one described in vernalisation and flowering (Lu et al., 2011; Noh et al., 2004). In particular, H3K27me3 was more prevalent in low expressed genes downstream the CDPK cascade. H3K27me3 has been previously linked to defence gene silencing and timed activation downstream of the JA signalling pathway in rice (Li et al., 2013), but its role in *Arabidopsis* immunity is less clear.

2 Implication of Histone H3, lysine 27 trimethylation in the transcriptional regulation of defence genes

2.1 Gene activation locally correlates with H3K27me3 removal during flg22-induced gene expression

In order to understand the dynamics of H3K27me3 during flg22-induced immune activation the levels of H3K27me3 were monitored by immunoblotting. *Arabidopsis* Col-0 seedlings were treated with 100 nM flg22 and samples were collected at 0, 7, 15, 30, 60 and 120 minutes after treatment. The time course indicated that global levels of H3K27me3 moderately increased following flg22 treatment (Figure **1.6**). This was an apparent contradiction with the fact that flg22 differentially expressed gene response is characterised by a greater up-regulation than down-regulation, specially shortly after flg22 exposure (Frei dit Frey et al., 2014; Zipfel et al., 2004). However,

this increase was seemingly temporary, and it is difficult to extrapolate from general levels of H3K27me3 to changes in gene expression. For this, other methods such as ChIP followed by qPCR analysis or sequencing are required.

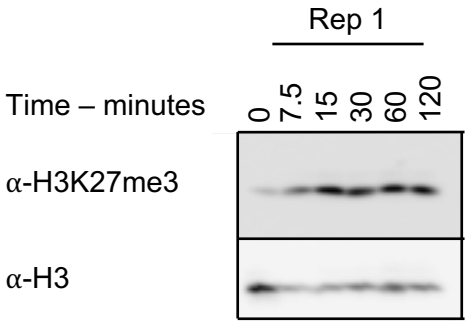

Figure 1.6. General levels of H3K27me3 following flg22 elicitation. Immunoblot of H3K27me3 and H3 levels in *Arabidopsis* seedlings treated with 100 nM flg22 over a time course. Samples were collected at 0, 7, 15, 30 60 and 120 minutes. Two more biological replicates were performed with similar results.

In order to monitor the correlation between flg22-induced gene expression and H3K27me3 of individual genes, ChIP in parallel with gene expression analyses were performed. 14 day-old *Arabidopsis* seedlings were treated with 100 nM flg22 and mock for 1 hour. Sample material was divided in two; for RNA extraction and for cross-linking treatment prior to ChIP. Two marker genes, *CYP82C2* and *WRKY75*, previously described as flg22-induced and identified as H3K27me3 enriched from the bioinformatic analysis were chosen (Supplementary table **S1.1**). The results elucidated a dynamic anti-correlation between gene expression and H3K27me3. The increase of gene expression of *CYP82C2* and *WRKY75* was mirrored with a decrease in H3K27me3 deposition (Figure **1.7**). These data strongly suggested that there is a close linkage between flg22-induced gene expression and the histone mark H3K27me3 at these loci.

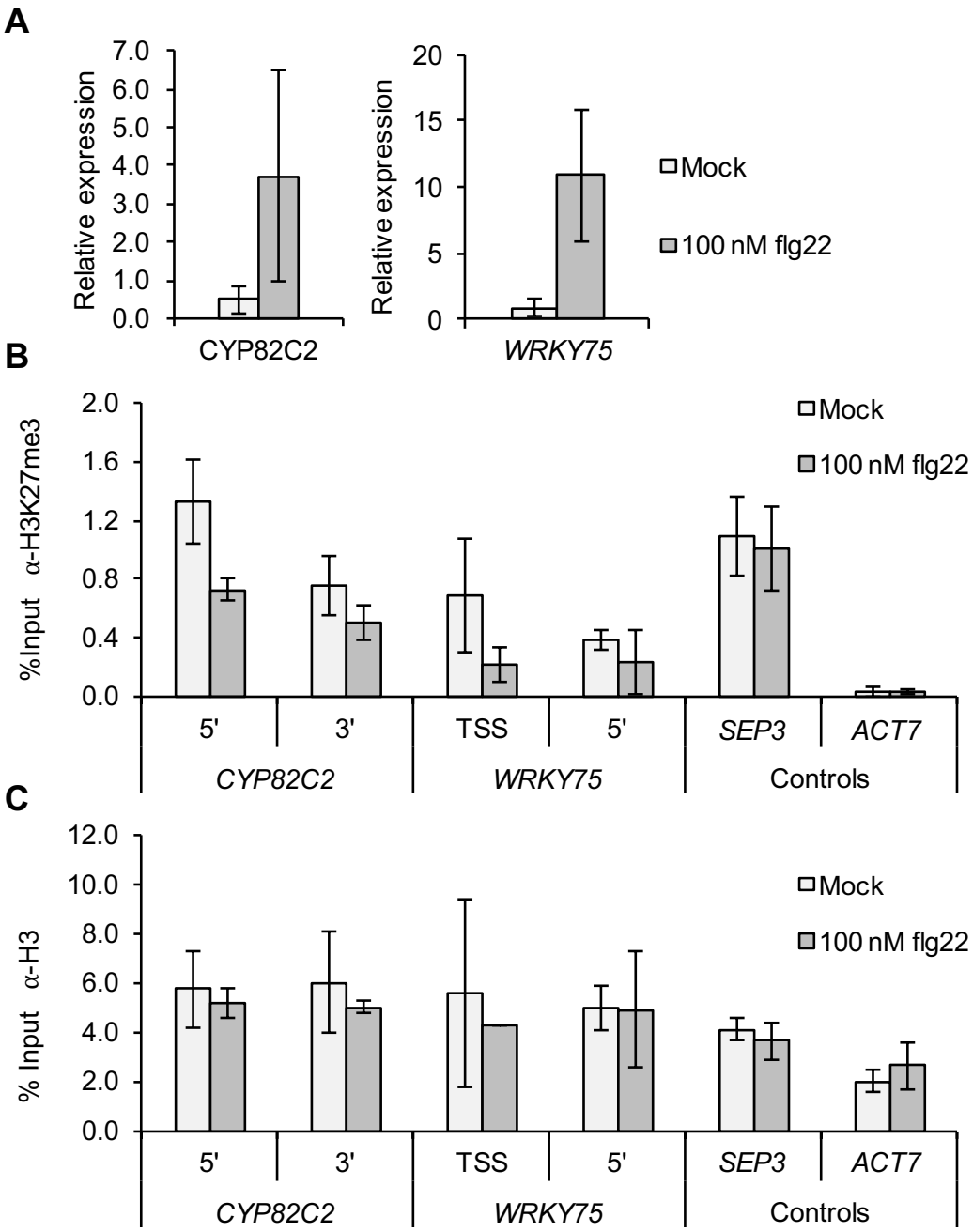

Figure 1.7. Dynamic anti-correlation between gene expression and H3K27me3 in response to flagellin. (A) qPCR analysis of *CYP82C2* and *WRKY75* gene expression on *Arabidopsis* Col-0 (wild-type) seedlings 1 hour after 100 nM flg22. (B and C) ChIP-qPCR analysis of *CYP82C2* and *WRKY75* loci 1 hour after 100 nM flg22. (B) ChIP anti-H3K27me3 and (C) control ChIP anti-H3. Data shown are means of three biological replicates. The differences were not statistically significant, two-sided T-test, p-value > 0.01. Error bars represent standard deviations. See Supplementary figure S1.3 for ChIP-qPCR primer localisation and corresponding levels of H3K27me3 as publicly described (epigara.biologie.ens.fr Roudier et al., 2011). *SEP3* and *ACT7* are positive (highly enriched in H3K27me3) and negative (depleted) control genes respectively.

2.2 Involvement of Calcium-dependent kinases in H3K27me3 de-repression

Flg22-induced, CDPK-dependent genes with low levels of expression showed the highest enrichment for H3K27me3 compare to MAPKs-dependent low-expressed genes (Figure **1.5**). Therefore, the next step was to test *in vivo* the correlation between flg22-induced gene expression and H3K27me3 deposition in Col-0 (wild type) and the triple CDPK (*CPK5*, *CPK6* and *CPK11*) knockout mutant *cpk5cpk6cpk11*.

Firstly, the *cpk5cpk6cpk11* triple mutant (Boudsocq et al., 2010), was genotyped and characterised by qPCR, proving to be homozygous for the T-DNA insertions and causing a reduction in transcript levels of ~1000-fold for *CPK5*, ~10-fold for *CPK6* and ~100-fold for CPK11 (Figure **1.8**, see T-DNA insertion genome position and amplification fragments in Supplementary figure S1.4, and Supplementary table S.2, for primer sequences).

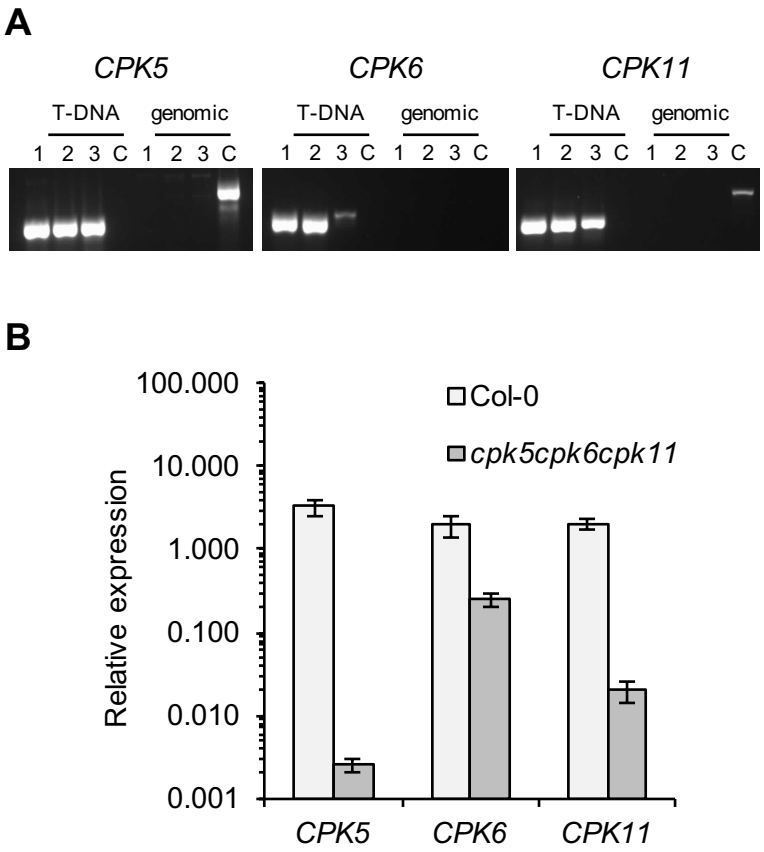

Figure 1.8. Calcium-dependent protein kinase (CDPK) triple mutant *cpk5cpk6cpk11* characterization. (A) Three independent lines (1, 2 and 3) were genotyped for each T-DNA insertion and absence of genomic fragment, compared with Col-0 (C). (B) qPCR analysis of *CPK5*, *CPK6* and *CPK11* transcript levels in the triple mutant *cpk5cpk6cpk11* compared to Col-0 (control), and referenced to the stably expressed genes *α-TUB* and *TIP41*. Data shown are means of three biological replicates. Error bars represent standard deviations.

Despite the triple mutant *cpk5cpk6cpk11* showing between a 1000- and 10-fold gene expression reduction for the *CPK5*, *CPK6* and *CPK11* (Figure **1.8 B**), *CYP82C2* and *WRKY75* gene expression was induced by flg22 in the triple mutant *cpk5cpk6cpk11*, and the levels of H3K27me3 varied accordingly (Figure **1.9**). *CYP82C2* flg22-induced gene expression was described as MAPK/CDPK synergistic, but *WRKY75* was described as *CDPK*-responsive (Boudsocq et al., 2010). However, *WRKY75* yielded a gene induction after flg22 treatment equivalent in the mutant and in the control (Figure **1.10**). This discrepancy can be partially explained since there are at least four CDPKs

involved in flg22 responses with additive effects (Boudsocq et al., 2010), but the quadruple mutant *cpk5cpk6cpk11* RNAi *cpk4* was not available for this work. Nevertheless, gene expression of another CDPK-responsive gene, *PHI-1* was impaired in the *cpk5cpk6cpk11* mutant. Following flg22 induction, *PHI-1* expression levels were significant reduced in the triple mutant in comparison to the control (Figure **1.10**). However, based on previously reported data (Roudier et al., 2011; Engelhorn et al., personal communication) H3K27m3 deposition in the promoter and the gene body of *PHI-1* is low, therefore it would be difficult to measure any change in H3K27m3 levels.

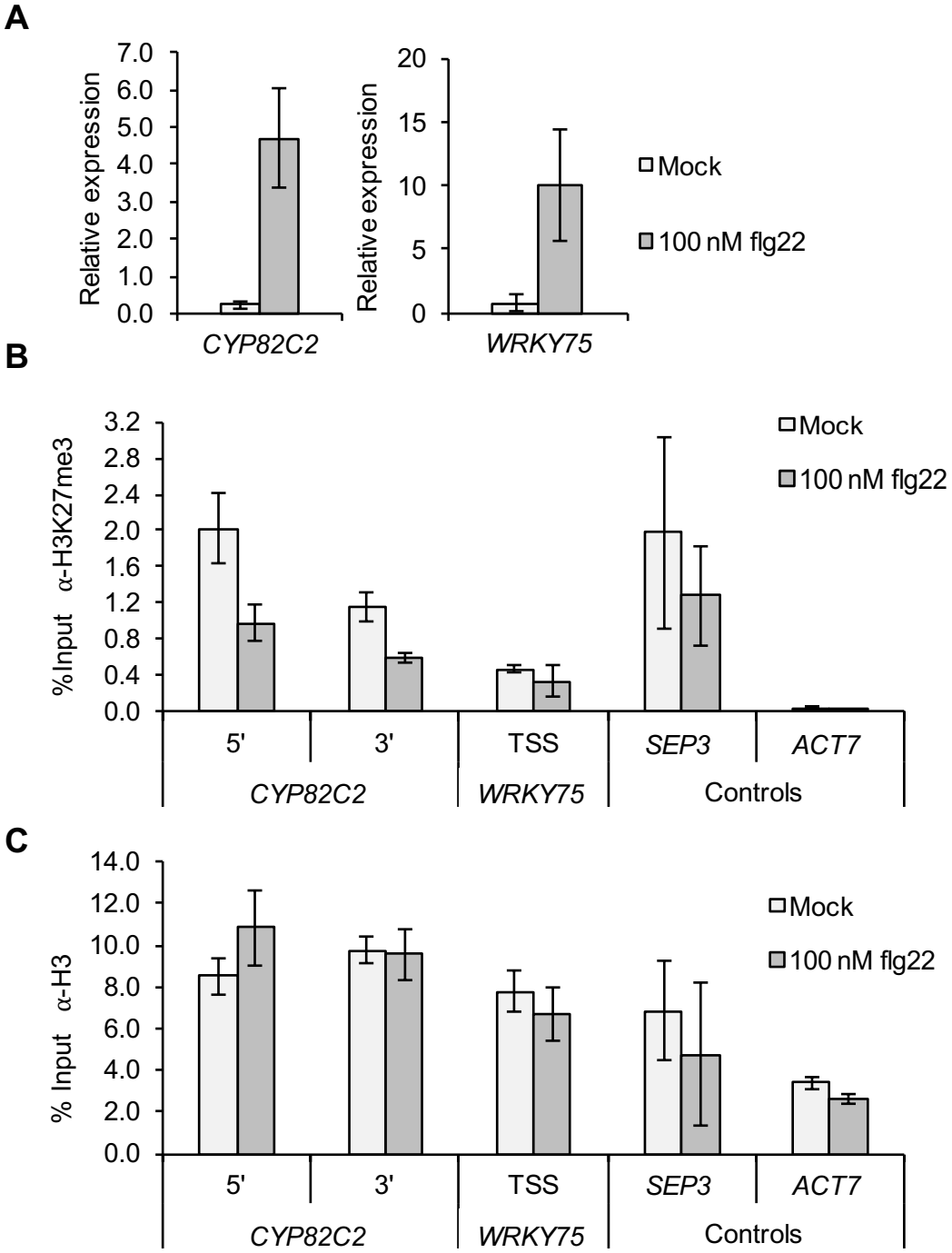

Figure 1.9. *CYP82C2* and *WRKY75* gene expression and H3K27me3 ChIP assay in triple mutant *cpk5cpk6cpk11*. (A) qPCR analysis of *CYP82C2* and *WRKY75* gene expression 1 hour after induction with 100 nM flg22. Gene expression was relative to reference genes □-*TUB* and *TIP41*. (B and C) ChIP-qPCR analysis of *CYP82C2* and *WRKY75* loci 1 hour after induction with 100 nM flg22. (B) ChIP anti-H3K27me3 and (C) control ChIP anti-H3. Data shown are means of technical replicates of a single experiment. Error bars represent technical replicates' standard deviations. *SEP3* and *ACT7* are positive (highly enriched in H3K27me3) and negative (depleted) control genes.

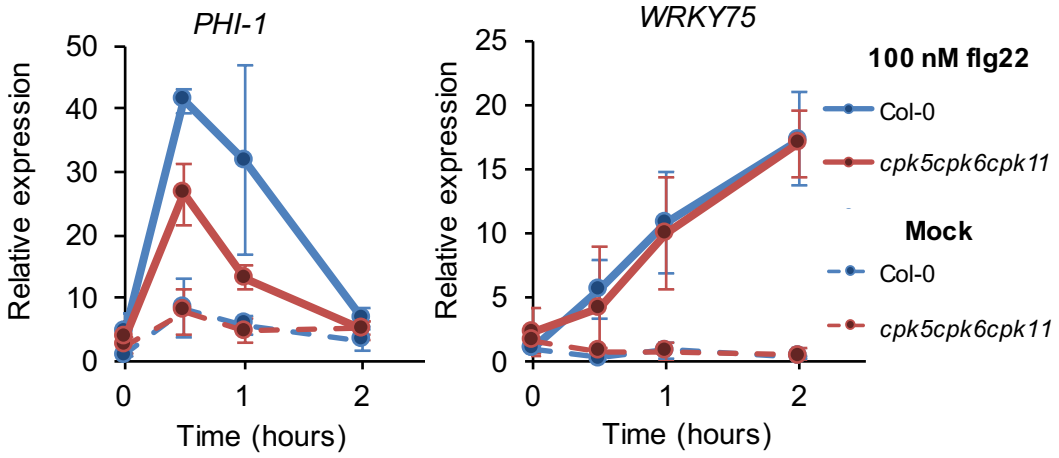

Figure 1.10. Only *PHI-1* expression is affected by the triple mutation in response to flagellin. Data shown are means of two biological replicates. Error bars represent standard deviations.

3 Histone-demethylases role in *Arabidopsis* defence against *P. syringae*

In rice upon pathogen perception, the histone demethylase Jumonji C protein JMJ705, a putative orthologue of *Arabidopsis* REF6, mediates gene activation through histone H3K27 demethylation (Li et al., 2013). In *Arabidopsis*, members of the Jumonji C family were shown to be upregulated following infection with the bacterial pathogen *P. syringae*. Specifically, *ELF6* and the gene AT1G62310 (also containing a jmjC domain) were significantly up-regulated when the infection was caused by the virulent strain *Pst* DC3000 compared to the failed infection caused by *hrpA* mutant, unable to deploy effector proteins (Lewis et al., 2015). The bioinformatics analysis also indicated that the expression of flg22-induced genes is repressed by H3K27me prior to elicitation. In order to directly investigate the role of histone demethylases in plant immunity we selected the *bona fide* H3K27 demethylases REF6 and ELF6 for further analysis. Previously published knockout mutants for *REF6* and *ELF6* genes, *ref6-1* and *elf6-3*, respectively (Crevillén et al., 2014; Lu et al., 2011), were acquired, propagated and genotyped for the selection of homozygous lines.

3.1 Demethylase susceptibility to bacterial infection

In order to further assess the role of H3K27me3 in plant defence, the immunity phenotypes of the two histone demethylase mutants *ref6-1* and *elf6-3* against the hemibiotroph bacteria *P. syringae* were evaluated. Both demethylase mutants were more susceptible than the control Col-0 plants to *Pst* DC3000 mutant Δ*AvrPto/AvrPtoB* (Figure **1.11**). The *Pst* DC3000 mutant Δ*AvrPto/AvrPtoB* lacking the mechanistically related effectors AvrPto and AvrPtoB was chosen due to its reduced virulence (Ntoukakis et al., 2009). Importantly, these experiments clearly demonstrated that histone demethylases positively regulate plant immunity.

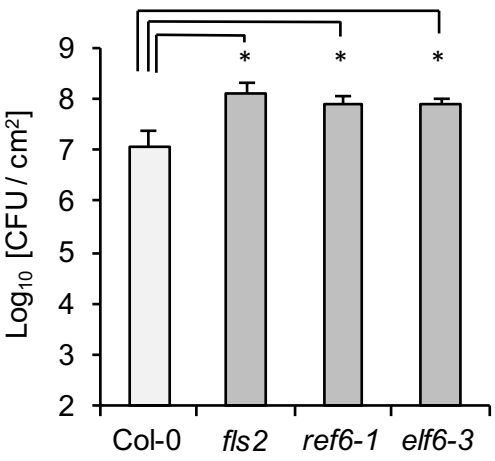

Figure 1.11. Histone demethylase mutants *ref6-1* and *elf6-3* are susceptible to the bacterial pathogen *Pst* DC3000 Δ*AvrPto/AvrPtoB*. 5 week-old plants were sprayed with OD_{600} 0.001 and samples were harvested 3 dpi for bacterial re-isolation. *fls2* is used as a susceptible control. One representative experiment out of two biological repeats is shown. Statistical significance determined by a two-sided T-test assuming equal variances, n = 6, "*" indicates p-value < 0.01.

3.2 Implications of ectopic *FRK1* histone methylation at the chromatin level

The bacterial growth curves highlighted the role of the histone demethylases in plant immunity. In order to understand the molecular mechanism underlying the enhanced susceptibility of the *ref6-1* mutant, the correlation between flg22-induced gene expression and H2K27me3 removal was evaluated in the mutant. For the analysis three genes were selected: *MYB122* as a H3K27me3 enriched gene, *PHI-1* as a CDPK-responsive and *FRK1* as MAPK-responsive gene.

In comparison to Col-0 seedlings, in the *ref6-1* mutant background *MYB122* showed a small reduction in flg22-induced gene up-regulation, but no difference was observed in the expression to flg22 were observed for *PHI-1* (Figure **1.12**). Surprisingly, *FRK1*, a gene utterly depleted of H3K27me3 marks along the gene body in the wild-type plants, Col-0 (Roudier et al., 2011), showed an impaired transcriptional response to flg22 (Figure **1.12**). However, a closer look into the *ref6-1* H3K27me3 deposition along the *FRK1* gene, revealed an unsuspected ectopic enrichment of the mark (Lu et al., 2011; Engelhorn et al., personal communication). The recent characterization of REF6 binding sites allowed the identification of two putative REF6 DNA binding sites near the promoter and 5 prime regions of *FRK1*, and the ChIP assay confirmed *FRK1* as a target of REF6 (Cui et al., 2016).

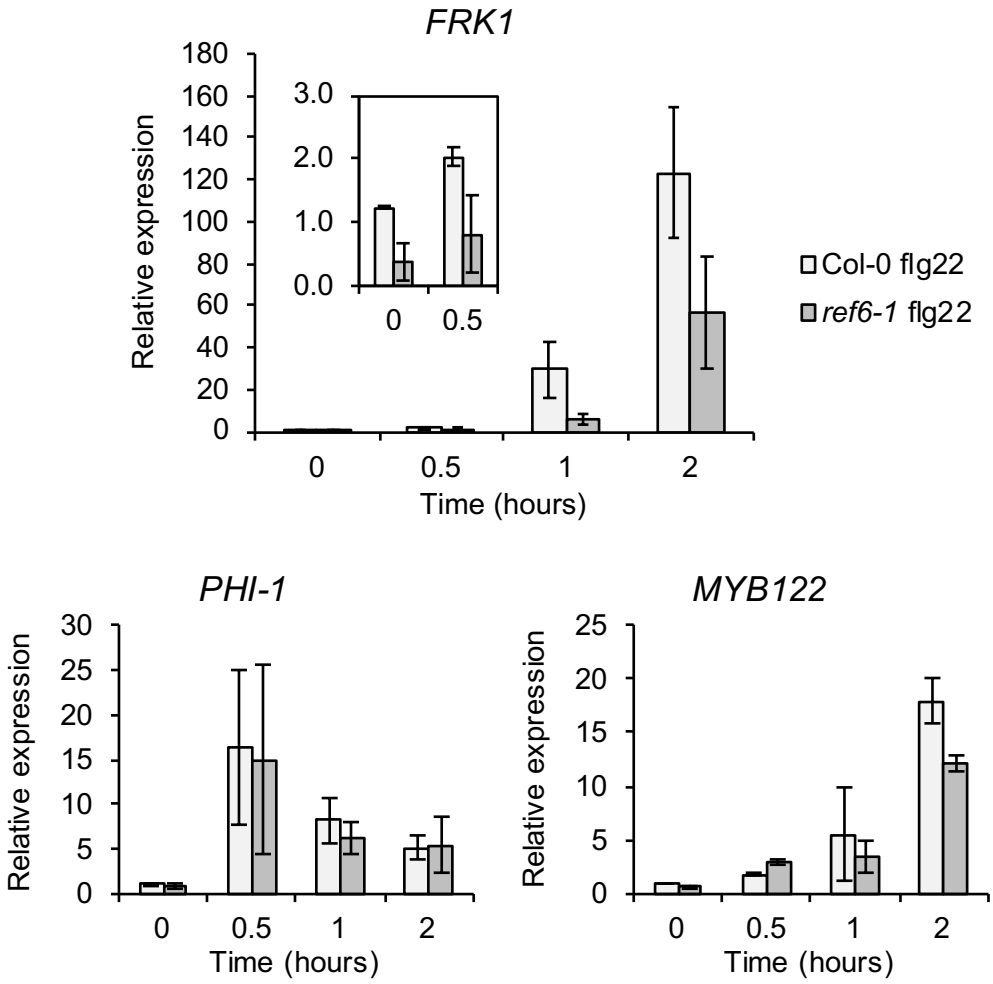

Figure 1.12. Expression profile of flg22-induced genes in the histone demethylase *ref6-1* mutant. flg22-induced gene up-regulation is impaired for certain defence-related genes for histone demethylase mutant *ref6-1* such as *FRK1* and *MYB122*. It can be observed (top figure, insert) that *FRK1* expression is diminished at the basal stage. *FRK1* transcript quantitation was assessed with two independent pairs of primers. Gene expression was quantified relative to reference genes *U-BOX*, *α-TUB* and *TIP41*. Data shown are means of two biological replicates. Error bars represent standard deviations.

In spite of *FRK1* impaired up-regulation in *ref6-1* compared to the wild-type (Figure **1.12**), in relative terms, *FRK1* showed an up-regulation upon flg22 treatment in the *ref6-1* mutant. To get a better insight into the mis-regulation of flg22-induced *FRK1* expression in the *ref6-1* mutant (lacking the H3K27me demethylase enzyme), a time course ChIP assay was performed. In parallel with the flg22-induced *FRK1* gene expression, a decrease in the H3K27me3 mark was observed (Figure **1.13**). These results suggest that REF6 maintains a hypo-methylated environment important for flg22-induced gene expression. However, REF6 is not strictly required for gene up-regulation, neither for H3K27me3 removal upon flg22 perception.

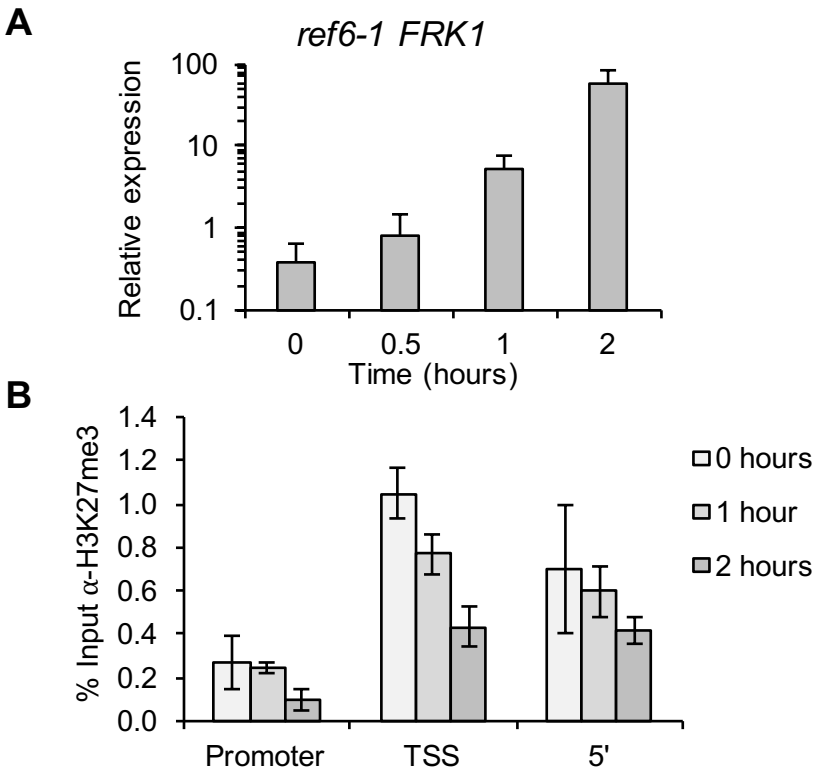

Figure 1.13. Correlation between histone mark H3K27me3 and gene expression at *FRK1* locus. (A) Relative expression of *FRK1* following flg22 induction (100 nM flg22) over a 2-hour time course. Experiments performed on 14 days old seedlings (same as in Figure **1.12** *FRK1*). (B) ChIP-qPCR analysis of ref6-1 FRK1 locus after 0 hours (control) 1 and 2 hours exposure to 100 nM flg22. Data shown are means of technical replicates of a single experiment. Error bars represent technical replicates' standard deviations.

3.3 Histone-demethylase *REF6* involvement in gene expression upon flg22 perception

To test whether this ectopic histone methylation deposition could extend to other defence-related genes than *FRK1*, the available REF6 ChIP data (Cui et al., 2016) were cross compared with the previously defined set of flg22-induced defence genes (Denoux et al., 2008). Out of 3091 REF6-DNA binding regions defined by ChIP-seq, corresponding to 2837 genes, 242 overlapped with flg22 induced genes. The overlap was significantly overrepresented with a p-value < 0.01 (using a hypergeometric probability test http://nemates.org/MA/progs/overlap_stats.html, out of the possible random sampling of two subsets of 2837 and 1611 genes with an overlap of 242 in a universe of 27655 genes annotated in the TAIR10 release 36). These 242 genes were in fact, highly recognised in orchestrating plant immunity. Genes as well characterised as *PHYTOALEXIN DEFICIENT 4* (*PAD4*), TFs *WRKY15*, *WRKY22*, *WRKY33* and *WRKY46*, *CYTOCHROME P450* (*CYP*) family *CYP81D8*, *CYP81F2*, receptor kinases *BAK1-ITERACTING RECEPTOR-LIKE KINASE 2* (*BIR2*), *CERK1*, *CYSTEINE-RICH RECEPTOR KINASE* (*CRK*) *CRK10*, *11*, *13*, *19* and *41*, *LECTIN RECEPTOR KINASE* (*LecRK*) *LecRK-IV.3*, *LecRK-V.5*, *LecRK-VI.3*, *LecRK-VII.2* and *LecRK-S.2*, *CALCIUM-DEPENDENT PROTEIN KINASE* (*CPK*) *CPK4*, or *MAP-kinase 5* (*MPK5*). A gene ontology analysis corroborated this idea, with especial emphasis on phosphorylation processes (Figure **1.14**, Table **1.2**).

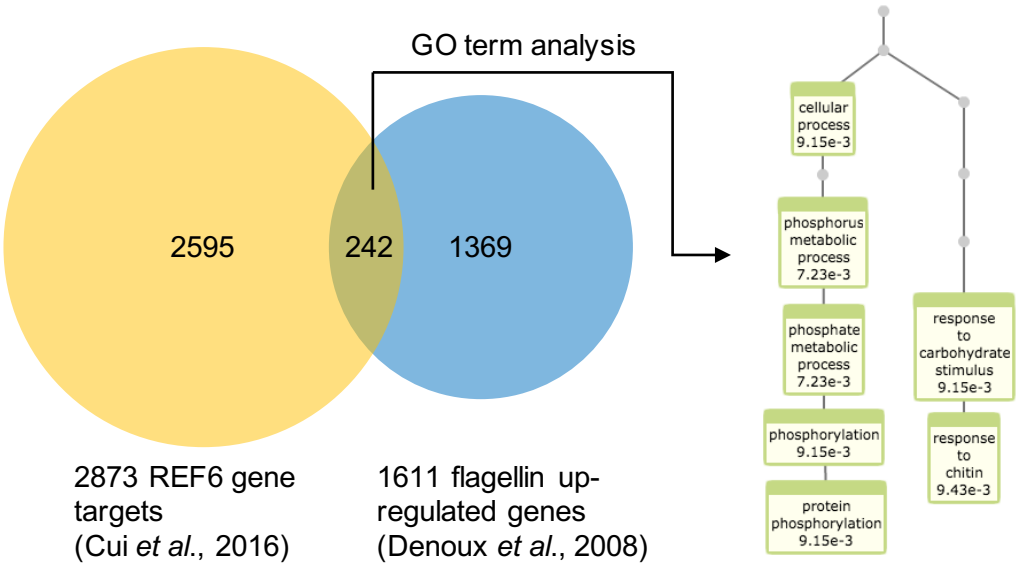

Figure 1.14. Defence genes are over-represented within the REF6 gene targets. (Left) Venn diagram illustrating the overlap between REF6 target genes and flagellin responsive genes and over-represented GO term analysis. (Right) GO terms of flagellin-induced (1611) and REF6-associated (2837) intersection (242), compared with *Arabidopsis* genome (http://virtualplant.bio.nyu.edu/cgi-bin/vpweb/). See also accompanying Table **1.2**).

Table 1.2. Table of selected GO terms of flagellin-induced (1611) and REF6-associated (2837) intersection (242), compared with the union set (only 3596 genes with at least one associated GO term). Protein phosphorylation is enriched for genes targeted by REF6 and activated by flg22.

Term	Observed Frequency	Expected Frequency	p-value
phosphorus metabolic process	42 genes out of 242, 17.4%	305 genes out of 3596, 8.5%	0.00543
phosphate metabolic process	42 genes out of 242, 17.4%	305 genes out of 3596, 8.5%	0.00543
protein phosphorylation	39 genes out of 242, 16.1%	282 genes out of 3596, 7.8%	0.00652
phosphorylation	39 genes out of 242, 16.1%	286 genes out of 3596, 8%	0.00652

Discussion

This chapter studies the correlation between histone mark H3K27me3 and gene expression during flagellin-induced gene expression. One of the most important limitations of the analysis is the combination of independently generated datasets. Two main precautions were taken against undesired sources of variance or data artefacts derived from this: the gene expression dataset chosen had been performed with similar experimental conditions (Table **1.1**; Denoux et al., 2008; Roudier et al., 2011). The comparability of the two datasets was further validated by the finding of strong correlations between histone marks and gene expression (Figure **1.1**).

The computational analysis demonstrated that histone marks can be interpreted as a proxy for gene expression levels with a remarkable degree of accuracy (Figure **1.1 C**). In addition, for stably expressed genes with very high and low levels of gene expression, chromatin marks associated with active transcription such as H3K4 di- and tri-methylation, as well as H2Bub and H3K36me3 strongly co-occurred. Repressive marks such as H3K27me1, DNA methylation and H3 enrichment (expected for more condensed chromatin) were highly correlated (Roudier et al., 2011; Sequeira-Mendes et al., 2014). Intriguingly, H3K27me3 did not strongly associate with either group, but remained poorly correlated except with its own environment, so that the appearance of H3K27me3 is not highly restricted to a few tens of base pairs (single nucleosome) but it rather spreads across several hundreds of base pairs (occurring at several adjacent nucleosomes).

Analysis of chromatin marks of flg22-induced genes showed that H3K27me3 accounted for an important contribution to the observed chromatin variance (Figure **1.2**), and was expected either on its own or in combination with other marks (Figure **1.3**). Interestingly, H3K27me3 is found in co-occurrence with histone marks related to gene activation, such as H3K4me, H3K36me, or H2Bub, as described in chromatin state 2 according to Sequeira-Mendes et al. (2014). A similar chromatin landscape has been described before for genes that, upon cellular program change (such as cell differentiation in animal cells) become active (Sachs et al., 2013). As in the case of cell differentiation-related genes in animals, flagellin-induced genes in plants may be

blocked by a repressor but ready to allow transcription by de-repression. Regulation by de-repression is a common mechanism observed in other contexts such as plant phytohormones signalling pathways (Robert-Seilaniantz et al., 2011).

The experiments presented in this chapter demonstrate the dynamic and intimately correlated nature of gene expression and the presence of H3K27me3 (Figures **1.7**, **1.9** and **1.13**). This local correlation was not mirrored at a global scale, where levels of H3K27me3 were at their highest a few minutes after flagellin induction and either decay or remain stable (Figure **1.6**). Increased levels of H3K27me3 have been previously reported for as long as up to a generation time. A jasmonic acid-responsive gene, *PLANT DEFENSIN 1.2* (*PDF1.2*) has been shown to have a transgenerational increase of H3K27me3 after successive rounds of infection with *Pst* DC3000 on the parental lines (Luna et al., 2012). In any case, to fully articulate the meaning of a change at a global scale, ChIP assay paired with genome-wide sequencing (ChIP-seq) is required. This would help to understand the apparent contradiction between the local and global observed responses.

When looking at different flagellin-induced signalling pathways, the bioinformatics analysis hinted that *CDPK* dependent genes with virtually no basal gene transcription are enriched in H3K27me3 (Figures **1.4** and **1.5**). However, in the *CDPK* triple mutant *cpk5cpk6cpk11* gene induction was correlated with histone H3K27me3 removal. On the basis of the *in vivo* experiments it is difficult to conclude positively on the involvement of CDPKs in the demethylation activation process (Figures **1.9** and **1.10**). Many reasons could account for these discrepancies. Beyond possible technical problems (though unlikely that two independent test should converge in false positive results, Figure **1.6**), it is worth discussing that the *CDPK* family contains 34 members (Cheng et al., 2002; Harper and Harmon, 2005). Out of these 34 proteins, the transient expression of a constitutively active form of almost each of the CDPKs induced the *NHL10* promoter-Luciferase reporter system. In particular, 6 of them (CPKac3, 4, 5, 6, 11 and 26) showed more than 5-fold induction (Boudsocq et al., 2010). In addition, most of the experiments describing CPK4, 5, 6 and 11 as the main drives of flagellin-induce gene expression within the CDPK family, were performed in protoplasts, whereas the experiments presented in this chapter were carried out on seedlings.

Recently, Latrasse et al. (2017) showed that histone deacetylase HD2B is a direct target of MPK3. Upon immune activation, MPK3 phosphorylates HD2B, mainly located in the nucleolus, translocating it to the nucleus, impacting on histone acetylation and ultimately on gene expression. On the opposite process, a histone acetyltransferase, HAC1, involves histone acetylation at defence-related loci *WRKY53*, *FRK1* or *NHL10* upon heat, cold and salt stresses (Singh et al., 2014). In the same line, loci *WRKY6*, *WRKY29* and *WRKY53*, showed an increased in H3K4me3 after a treatment with the SA synthetic analogue acibenzolar S-methyl (BTH) (Jaskiewicz et al., 2011). Unfortunately, at the time of writing, there was no genome-wide data for histone acetylation. In the present study acetylation data were not included, limiting the depth of the analysis. Genome-wide data were the key experiment providing detailed proof of the role of histone acetylation during flagellin perception. Hyper-acetylated genes were over-represented for defence response and phosphorylation GO terms (Latrasse et al., 2017). On the other hand, hypo-acetylated genes presented nitrogen metabolism and plastid organization terms, linking phosphorylation cascades through histone deacetylation with the current understanding of the chloroplast shutdown during early defence responses (de Torres Zabala et al., 2015).

Histone H3K27 demethylases *ref6-1* and *elf6-3* mutants showed increased susceptibility to the hemi-biotroph pathogen *Pst* DC3000 mutant Δ*AvrPto/AvrPtoB* (Figure **1.11**). In agreement, the rice *REF6* homologue *JMJ705* over-expressing mutants showed increased resistance to the bacterial pathogen *Xanthomonas oryzae*, and mutant lines resulted in more susceptible plants (Li et al., 2013). In addition, *JMJ705* positively contributed to the dynamic H3K27me3 removal from defence loci upon Me-JA induction (Li et al., 2013). Others had previously shown interactions between hormone pathway components and histone methylation (Berr et al., 2010; Luna et al., 2012). This is somewhat reminiscent of the case described here for the *FRK1* locus in *Arabidopsis* response to flagellin (Figures **1.12** and **1.13**). However, there are no data for ectopic hyper-methylation in a *JMJ705* mutant in rice.

In the *Arabidopsis ref6-1* mutant background, H3K27me3 hyper-methylated regions significantly over-lap with REF6 binding sites (Cui et al., 2016), suggesting the dynamic nature of the histone methylation/demethylation cycles. This may be a

mechanism of maintaining genes poised, though blocked, for a subsequent rapid gene expression, such as the case of *FRK1* and possibly *MYB122* (Figures **1.12** and **1.13**). The overlap between genes bound by REF6 and flagellin-induced genes revealed GO terms strongly involved in defence, related to phosphorylation processes, suggesting that the described kinase *FRK1* locus may not be an isolated case (Figure **1.14** and Table **1.2**). Among these kinases, there were five L-type lectin receptor kinases (LecRK), out of 20 of these genes in *Arabidopsis* recently involved in the evolutionary race for pathogen perception and defence specificity (Wang and Bouwmeester, 2017; Wang et al., 2015a).

Since brassinosteroids are phytohormones involved at the crosstalk between development and immunity (Lozano-Durán and Zipfel, 2015), another interesting aspect of histone demethylases involvement in plant defences that could further help to understand the described susceptible phenotypes of the *ref6-1* and *elf6-3* mutants (Figure **1.11**), is the mis-regulation of several brassinosteroid-inducible genes in the *ref6-1* and *elf6-3* mutants (Yu et al., 2008). ELF6 and REF6 were described interactors of the TFs BRI1-EMS-SUPPRESSOR 1 (BES1) and BRASSINAZOLE RESISTANT 1 (BZR1) through their C-terminal zing finger domain (Yu et al., 2008), the same domain described to be essential for its DNA binding activity (Cui et al., 2016).

From the literature and results presented in this chapter, arise several fundamental questions. Is H3K27me3 dictating the fate of transcription of flagellin-inducible genes? Does H3K27me3 have to be removed before the polymerase can read through? If so, there must be another enzyme, besides REF6 capable of doing so in the short term (Figure **1.13**), maybe ELF6. The alternative hypothesis would be to regard H3K27me3 as a helper, or a "cookie", on the onset of gene expression, whose enzymatic removal is non-sufficient and non-necessary for transcription assembly, and that transcription could excise the mark on its own. And finally, in the cell-to-cell immunity model, what is the interpretation of partially enriched chromatin marks, being bimodal indexes at a singular locus, in terms of different chromatin states between different cells remains an open question.

Chapter 2. Screening disease susceptibility of Chromatin remodelling ATPases

Introduction

Through evolution plants have developed sophisticated mechanism to sense and respond accordingly to biotic threats. One such stress are pathogen infections. Pathogen perception leads to rapid and strong changes in gene expression (Kong et al., 2015; Lewis et al., 2015; Tao et al., 2003; Windram et al., 2012). Complex as they are, gene expression mechanisms remain largely elusive. However, it is well-known that some phytohormones play a role in plant immunity by de-repressing gene transcription. Historically, two major phytohormones pathways have been implicated in plant defence responses; the salicylic acid (SA) pathway and the ethylene/jasmonic acid (ET and JA) pathway (Robert-Seilaniantz et al., 2011). The SA pathway is related to defence against biotrophic pathogens. In addition, it is responsible for the establishment of primed states distal to the focus of infection termed systemic acquired resistance (SAR). In the presence of SA, the transcriptional coactivator NPR1 becomes nuclear-localised and promotes the transcription of the pathogen responsive genes, *PR* genes, such as *PR1* (Spoel et al., 2003, 2009). The SA receptor remains unclear, but the regulation of *PR1* is also affected by proteins involved in DNA repair mechanisms (Fu and Dong, 2013; Song et al., 2011).

In response to wounding by insects and infections by necrotrophic pathogens plants induce JA biosynthesis from its precursor, the linolenic acid (Gfeller et al., 2010; Glauser et al., 2008). JA metabolites promote degradation of the JAZ family of transcriptional repressors. JA metabolites act as a molecular glue between the JAZ proteins and the co-receptor COI1 E3 ligase adaptor protein (Chini et al., 2007; Thines et al., 2007; Yan et al., 2007). JAZ proteins exert gene repression by means of linking transcription factors, such as MYC2, to the general transcription repressor TPL (Pauwels and Goossens, 2011). JAZ proteins have been shown to require HDA6, a

histone deacetylase, for the repression of ethylene (ET)-dependent genes *EIN3/EIL1* (Zhu et al., 2011). In fact, HDA6 and the closely related HDA19, had been previously associated with the regulation of JA/ET pathway-dependent genes such as *ERF1* or *VSP2*, a gene in the JA signalling pathway that requires MYC2 for transcription, (Wu et al., 2008; Zhou et al., 2005). SYD, one of the canonical SWI/SNF chromatin remodelling ATPases is recruited to the *MYC2* and *VSP2* promoters upon wounding, and it is involved in JA-mediated pathways since *syd* null mutants show enhanced susceptibility to the necrotrophic fungus *Botrytis cinerea* but not to the bacterium *Pseudomonas syringae* (Walley et al., 2008).

Chromatin Remodelling ATPases (CRAs) share a mechanism of binding to the DNA-nucleosome complex, but their different involvement in DNA-dependent processes (i.e. replication, transcription, DNA repair) is mediated by their side domains, away from the conserved catalytic domains (Flaus et al., 2006; Knizewski et al., 2008; Liu et al., 2017). So far, the canonical CRAs *SYD*, *PIE1* and *BRM* have been shown to have an important role in the regulation of *Arabidopsis* immunity (Johnson et al., 2015; March-Díaz et al., 2008; Walley et al., 2008). Similarly, in rice, Ris1-related protein BRHIS1 interacts with histone variants and suppresses activation of immunity. *BRHIS* undergoes downregulation and decreases its presence at immunity-related loci upon pathogen challenge in a SA-independent manner (Li et al., 2015b). The two closest homologues of the BRHIS1 in Arabidopsis, FRG1 and FRG2, are associated with the RNA directed DNA methylation machinery (RdDM), (Groth et al., 2014), which in turn has been linked with biotic stress responses (Dowen et al., 2012). However, the CRAs are a large family in eukaryotes with 4 distinctive subfamilies (Clapier and Cairns, 2009) and it is far from being fully explored.

Plant immunity relies on the cellular perception and proportionate response to pathogenic microorganisms. Exacerbated defence responses lead to auto-immunity, with developmental costs and reduced seed yield (Bowling et al., 1997; Brown, 2002; Tian et al., 2003). Nucleosome re-organization of SA pathway-related promoter regions has been associated with spurious gene expression and auto-immune phenotypes (Mozgová et al., 2015). Therefore, it was expected that enhancements (artificial or natural) towards improving certain plant defences would come with developmental fitness costs or imbalances towards other defence mechanisms, such as

favouring either biotrophic *versus* necrotrophic or favouring different feeding insect strategies (Gurr and Rushton, 2005; Karasov et al., 2017; Li et al., 2015a). However, recent paradigm-shifting research is showing that this is not necessarily the case, especially if there is a way to by-pass hormone networks crosstalk (Campos et al., 2016; Xu et al., 2017). Interestingly, chromatin remodelling plays a role in the cross-talk between hormone pathways. BRM represses ABA regulated genes in the absence of ABA signalling, preventing precocious activation of stress responses during germination (Han et al., 2012).Upon ABA stimulation, BRM is phosphorylated restoring ABA responsiveness (Peirats-Llobet et al., 2016). Thus, master regulator proteins, such as chromatin remodelling proteins that could interact with several thousands of loci at a time (controlling nucleosome repositioning and spacing) have the potential to alter the whole plant homeostasis during plant immunity activation.

In this chapter a screen testing twenty-five CRAs for disease susceptibility to *P. syringae*, identified six very promising CRAs, some acting like positive regulators of immunity and some acting like negative regulators. Although some CRAs are transcriptionally responsive to the hormone, no evident link with JA responses could be found. CRAs are involved in defence processes and they may be involved in regulating the complex balance between growth and defence. Here it is presented an example of a conserved genetic mutation that increases performance at both developmental and defence level.

Results

1 Novel chromatin remodelling ATPases associated to plant immunity

1.1 CRAs mutant collection

41 CRA genes were identified in *Arabidopsis* (Flaus et al., 2006; Knizewski et al., 2008). A reverse genetics approach was used to identify CRAs involved in plant defence. For this, the T-DNA insertion available collections (SALK, SAIL and Gene Trap lines, http://signal.salk.edu/cgi-bin/tdnaexpress, Alonso et al., 2003) were used. Two independent lines were chosen for each gene when possible, in order to ensure that the targeted gene affected by the insertion was responsible for the phenotype observed. The T-DNA insertions chosen were within the promoter or the 5' region of the gene body in order to obtain knockout mutants. Out of the 41 CRA genes, 80 mutants were obtained from NASC. Two mutants were identified for 39 CRA genes, only one mutant was available for the genes AT3G54280 and AT5G43530.

To obtain homozygous lines the mutants were propagated and genotyped, yielding 61 T-DNA homozygous mutants. For 22 genes, both mutants were isolated as homozygous, 14 genes had only one homozygous mutant line and for 4 genes (*INO80*, *PKR1*, AT3G54280 and AT5G43530) no homozygous plant for the T-DNA insertion were found (Supplementary table **S2.1**).

1.2 CRAs bacterial *Pst* DC3000 susceptibility screening

Twenty-five CRA genes were selected for bacterial pathogen screening. They were selected based on expression profile after flagellin and/or *Pst* DC3000 perception, availability of homozygous lines and selecting at least one gene of each subfamily within the CRA family (Table **2.1** and Supplementary table **S2.1**). Selected lines were infected by spray inoculation with a mutant of the bacterial pathogen *P. syringae* pathovar *tomato* (*Pst*) DC3000 and DC3000 Δ*avrPto*Δ*avrPtoB*. Δ*avrPto*Δ*avrPtoB* was used to ensure milder infections in order to differentiate subtle phenotypes (Xin

and He, 2013). To exclude the possibility of AvrPto or AvrPtoB targeting the CRA activity, those mutants that resulted in a phenotype of interest, were also tested with the wildtype strain *P. syringae* DC3000 (*Pst*).

Mutants from six different CRAs showed increased susceptibility or increased resistance to *Pst* DC3000 Δ*avrPto*Δ*avrPtoB* infection compared with the control *Arabidopsis thaliana* Col-0; *FRG2*, *EDA16*, *ETL1*, *RAD54*, *PKR2* and *CHR17* (Table **2.1**). Similarly to previous reports using wildtype *Pst* DC3000 (Walley et al., 2008), *SYD* mutants did not show differential susceptibility to *Pst* DC3000 Δ*avrPto*Δ*avrPtoB*. *PIE1* mutant *pie1-5* was described as more resistant to *Pst* DC3000 infection (March-Díaz et al., 2008). However, this mutant was not isolated as homozygous plant in the present work. The *PIE1* mutant tested within the CRAs collection, SALK_116597 with the insertion on the promoter region, did not show a phenotype. Neither a developmental phenotype was observed, in contrast to the previously published phenotype for *pie1-5* (March-Díaz et al., 2008).

The *RAD54* mutant with the insertion on the promoter was more susceptible to *Pst* DC3000 Δ*avrPto*Δ*avrPtoB*. It was previously shown, that RAD51D interacts with RAD51 (Tambini et al., 2010) which in turn works closely with RAD54 (Alexeev et al., 2003; Alexiadis and Kadonaga, 2002). Interestingly, similar susceptible phenotypes were previously observed for the triple mutant of RAD51D physical interactors, SA-related proteins SNI1, SSN2 and NPR1, *sni1npr1ssn2* (Song et al., 2011).

Resistant phenotypes were observed for the mutants of two genes within the yeast homolog Ris1 subfamily, *EDA16*, and *FRG2* (*CHR28*). *ETL1* mutants also showed a resistant phenotype. Interestingly, ETL1 has been mechanistically related to FRG2 and FRG1 (Han et al., 2014). For *FRG2*, two independent mutants, *frg2-1* and *frg2-2*, showed increased resistance, although *frg2-2* to a lesser extent than *frg2-1*. Consistent with the results here presented, the RNAi lines for the rice homolog of *FRG2*, *BHRIS1*, showed a similar resistant phenotype in the pathosystem rice-*Magnaporthe oryzae* (Li et al., 2015).

Table 2.1. Chromatin remodelling ATPases sorted by phylogeny (http://www.phylogeny.fr). Includes known gene expression from public databases, developmental (either observed or previously described) and immune phenotype (Green background for resistant, orange for susceptible phenotypes and grey for previously described).

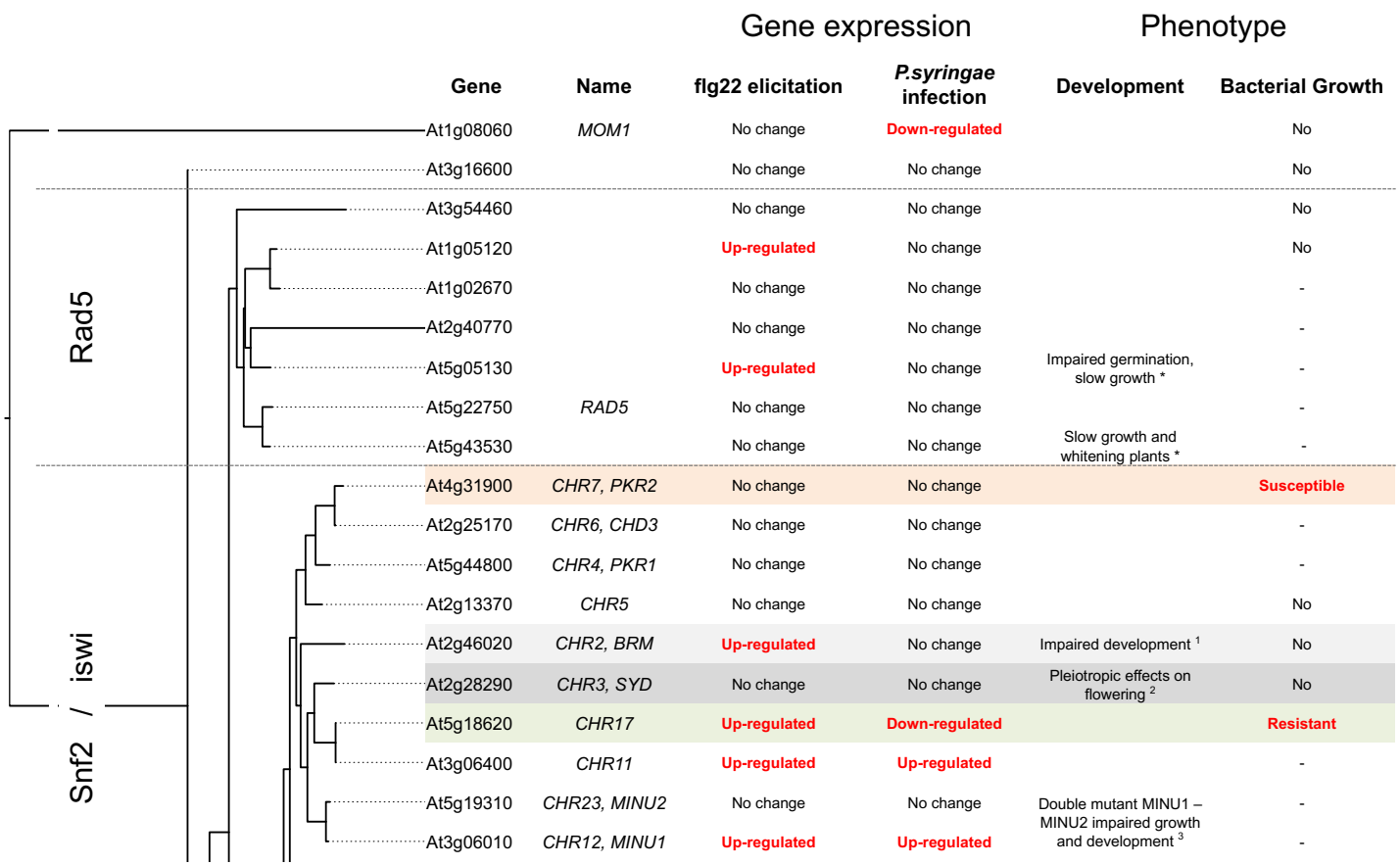

		Gene expression		Phenotype	
Gene	Name	flg22 elicitation	*P.syringae* infection	Development	Bacterial Growth
At1g08060	*MOM1*	No change	Down-regulated		No
At3g16600		No change	No change		No
At3g54460		No change	No change		No
At1g05120		Up-regulated	No change		No
At1g02670		No change	No change		-
At2g40770		No change	No change		-
At5g05130		Up-regulated	No change	Impaired germination, slow growth *	-
At5g22750	*RAD5*	No change	No change		-
At5g43530		No change	No change	Slow growth and whitening plants *	-
At4g31900	*CHR7, PKR2*	No change	No change		Susceptible
At2g25170	*CHR6, CHD3*	No change	No change		-
At5g44800	*CHR4, PKR1*	No change	No change		-
At2g13370	*CHR5*	No change	No change		No
At2g46020	*CHR2, BRM*	Up-regulated	No change	Impaired development [1]	No
At2g28290	*CHR3, SYD*	No change	No change	Pleiotropic effects on flowering [2]	No
At5g18620	*CHR17*	Up-regulated	Down-regulated		Resistant
At3g06400	*CHR11*	Up-regulated	Up-regulated		-
At5g19310	*CHR23, MINU2*	No change	No change	Double mutant MINU1 – MINU2 impaired growth and development [3]	-
At3g06010	*CHR12, MINU1*	Up-regulated	Up-regulated		-

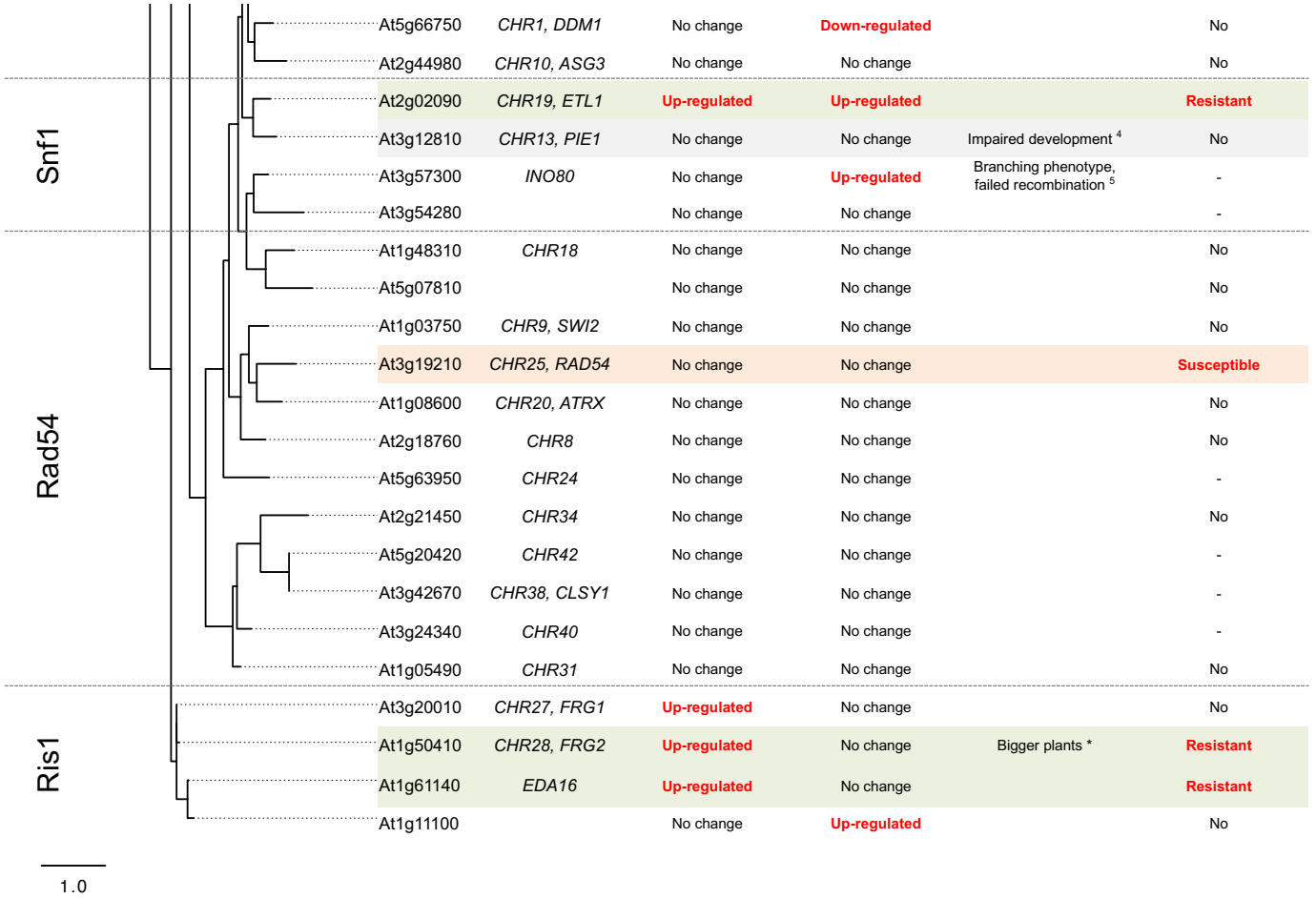

At5g66750	*CHR1, DDM1*	No change	**Down-regulated**		No
At2g44980	*CHR10, ASG3*	No change	No change		No
At2g02090	*CHR19, ETL1*	**Up-regulated**	**Up-regulated**		**Resistant**
At3g12810	*CHR13, PIE1*	No change	No change	Impaired development [4]	No
At3g57300	*INO80*	No change	**Up-regulated**	Branching phenotype, failed recombination [5]	-
At3g54280		No change	No change		-
At1g48310	*CHR18*	No change	No change		No
At5g07810		No change	No change		No
At1g03750	*CHR9, SWI2*	No change	No change		No
At3g19210	*CHR25, RAD54*	No change	No change		**Susceptible**
At1g08600	*CHR20, ATRX*	No change	No change		No
At2g18760	*CHR8*	No change	No change		No
At5g63950	*CHR24*	No change	No change		-
At2g21450	*CHR34*	No change	No change		No
At5g20420	*CHR42*	No change	No change		-
At3g42670	*CHR38, CLSY1*	No change	No change		-
At3g24340	*CHR40*	No change	No change		-
At1g05490	*CHR31*	No change	No change		No
At3g20010	*CHR27, FRG1*	**Up-regulated**	No change		No
At1g50410	*CHR28, FRG2*	**Up-regulated**	No change	Bigger plants *	**Resistant**
At1g61140	*EDA16*	**Up-regulated**	No change		**Resistant**
At1g11100		No change	**Up-regulated**		No

1: Bezhani et al., 2007. 2: Wagner and Meyerowitz, 2002 3: Sang et al., 2012. 4: March-Díaz et al., 2008. 5: Fritsch et al., 2004 * Observed in this work.

1.3 CRAs Jasmonic acid screening

Different phytohormones regulate specific defensive pathways and the balance between immune responses and growth. Pathogens therefore target several hormonal signalling pathways at various levels as part of their efforts to dampen and control the plant immune response. For example, *Pst* DC3000 strain produces a mimic of JA, known as coronatine with roles in pathogenesis such as overcoming stomatal defences, mediating disease symptoms or inducing susceptibility in systemic tissues (Bender et al., 1999; Xin and He, 2013). In fact, *COI1*, the JA co-receptor was originally isolated as the first mutation yielding plants insensitive to coronatine, to methyl JA and more resistant to bacterial infection (Feys et al., 1994; Xie et al., 1998). Thus, given the importance of JA in plant defence and JAZ/MYC2 mechanism of action linked with histone modification and chromatin remodelling the role of CRAs as JA-pathway components was investigated.

JA gene regulation

Public datasets (http://bar.toronto.ca, Toufighi et al., 2005) were used to select from 41 CRAs a list of 9 genes responsive to phytohormones (Figure **2.1**). For example, AT1G02670 and AT5G43530 showed, respectively, a moderate and an intense up-regulation under different phytohormones treatment. For these 9 genes, transcript levels were quantified by quantitative real-time PCR (qPCR) in two weeks old seedlings, treated with 50 µM JA and alternatively treated with the bacterial analogue coronatine (1 µM) for 30 minutes, one hour and three hours (Figure **2.1 A**, **2.1 B** and **2.1 C**).

Consistent with the public database, The gene AT1G02670 was up-regulated by JA and coronatine. However, in the case of AT5G43530, the reported regulation could only be reproduced in the coronatine-treated samples. Since coronatine is more stable than JA metabolites, it was expected to find that coronatine-treated samples tended to

show more obvious changes for most genes tested. In general, in accordance with the public database, none of these genes showed massive expression changes, but rather confined to the 2 to 4-fold range.

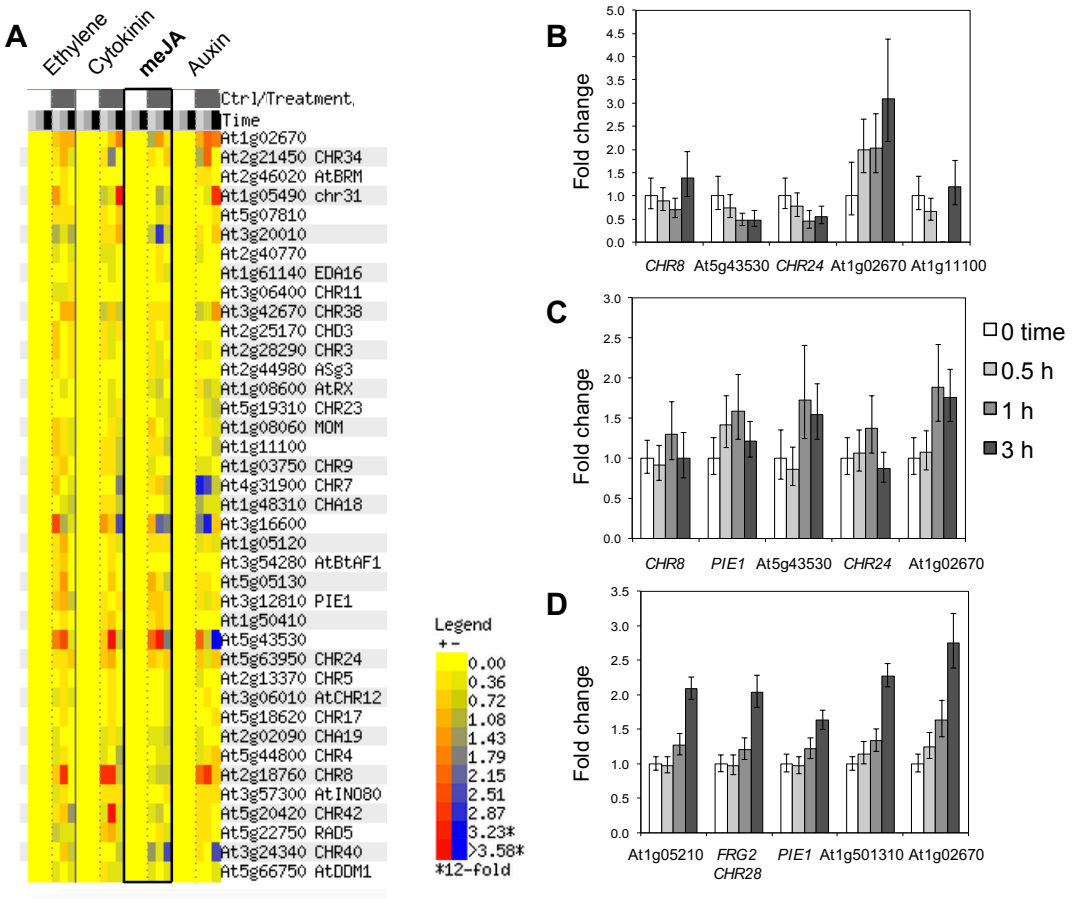

Figure 2.1. Comparative gene expression of CRAs upon phytohormones treatment. (A) Publicly available gene expression data (Toufighi et al., 2005) collected and analysed for 41 putative CRAs *Arabidopsis* genes http://bar.utoronto.ca/affydb/cgi-bin/affy_db_exprss_browser_in.cgi?pub=&dataset=atgenexp_pathogen. (B), (C) and (D): Relative gene expression time course of selected ATP-CR in two weeks old wild-type (Col-0) seedlings treated with (B) 50 µM JA, (C) and (D) 1 µM coronatine. The reference gene was ACTIN8 and the basal condition was 0 time. Values represent technical replicates mean ± standard deviation.

MeJA root growth inhibition

The CRA collection was tested for JA-mediated responses using seedlings assays. JA treatment of *Arabidopsis* seedlings causes growth arrest and accumulation of secondary metabolites such as anthocyanins. To test the ability to respond to the JA pathway, *Arabidopis* seedlings were exposed to MeJA and the effects on root length and anthocyanin accumulation were reported. As a control, the mutant of the JA receptor, *coi1-3* was included.

Root length analysis of seedlings germinated and grown for 8 days in plates containing 50 μM meJA showed that the variation between lines and controls was moderate. In some cases, like both lines for gene *CHR5*, they were greener and bigger than controls (Figure **2.2 B**). The two independent mutant lines for *CHR17* showed some degree of JA tolerance (lines 49 and 50 in picture S10). The only homozygous line available for *CHR24* showed what looked like an exacerbated response, with smaller and especially purple plants (line 54 in picture S11). None of the mutants showed an unresponsive phenotype, such as the JA co-receptor *coi1-3* mutant.

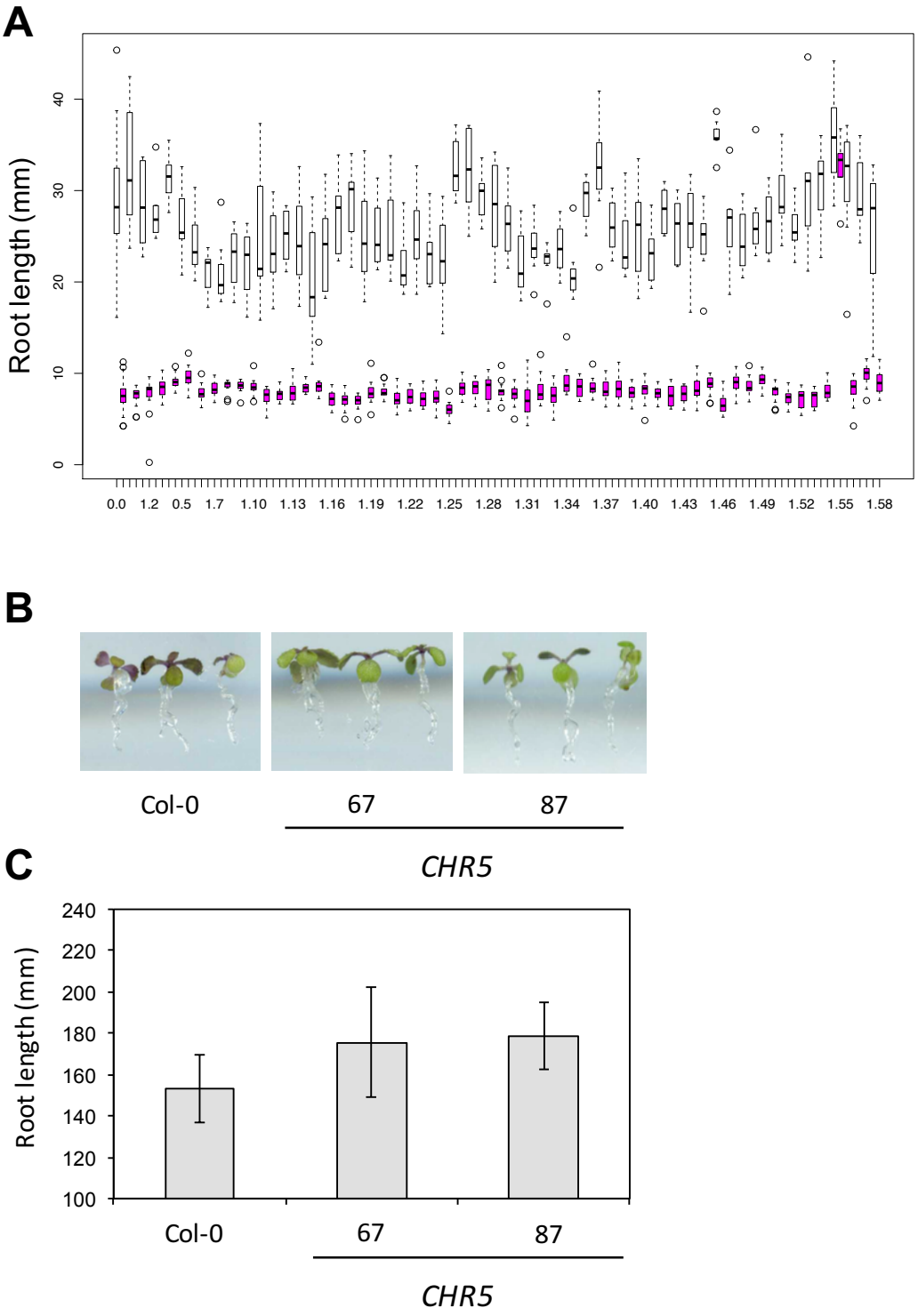

Figure 2.2. JA mediated growth repression. (A) 14 days old seedlings grown in JP + 50 µM meJA root size (violet) and controls, grown in JP medium (white). (B) Picture of three 14 days old seedlings grown in JP + 50 µM meJA in the same plate for Col-0 (control) 76 and 87 *chr5* mutants. T-DNA insertion mutants appear greener and slightly bigger. (C) Root length measured in cm (measured with ImageJ software) for 15 to 20 seedlings grown in JP + 50 µM meJA. Values represent mean ± standard deviation.

MeJA anthocyanin production

Anthocyanins production was only measured for those lines that visually showed a prominent phenotype (purple-violet tones) in comparison with control plants (Col-0 growing in the same plate). Only the homozygous line L49 (SALK_139387C), T-DNA insertion for AT5G18620, *CHR17* (Figure **2.3**) showed a clear reduction in anthocyanin accumulation compared to control plants.

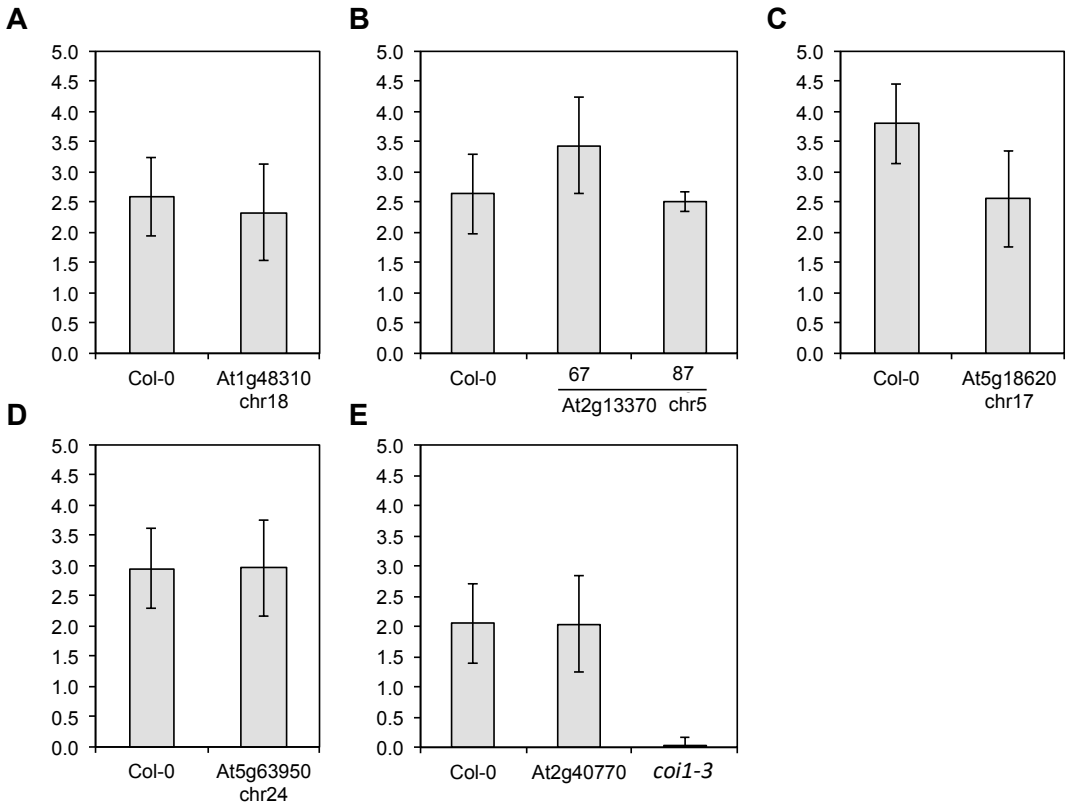

Figure 2.3. Anthocyanin content in CRAs mutants. Anthocyanin content was measured for plants displaying a visual phenotype; plants apparently greener (potentially having less anthocyanins, such as lines 67 and 87 (At213370, Chr5) or hypersensitive, like At5g63950 (see line 54 in supplementary picture 11). However, the visual observations did not correspond very accurately with the anthocyanin concentrations measured. The *coi1-3* null mutant was included as a control unaffected by JA (E).

2 Growth/immunity chromatin interplay: FRG2/ETL1 case study

2.1 *frg2-1* & *etl1-1* developmental phenotypes

Most CRAs T-DNA insertion mutants, as noted in Table **2.1**, did not show any apparent developmental phenotype. However, two mutants did show consistent differences with the control Col-0 plants. The *etl1-1* mutant presented the rosette leaves folded in a "u-shape" that could be affecting the bacterial surface distribution and infection, and hence the observed resistant phenotype (Figure **2.4**). However, in comparison with wild type plants, the second T-DNA insertion mutant *etl1-2*, was more resistant to *Pst* DC3000 and had no obvious developmental phenotype (Supplementary figure **S2.1**). In addition, the *frg2-1* mutant, showed increased resistance to *Pst* DC3000 and had a larger leaf surface area than control plants (Figure **2.5**). Taken together, these results suggest that the processes related to the mechanistically-associated proteins FRG/ETL1 could be involved in immunity and development. It is worth remarking that with *FRG2* as well as with *ETL1*, only one of the T-DNA lines showed the described phenotype clearly. It is therefore necessary to approach these results and the conclusions that may be taken from them with the due caution.

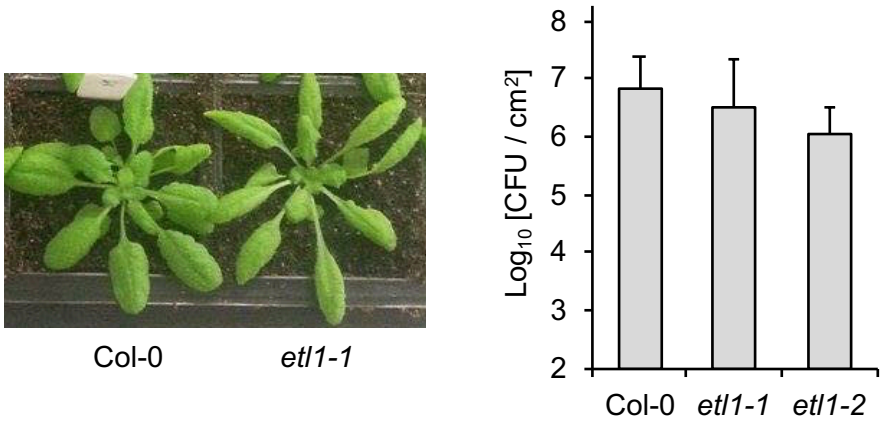

Figure 2.4. *etl1-1* plants show a leaf phenotype, as well as being more resistant to bacterial infection. The rosette leaves of *etl1-1* mutant folded into a "u-shape" and was more resistant to *Pst* DC3000 Δ*avrPto*Δ*avrPtoB* compared with Col-0 (control).

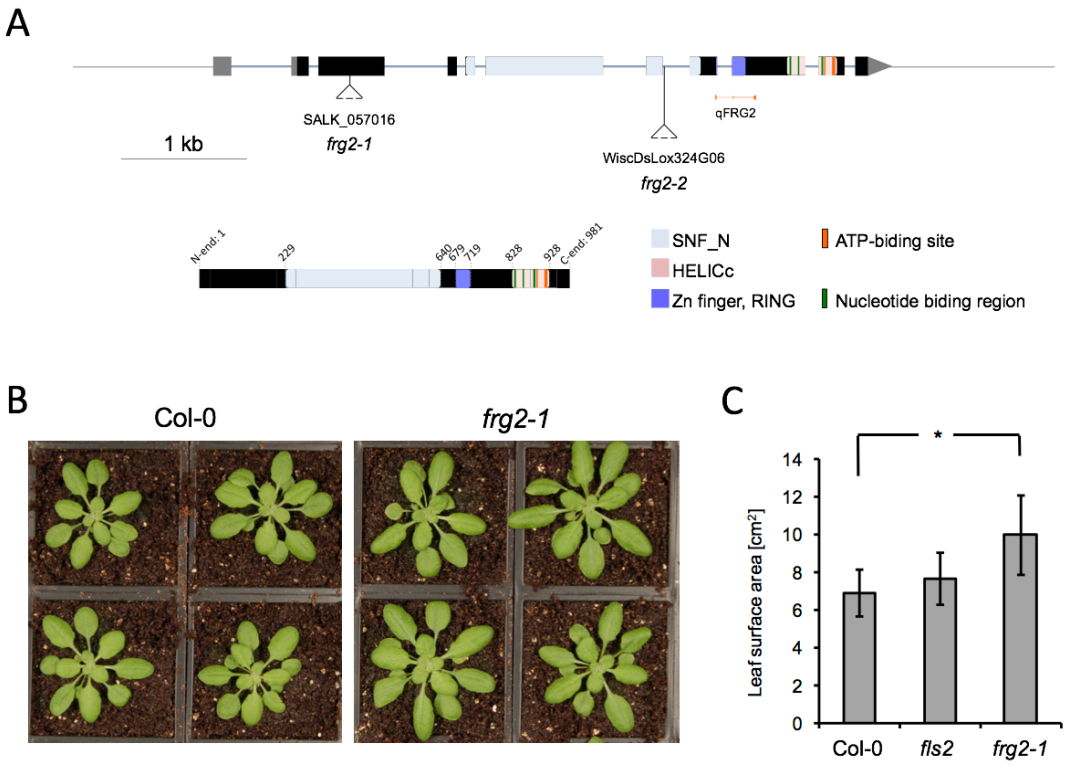

Figure 2.5. *fgr2-1* mutants have greater leaf surface than wild type control (Col-0) under normal growth conditions. (A) T-DNA insertion position along the *FRG2* gene. (B) Observed growth phenotype of *frg2-1* lines in normal growth conditions (no stressed applied). (C) Measured leaf surface area and statistically significant difference between Col-0 and *frg2-1* (two-sided T-test, n = 24, "*" p-value < 0.01).

2.2 *frg2-1* growth phenotype is retained across abiotic and biotic stresses

frg2-1 mutants remained larger than wild type throughout the biotic and abiotic stresses tested. As expected, NaCl and flagellin caused a growth reduction. Interestingly, the *frg2-1* mutant plants retained their growth advantage over control plants under the stresses (Figure **2.5**), suggesting that *frg2-1* growth phenotype may not be directly linked with defence signalling pathways.

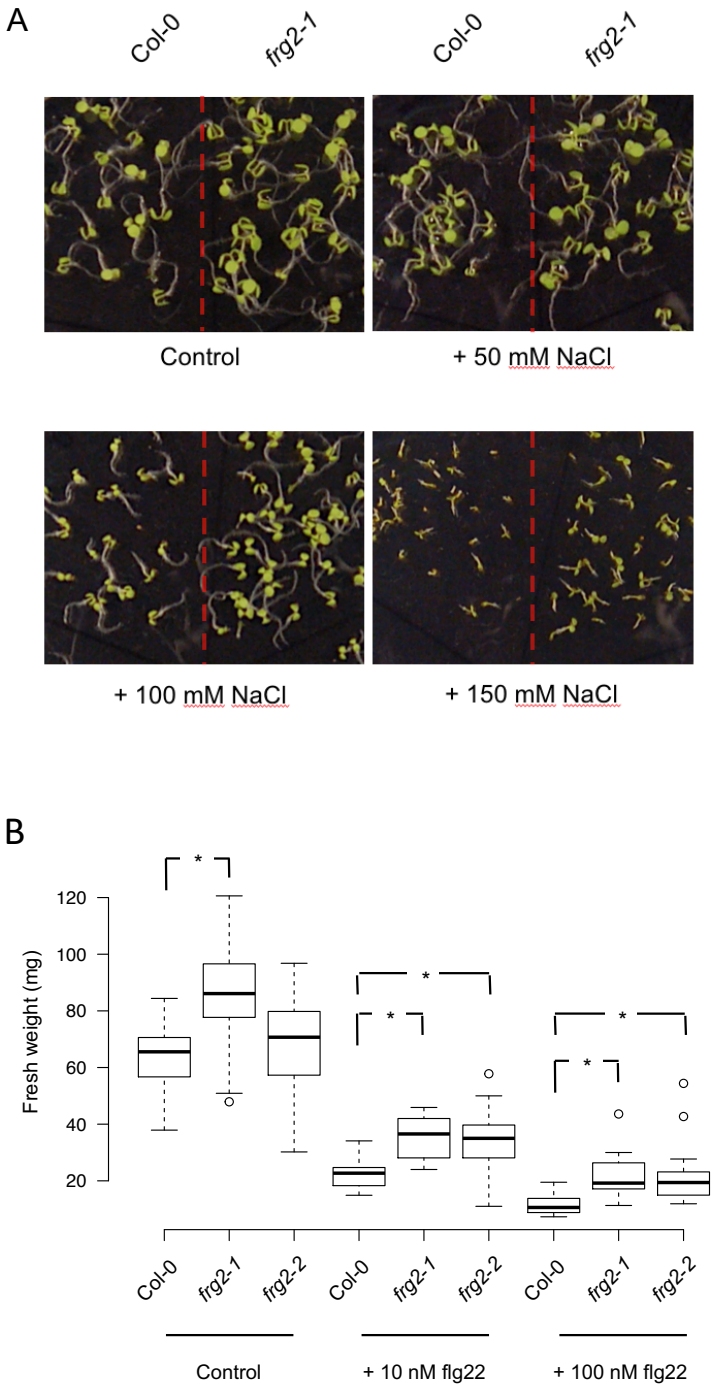

Figure 2.6. *frg2-1* is bigger than wild type and this difference is kept across abiotic and biotic stresses. (A) Seedlings germinated in ½ MS medium containing different concentrations of NaCl 0 (control), 50, 100 and 150 mM NaCl. (B) Seedling growth inhibition assay. Seedlings transferred to ½ MS liquid medium containing concentrations of flg22 (0–control, 10 and 100 nM). Statistically significant differences between Col-0 and *frg2-1*, and between Col-0 and *frg2-2* (two-sided T-test, n = 30, "*" p-value < 0.01).

2.3 *FRG2* negatively affects general immunity

In addition to the observed developmental phenotype for *frg2-1*, both mutants *frg2-1* and *frg2-2* showed an increased resistance against the pathogenic bacteria *Pst* DC3000 Δ*avrPto*Δ*avrPtoB* (Table **2.1** and Figure **2.6**). Plant significantly different in their defence against hemibiotroph pathogen such as *Pseudomonas* and necrotroph pathogens such as *B. cinerea*. In order to test the involvement of *FRG2* in general defence mechanisms or those particular to the biotrophic/necrotrophic responses, *frg2-1* plants were subjected to a detached leaves *Botrytis* infection assay. This resulted in mild enhanced resistance in the mutant lines compared with the control, suggesting that *FRG2* role in plant defence may be independent of the pathogen's lifestyle.

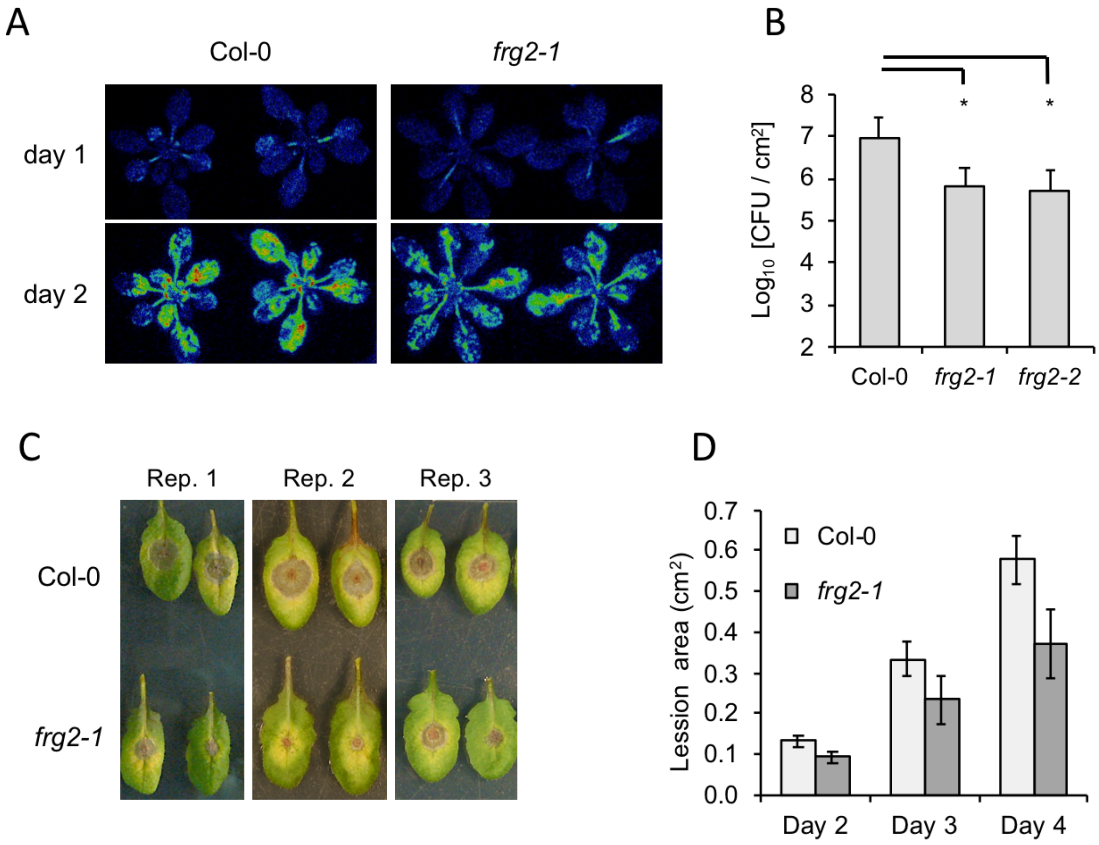

Figure 2.7. *frg2-1* is more resistant to the biothrophic bacteria *P. syringae* without compromising defences against the necrotrophic fungus *B. cinerea*. (A) Col-0 and *frg2-1* adult plants (5 weeks old) spray-infected with *Pst* DC3000 LUX. Photek images taken after 1 and 2 days after infection. (B) *Pst* DC3000 Δ*avrPto*Δ*avrPtoB* bacterial growth 3 days after spray infection of Col-0 *frg2-1* and *frg2-2* plants. Statistical significance determined by a two-sided T-test (on Log_{10}[colony forming units / cm^2]) assuming equal variances, n = 6, "*" indicates p-value < 0.01. Error bars represent standard deviation. (C and D) Detached leaf assay symptoms 3 days after inoculation (C) and measurements of affected area by *B. cinerea* var *Pepper*, third repeat representative of the other two experiments (D). Error bars represent the standard error of the mean, and the differences observed were not significant on a two-sided T-test (n = 20, p value > 0.01).

Discussion

Based on the two main premises that (1) chromatin remodelling is an important component in transcription (Clapier and Cairns, 2009) and (2) the necessity of gene reprograming in coordinating the plant defence mechanisms (Jenner and Young, 2005), a reverse-genetic screening was conducted on CRAs T-DNA mutant collection by infecting with *P. syringae Pst* DC3000. The screening showed, as hypothesised, that some CRAs may play a specific role in plant immune responses.

In agreement with previously published data, the *syd* mutant tested did not show a difference with the bacterium *P. syringae* (Walley et al., 2008). In contrast, no significant differences in bacterial proliferation were observed with the tested mutant of *PIE1*, SALK_116597C, where an increased resistance was described for the mutant *pie1-5* (March-Diaz et al., 2008). A genetic screening using the T-DNA insertion lines presents several limitations that can account for either false negatives, as well as false positives. False positives can be due to multiple T-DNA insertion and untargeted gene knockouts. Approximately, 50% of the SALK T-DNA lines contain more than one insertion (Alonso et al., 2003). This problem is minimised by genotyping after propagating, and if needed, by back-crossing the line with the wild type parent (although, in the interest of time, this last measure was not taken before performing the screening). The risk of false negatives (as the tested *PIE1* line might be) can be due to active forms of the protein still being assembled, despite the genomic DNA insertion. This could happen if the catalytic centre of the enzyme is unaffected by the insertion (for instance being in the 5' upstream region from the insertion) or due to the maturation of the transcript that removes the T-DNA re-connecting viable exons. Furthermore, the *Arabidopsis* genome possesses sufficient gene redundancy and compensatory mechanisms to render it capable of absorbing some potential deleterious mutations without an observable phenotype (Bolle et al., 2011; Bouché and Bouchez, 2001; Briggs et al., 2006).

Gene duplication is indeed a common phenomenon in the *Arabidposis* genome and in general in angiosperms (Blanc et al., 2003; Bowers et al., 2003; Langham et al., 2004), and can be also observed in the CRA family. On the closely related pair

CHR12/*CHR23* (also known as *MINU1*/*MINU2*), while single mutants did not display any distinguishable phenotype, the double mutation displayed aberrant meristematic cell division and embryonic lethality (Sang et al., 2012). Similarly, in the ISWI sub-family composed of *CHR11* and *CHR17*, only the double mutants displayed strong developmental phenotypes (Li et al., 2012). More than 3000 genes showed altered expression in the double mutant, and these had a disrupted nucleosome distribution pattern over the gene body. The first nucleosome after the transcription start site was not affected; only following nucleosomes within the gene body lacked the characteristic regularity of actively transcribed genes (Dong et al., 2013; Li et al., 2012, 2014). These results indicate that nucleosome positioning is initiated by some chromatin remodelling components other than CHR11/CRH17 (ISWI) complexes, and that these complexes have an effect on gene expression by helping in nucleosome spacing.

Previous results produced in the laboratory had shown by protein IP followed by mass spec histone acetyltransferase HAG1 (also known as GENERAL CONTROL NONDEREPRESSIBLE 5, or GCN5) interaction with chromatin remodelling ATPases CHR11/CHR17 (ISWI), *Arabidopsis* Chd1 homolog CHR5, and PKL (Mastorakis et al., in preparation). All of these CRAs are closely related, and possess a HAND-SANT-SLIDE C-terminal domain (Knizewski et al., 2008). This interaction makes sense, since the SANT domain has been associated *in vitro* to histone acetyl-transferase activity (Boyer et al., 2002). The group and others (Kong et al., 2017; Piquerez et al., in preparation) have demonstrated that histone acetyltransferase HAG1 is involved in plant defence. In line with these results, ISWI *CHR17* mutant SALK_080144C showed a resistant phenotype. *PKR2* (closely related to *PKL*, which was not tested) line SALK_115303C showed a susceptible phenotype.

Both mutant lines of *RAD54* appeared more susceptible than the control. *RAD54* has been extensively characterised as a DNA repair component through the homologous recombination pathway (Hirakawa et al., 2017; Osakabe et al., 2006; Shaked et al., 2006). Even though there is ample evidence of oxidative stress events and DNA damage both during abiotic and biotic stresses (Baxter et al., 2014; Mittler et al., 2011), there is little knowledge on *RAD54* during biotic stress. Only two conflicting reports associate its function with geminiviral replication, where it may play a role but

it is not essential (Kaliappan et al., 2012; Richter et al., 2015). However, closely related proteins working within the homologous recombination pathway, or even directly interacting with RAD54, have been linked with defence responses through SA-dependent gene de-repression. SNI1 acts as a negative regulator of NPR1 (Li et al., 1999; Pape et al., 2010) possibly through the interaction with an unknown DNA-binding protein (Song et al. 2011). Upon defence activation, SSN2 (a protein containing a SWIM, SWI2/SNF2 and MuDR, domain) together with RAD51D are recruited to the *PR1* promoter, possibly mediating SNI1 removal (Durrant et al., 2007; Song et al., 2011). RAD54 direct interactor RAD51 (Klutstein et al., 2008) is also recruited to the *PR1* promoter (Wang et al., 2010).

It therefore remains to be determined whether RAD54 exercises an active role in plant defences, perhaps taking a place within the RAD51 complex, to regulate gene expression during SA elicitation (Song et al., 2011). If this was the case, it would be interesting to see if it responds directly to SA, or to elevated levels of oxidative potential. However, it could be that the *rad54* mutants simply do not cope well with the oxidative stresses generated during plant immune activation that eventually render them less fit and less likely to survive. To test this, infections with different *Pseudomonas* strains (with different levels of response) followed by DNA damage assays (such as comet assays) could be used.

FRG2 mutants displayed a resistant phenotype, bigger leaf surface area, as well as an increased tolerance to biotic and abiotic stress. In agreement with that, RNAi lines for the rice homolog of *FRG2*, *BHRIS1*, showed a similar resistant phenotype in the pathosystem rice-*Magnaporthe oryzae* (Li et al., 2015). *FRG2* and *FRG1*, co-express with the de novo DNA methylation pathway RdDM (Groth et al., 2014). They are involved in gene silencing through the RdDM pathway, but also independently (Han et al., 2014). Mutations in the DNA methylation pathway display increased resistance to *P. syringae* (Dowen et al., 2012). By contrast, some other CRAs are associated to DNA methylation patterns and development. For example, PKL has a role in stabilizing nucleosomes for Pol V stabilisation and subsequent DNA methylation in a CHH context (Yang et al., 2017), and it is directly involved in promoting development and growth closely related to the phytohormone gibberellic acid (GA) (Park et al., 2017; Yang et al., 2017). Questions that remain are what is then the link between

FRG2 and development? Do FRGs and PKL work at opposite ends of similar processes? Is FRG2 related to the SA pathways?

Chapter 3. EDA16 plays a role in moderating plant defences

Introduction

The plant innate immune system is greatly tuneable and capable of precisely assessing and responding to the various threats encountered in nature. Because any action, growth or defence has its intrinsic costs, whatever the ecological strategy of a plant may be, the responses to the environment need to be tightly controlled. Therefore, after pathogen recognition the plant must mount an adequate response. Since different microbes present different lifestyles, plants deflect them with specific mechanisms. Depending on the virulence of the infection, some defensive strategies will be more cost-effective than others.

Plant immunity is commonly divided into two layers for simplicity (Jones and Dangl, 2006). The first layer corresponds to surface detection of a potential danger. Conserved pathogen-associated molecular patterns (PAMPs) are recognised by transmembrane receptors leading to the activation of a PAMP-triggered immunity (PTI). PTI is characterised by a quick burst of reactive oxygen species (ROS), stomatal closure and gene expression changes leading to the production of secondary metabolites and cell wall thickening (Macho and Zipfel, 2014). One of the best studied PAMPs is the 22 amino acid conserve peptide from the flagellin protein (flg22) of the bacterial pathogen *P. syringae* flagellum (Chinchilla et al., 2006; Gómez-Gómez and Boller, 2000). Flg22 perception triggers significant gene expression changes with more than 1500 genes differentially expressed within an hour following elicitation (Denoux et al., 2008; Zipfel et al., 2004). These responses are often enough to ward off opportunistic or unspecialised pathogens. However, successful pathogens have evolved to avoid PTI by delivering inside the plant cell sets of effector proteins and small molecules that interfere with PTI signalling and responses (Dodds and Rathjen, 2010).

In turn, plants have adapted to detect effectors with cytosolic receptors that either interact directly with the effectors or indirectly by guarding the targets (or even sometimes decoy targets) of the effectors (van der Hoorn and Kamoun, 2008; Jones and Dangl, 2006). This effector-triggered immunity (ETI) leads to a somewhat similar gene reprograming to PTI, but with a stronger response (Tsuda et al., 2009). Indeed, PTI induced by flg22 and ETI induced by the *P. syringae* effector AvrRpt2 extensively share mechanisms for the transduction of the signal (Qi et al., 2011). ETI leads to an intense oxidative burst followed by localised cell death at the infection site known as the hyper-sensitive response (HR; Coll et al., 2011; Mur et al., 2008). HR is commonly followed by a systemic acquired resistance mediated by salicylic acid (SA) and other small molecules moving across tissues (Fu and Dong, 2013; Shirasu et al., 1997).

However, defences against pathogens that feed on dead tissue, such as necrotrophic fungi, are primarily coordinated by the jasmonic acid family of hormones (JA). JA and SA responses are complex and partially antagonistic, but other hormones also play a major role in plant immunity (Robert-Seilaniantz et al., 2011). For example the plant hormone abscisic acid (ABA) moderates and dampens PTI defence responses (Mbengue et al., 2016; Stec et al., 2016). Therefore, the extreme effects of ETI and other defensive responses are tightly regulated to prevent inappropriate outcomes or autoimmunity (Rodriguez et al., 2016).

Negative regulators of immunity moderate the development and escalation of defence responses. Some act as passive repressing mechanisms at the transcriptional level. For example, JAZ proteins, co-receptors of JA (Chini et al., 2007; Thines et al., 2007; Yan et al., 2007), block the activation of transcription factors (TFs) at their genomic loci by recruiting histone deacetylase (Devoto et al., 2002; Zhou et al., 2005). Upon JA signalling, JAZ proteins are degraded and gene expression is de-repressed (Pauwels and Goossens, 2011). Other negative regulators of defences act during immunity. For example at the cell surface, after flg22-mediated activation, the flagellin receptor FLS2 is ubiquitinated and subsequently degraded as a mechanism of attenuating the signal (Lu et al., 2011). At the transcriptional level, transcription factors (TFs) WRKY18 and WRKY40 act redundantly as negative modulators of defences in response to flg22 (Birkenbihl et al., 2017). Other than TFs, chromatin remodelling factors also affect plant defence gene expression (Ma et al., 2011). For example,

chromatin remodelling ATPase SYD may be a negative regulator of the SA pathway (Bezhani et al., 2007) and also regulates a subset of genes within the JA hormone responses (Walley et al., 2008). Other chromatin remodelling ATPases, such as PIE1 (March-Díaz et al., 2008), and DDM1 (Li et al., 2010) are also associated with gene silencing and negative regulation of plant defences.

The screening presented in Chapter 2 resulted in the discovery of chromatin remodelling ATPase *Arabidopsis* mutants with altered susceptibility to the bacterial pathogen *P. syringae*. From the Ris-1 subfamily, *FRG2* was identified as a defence-related gene. Consistent with the notion that the role of chromatin remodelling in plant defence is conserved across flowering plants, *BRHIS1*, the rice putative orthologue *BRHIS1* has being previously described as defence-related gene (Li et al., 2013). In this chapter, another Ris-1 subfamily gene, *EDA16* is described as a novel defence-related chromatin remodelling ATPase. The results with *eda16* mutants highlight the role of *EDA16* in plant defences. Transcriptomic data, pathogen assays, together with other cell biology and molecular assays performed, indicated that EDA16 acts as a negative regulator of plant immunity by moderating excessive immune responses.

Results

1. EDA16 is a negative regulator of immunity

1.1 *EDA16* is up-regulated after bacterial perception

Transcriptomic databases suggested that *EDA16* expression was regulated by PAMPs such as the flg22 flagellin peptide, as well as by pathogens such as *P. syringae* (Chapter 2, Table **2.1**). To confirm this, *EDA16* expression was monitored by qPCR on samples from *Arabidopsis* Col-0 seedlings treated with 100 nM flg22 and on adult plants infiltrated with *Pst* DC3000. After both treatments, *EDA16* showed a modest but consistent, up-regulation of about 2 to 4 fold, suggesting a further function of EDA16 during the PAMP-associated response (figure **3.1**).

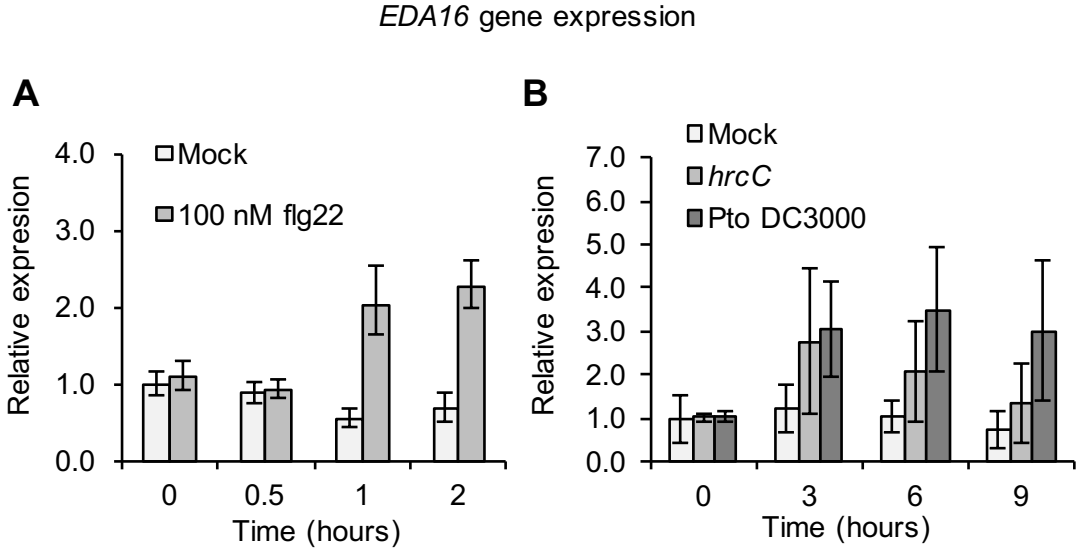

Figure 3.1. *EDA16* expression following pathogen perception. (A) 2 week-old *Arabidopsis* plants were elicited with 100 nM flg22 or water (mock). (B) 5-week old *Arabidopsis* plants were infiltrated with *Pst* DC3000, *Pst* DC3000 *hrcC* (OD_{600} 0.1) or 10 mM $MgCl_2$ (mock). *EDA16* gene expression was monitored by qPCR. For (A), data shown correspond to one biological repeat and error bars represent technical replicates standard deviations, and for (B), data shown are means of three biological replicates and error bars represent standard deviations.

1.2 Different *eda16* mutants display opposite susceptibility phenotypes during bacterial infection

In the original screening (Chapter 2, 1.2 CRAs bacterial *Pst* DC3000 susceptibility screening) CRA mutants were spray-infected with the bacterial pathogen *Pst* DC3000 Δ*avrPto*Δ*avrPtoB* in order to attain a less virulent infection (Ntoukakis et al., 2009). *eda16-1* was used as the mutant for *EDA16* in the screening and produced a susceptible phenotype (Figure **3.2 B**). In order to understand the role of *EDA16* during immunity, two more T-DNA insertion lines distributed along *EDA16* gene were obtained as homozygous lines (Alonso et al., 2003) and their immune phenotype using bacterial growth assays with *Pst* DC3000 (wild type) was studied. *eda16-1* has a T-DNA insertion in the promoter region and *eda16-3* and *eda16-5* have T-DNA insertions within the conserved catalytic SNF/HELICc domains (Figure **3.2 A**). *eda16-1* showed a small but consistent (through multiple experiments) increased susceptibility to *Pst* DC3000 (Figure **3.2 C**), whereas *eda16-3* and *eda16-5* showed increased resistance (Chapter 2, Table **2.1** and Figure **3.2 C**). To explain the discrepancy between the lines phenotypes, given that the 3 T-DNA insertions are split across the gene locus (Figure **3.2 A**), *EDA16* transcript integrity was tested in the mutants. *eda16-1* (promoter insertion) showed no transcript disruption while the other two lines, *eda16-3* and *eda16-5* produced truncated *EDA16* mRNAs (knock-outs, KOs; Figure **3.2 D**). Surprisingly, the expression levels of *EDA16* showed that *eda16-1* had higher steady state levels. Most importantly, in the *eda16-1* background the *EDA16* transcript over-responded to flg22 treatment, compared to wild type (Figure **3.2 E**). This suggests that the *eda16-1* susceptibility phenotype (Figure **3.2 B**) could be due to *EDA16* overexpression (OE). EDA16 therefore appears to act as a negative regulator of immunity in response to the bacterial pathogen *Pst* DC3000.

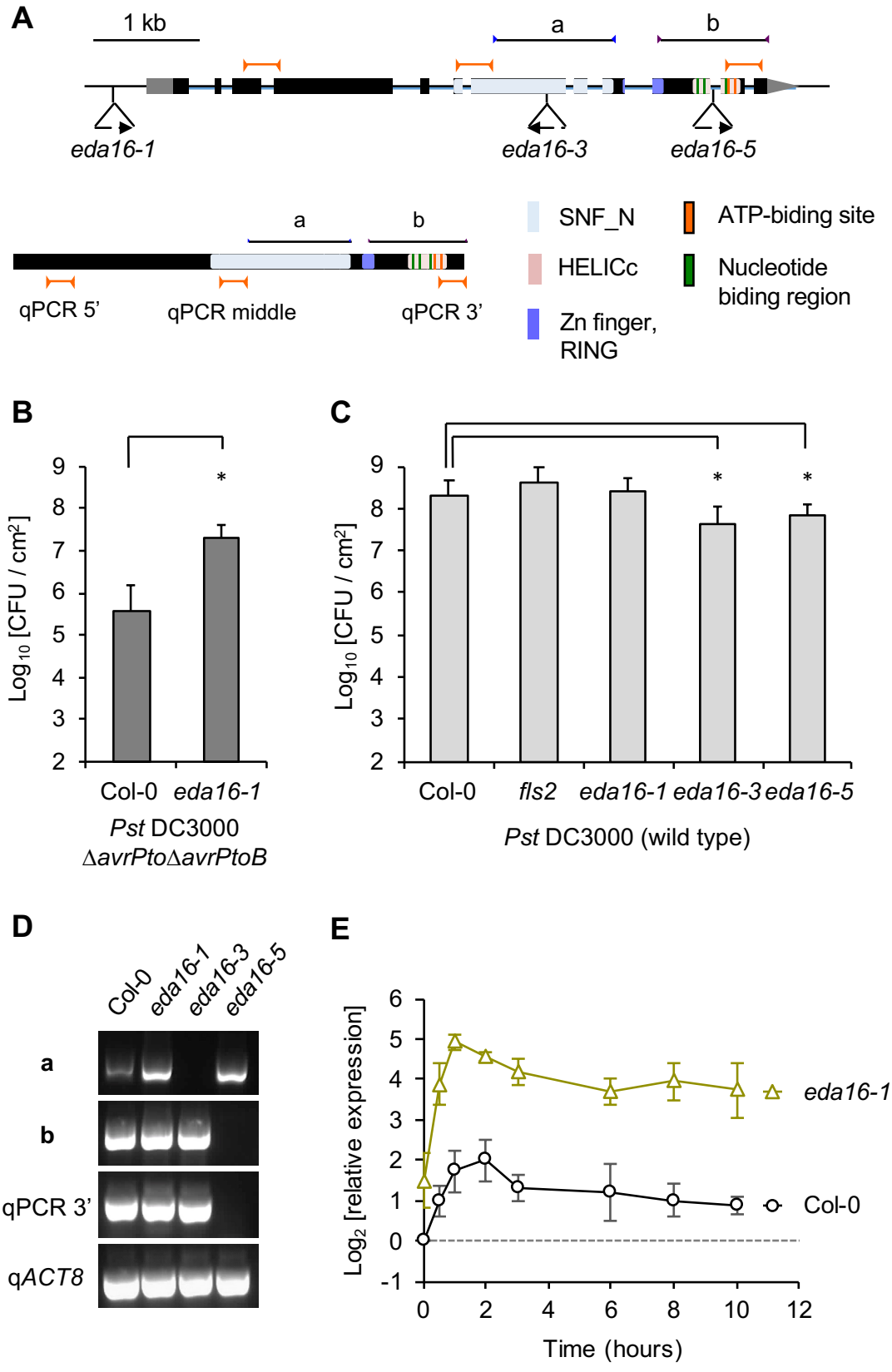
A
1 kb
a
b
eda16-1
eda16-3
eda16-5
qPCR 5'
qPCR middle
qPCR 3'
SNF_N
HELICc
Zn finger, RING
ATP-biding site
Nucleotide biding region
B
Log10 [CFU / cm2]
Col-0
eda16-1
Pst DC3000 ΔavrPtoΔavrPtoB
C
Col-0
fls2
eda16-1
eda16-3
eda16-5
Pst DC3000 (wild type)
D
Col-0
eda16-1
eda16-3
eda16-5
a
b
qPCR 3'
qACT8
E
Log2 [relative expression]
Time (hours)
eda16-1
Col-0

Figure 3.2. *EDA16* T-DNA insertion lines characterisation. (A) *EDA16* gene and transcript model showing *eda16-1*, *eda16-3* and *eda16-5* T-DNA insertion sites as well as predicted protein domains. (B and C) Growth of *Pst* DC3000 Δ*avrPto*Δ*avrPtoB* (B) and wild type (C) on Col-0 and *eda16* mutants *Arabidopsis* plants 3 days after spray inoculation. Statistical significance determined by a two-sided T-test (on Log_{10}[colony forming units / cm^2]) assuming equal variances, n = 6, "*" indicates p-value < 0.01. Error bars represent standard deviation. (D) PCR products for *EDA16* transcript fragments "a", "b" and 3' qPCR fragments. ACT8 was included as loading control. (E) qPCR analysis of *EDA16* expression in wild-type (Col-0) and *eda16-1* mutant seedlings following elicitation with 100 nM flg22. *EDA16* transcript was monitored with 3 probes distributed along the gene and referenced to the stably expressed genes *α-TUB*, *ACT8* and *TIP41*. Data shown are means of two biological replicates and error bars represent standard deviations.

1.3 Necrotroph *B. cinerea* infection on *eda16* mutants

Defence responses to pathogens with different lifestyles, namely necrotrophic, biotrophic or hemibiotrophic pathogens are specialised and often involve antagonistic pathways. For example, chromatin remodelling ATPase *SYD* mutants only showed a phenotype against the fungus *B. cinerea* (Walley et al., 2008). To investigate the role of *EDA16* in defence against the necrotrophic fungi *B. cinerea*, *eda16* mutants were subjected to a detached leaf infection assay (Windram et al., 2012). The three *eda16* mutants' immunity phenotypes against *B. cinerea* were indistinguishable compared to Col-0 control plants (Figure **3.3**), suggesting that *EDA16* role in plant defence is restricted other pathogens than *B. cinerea*, perhaps only to bacterial pathogens, or at least to pathogens with a biotrophic or hemibiotrophic lifestyle. Further experiments would be required with different pathogens like the biotrophic fungus *Hyalonospora arabidopsidis* or the Oomycete *Albugo candida*, in order to better understand whether the role of EDA16 is in fact restricted to bacterial pathogens.

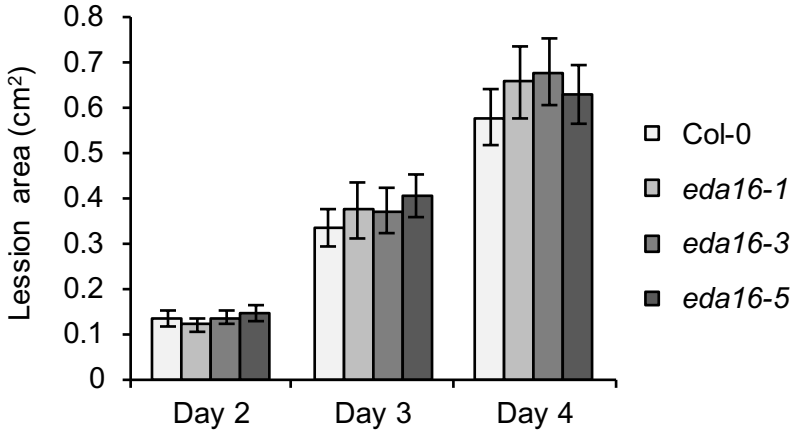

Figure 3.3. *B. cinerea* infection on *eda16* mutants. *B. cinerea* var *pepper* inoculated on *Arabidopsis* detached leaves. Leaves number 7, 8 or 9 were collected from adult plants. Lesion surface area was measured 1 to 4 days after inoculation of $4x10^5$ spores. Data shown are means from one biological repeat of three performed. Error bars represent standard errors, n = 20.

2 PAMP- and effector-triggered responses are not altered in *eda16* mutants

The next step was to pinpoint at which layer of immunity EDA16 could be acting. For this, flg22-based assays and infections with the avirulent *Pst* DC3000 carrying the effector AvrRpt2 were performed.

2.1 Flagellin responses are maintained in *eda16* mutants

Since *EDA16* gene expression is inducible by the flg22 flagellin-derived peptide, and responses to flagellin constitute one of the best characterised examples of PTI, the *eda16* mutants were tested for responses to flg22. During PTI, ROS production is directly mediated by protein phosphorylation and Ca^{2+} influx (Kimura et al., 2012), and can be triggered independently or even before gene expression changes (Kadota et al., 2015; Macho and Zipfel, 2014). The combination of all PTI responses affect in the long term developmental outcomes and result in, for instance, growth arrest (Huot et al., 2014). Here, short- (ROS burst), medium- (defence-related gene expression over a time course) and long-term responses (growth inhibition) were tested.

ROS assay

To test early PTI responses, ROS production caused by flg22 perception was assessed on adult leaves of the three *eda16* mutants. The results did not show a consistent difference between the ROS production of the truncated mutants (*eda16-3* and *eda16-5*), the wild type (Col-0) or the OE mutant *eda16-1* (Figure **3.4**). These results suggest that *EDA16* is not involved in the early production of ROS after flg22 exposure.

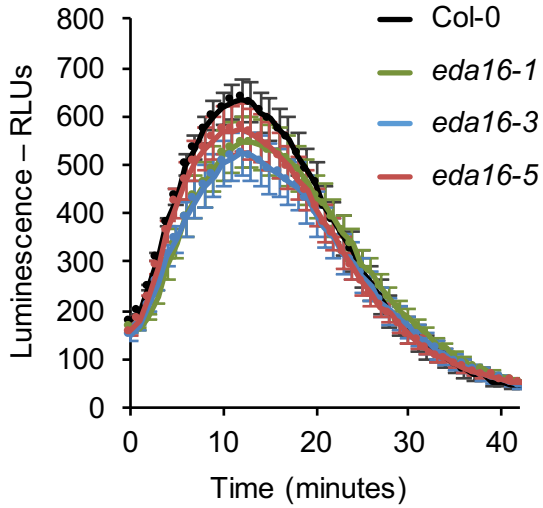

Figure 3.4. ROS burst following flg22 elicitation in *eda16* mutants. The assay was performed on leaf disks from adult plants kept for 8 hours in darkness, then exposed to 100 nM flg22 with Luminol® and HR peroxidase. Data shown are means of one experiment (n = 24) out of three biological repeats. Error bars represent standard error of the mean.

Defence marker genes responses were unaltered in *eda16* mutants

To pinpoint in which pathway and the dynamics that EDA16 may be involved during the gene reprograming following flg22 perception, the expression of well-characterised marker genes was monitored. MAP kinase responsive gene *FRK1*, CDPK responsive gene *PHI-1* (Boudsocq et al., 2010) and the fgl22 and SA-responsive gene *CBP60g* (Wang et al., 2011) were monitored over a 10-hour time course of exposure to 100 nM flg22. The expression of these flg22-induced marker genes was undistinguishable in the *eda16* mutants compared with the control (Col-0). These results suggest that the early PAMP-induced transcriptional changes are not affected by *EDA16* at early time points.

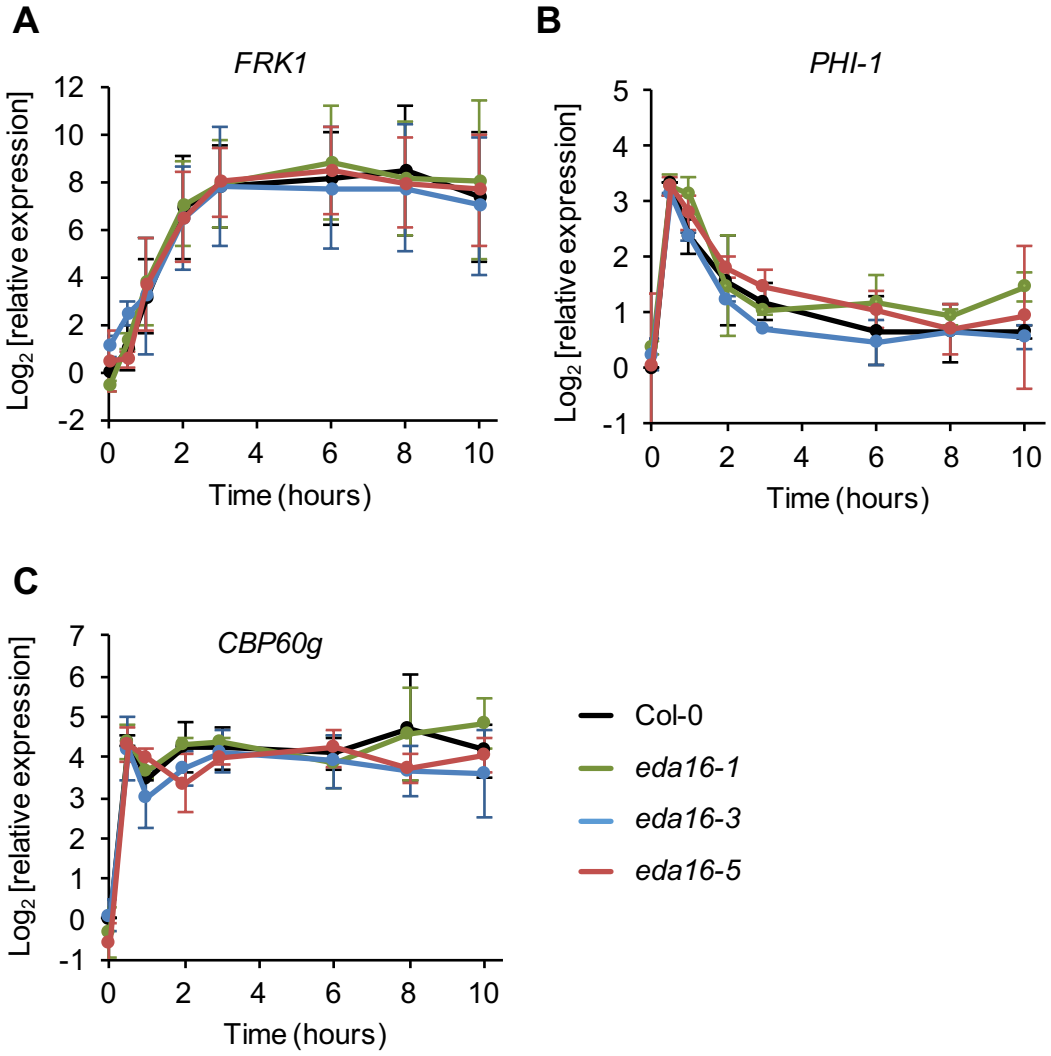

Figure 3.5. Flg22-induced gene expression of PTI marker genes in *eda16* mutants. qPCR analysis on wild-type (Col-0) and mutants *eda16-1* (OE), *eda16-3* and *eda16-5* (KO) seedlings following elicitation with 100 nM flg22 (A) *FRK1*, (B) *PHI-1*, and (C) *CBP60g* gene expression. Gene expression was referenced to *α-TUB* gene. Data shown are means of two biological replicates and error bars represent standard deviations.

The gene expression of SA-induced *PR1* was also monitored over the 10 hours time course after flagellin exposure. However, the results were not reproducible, depicting almost an erratic gene expression profile (Supplementary Figure **S3.2**). Therefore, the mutants were treated with 500 µM SA and gene expression of *PR1* as well as *CBP60g* was monitored. When applying SA, *PR1* expression was induced consistently across the mutants and control, suggesting no SA-mediated gene expression deficiencies (Figure **3.6**).

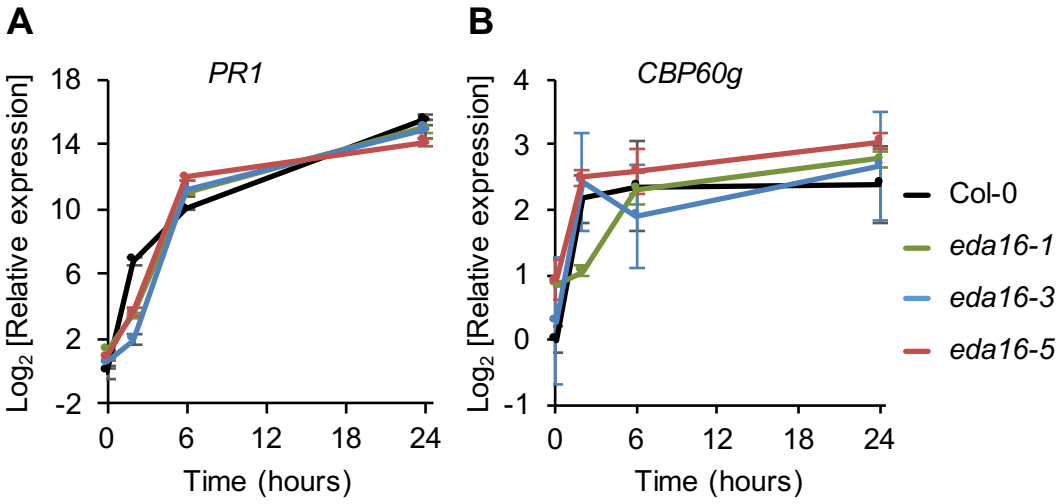

Figure 3.6. SA elicited *PR1* and *CBP60g* gene expression in *eda16* mutants. qPCR analysis on wild-type (Col-0) and mutants *eda16-1* (OE), *eda16-3* and *eda16-5* (KO) seedlings following elicitation with 500 µM SA (A) *PR1* and (B) *CBP60g* gene expression. Gene expression was referenced to *α-TUB* gene. Data shown were collected in one experiment and error bars represent standard deviations of the technical replicates.

Growth inhibition assay

For the growth inhibition assay, seedlings are allowed to germinate and begin growing. After a week they are moved to liquid medium supplemented with the elicitor (0– control, 1, 10 or 100 nM flg22), and are grown for one more week in these conditions. The *fls2* mutant, lacking the flagellin receptor FLS2, was used as an insensitive control (Chinchilla et al., 2006). The assay showed that flg22 could inhibit equally the growth of *Arabidopsis* seedlings irrespective of the *eda16* mutations (Figure **3.7**).

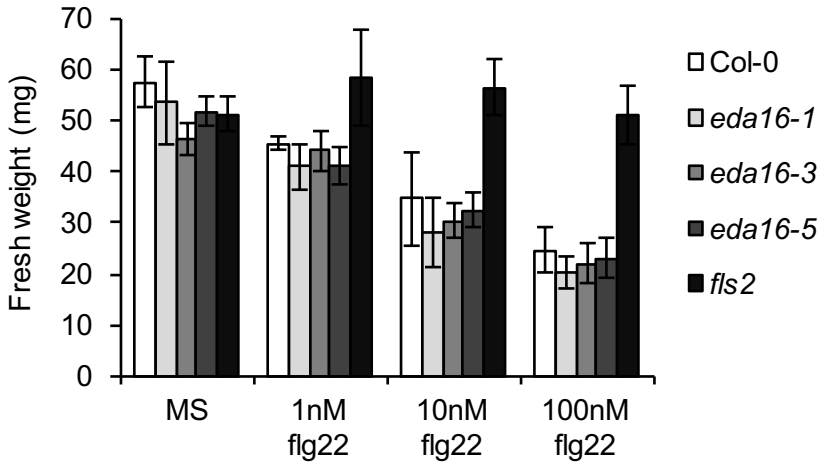

Figure 3.7. flg22 growth inhibition assay. Seedlings were grown for a week in solid medium and then moved to liquid medium containing different concentrations of flg22 and allow growing for one more week. Showing standard deviations (n = 6), two biological repeats merged. *fls2* mutant is used here as a negative control.

2.2 ETI responses were unaltered in *eda16* mutants

The second layer of plant immunity consist of cytoplasmic receptors that mediate the gene-to-gene recognition, or ETI (Jones and Dangl, 2006). To test EDA16 responses to an avirulent effector, adult plants were syringe-infiltrated with *Pst* DC3000 expressing the effector AvrRpt2. Two different types of assays were performed; (1) ion leakage assays, a proxy measurement of cell death generated by the plant as a defence measure in response to the effector recognition, and (2) bacterial growth assays, quantifying the bacteria ability to survive in the potentially immune-compromised *eda16* mutants.

The results of the ion leakage experiments and the infections with a strain carrying an effector recognised by *Arabidopsis* suggested that ETI is not compromised in *eda16* mutants, since comparable levels of cell death were attained in the control (Figure **3.8 A**). The bacterial growth assays supported this conclusion, where *eda16* mutants and the control AvrRpt2 were equally effective impeding the bacterial growth (Figure **3.8 B**).

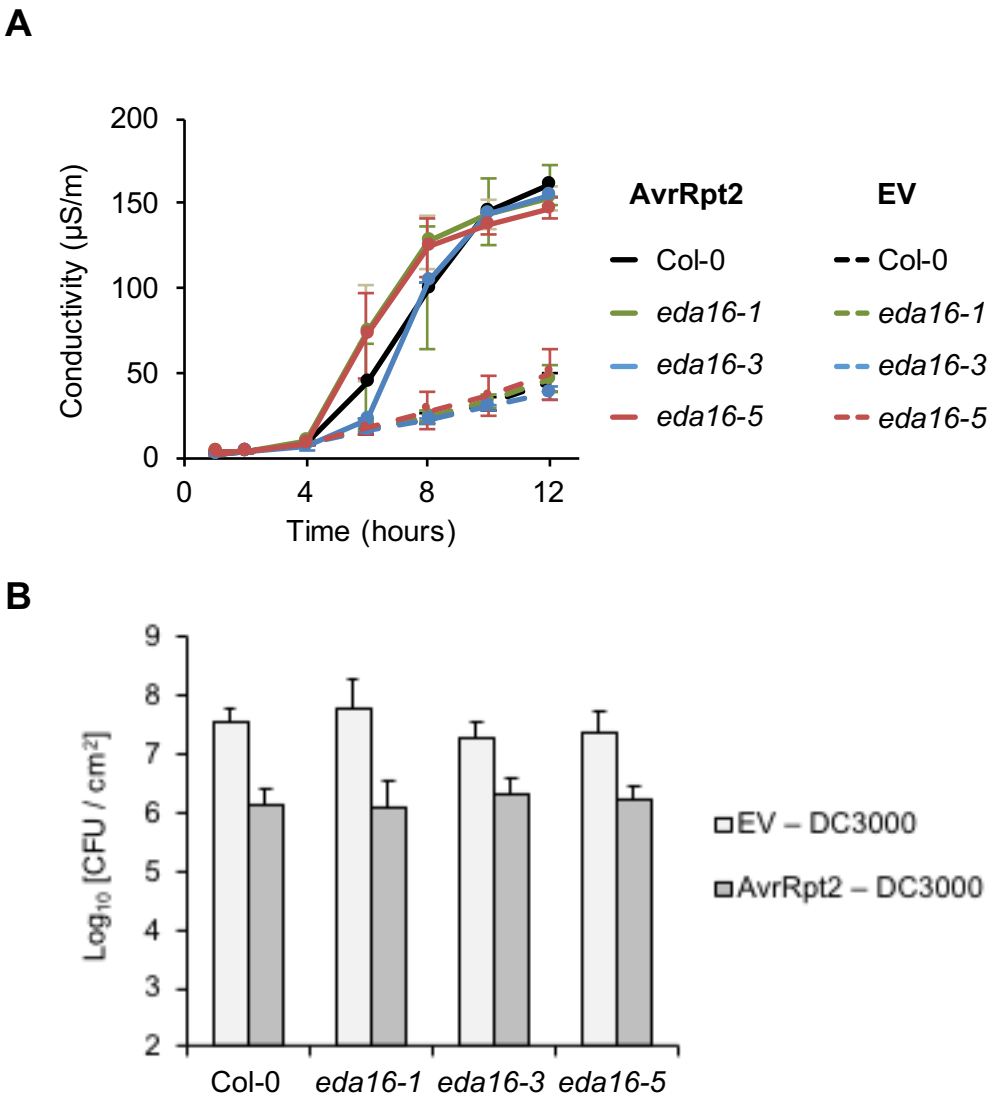

Figure 3.8. AvrRpt2-induced ETI is not impaired in *eda16* mutants. (A and B) Ion leakage, and bacterial growth of *Pst* DC3000 transformed with an empty vector (EV) as a control and with AvrRpt2 on Col-0 (wild-type) and *eda16* mutants adult plants. (A) Plants were syringe-infiltrated and leaf disks were collected and kept in sterile water. Conductivity measurements (microsiemens per meter) were taken from the solution for 12 hours as a quantitative measure of ion leakage from dead cells. (B) Growth of *Pst* DC3000 EV and AvrRpt2 3 days after syringe infiltration. Data shown from one experiment representative of three performed. Error bars represent standard deviation (n = 6). Differences were not statistically significant (Two-sided T-test assuming equal variances).

3 EDA16 localisation and functional characterisation

EDA16 has been annotated as a nuclear-localised chromatin remodelling ATPase based on protein homology and sequence similarity (http://www.arabidopsis.org). To confirm EDA16 localisation and allow future biochemical work, such as identification of interactors by mass-spectrometry or *in vitro* protein activity assays, *EDA16* cDNA was cloned and tagged with a C-terminal EYFP-HA tag. The upstream promoter used was the cauliflower mosaic virus 35S (Earley et al., 2006).

3.1 Nuclear localisation of EDA16

The 35S:cEDA16-EYFP-HA construct was transiently expressed in *N. benthamiana dcl2dcl3* double knock out plants (impaired in the RNA silencing pathway; Dadami et al., 2013; Katsarou et al., 2016) using *A. tumefaciens* infiltration. Using confocal microscopy, EDA16 was confirmed to be nuclear-localised (Figure **3.9**, left). As a control, GFP-tagged histone H2B (H2B-GFP; Rosa et al., 2014) was also observed in the nucleus, but to a greater extent than EDA16 (Supplementary figure **S3.3**). In addition, it is noticeable that expression in *N. benthamiana* (wild type) was never achieved with this construct using the cauliflower mosaic virus 35S promoter, whereas GFP-tagged H2B did not show this problem (data not shown). It would be therefore interesting to dedicate further research attempting to understand post transductional regulation (such as UTR regulation) of *EDA16*.

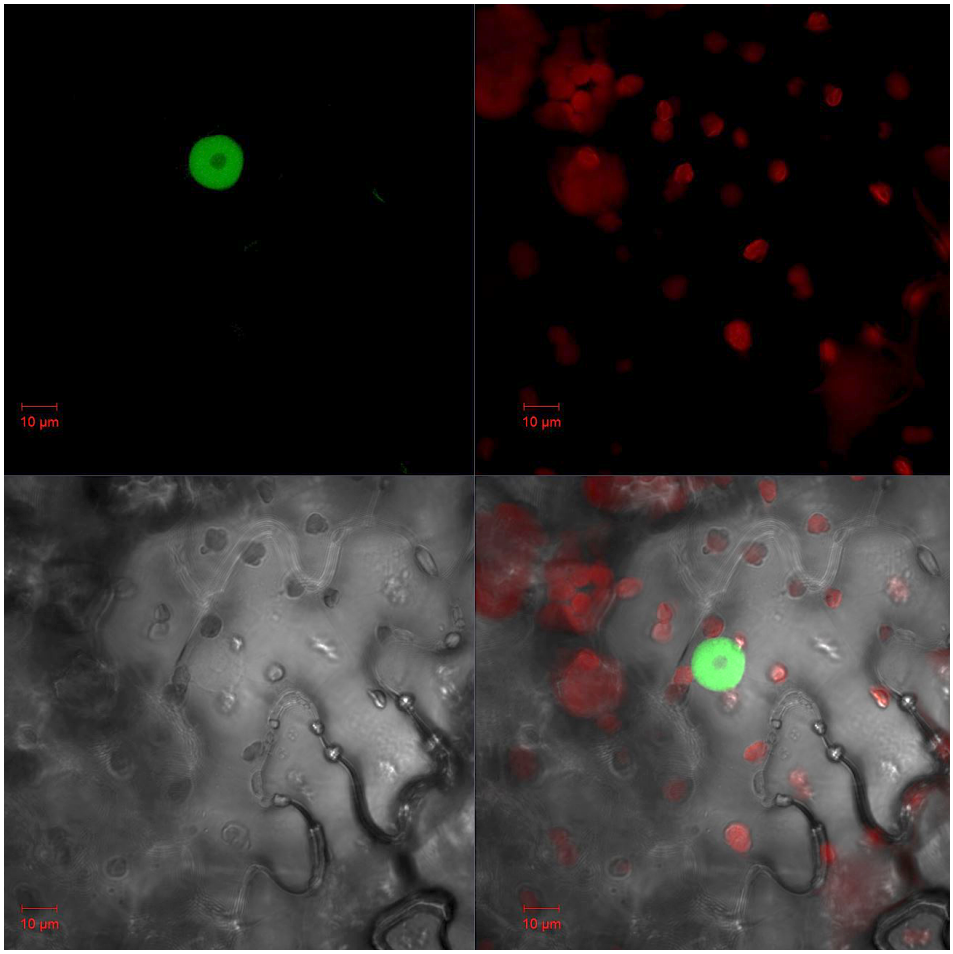

Figure 3.9. Nuclear localization of EDA16. 35S:cEDA16-EYFP-HA construct was transiently expressed in *N. benthamiana dcl2dcl3*. Subcellular localisation was observed by confocal microscopy. Top left: EYFP channel, top right: red fluorescence (chlorophyll A), bottom left: transmission field (cell boundaries) and bottom right: merged. Bar = 10 µm.

3.2 Relevance of EDA16 during flg22-induced nuclear reorganization

To study the involvement of EDA16 in active chromatin remodelling, fluorescence recovery after photo-bleaching (FRAP) assays were performed on H2B-GFP *Arabidopsis* stable lines, in Col-0 background (as a control) and *eda16-5* background. FRAP assays allow the inference of molecular dynamics of the fluorophore diffusion. In this case, H2B-GFP is taken as a measurement of nucleosome diffusion, which in turn can be affected by the nuclear cell phase and developmental stage, and in general by the DNA dynamical processes, such as replication or transcription (Cuvier and Fierz, 2017; Rosa et al., 2014). Since cells at different developmental stages in the roots show very different FRAP behaviours (Rosa et al., 2014), only mature mesophyll cells with big (greater than 5 μm) elongated nuclei were chosen (see Supplementary figure **S3.4**).

FRAP assays showed the nuclear dynamics after flg22 on the wild-type background (Col-0) and *eda16-5* expressing H2B-GFP. Seedlings were not treated (resting state) or treated with flg22 for 10 minutes and 2 hours. Then a true leaf was detached and prepared in water for confocal imaging following the dynamics in nuclei from mature cells for 20 minutes. The mutant *eda16-5* recovered the fluorescence more slowly than the control at the resting state, showing seemingly slower diffusion rates in *eda16-5* mutant (however, the estimated half-times, $t_{1/2}$, were not statistically different Supplementary table **S3.1**). These small differences could be accounted by a more restricted chromatin conformation in the resting state than that of the control (Figure **3.10 A**).

To validate this, other alternative hypotheses should be examined. For example, the availability of H2B-GFP measured by alternative methods to microscopy, such as protein immunoblotting, in the mutant compared to the control. In addition, recent techniques dedicated to explore the 3D conformation of chromatin, such as Chromosome Conformation Capture (3C) or 3C pair with deep sequencing (Hi-C; Lieberman-Aiden et al., 2009) could help to understand at what level *eda16-5* chromatin configuration would differ from that of Col-0 seedlings. Hi-C is a genome-

wide technique based on chromatin fragmentation and DNA re-ligation to closely located fragments providing information regarding chromosomal interactions (Dekker et al., 2013; Rodriguez-Granados et al., 2016).

The flg22 treatment had an observable impact on chromatin dynamics, extrapolated from increased H2B-GFP diffusion rates at both times (Supplementary figure **S3.5**). This was evident as well on the $t_{1/2}$ values for FRAP (Supplementary table **S3.1**), although the differences in $t_{1/2}$ were not statistically significant. *eda16-5* 35S::H2B-GFP and the control (Col-0 35S::H2B-GFP) behaved similarly when exposed to flg22 (Figure **3.10 B** and **C** and Supplementary table **S3.1**). Interestingly, a short exposure of 10 min to flg22 was enough to affect the H2B-GFP diffusion rates (in fact, with less variation than a longer exposure of 2 hours Figure **3.10 B** and **C**, stronger fluorescence recovery, Supplementary figure **S3.5** and shorter $t_{1/2}$, Supplementary table **S3.1**).

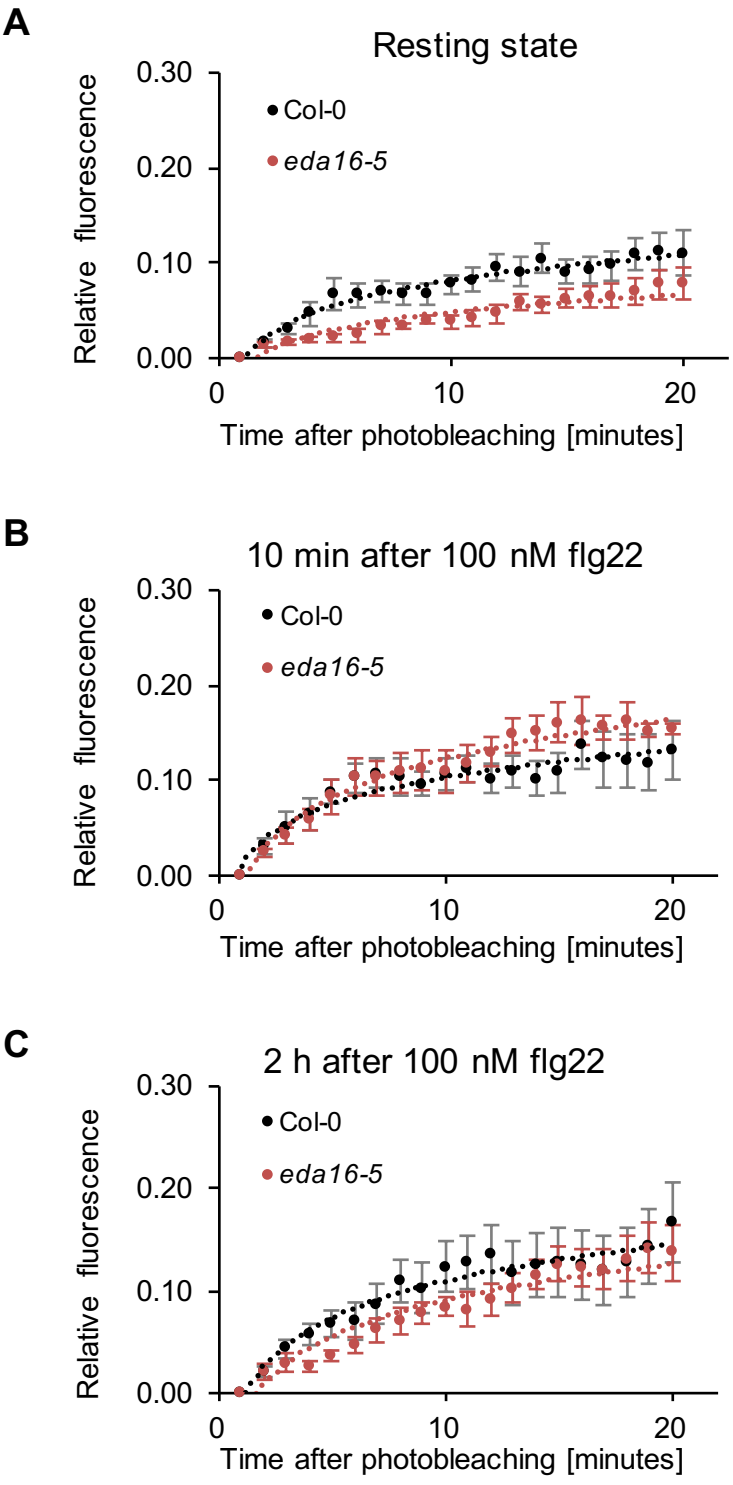

Figure 3.10. Altered chromatin in *eda16-5* mutant at the resting state. FRAP data collected from seedling leaf tissue. H2B-GFP in Col-0 and *eda16-5*. The seedlings were exposed to water (A) or 100 nM flg22 for 10 minutes (B) or 2 hours (C). Data points are averages of at least 8 nuclei for each condition and genotype. Error bars represent standard error of the mean. See also Supplementary table **S3.1** for estimated half-times for each condition.

4 RNA-seq transcriptomic analysis of flagellin treated *eda16* mutants

To gain an insight into *EDA16* function in plant immunity, the consequences of loss and gain of *EDA16* transcript on gene expression and nucleosome positioning after PAMP perception were examined using the described mutants *eda16-1* (OE) and *eda16-5* (KO). Unfortunately, none of the defence marker genes tested (*FRK1*, *PHI-1* and *CBP60g*) indicated any particular time-point when *EDA16* impact on gene expression could be greatest (Figure **3.2**). Therefore, taking into account that flg22 induced a peak of gene expression after two hours of exposure in both Col-0 and in the OE mutant *eda16-1*, this time was chosen to perform genome-wide transcriptomic analysis. Samples were collected from Col-0 (wild-type), *eda16-1* (OE) and *eda16-5* (KO) mutant seedlings, either mock or treated with 100 nM flg22 for 2 hours.

The first raw analysis of the RNA-seq data showed that the majority of the variance could be attributed to the flg22 treatment. When analysed for the first 500 genes sorted by variance, principal component 1 (PC1) explained 90% of the variance, clearly separating treated from untreated samples (Figure **3.11 A**). The samples separated by genotype on PC3, accounting for over 1% of the variance. As expected, *eda16-1* (OE) and *eda16-5* (KO) had greater differences between themselves than compared to Col-0 (Figure **3.11 B**). Consistent levels of variance were found attributed to the replicates (principal component 2, figure **3.11 A** and figure **3.11 C**). To control for a possible batch effect, genes differentially expressed between replicates were defined using relax parameters to ensure that most variation due to replicates was detected (p-value < 0.01, fold-change > square root of 2). Identified genes varying by replicate (1732 genes were considered as different between replicates) did not show any defence related GO term enrichment, Fisher's exact test with FDR correction, p-value < 0.01 (Supplementary figure **S3.6** and Supplementary Table **3.1**). To ensure meaningfulness of the results found hereon, they were compared with the replicate-varying genes and removed from interest groups if present.

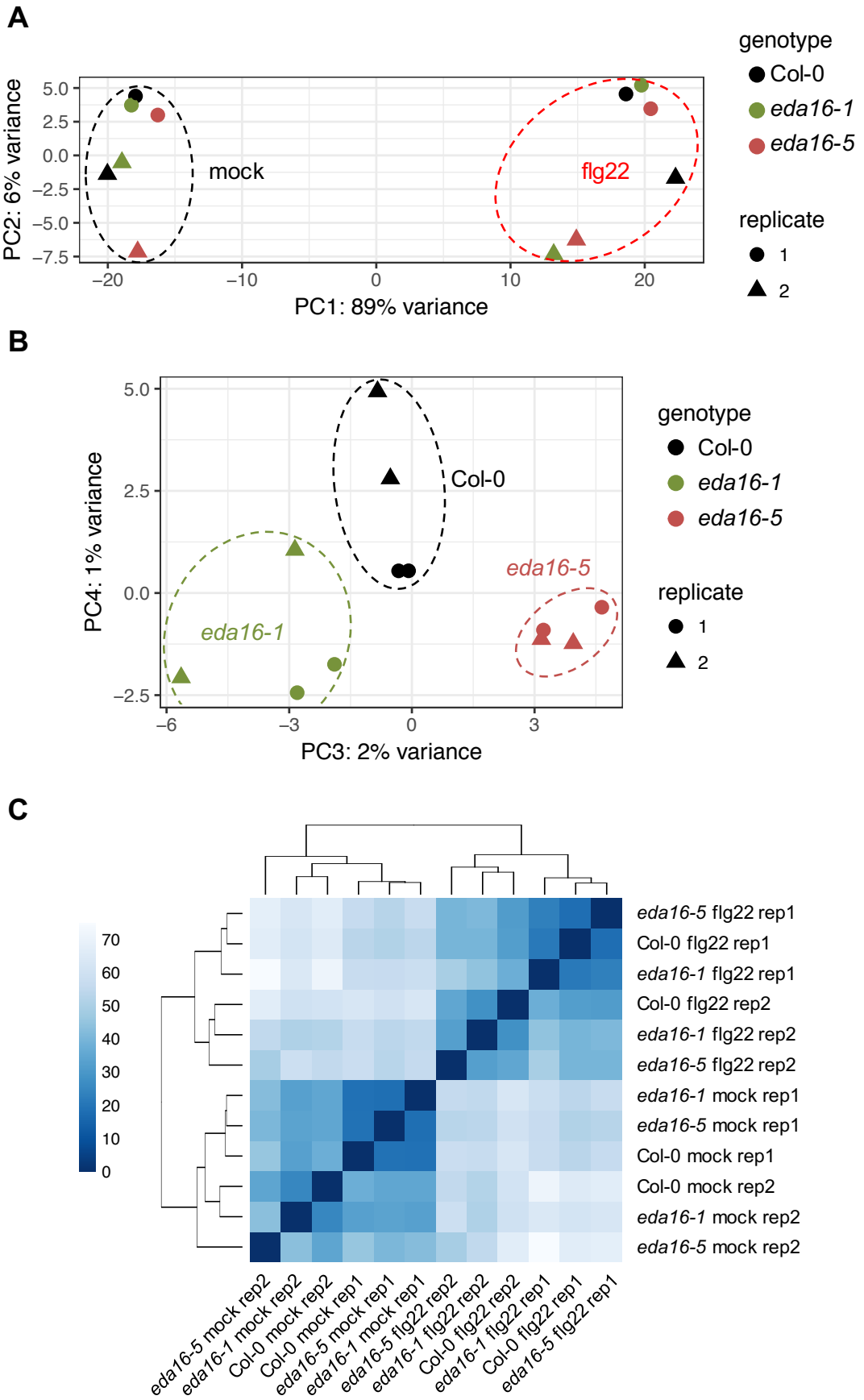
A
genotype
Col-0
eda16-1
eda16-5
replicate
1
2
PC2: 6% variance
PC1: 89% variance
mock
flg22
B
PC4: 1% variance
PC3: 2% variance
Col-0
eda16-1
eda16-5
C
eda16-5 flg22 rep1
Col-0 flg22 rep1
eda16-1 flg22 rep1
Col-0 flg22 rep2
eda16-1 flg22 rep2
eda16-5 flg22 rep2
eda16-1 mock rep1
eda16-5 mock rep1
Col-0 mock rep1
Col-0 mock rep2
eda16-1 mock rep2
eda16-5 mock rep2

Figure 3.11. RNA-seq variance analysis demonstrates flg22 high impact on gene expression compared to genotype. (A and B) Principal component analysis performed for the 500 genes with the greatest variance. Circles represent samples from the first biological repeat and triangles from the second; Black is Col-0, green is *eda16-1* and red *eda16-5*. (A) PC1 and PC2 shows the strong (~90%) contribution to the variance is accounted by the flg22 treatment. (B) PC3 and PC4 shows a separation of the samples according to their genotype. (C) Heat map of distance matrix and hierarchical clustering for each sample. If gene expression, measured as read counts per transcript, is more similar between samples, values will be low (when comparing the same sample, it yields a trivial value of 0, following the inverse diagonal). Log_2 scale data counts normalised with respect to library size and minimizing differences between samples for rows with small counts (Love et al., 2014).

Flagellin treatment

As expected from the first analysis (Figure **3.11**), the flg22 treatment had a massive impact on gene expression across the samples (Birkenbihl et al., 2017; Denoux et al., 2008; Navarro et al., 2004; Zipfel et al., 2006). 1520 genes were identified as differentially expressed across genotypes (fold-change > 2 and p-value < 0.01), of which only 5 (less than 0.5%) were affected by replicate. Most of them, 1400, were up-regulated (Supplementary figure **S3.7** and Supplementary table **S3.3**). GO terms for up-regulated and down-regulated genes confirmed the success of the treatment; expected enriched GO terms in up-regulated genes included defence hormone terms, response to chitin, wounding or oxidative burst involve in defence, while down regulated genes presented terms such as response to brassinosteroid or cell wall organization and loosening.

Genotype effect

Comparing the three genotypes across treatments (Col-0 treated vs. *eda16-1* treated, Col-0 untreated vs. *eda16-1* untreated, and so forth), 20 genes were found to be differentially regulated, with stringent fold-change > 2 and p-value < 0.01 (Figure **3.11** and Supplementary table **S3.4** for adjusted p-values). GO term analysis for this group of genes showed relevant terms such as chromatin assembly or disassembly or response to hydrogen peroxide (Fisher's exact test p-value < 0.05). For most of these genes (excluding cis-affected *EDA16*, AT1G61140, and contiguous gene AT1G61150), *eda16-1* (OE) showed less expression than Col-0, and far less than *eda16-5* (KO) mutant, suggesting a role of EDA16 in repressing gene expression. Interestingly, 4 of these genes were also responsive to flg22 treatment, and *eda16-1* showed a lesser (or not significant) up-regulation. These genes encoded two heat-shock factors, heat shock transcription factor A2 (HSFA2) and heat shock protein 17.6A (HSP17.6A), a peroxidase (PX52) involved in lignin production (Fernández-Pérez *et al.*, 2015) and a N-acetyl transferase (NATA1) responsive to MeJA and ABA (Lemarié et al., 2015; Lou et al., 2016).

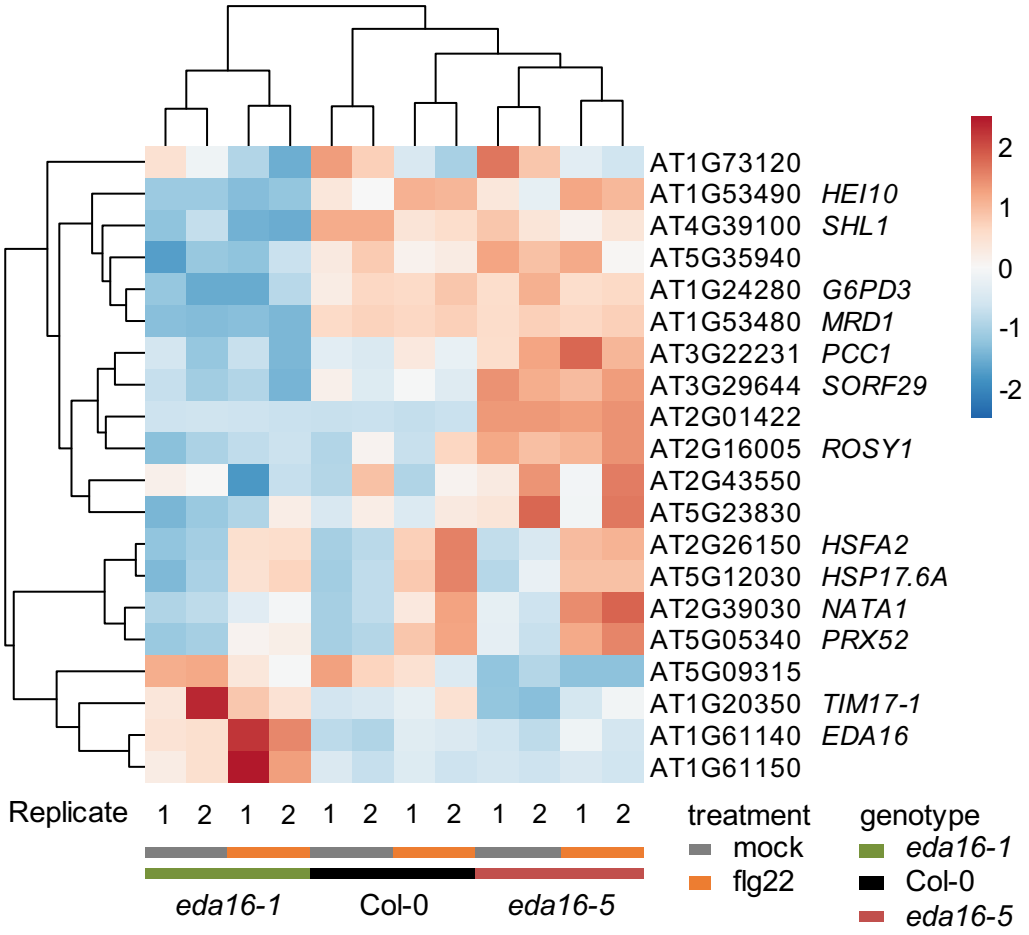

Figure 3.12. Relative gene expression heat map for differentially expressed genes between genotypes and hierarchical clustering. Mutants cluster together according to gene expression similarity, and also treatments. *eda16-1* (OE) shows the greatest differences with *eda16-5* (KO) and Col-0. These genes were defined as DEG according to stringent criteria (fold-change > 2 and p-value < 0.01) in the either of the six pairwise comparisons: Col-0 mock vs *eda16-1* mock, Col-0 flg22 vs *eda16-1* flg22, Col-0 mock vs *eda16-5* mock, Col-0 flg22 vs *eda16-5* flg22, *eda16-1* mock vs *eda16-5* mock or *eda16-1* flg22 vs *eda16-5* flg22.

Table 3.1. Statistically enriched GO terms of genes different by genotype. Significance stablished with Fisher's Exact test, VirtualPlant 1.3 (http://virtualplant.bio.nyu.edu/cgi-bin/vpweb/).

Term	Observed Frequency	Expected Frequency	p-value	Genes
Response to oxidative stress	4 out of 16 genes, 25%	278 out of 24961 genes, 1.1%	0.00164	*HSFA2*, *HSP17.6A*, *PRX52*, AT1G73120
Response to high light intensity	2 out of 16 genes, 12.5%	48 out of 24961 genes, 0.2%	0.00972	*HSFA2*, *HSP17.6A*
Response to hydrogen peroxide	2 out of 16 genes, 12.5%	44 out of 24961 genes, 0.2%	0.00972	*HSFA2*, *HSP17.6A*

Chromatin remodelling proteins may affect transcription in less direct and subtler way than TF. With this idea, the criteria for differentially expressed gene discovery were adjusted, maintaining it within commonly accepted boundaries of significance (Schurch et al., 2016), fold-change > square root of 2 (1.4142), and p-value < 0.05. Then, 45 genes were found as differentially regulated (Supplementary figure **S3.7**). Again, confirming the previous results with more stringent parameters (Figure **3.12**), GO term analysis showed an enrichment for responses to stress, chemical stimulus, toxin metabolic processes and oxidative stress, Fisher's exact test p-value < 0.01 (Supplementary Table 3.3).

In all, the transcriptional data analysis showing more genes repressed in *eda16-1* (OE) compared to Col-0 and especially compared to *eda16-5* (KO), suggested a role of *EDA16* as a transcription repressor, and even if on a small scale, with an impact on defence-related genes. The next step to understand EDA16 action on chromatin remodelling will be to compare the transcriptomic data with the MNase-seq data, potentially revealing a mechanism of action for gene repression.

Discussion

EDA16 expression induction after bacteria perception suggested that *EDA16* is a relevant gene in plant defence (Figures **3.1**, **3.2 D**, and Table N2.1 in chapter 2). The characterisation of the OE and the KO mutants indicated a negative action of *EDA16* over the plant's ability to control the bacterial infection (Figure **3.2**). *eda16-1* OE mutant was able to up-regulate *EDA16* with a similar pattern to Col-0, but about one order of magnitude higher (Figure **3.2 D**). This suggested an active role of EDA16 protein on immunity repression during defence activation. This hypothesis was, at least partially, supported by the RNA-seq analysis findings, where the overexpression of *EDA16* caused gene repression of a few defence-related genes, and higher gene expression for the same genes in the KO mutant (Figure **3.12**). Further testing (by qPCR for instance) will strengthen the understanding on the mis-regulation of these genes with experiments such as monitoring gene expression over a time course response. Finding EDA16 as a negative regulator of immunity activated during immunity is not such a paradox or futile cycle. Indeed, in the literature, there are other negative regulators of immunity up-regulated during defence processes. For instance, TF from the WRKY family, *WRKY18* and *WRKY40* are up-regulated in response to flg22, leading to defence-related gene down-regulation. In this manner, they are expected to control exaggerated defence responses (Birkenbihl et al., 2017; Li et al., 2017).

Recently, it has been shown that some transcriptional regulator networks mediate (or prevent) the escalation of PTI towards ETI (Hatsugai et al., 2017). Thus, it is possible that *EDA16* helps to block the development of ETI, unless perhaps further positive regulators are recruited. The ETI experiments suggested that indeed, ETI is not compromised in *eda16* mutants when triggered with bacteria carrying the effector AvrRpt2 (Figure **3.8**). It is worth pointing out that the different phenotypes observed in *eda16* mutants when infecting by spraying (Figure **3.2 B**) were reduced when the plants are syringe-infiltrated (Figure **3.7**, EV) and no differences are seen during ETI assays (Figure **3.8**, AvrRpt2). These differences, together with the RNA-seq data, may indicate that *EDA16* is involved in repressing defence processes, mainly other than

PTI, either those related to late oxidative stress leading to HR or perhaps early stomatal control and leaf penetration.

The transcriptomic data showed only a few genes were differentially expressed in the mutants compared to the control. However, this was the case for other chromatin remodelling ATPases (Bezhani et al., 2007). Four genes attracted special attention since they were flg22-induced to a different extend in the mutants and had associated GO terms in response to oxidative stress (Table **3.1**). Two heat shock related proteins, the TF HEAT SHOCK TRANSCRIPTION FACTOR A2 (HSFA2) and HSP17.6A, are partially silenced in the OE mutant (Figure **3.12**). *HSFA2* is inducible by a series of environmental stresses, such as oxidative stress or the combination of heat and light (Nishizawa et al., 2006). Intriguingly, peroxidase *PRX52*, involved in lignin production (Fernández-Pérez *et al.*, 2015), is also partially silenced in *eda16-1* OE mutant. N-acetyl transferase 1 (NATA1), also de-regulated in the OE mutant, is involved in hydrogen peroxide detoxification during HR (Lou et al., 2016). It may be revealing of EDA16 function during plant immunity, the fact that *EDA16* is up-regulated by oxidative stress (Xu et al., 2015) and UV light (Kilian et al., 2007). Since both stresses can cause DNA damage, and other chromatin remodelling factors such as ATPase RAD54 are involved in DNA repair mechanisms (Hirakawa et al., 2017; Osakabe et al., 2006), it is tempting to speculate with EDA16 involvement in DNA damage repair triggered by defence-induced oxidative stress. However, the evidence presented here indicates that EDA16 would act as a transcription repressor favouring conditions less toxic at the DNA level, or at least, conditions involving less oxidative stress.

NATA1 acetyltransferase is greatly induced by MeJA, coronatine and ABA (Lemarié et al., 2015; Lou et al., 2016). Even though JA responses were not tested following the expression of JA-responsive genes, *eda16-1* did not produce any remarkable phenotype on JA-induced growth inhibition assays (data shown on Chapter 2, 2.1 CRAs Jasmonic acid screening). In addition, no phenotype was observed when infecting *eda16* mutants with the necrotrophic fungus *B. cinerea* (Figure **3.8**). Defences against the necrotrophic pathogen *B. cinerea* rely on an functional JA-signalling pathway (Robert-Seilaniantz et al., 2011), and phenotypes have been reported in the case of mutated components at the chromatin remodelling level

(Walley et al., 2008). Thus, it can be expected that *EDA16* has no major role mediating in the JA pathway, and therefore future experiments exploring the ABA pathway may help to unveil *EDA16* genetic network.

The nuclear localisation of EDA16 shown in this chapter (Figure **3.9**), together with the presence of SNF/ATPase domains within the protein, could suggest a conserved role of EDA16 interacting with chromatin. FRAP assays performed on *eda16-5* and Col-0 stably expressing H2B-GFP were insufficient to conclude an involvement of EDA16 on flagellin-induced gene reprograming (Figure **3.10**), and even the differences at the basal state (not induced) where small (Supplementary table **S3.1**). It could be speculated that EDA16 played a role in chromatin remodelling under specific conditions (such as DNA stress, similar to other CRAs like RAD54; Osakabe et al., 2006).However, FRAP data was collected from a very specific set of cells (fully mature mesophyll cells with extended areas, and with big elongated nuclei; see Supplementary figure **S3.4**). Therefore, other cell types and developmental stages should be examined before the findings could be generalised. In this line, gene expression at different developmental tissues can vary considerably (Schmid et al., 2005). Future efforts to pair single-cell gene expression and live-cell imaging approaches (Rosa and Shaw, 2013) may help to understand the cellular response to pathogen cues and more specifically, the role of EDA16 in different cell types and developmental stages.

To further elucidate changes in chromatin structure related to this study, an MNase-seq analysis has been undertaken and results are currently being analysed. These data will show how the nucleosome positioning changes after a dramatic gene reprograming such as the one triggered by flagellin, and the impact of EDA16 in this process, as well as in nucleosome positioning at the resting state. Future experiments with GFP-tagged lines may allow ChIP followed by mass-spectrometry for protein complex determination and ChIP followed by next-generation sequencing for DNA binding sites and direct target determination. A construct with EDA16 cDNA tagged with a C-terminal HA peptide under the control of a dexamethasone-inducible promoter will allow to study system with EDA16 controlled induction for activity assays and infection assays.

Additionally, it will be important testing non-transcriptional responses such as stomatal opening due to bacterial manipulation, later HR development and DAB staining to explore hydrogen peroxide production after flagellin exposure or perhaps with the expression of an effector protein *in planta*, and further transcriptomic experiments using virulent and avirulent pathogenic bacteria and later time points. These experiments will allow to test whether EDA16 is a target of bacterial effectors, manipulated by them to favour the course of the infection.

Concluding discussion

Datamining, H3K27me3 and gene regulation

In this era of numerous genome-wide datasets and publicly available resources, it is not only an advantage but a necessity to understand how to combine and exploit this wealth of knowledge. In the Chapter 1 of results, an analysis of several chromatin marks over defence-related genes led to the detection and subsequent verification of histone H3K27me3 as an important mark in regulating the expression of flagellin-induced genes. The results presented in this chapter support the notion of H3K27me3 as a repressive mark, associated with lowly expressed genes. Given that defence activation may lead to growth arrest, it is not surprising that their expression is regulated at multiple levels including gene repression by H3K27me3 deposition (Figure **D.1**).

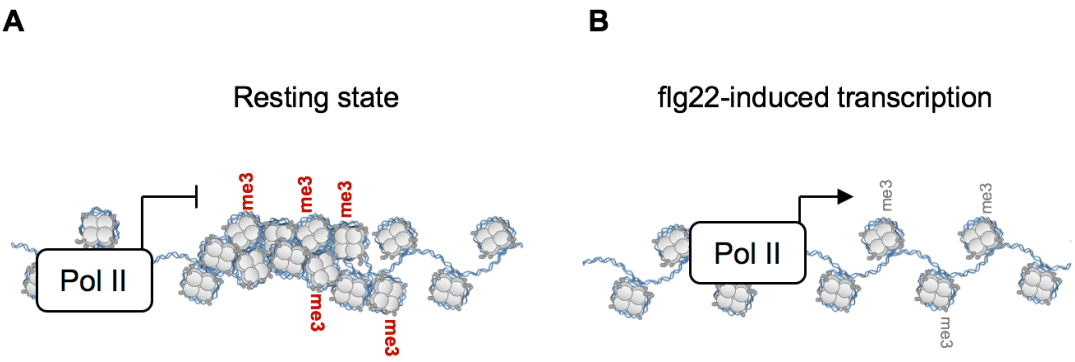

Figure D.1. Gene repression via H3K27me3. (A) In the resting state, genes that normally have low or no detectable expression are associated with the repressive histone mark H3K27me3, represented in with **me3** in red, leading to a repressive chromatin conformation state. (B) During the flg22-induced transcription, specific defence genes that presented H3K27me3 are now depleted of the mark.

The bioinformatics analysis presented here suggested an enrichment in H3K27me3 for the calcium-dependent protein kinase (CDPKs) responsive genes. CDPK kinases are activated downstream the perception of PAMPs such as flagellin through ion calcium fluxes (Boudsocq et al., 2012; Ludwig et al., 2004). At least four CDPKs, CPK4, 5, 6 and 11, are responsible of the transcriptional reprogramming at the initial PAMP signalling cascade (Boudsocq et al., 2010). These kinases localise to the nucleus in the presence of bacterial effectors such as AvrRpt2 and phosphorylate certain WRKY TF contributing to the activation of ETI (Gao et al., 2013). In this work, qPCR and ChIP assays explored a potential link between the CDPK pathway and chromatin remodelling processes activating transcription through histone H3K27 demethylation during the onset of PTI. Unfortunately, due to the partial redundancy in the CPK family, the potential connection between the CDPKs and the histone demethylase enzymes remained conjecture. Future work with stronger *cpks* mutants revealing diminished reduction of H3K27me3 paired with delayed or impaired gene expression may lead to further *in vitro* kinase assays and protein co-IP exploring CDPKs directly targeting and phosphorylating histone demethylase enzymes.

The question that naturally follows concerns the role of the enzymes depositing, maintaining and removing the H3K27me3 mark. More specially the role of those enzymes dedicated to remove the mark prior to flagellin-induced gene expression, and the signalling cascade leading to this enzymatic activation following the onset of immunity.

The bacterial growth assays with the *bona fide* H3K27me3 demethylase mutants *ref6-1* and *elf6-3* revealed the importance of these enzymes in the fitness of the plant facing a biotic stress (Figure **1.11**). It remains to be answered whether REF6 plays a direct role upon immunity activation or if the *ref6-1* mutant is (generally) transcriptionally disadvantaged due to the accumulated number of hyper-methylated regions. However, the significant overlap between the genes targeted by REF6 and the flg22-induced genes, together with the relevance of these common genes in defence processes (illustrated by the phosphorylation GO term enrichment), suggests that REF6 plays a role in regulating the chromatin landscape of flagellin-induced genes. Moreover, the *REF6* putative orthologue in rice, *JMJ05,* exhibit a similar immune phenotype (Li et

al., 2013), suggesting that the role of histone demethylases in plant immunity is conserved across flowering plants.

In this work, the PTI marker gene *FRK1* has been shown to respond differently to flagellin in the *ref6-1* mutant, corresponding to the respective levels of H3K27me3 (Figures **1.12** and **1.13** and summarised in Figure **D.2**). These results demonstrate an alternative tool to further study the dynamic turnover of histone methylation/demethylation by closely characterising the H3K27me3 deposition in response to flagellin in the demethylase mutant background. Previous studies on the dynamics of H3K27me3 have focused on aspects such as the effect of vernalisation on repressing flowering loci (De Lucia et al., 2008; Sung and Amasino, 2004). However, the dynamic removal of H3K27me3 during warm periods has been only approached as a mathematical simulation (Angel et al., 2011).

FRK1 is a flagellin-induced gene which accumulates ectopic H3K27 methylation in the *ref6-1* mutant. This may imply a highly dynamic chromatin environment, where the action of histone methylation complexes such as the polycomb repressive complex 2 (PRC2) is immediately reversed by REF6 demethylase (Figure **D.2** and Supplementary figure **S1.5)**. It is unlikely that *FRK1* is an isolated case, given the high number of ectopically hyper-methylated loci found in the *ref6-1* mutant (Cui et al., 2016; Lu et al., 2011). This leads to exciting questions where the proposed study of *FRK1* induction on the demethylase background may prove as a useful model system. Firstly, how often does this histone methylation/demethylation cycle occur? It will be fundamental to clarify if H3K27me3 deposition (and re-setting the chromatin landscape) happens once in the cell cycle after DNA replication.

Furthermore, H3K27me3 deposition overlaps with the deposition of LIKE HETEROCHROMATIN PROTEIN 1 (LHP1, a component of the PRC2; Turck et al., 2007) in the surroundings of *FRK1*. A single peak of REF6 is observed in the middle of *FRK1* transcribed region, where very low levels of both, histone methylation and LHP1 are reported for wildtype plants (Liu et al., 2018 see Supplementary figure **S1.5**). The results showing *ref6-1* and *elf6-3* mutants more susceptible to *Pseudomonas* infection together with a hyper-methylated *FRK1* locus (Figures **1.11** and **1.13**), suggest a key role for the REF6 binding site (in processes such as plant

defences) versus PRC2 (and LHP1) with little DNA-binding specificity and a mechanism of action based on high processivity along the DNA. In summary, it remains a matter of speculation whether the gene-specific histone methylation pattern is achieved through the selective action of the demethylase enzymes. And finally, is there a tissue/developmental stage were loci such as *FRK1* are highly methylated and have a physiological function? The system proposed here, exploring flg22-induced *FRK1* gene expression in the *ref6-1* background provides a useful tool to study H3K27 dynamic demethylation especially combined with other mutations such as the double mutant *ref6*/*elf6*.

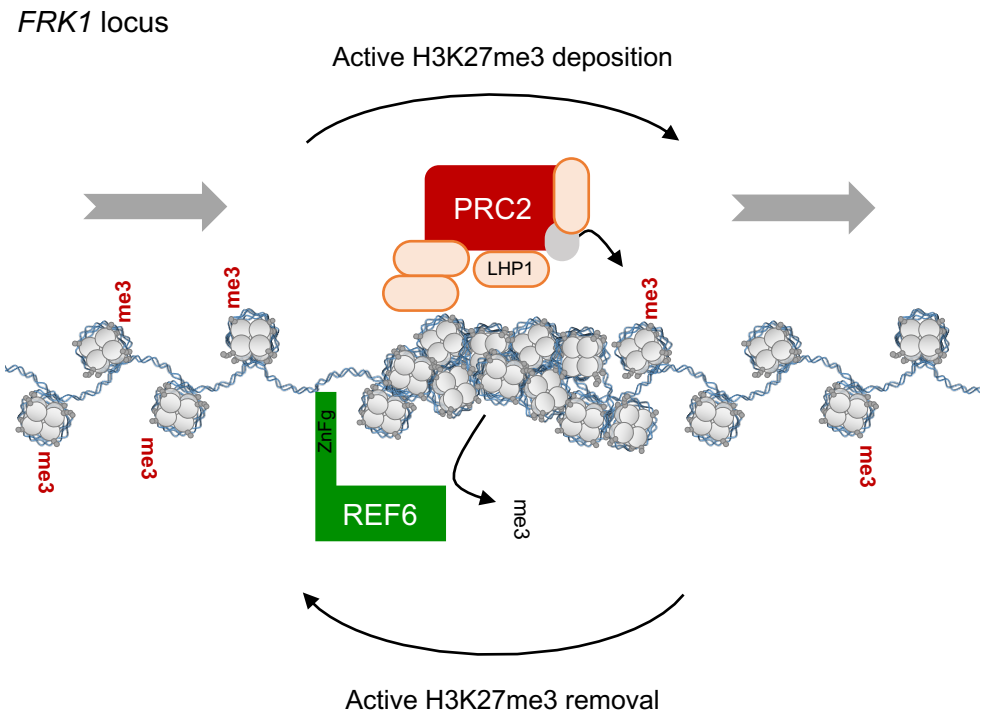

Figure D.2. Dynamic H3K27 methylation/demethylation at the *FRK1* locus. Histone methyltransferase complexes such as polycomb repressive complex 2 (PRC2) mediate H3K27me3 deposition. Jmj-C demethylase REF6 binds to DNA through its zing fingers domain (ZnFg) and mediates the demethylation of H3K27.

EDA16 as a negative regulator of immunity

EDA16 was originally described as a gene related to the development of the female gamete. The use of a gene trap collection allowed the identification of *EDA16* as a mutant showing a heterozygous transmission ratio near 0.5, instead of 0.75 on the gene trap selective marker (as it would be expected of embryo lethality). Further microscopy characterisation showed embryo sac arrested at varying stages of development within the same silique. Hence, the name embryo sac development arrest 16 (Pagnussat et al., 2005). However, no information about the position of the insertion was provided. Even though *eda16-2* (SALK_107256) and *eda16-4* (SAIL_1156_D12C1) were never characterised as homozygous (and so, not presented in this work), *eda16-3* and *eda16-5* homozygous mutants described in this thesis displayed no obvious developmental phenotypes and yielded copious amounts of seeds. Interestingly, *EDA16* gene expression (the strongest within the Ris-1 sub-family) is stronger in senescent tissue, mature siliques and in the seeds than it is in the flowers (http://bar.utoronto.ca/; Groth et al., 2014). However, the change was not considered significant (perhaps due to the low fold change) by authors studying gene reprograming during senescence (Breeze et al., 2011; Buchanan-Wollaston et al., 2005).

During senescence, as macromolecules break down ROS may be produced generating oxidative stress. Conversely, drought and other abiotic stresses may lead to senescence through ROS accumulation (Lee et al., 2012). As revealed by the RNA-seq data presented in Chapter 3 (RNA-seq transcriptomic analysis of flagellin treated *eda16* mutants), 4 genes up-regulated by flagellin were affected in the *eda16* mutants with functions related to oxidative stress. *EDA16* would be therefore involved in several different biological functions; gamete formation (Pagnussat et al., 2005), seed maturation and senescence (based on transcriptomic data: http://bar.utoronto.ca/; Groth et al., 2014), and according to the results here presented, oxidative stress moderation (RNA-seq data, Figure **3.12**) and plant defences (gene expression analysis and pathogen growth experiments Figures **3.1** and **3.2**).

There is a considerable overlap in hormone signalling during senescence and immunity. Hormones such as ET, JA or ABA play a role in both. Interestingly, there is an inhibition (although moderate) in *EDA16* gene expression by ABA in the mesophyll cells and no effect on the guard cells (Yang et al., 2008). Perhaps, the explanation could be that ABA on mature leaves acts as pro-senescence signal, while EDA16 may slow down ROS and cell aging. The ABA signalling pathway is an important target for *Pst* DC3000 effectors such as AvrPto (de Torres-Zabala et al., 2007). The similarities in the phenotypes between *Pst* DC3000 and Δ*AvrPto/AvrPtoB* mutant suggest that EDA16 exerts its negative action on plant defences regardless of an influence from the effectors AvrPto or AvrPtoB (Supplementary figure **S3.1**). However, the possibility of other effectors manipulating EDA16 (directly or indirectly) should not altogether be excluded. Especially as *EDA16* remains up-regulated a long time after infection (at least more than 8 hours) by wild-type *Pst* DC3000 but not with a bacteria lacking the ability to inject effectors *hrcC* (Figure **3.1** and model Figure **D.3**) or *hrpA*, (Lewis et al., 2015). It should be noted that in these experiments the amount of bacteria long after treatment may not be comparable between plants infected with *Pst* DC3000 wildtype and the ones infected with the bacteria lacking effectors (Lewis et al., 2015).

When infiltrating with avirulent *Pst* DC3000 AvrRpt2, *eda16* mutants responded in the same degree as the control in terms of cell death and bacterial growth (Figure **3.7**), suggesting that EDA16 has no function in AvrRpt2-induced ETI. Nevertheless, other effector recognition by R proteins cause the up-regulation of *EDA16* more than two-fold. AvrRpm1 caused *EDA16* up-regulation (after 3 and 6 hours) and so did AvrRps4 in a EDS1-dependent and PAD4 synergistic manner (Bartsch et al., 2006). The expression of *EDA16* was not studied in this work upon infection with AvrRpt2, but the corresponding resistance (R) proteins RPS2 and RPM1 (detecting AvrRpm1) react to modifications on the same protein (Kim et al., 2005), and belong to the coil-coil (CC) NB-LRR subfamily of R proteins, while RPS4 contains a N-terminal domain with a Toll/interleukin-1 receptor (TIR; Gassmann et al., 1999). Future experiments with bacteria carrying AvrRpm1 and AvrRps4 effectors or *in planta* inducible expression in *eda16* mutants background may shed light into the role of EDA16 in ETI mediated pathways.

The results presented in this work together with the available transcriptomic data indicate that *EDA16* responds to different challenges that imply to a greater or lesser extend oxidative stress. The production of ROS upon flagellin perception was not altered in *eda16* mutants (Figure **3.4**). Early ROS is mainly dependent on the NADPH oxidase RESPIRATORY BURST OXIDASE HOMOLOGUE D (RBOHD, Kadota et al., 2015). RBOHD is controlled by Ca^{2+}, Ca^{2+}-dependent protein kinases and it is rapidly phosphorylated by BIK1 at the plasma membrane level independently of gene transcription (Dubiella et al., 2013; Kadota et al., 2004, 2014). Therefore, it was unlikely that EDA16, being nuclear localised (Figure **3.9**), would participate in the generation of rapid ROS at the plasma membrane level.

RBOHD produces the unstable free radical superoxide (O_2^-) towards the apoplastic space, that generates hydrogen peroxide (H_2O_2) (Marino et al., 2012; Torres et al., 2002). Recently, the plant aquaporin PLASMA MEMBRANE INTRINSIC PROTEIN 1;4 (PIP1;4) has emerged as an important H_2O_2 importer (Tian et al., 2016), facilitating plant defence responses through increasing the intracellular levels of H_2O_2 (Chaouch et al., 2012; Tian et al., 2016). In addition, other organelles such as chloroplasts, mitochondrion and peroxisomes can release ROS within the cell (Noctor et al., 2017). In addition, it is worth mentioning that oxidative stress can cause DNA damage, and other chromatin remodelling factors such as ATPase RAD54 are involved in DNA repair mechanisms (Hirakawa et al., 2017; Osakabe et al., 2006).

The emerging picture predicts that EDA16 acts in response to ROS, to keep the cell homeostasis and protect the cell from the intense effects of oxidative stress. This action would make sense during moderate responses such as PTI, where at the cellular level self-preservation survival strategies would be preferred (since no cellular death is observed, Figure **D.3 A**). However, during ETI responses, where HR causes cell death, there would be no need for a moderating activity within the cell (Figure **D.3 D**).

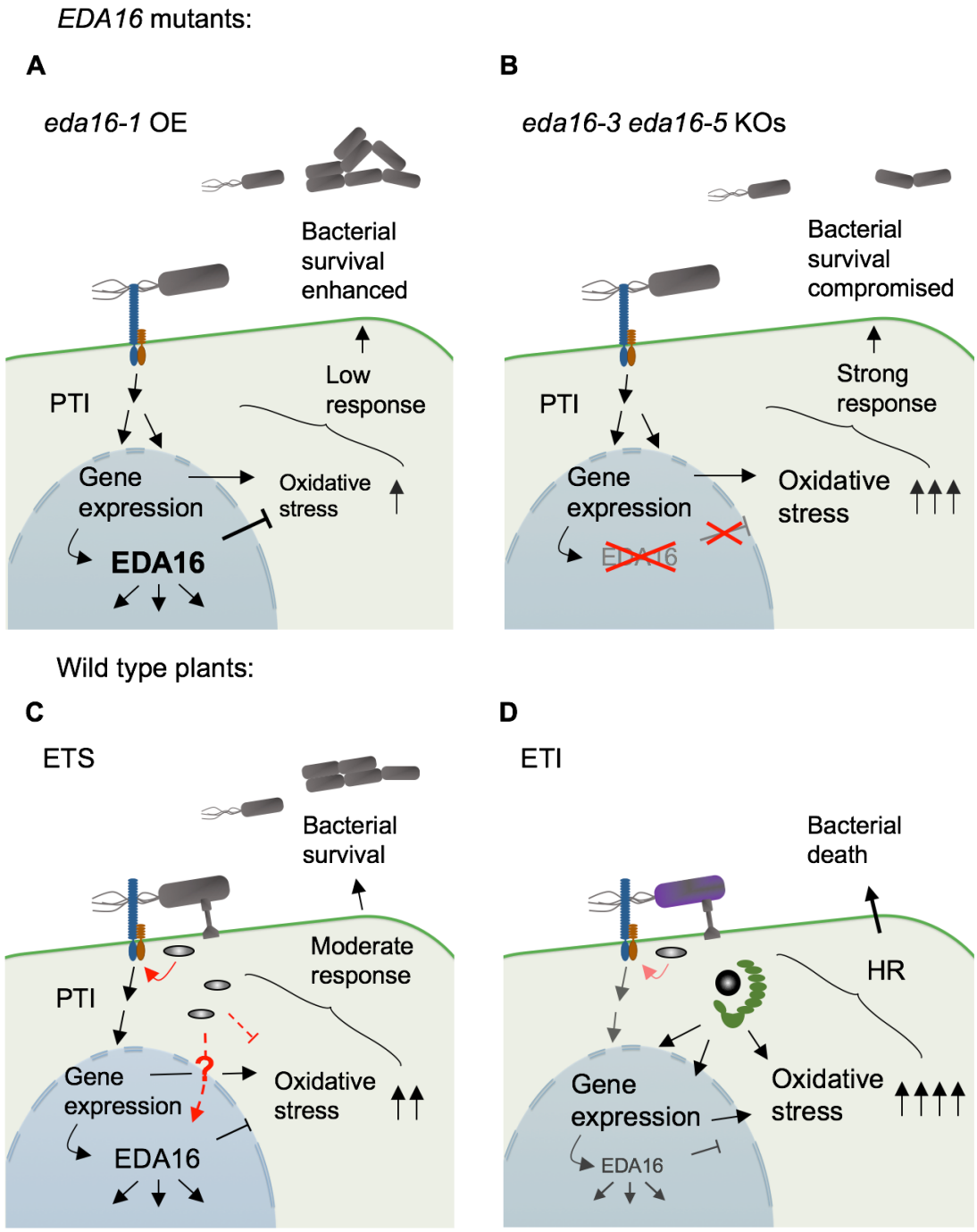

Figure D.3. Proposed EDA16 mechanism of action during immunity. (A) and (B) Observed phenotypes in *eda16* mutants are in agreement with RNA-seq data in a model where EDA16 moderates oxidative stress induced by immunity activation. (C) Extending the model even further, any negative regulator of defence mechanisms may be potentiated by bacterial effectors (effector-triggered susceptibility; ETS), (D) unless these effectors are recognised by their corresponding R proteins triggering ETI that leads to HR and cell death.

Histone marks and chromatin remodelling during plant defence

Histone marks are closely related to the activity of other chromatin remodelling factors such as the ATP-dependent chromatin remodelling complexes. These complexes often carry histone modification reader domains and in some cases they also have subunits with histone-modifying capabilities (Flaus and Owen-Hughes, 2011).

1. H3K27me3 and chromatin remodelling ATPases

In the case of H3K27me3 repressed flowering loci, chromatin remodelling ATPases SYD and BRM are redundantly required to overcome gene repression and control floral organ development (Li et al., 2015a; Wu et al., 2012). SYD has been associated with defence against necrotrophic pathogens through the direct activation of JA-related *MYC2* and *VSP2* gene expression upon wounding (Walley et al., 2008). Marker genes of the SA pathway such as *PR1* are upregulated in the *brm* (Bezhani et al., 2007), again suggesting possible overlapping functions giving the known antagonism between the JA and SA pathways. To make things more complicated, the *MYC2* locus is not enriched in H3K27me3 but *PR1* is (Roudier et al., 2011; Zhang et al., 2016). *PR1* was not detected with the bioinformatics analysis since it does not respond very robustly to flg22 (Supplementary figure **3.1**). In any case, *PR1* is heavily regulated at the chromatin level (Alvarez-Venegas et al., 2007; Choi et al., 2012). Together, these findings suggest that SYD and BRM may be involved in overcoming H3K27me3 gene repression, but it is unlikely that they directly target this mark. In support of this, recently BRM has been recently found to co-occur at genomic loci with histone demethylase REF6 (Li et al., 2016). This concerted targeting does not happen at *PR1* locus in 14 days old seedlings, but it happens at *FRK1* and other defence-related loci such as *MPK11* and other coding regions of receptor-like kinases (Li et al., 2016). None of the *brm* mutants used in this work resulted in an increased resistance/susceptibility phenotype when infected with Δ*AvrPto/AvrPtoB* (Table **2.1**). Future experiments may involve testing double mutants *brm*/*syd* to cover partial redundancies or double mutants compensating with polycomb components such as LHP1 or CURLY LEAF (CLF), in opposite methylation/demethylation pathways.

2. EDA16 and histone marks

The RNA-seq analysis showed the repression of *HSFA2*, a heat shock factor gene, in the *eda16-1* OE background. *HSFA2* gene activation is also regulated by histone acetylation. Acetyltransferase *GCN5* mutations compromise *HSFA2* responsiveness to heat stress (Hu et al., 2015). Interestingly, the group has observed that *gcn5* mutants are impaired in the regulation of flagellin-induced genes (Piquerez et al., in preparation). This suggests opposite roles on specific loci between histone acetylation dependent on GCN5, and EDA16 during plant defences.

Furthermore, chromatin interacting *SHORT LIFE 1* (*SHL1*) gene was repressed in the *eda16-1* OE background. SHL1 and paralog protein EARLY BOLTING IN SHORT DAYS (EBS) are partially redundant in repressing flowering loci (and also other TF involved in plant defences such as *WRKY18*, *22*, *MYB77* or *JAZ7*). They bind to di and tri-methylated H3K4 through their PHD domains and exert their repressive action through the recruitment of histone deacetylase HDA6 (Lopez-Gonzalez et al., 2014; Narro-Diego et al., 2017).

The ATPases are considered the central subunit of the chromatin remodelling protein complexes. Therefore, a genetic interaction between EDA16 and chromatin associated protein SHL1 could be expected. In addition, EDA16 is predicted to associate with SUMO1 (https://string-db.org/) and HSFA2 protein SUMOylation is associated with stress regulation (Cohen-Peer et al., 2010). SHL1 also interacts with SUMO1 (Araport, BioGRID Interaction Data Set, https://thebiogrid.org/, Elrouby and Coupland, 2010). Thus, future experiments involving EDA16 protein complex determination by mass-spectrometry will help to understand the potential mechanism of action through direct interactions.

Ris-1 subfamily and other CRAs influencing immunity

CHR27 and CHR28 members of the Ris-1 subfamily were renamed to SNF2- ring-helicase–like1 and -2, FRG1 and FRG2 and by extension the rest of the family FRG3, FRG4 (EDA16) and FRG5 (Groth et al., 2014). FRG1 and FRG2 have redundant roles in RNA-directed DNA methylation (RdDM). However, other family members did not show an impact on DNA methylation (Groth et al., 2014). At the same time, FRG1 and FRG2 were shown to interact with SUVR2 methyltransferase and contribute to RdDM-independent gene silencing (Han et al., 2014). The mass-spectrometry analysis of FRG1 and SURV2 interactor ETL19 (that also showed a phenotype in the bacterial screening, Table **2.1**) showed that these proteins strongly interact with structural components such as tubulin, actin and clathrin, as well as heat shock proteins, auxiliary helicases, ubiquitin-like proteins, and histone methylation co-factor biosynthetic enzymes (Han et al., 2014).

How these functions lead to a resistant phenotype against *Pst* Δ*AvrPto/AvrPtoB* (Figure **2.1**) in both *frg2-1* and *frg2-2* mutants, whilst also providing bigger plants (Figure **2.1**), remains to be explained. Both *FRG2* and *FRG1* are down-regulated by necrotrophic fungus *B. cinerea* (Windram et al., 2012), while in rice, the *FRG2* putative orthologue *BRHIS1* was associated with plant resistance to the necrotrophic fungus *M. oryzae*, and the presence of the defence-priming compound (1,2-benzisothiazol-3(2h)-one,1, 1-dioxide) down-regulated *BRHIS1* expression (Li et al., 2015b). The results with *frg2-1* infected with *B. cinerea* showed a less affected trend for *frg2-1* compared to control although these differences were not statistically significant (Figure **2.1**).

Taken together these results make *FRG2* an interesting target for further research in crop engineering, increasing resistance without compromising growth across plant species.

Bibliography

Alexeev, A., Mazin, A., and Kowalczykowski, S.C. (2003). Rad54 protein possesses chromatin-remodeling activity stimulated by the Rad51-ssDNA nucleoprotein filament. Nat. Struct. Biol. *10*, 182–186.

Alexiadis, V., and Kadonaga, J.T. (2002). Strand pairing by Rad54 and Rad51 is enhanced by chromatin. Genes Dev. *16*, 2767–2771.

Alonso, J.M., Stepanova, A.N., Leisse, T.J., Kim, C.J., Chen, H., Shinn, P., Stevenson, D.K., Zimmerman, J., Barajas, P., Cheuk, R., et al. (2003). Genome-Wide Insertional Mutagenesis of Arabidopsis thaliana. Science (5633). *301*, 653–657.

Alvarez, M.E., Nota, F., and Cambiagno, D.A. (2010). Epigenetic control of plant immunity. Mol. Plant Pathol. *11*, 563–576.

Alvarez-Venegas, R., Abdallat, A. Al, Guo, M., Alfano, J.R., and Avramova, Z. (2007). Epigenetic control of a transcription factor at the cross section of two antagonistic pathways. Epigenetics *2*, 106–113.

Anders, S., Pyl, P.T., and Huber, W. (2015). HTSeq-A Python framework to work with high-throughput sequencing data. Bioinformatics *31*, 166–169.

Angel, A., Song, J., Dean, C., and Howard, M. (2011). A Polycomb-based switch underlying quantitative epigenetic memory. Nature *476*, 105–109.

Archer, N., Walsh, M.D., Shahrezaei, V., and Hebenstreit, D. (2016). Modeling Enzyme Processivity Reveals that RNA-Seq Libraries Are Biased in Characteristic and Correctable Ways. Cell Syst. *3*, 467–479.e12.

Asselbergh, B., Vleesschauwer, D., and Höfte, M. (2008). Global switches and fine-tuning-ABA modulates plant pathogen defense. Mol. Plant-Microbe Interact. *21*, 709–719.

Atkinson, N.J., and Urwin, P.E. (2012). The interaction of plant biotic and abiotic stresses: From genes to the field. J. Exp. Bot. *63*, 3523–3544.

Bannister, A.J., and Kouzarides, T. (2011). Regulation of chromatin by histone

modifications. Cell Res. *21*, 381–395.

Bartels, S., Lori, M., Mbengue, M., Verk, M. Van, Klauser, D., Hander, T., Böni, R., Robatzek, S., and Boller, T. (2013). The family of peps and their precursors in arabidopsis: Differential expression and localization but similar induction of pattern-Triggered immune responses. J. Exp. Bot. *64*, 5309–5321.

Barth, T.K., and Imhof, A. (2010). Fast signals and slow marks: the dynamics of histone modifications. Trends Biochem. Sci. *35*, 618–626.

Bartsch, M., Gobbato, E., Bednarek, P., Debey, S., Schultze, J.L., Bautor, J., and Parker, J.E. (2006). Salicylic Acid – independent ENHANCED DISEASE SUSCEPTIBILITY1 signaling in Arabidopsis immunity and cell death Is regulated by the monooxygenase FMO1 and the nudix hydrolase NUDT7. Plant Cell *18*, 1038–1051.

Baxter, A., Mittler, R., and Suzuki, N. (2014). ROS as key players in plant stress signalling. J. Exp. Bot. *65*, 1229–1240.

Bender, C.L., Alarcón-Chaidez, F., and Gross, D.C. (1999). Pseudomonas syringae phytotoxins: mode of action, regulation, and biosynthesis by peptide and polyketide synthetases. Microbiol. Mol. Biol. Rev. *63*, 266–292.

Berr, A., McCallum, E.J., Alioua, A., Heintz, D., Heitz, T., and Shen, W.-H. (2010). Arabidopsis Histone Methyltransferase SET DOMAIN GROUP8 Mediates Induction of the Jasmonate/Ethylene Pathway Genes in Plant Defense Response to Necrotrophic Fungi. PLANT Physiol. *154*, 1403–1414.

Berriri, S., Gangappa, S.N., and Kumar, S.V. (2016). SWR1 Chromatin-Remodeling Complex Subunits and H2A.Z Have Non-overlapping Functions in Immunity and Gene Regulation in Arabidopsis. Mol. Plant *9*, 1051–1065.

Bertani, G. (1951). Studies on lysogenesis. I. The mode of phage liberation by lysogenic Escherichia coli. J. Bacteriol. *62*, 293–300.

Bethke, G., Unthan, T., Uhrig, J.F., Pöschl, Y., Gust, A. a., Scheel, D., and Lee, J. (2009). Flg22 regulates the release of an ethylene response factor substrate from MAP kinase 6 in Arabidopsis thaliana via ethylene signaling. Proc. Natl. Acad. Sci. U. S. A. *106*, 8067–8072.

Bezhani, S., Winter, C., Hershman, S., Wagner, J.D., Kennedy, J.F., Kwon, C.S.,

Pfluger, J., Su, Y., and Wagner, D. (2007). Unique, Shared, and Redundant Roles for the Arabidopsis SWI/SNF Chromatin Remodeling ATPases BRAHMA and SPLAYED. Plant Cell *19*, 403–416.

Birkenbihl, R.P., Kracher, B., and Somssich, I.E. (2017). Induced Genome-Wide Binding of Three Arabidopsis WRKY Transcription Factors during Early MAMP-Triggered Immunity. Plant Cell *29*, 20–38.

Blanc, G., Hokamp, K., and Wolfe, K.H. (2003). A recent polyploidy superimposed on older large-scale duplications in the Arabidopsis genome. Genome Res. *13*, 137–144.

Blosser, T.R., Yang, J.G., Stone, M.D., Narlikar, G.J., and Zhuang, X. (2009). Dynamics of nucleosome remodelling by individual ACF complexes. Nature *462*, 1022–1027.

Bolle, C., Schneider, A., and Leister, D. (2011). Perspectives on Systematic Analyses of Gene Function in Arabidopsis thaliana: New Tools, Topics and Trends. Curr. Genomics *12*, 1–14.

Boter, M., Golz, J.F., Giménez-Ibañez, S., Fernandez-Barbero, G., Franco-Zorrilla, J.M., and Solano, R. (2015). FILAMENTOUS FLOWER Is a Direct Target of JAZ3 and Modulates Responses to Jasmonate. Plant Cell *27*, 3160–3174.

Bouché, N., and Bouchez, D. (2001). Arabidopsis gene knockout: Phenotypes wanted. Curr. Opin. Plant Biol. *4*, 111–117.

Boudsocq, M., Willmann, M.R., McCormack, M., Lee, H., Shan, L., He, P., Bush, J., Cheng, S.-H., and Sheen, J. (2010). Differential innate immune signalling via Ca2+ sensor protein kinases. Nature *464*, 418–422.

Boudsocq, M., Droillard, M.-J., Regad, L., and Laurière, C. (2012). Characterization of Arabidopsis calcium-dependent protein kinases: activated or not by calcium? Biochem. J. *447*, 291–299.

Bowers, J.E., Chapman, B.A., Rong, J., and Paterson, A.H. (2003). Unravelling angiosperm genome evolution by phylogenetic analysis of chromosomal duplication events. Nature *422*, 433–438.

Bowling, S.A., Clarke, D.J., Liu, Y., Klessig, D.F., and Dong, X. (1997). The cpr5 Mutant of Arabidopsis Expresses Both NPR1-Dependent and NPR1-

Independent Resistance. Plant Cell *9*, 1573–1584.

Boyer, L.A., Langer, M.R., Crowley, K.A., Tan, S., Denu, J.M., and Peterson, C.L. (2002). Essential role for the SANT domain in the functioning of multiple chromatin remodeling enzymes. Mol. Cell *10*, 935–942.

Breeze, E., Harrison, E., McHattie, S., Hughes, L., Hickman, R., Hill, C., Kiddle, S., Kim, Y. -s., Penfold, C.A., Jenkins, D., et al. (2011). High-Resolution Temporal Profiling of Transcripts during Arabidopsis Leaf Senescence Reveals a Distinct Chronology of Processes and Regulation. Plant Cell *23*, 873–894.

Briggs, G.C., Osmont, K.S., Shindo, C., Sibout, R., and Hardtke, C.S. (2006). Unequal genetic redundancies in Arabidopsis - a neglected phenomenon? Trends Plant Sci. *11*, 492–498.

Brown, J.K.M. (2002). Yield penalties of disease resistance in crops. Curr. Opin. Plant Biol. *5*, 339–344.

Buchanan-Wollaston, V., Page, T., Harrison, E., Breeze, E., Pyung, O.L., Hong, G.N., Lin, J.F., Wu, S.H., Swidzinski, J., Ishizaki, K., et al. (2005). Comparative transcriptome analysis reveals significant differences in gene expression and signalling pathways between developmental and dark/starvation-induced senescence in Arabidopsis. Plant J. *42*, 567–585.

Buscaill, P., and Rivas, S. (2014). Transcriptional control of plant defence responses. Curr. Opin. Plant Biol. *20*, 35–46.

Campos, M.L., Yoshida, Y., Major, I.T., De Oliveira Ferreira, D., Weraduwage, S.M., Froehlich, J.E., Johnson, B.F., Kramer, D.M., Jander, G., Sharkey, T.D., et al. (2016). Rewiring of jasmonate and phytochrome B signalling uncouples plant growth-defense tradeoffs. Nat. Commun. *7*.

Cattell, R.B. (1966). The scree test for the number of factors. Multivariate Behav. Res. *1*, 245–276.

Chang, S.S., Park, S.K., Kim, B.C., Kang, B.J., Kim, D.U., and Nam, H.G. (1994). Stable genetic transformation of Arabidopsis thaliana by Agrobacterium inoculation in planta. Plant J. *5*, 551–558.

Chaouch, S., Queval, G., and Noctor, G. (2012). AtRbohF is a crucial modulator of defence-associated metabolism and a key actor in the interplay between

intracellular oxidative stress and pathogenesis responses in Arabidopsis. Plant J. *69*, 613–627.

Chen, Z., Kloek, A.P., Boch, J., Katagiri, F., and Kunkel, B.N. (2000). The Pseudomonas syringae avrRpt2 gene product promotes pathogen virulence from inside plant cells. Mol. Plant. Microbe. Interact. *13*, 1312–1321.

Cheng, S., Willmann, M.R., Chen, H., and Sheen, J. (2002). Update on Calcium Signaling through Protein Kinases . The Arabidopsis Calcium-Dependent Protein Kinase Gene Family 1. Plant Physiol. *129*, 469–485.

Cheong, Y.H., Moon, B.C., Kim, J.K., Kim, C.Y., Kim, M.C., Kim, I.H., Park, C.Y., Kim, J.C., Park, B.O., Koo, S.C., et al. (2003). BWMK1, a rice mitogen-activated protein kinase, locates in the nucleus and mediates pathogenesis-related gene expression by activation of a transcription factor. Plant Physiol. *132*, 1961–1972.

Chinchilla, D., Bauer, Z., Regenass, M., Boller, T., and Georg, F. (2006). The Arabidopsis Receptor Kinase FLS2 Binds flg22 and Determines the Specificity of Flagellin Perception. Plant Cell *18*, 465–476.

Chini, A., Fonseca, S., Fernández, G., Adie, B., Chico, J.M., Lorenzo, O., García-Casado, G., López-Vidriero, I., Lozano, F.M., Ponce, M.R., et al. (2007). The JAZ family of repressors is the missing link in jasmonate signalling. Nature *448*, 666–671.

Chodavarapu, R.K., Feng, S., Bernatavichute, Y. V., Chen, P.-Y., Stroud, H., Yu, Y., Hetzel, J.A., Kuo, F., Kim, J., Cokus, S.J., et al. (2010). Relationship between nucleosome positioning and DNA methylation. Nature *466*, 388–392.

Choi, S.M., Song, H.R., Han, S.K., Han, M., Kim, C.Y., Park, J., Lee, Y.H., Jeon, J.S., Noh, Y.S., and Noh, B. (2012). HDA19 is required for the repression of salicylic acid biosynthesis and salicylic acid-mediated defense responses in Arabidopsis. Plant J. *71*, 135–146.

Clapier, C.R., and Cairns, B.R. (2009). The Biology of Chromatin Remodeling Complexes. Annu. Rev. Biochem. *78*, 273–304.

Cohen-Peer, R., Schuster, S., Meiri, D., Breiman, A., and Avni, A. (2010). Sumoylation of Arabidopsis heat shock factor A2 (HsfA2) modifies its activity

during acquired thermotholerance. Plant Mol. Biol. *74*, 33–45.

Coll, N.S., Epple, P., and Dangl, J.L. (2011). Programmed cell death in the plant immune system. Cell Death Differ. *18*, 1247–1256.

Couto, D., and Zipfel, C. (2016). Regulation of pattern recognition receptor signalling in plants. Nat. Rev. Immunol. *16*, 537–552.

Crevillén, P., Yang, H., Cui, X., Greeff, C., Trick, M., Qiu, Q., Cao, X., and Dean, C. (2014). Epigenetic reprogramming that prevents transgenerational inheritance of the vernalized state. Nature *515*, 587–590.

Cui, H., Tsuda, K., and Parker, J.E. (2015). Effector-Triggered Immunity: From Pathogen Perception to Robust Defense. Annu. Rev. Plant Biol. *66*, 487–511.

Cui, X., Lu, F., Qiu, Q., Zhou, B., Gu, L., Zhang, S., Kang, Y., Cui, X., Ma, X., Yao, Q., et al. (2016). REF6 recognizes a specific DNA sequence to demethylate H3K27me3 and regulate organ boundary formation in Arabidopsis. Nat. Genet. *48*, 694–699.

Cuppels, D.A. (1986). Generation and characterization of Tn5 insertion mutations in Pseudomonas syringae pv. tomato. Appl. Environ. Microbiol. *51*, 323–327.

Cuvier, O., and Fierz, B. (2017). Dynamic chromatin technologies: from individual molecules to epigenomic regulation in cells. Nat. Rev. Genet. *18*, 457–472.

Dadami, E., Boutla, A., Vrettos, N., Tzortzakaki, S., Karakasilioti, I., and Kalantidis, K. (2013). DICER-LIKE 4 But Not DICER-LIKE 2 may have a positive effect on potato spindle tuber viroid accumulation in nicotiana benthamiana. Mol. Plant *6*, 232–234.

Davie, J.R. (2003). Inhibition of histone deacetylase activity by butyrate. J. Nutr. *133*, 2485S–2493S.

Deal, R.B., Topp, C.N., McKinney, E.C., and Meagher, R.B. (2007). Repression of flowering in Arabidopsis requires activation of FLOWERING LOCUS C expression by the histone variant H2A.Z. Plant Cell *19*, 74–83.

Dekker, J., Marti-Renom, M.A., and Mirny, L.A. (2013). Exploring the three-dimensional organization of genomes: Interpreting chromatin interaction data. Nat. Rev. Genet. *14*, 390–403.

Denby, K.J., Kumar, P., and Kliebenstein, D.J. (2004). Identification of Botrytis cinerea susceptibility loci in Arabidopsis thaliana. Plant J. *38*, 473–486.

Denoux, C., Galletti, R., Mammarella, N., Gopalan, S., Werck, D., De Lorenzo, G., Ferrari, S., Ausubel, F.M., and Dewdney, J. (2008). Activation of defense response pathways by OGs and Flg22 elicitors in Arabidopsis seedlings. Mol. Plant *1*, 423–445.

Devoto, A., Nieto-Rostro, M., Xie, D., Ellis, C., Harmston, R., Patrick, E., Davis, J., Sherratt, L., Coleman, M., and Turner, J.G. (2002). COI1 links jasmonate signalling and fertility to the SCF ubiquitin-ligase complex in Arabidopsis. Plant J. *32*, 457–466.

Dobin, A., Davis, C.A., Schlesinger, F., Drenkow, J., Zaleski, C., Jha, S., Batut, P., Chaisson, M., and Gingeras, T.R. (2013). STAR: Ultrafast universal RNA-seq aligner. Bioinformatics *29*, 15–21.

Dodds, P.N., and Rathjen, J.P. (2010). Plant immunity: towards an integrated view of plant–pathogen interactions. Nat. Rev. Genet. *11*, 539–548.

Dong, J., Gao, Z., Liu, S., Li, G., Yang, Z., Huang, H., and Xu, L. (2013). SLIDE, The protein interacting domain of imitation switch remodelers, binds DDT-domain proteins of different subfamilies in chromatin remodeling complexes. J. Integr. Plant Biol. *55*, 928–937.

Dowen, R.H., Pelizzola, M., Schmitz, R.J., Lister, R., Dowen, J.M., Nery, J.R., Dixon, J.E., and Ecker, J.R. (2012). Widespread dynamic DNA methylation in response to biotic stress. Proc. Natl. Acad. Sci. *109*, E2183–E2191.

Drobic, B., Pérez-Cadahía, B., Yu, J., Kung, S.K.P., and Davie, J.R. (2010). Promoter chromatin remodeling of immediate-early genes is mediated through H3 phosphorylation at either serine 28 or 10 by the MSK1 multi-protein complex. Nucleic Acids Res. *38*, 3196–3208.

Dubiella, U., Seybold, H., Durian, G., Komander, E., Lassig, R., Witte, C.-P., Schulze, W.X., and Romeis, T. (2013). Calcium-dependent protein kinase/NADPH oxidase activation circuit is required for rapid defense signal propagation. Proc. Natl. Acad. Sci. *110*, 8744–8749.

Durrant, W.E., and Dong, X. (2004). Systemic acquired resistance. Annu. Rev.

Phytopathol. *42*, 185–209.

Durrant, W.E., Wang, S., and Dong, X. (2007). Arabidopsis SNI1 and RAD51D regulate both gene transcription and DNA recombination during the defense response. Proc. Natl. Acad. Sci. *104*, 4223–4227.

Dyer, P.N., Edayathumangalam, R.S., White, C.L., Bao, Y., Chakravarthy, S., Muthurajan, U.M., and Luger, K. (2004). Reconstitution of Nucleosome Core Particles from Recombinant Histones and DNA. Methods Enzymol. *375*, 23–44.

Earley, K.W., Haag, J.R., Pontes, O., Opper, K., Juehne, T., Song, K., and Pikaard, C.S. (2006). Gateway-compatible vectors for plant functional genomics and proteomics. Plant J. *45*, 616–629.

Elrouby, N., and Coupland, G. (2010). Proteome-wide screens for small ubiquitin-like modifier (SUMO) substrates identify Arabidopsis proteins implicated in diverse biological processes. Proc. Natl. Acad. Sci. *107*, 17415–17420.

Fabro, G., Steinbrenner, J., Coates, M., Ishaque, N., Baxter, L., Studholme, D.J., Körner, E., Allen, R.L., Piquerez, S.J.M., Rougon-Cardoso, A., et al. (2011). Multiple candidate effectors from the oomycete pathogen hyaloperonospora arabidopsidis suppress host plant immunity. PLoS Pathog. *7*.

Fan, J., Crooks, C., and Lamb, C. (2008). High-throughput quantitative luminescence assay of the growth in planta of Pseudomonas syringae chromosomally tagged with Photorhabdus luminescens luxCDABE. Plant J. *53*, 393–399.

Farrona, S. (2004). The Arabidopsis thaliana SNF2 homolog AtBRM controls shoot development and flowering. Development *131*, 4965–4975.

Farrona, S., Hurtado, L., and Reyes, J.C. (2007). A Nucleosome Interaction Module Is Required for Normal Function of Arabidopsis thaliana BRAHMA. J. Mol. Biol. *373*, 240–250.

Fernández-Calvo, P., Chini, A., Fernández-Barbero, G., Chico, J.-M., Gimenez-Ibanez, S., Geerinck, J., Eeckhout, D., Schweizer, F., Godoy, M., Franco-Zorrilla, J.M., et al. (2011). The *Arabidopsis* bHLH Transcription Factors MYC3 and MYC4 Are Targets of JAZ Repressors and Act Additively with MYC2 in the Activation of Jasmonate Responses. Plant Cell *23*, 701–715.

Fernández-Pérez, F., Pomar, F., Pedreño, M.A., and Novo-Uzal, E. (2015). The suppression of AtPrx52 affects fibers but not xylem lignification in Arabidopsis by altering the proportion of syringyl units. Physiol. Plant. *154*, 395–406.

Feys, B., Benedetti, C.E., Penfold, C.N., and Turner, J.G. (1994). Arabidopsis Mutants Selected for Resistance to the Phytotoxin Coronatine Are Male Sterile, Insensitive to Methyl Jasmonate, and Resistant to a Bacterial Pathogen. Plant Cell *6*, 751–759.

Flaus, A., and Owen-Hughes, T. (2011). Mechanisms for ATP-dependent chromatin remodelling: The means to the end. FEBS J. *278*, 3579–3595.

Flaus, A., Martin, D.M.A., Barton, G.J., and Owen-Hughes, T. (2006). Identification of multiple distinct Snf2 subfamilies with conserved structural motifs. Nucleic Acids Res. *34*, 2887–2905.

Fonseca, S., Chini, A., Hamberg, M., Adie, B., Porzel, A., Kramell, R., Miersch, O., Wasternack, C., and Solano, R. (2009). (+)-7-iso-Jasmonoyl-L-isoleucine is the endogenous bioactive jasmonate. Nat. Chem. Biol. *5*, 344–350.

Frei dit Frey, N., Garcia, A., Bigeard, J., Zaag, R., Bueso, E., Garmier, M., Pateyron, S., de Tauzia-Moreau, M.-L., Brunaud, V., Balzergue, S., et al. (2014). Functional analysis of Arabidopsis immune-related MAPKs uncovers a role for MPK3 as negative regulator of inducible defences. Genome Biol. *15*, R87.

Fritsch, O., Benvenuto, G., Bowler, C., Molinier, J., and Hohn, B. (2004). The INO80 Protein Controls Homologous Recombination in Arabidopsis thaliana Short Article. *16*, 479–485.

Fu, Z.Q., and Dong, X. (2013). Systemic Acquired Resistance: Turning Local Infection into Global Defense. Annu. Rev. Plant Biol. *64*, 839–863.

Fu, Z.Q., Yan, S., Saleh, A., Wang, W., Ruble, J., Oka, N., Mohan, R., Spoel, S.H., Tada, Y., Zheng, N., et al. (2012). NPR3 and NPR4 are receptors for the immune signal salicylic acid in plants. Nature *486*, 228–232.

Gao, X., Chen, X., Lin, W., Chen, S., Lu, D., Niu, Y., Li, L., Cheng, C., McCormack, M., Sheen, J., et al. (2013). Bifurcation of Arabidopsis NLR Immune Signaling via Ca2+-Dependent Protein Kinases. PLoS Pathog. *9*.

Gassmann, W., Hinsch, M.E., and Staskawicz, B.J. (1999). The Arabidopsis RPS4

bacterial-resistance gene is a member of the TIR-NBS-LRR family of disease-resistance genes. Plant J. *20*, 265–277.

Gfeller, A., Liechti, R., and Farmer, E.E. (2010). Arabidopsis jasmonate signaling pathway. Sci. Signal. *3*, cm4.

Glauser, G., Grata, E., Dubugnon, L., Rudaz, S., Farmer, E.E., and Wolfender, J.L. (2008). Spatial and temporal dynamics of jasmonate synthesis and accumulation in Arabidopsis in response to wounding. J. Biol. Chem. *283*, 16400–16407.

Glazebrook, J. (2005). Contrasting Mechanisms of Defense Against Biotrophic and Necrotrophic Pathogens. Annu. Rev. Phytopathol. *43*, 205–227.

Gómez-Gómez, L., and Boller, T. (2000). FLS2: An LRR Receptor-like Kinase Involved in the Perception of the Bacterial Elicitor Flagellin in Arabidopsis. Mol. Cell *5*, 1003–1011.

Groth, M., Stroud, H., Feng, S., Greenberg, M.V.C., Vashisht, A.A., Wohlschlegel, J.A., Jacobsen, S.E., and Ausin, I. (2014). SNF2 chromatin remodeler-family proteins FRG1 and -2 are required for RNA-directed DNA methylation. Proc. Natl. Acad. Sci. *111*, 17666–17671.

Gurr, S.J., and Rushton, P.J. (2005). Engineering plants with increased disease resistance: What are we going to express? Trends Biotechnol. *23*, 275–282.

Han, S.-K., Sang, Y., Rodrigues, A., Wu, M.-F., Rodriguez, P.L., and Wagner, D. (2012). The SWI2/SNF2 Chromatin Remodeling ATPase BRAHMA Represses Abscisic Acid Responses in the Absence of the Stress Stimulus in Arabidopsis. Plant Cell *24*, 4892–4906.

Han, Y.-F., Dou, K., Ma, Z.-Y., Zhang, S.-W., Huang, H.-W., Li, L., Cai, T., Chen, S., Zhu, J.-K., and He, X.-J. (2014). SUVR2 is involved in transcriptional gene silencing by associating with SNF2-related chromatin-remodeling proteins in Arabidopsis. Cell Res. *24*, 1445–1465.

Harper, J.F., and Harmon, A. (2005). Plants, symbiosis and parasites: a calcium signalling connection. Nat. Rev. Mol. Cell Biol. *6*, 555–566.

Hatsugai, N., Igarashi, D., Mase, K., Lu, Y., Tsuda, Y., Chakravarthy, S., Wei, H., Foley, J.W., Collmer, A., Glazebrook, J., et al. (2017). A plant effector-triggered immunity signaling sector is inhibited by pattern-triggered immunity. *36*, 2758–

2769.

Hirakawa, T., Hasegawa, J., White, C.I., and Matsunaga, S. (2017). RAD54 forms DNA repair foci in response to DNA damage in living plant cells. Plant J. *90*, 372–382.

Holsters, M., Silva, B., Van Vliet, F., Genetello, C., De Block, M., Dhaese, P., Depicker, A., Inzé, D., Engler, G., Villarroel, R., et al. (1980). The functional organization of the nopaline A. tumefaciens plasmid pTiC58. Plasmid *3*, 212–230.

Honda, S.I., Hongladarom, T., and Laties, G.G. (1966). A new isolation medium for plant organelles. J. Exp. Bot. *17*, 460–472.

van der Hoorn, R.A.L., and Kamoun, S. (2008). From Guard to Decoy: A New Model for Perception of Plant Pathogen Effectors. PLANT CELL ONLINE *20*, 2009–2017.

Hou, Y., Wang, L., Wang, L., Liu, L., Li, L., Sun, L., Rao, Q., Zhang, J., and Huang, S. (2015). JMJ704 positively regulates rice defense response against Xanthomonas oryzae pv. oryzae infection via reducing H3K4me2/3 associated with negative disease resistance regulators. BMC Plant Biol. *15*, 286.

Houben, A., Wako, T., Furushima-Shimogawara, R., Presting, G., Künzel, G., Schubert, I., and Fukui, K. (1999). The cell cycle dependent phosphorylation of histone H3 is correlated with the condensation of plant mitotic chromosomes. Plant J. *18*, 675–679.

Houben, A., Demidov, D., Caperta, A.D., Karimi, R., Agueci, F., and Vlasenko, L. (2007). Phosphorylation of histone H3 in plants-A dynamic affair. Biochim. Biophys. Acta - Gene Struct. Expr. *1769*, 308–315.

Hu, Z., Song, N., Zheng, M., Liu, X., Liu, Z., Xing, J., Ma, J., Guo, W., Yao, Y., Peng, H., et al. (2015). Histone acetyltransferase GCN5 is essential for heat stress-responsive gene activation and thermotolerance in Arabidopsis. Plant J. *84*, 1178–1191.

Huot, B., Yao, J., Montgomery, B.L., and He, S.Y. (2014). Growth-defense tradeoffs in plants: A balancing act to optimize fitness. Mol. Plant *7*, 1267–1287.

HwangBo, K., Son, S.H., Lee, J.S., Min, S.R., Ko, S.M., Liu, J.R., Choi, D., and Jeong,

W.J. (2010). Rapid and simple method for DNA extraction from plant and algal species suitable for PCR amplification using a chelating resin Chelex 100. Plant Biotechnol. Rep. *4*, 49–52.

Iwasaki, M., and Paszkowski, J. (2014). Identification of genes preventing transgenerational transmission of stress-induced epigenetic states. Proc. Natl. Acad. Sci. *111*, 8547–8552.

Janeway, C.A. (1989). Approaching the asymptote? Evolution and revolution in immunology. In Cold Spring Harbor Symposia on Quantitative Biology, pp. 1–13.

Jaskiewicz, M., Conrath, U., and Peterhänsel, C. (2011). Chromatin modification acts as a memory for systemic acquired resistance in the plant stress response. EMBO Rep. *12*, 50–55.

Jenner, R.G., and Young, R.A. (2005). Insights into host responses against pathogens from transcriptional profiling. Nat. Rev. Microbiol. *3*, 281–294.

Johnson, K.C.M., Xia, S., Feng, X., and Li, X. (2015). The Chromatin Remodeler SPLAYED Negatively Regulates SNC1-Mediated Immunity. Plant Cell Physiol. *56*, 1616–1623.

Jones, J.D.G., and Dangl, J.L. (2006). The plant immune system. Nature *444*, 323–329.

Joshi, A.A., and Struhl, K. (2005). Eaf3 chromodomain interaction with methylated H3-K36 links histone deacetylation to pol II elongation. Mol. Cell *20*, 971–978.

Kadota, Y., Goh, T., Tomatsu, H., Tamauchi, R., Higashi, K., Muto, S., and Kuchitsu, K. (2004). Cryptogein-Induced Initial Events in Tobacco BY-2 Cells: Pharmacological Characterization of Molecular Relationship among Cytosolic Ca2+ Transients, Anion Efflux and Production of Reactive Oxygen Species. Plant Cell Physiol. *45*, 160–170.

Kadota, Y., Sklenar, J., Derbyshire, P., Stransfeld, L., Asai, S., Ntoukakis, V., Jones, J.D., Shirasu, K., Menke, F., Jones, A., et al. (2014). Direct Regulation of the NADPH Oxidase RBOHD by the PRR-Associated Kinase BIK1 during Plant Immunity. Mol. Cell *54*, 43–55.

Kadota, Y., Shirasu, K., and Zipfel, C. (2015). Regulation of the NADPH Oxidase

RBOHD during Plant Immunity. Plant Cell Physiol. *56*, 1472–1480.

Kaliappan, K., Choudhury, N.R., Suyal, G., and Mukherjee, S.K. (2012). A novel role for RAD54: this host protein modulates geminiviral DNA replication. FASEB J. *26*, 1142–1160.

Karasov, T.L., Chae, E., Herman, J.J., and Bergelson, J. (2017). Mechanisms to Mitigate the Trade-Off between Growth and Defense. Plant Cell *29*, 666–680.

Katari, M.S., Nowicki, S.D., Aceituno, F.F., Nero, D., Kelfer, J., Thompson, L.P., Cabello, J.M., Davidson, R.S., Goldberg, A.P., Shasha, D.E., et al. (2010). VirtualPlant: A Software Platform to Support Systems Biology Research. Plant Physiol *152*, 500–515.

Katavic, V., Haughn, G.W., Reed, D., Martin, M., and Kunst, L. (1994). In planta transformation of Arabidopsis thaliana. MGG Mol. Gen. Genet. *245*, 363–370.

Katsarou, K., Mavrothalassiti, E., Dermauw, W., Van Leeuwen, T., and Kalantidis, K. (2016). Combined Activity of DCL2 and DCL3 Is Crucial in the Defense against Potato Spindle Tuber Viroid. PLoS Pathog. *12*.

Kilian, J., Whitehead, D., Horak, J., Wanke, D., Weinl, S., Batistic, O., D'Angelo, C., Bornberg-Bauer, E., Kudla, J., and Harter, K. (2007). The AtGenExpress global stress expression data set: Protocols, evaluation and model data analysis of UV-B light, drought and cold stress responses. Plant J. *50*, 347–363.

Kim, M.G., Da Cunha, L., McFall, A.J., Belkhadir, Y., DebRoy, S., Dangl, J.L., and Mackey, D. (2005). Two Pseudomonas syringae type III effectors inhibit RIN4-regulated basal defense in Arabidopsis. Cell *121*, 749–759.

Kimura, S., Kaya, H., Kawarazaki, T., Hiraoka, G., Senzaki, E., Michikawa, M., and Kuchitsu, K. (2012). Protein phosphorylation is a prerequisite for the Ca 2+-dependent activation of Arabidopsis NADPH oxidases and may function as a trigger for the positive feedback regulation of Ca 2+ and reactive oxygen species. Biochim. Biophys. Acta - Mol. Cell Res. *1823*, 398–405.

King, E.O., Ward, M.K., and Raney, D.E. (1954). Two simple media for the demonstration of pyocyanin and fluorescin. J. Lab. Clin. Med. *44*, 301–307.

Klutstein, M., Shaked, H., Sherman, A., Avivi-Ragolsky, N., Shema, E., Zenvirth, D.,

Levy, A.A., and Simchen, G. (2008). Functional conservation of the yeast and Arabidopsis RAD54-like genes. Genetics *178*, 2389–2397.

Knizewski, L., Ginalski, K., and Jerzmanowski, A. (2008). Snf2 proteins in plants: gene silencing and beyond. Trends Plant Sci. *13*, 557–565.

Kong, L., Qiu, X., Kang, J., Wang, Y., Chen, H., Huang, J., Qiu, M., Zhao, Y., Kong, G., Ma, Z., et al. (2017). A Phytophthora Effector Manipulates Host Histone Acetylation and Reprograms Defense Gene Expression to Promote Infection. Curr. Biol. *27*, 981–991.

Kong, W., Chen, N., Liu, T., Zhu, J., Wang, J., He, X., and Jin, Y. (2015). Large-scale transcriptome analysis of cucumber and botrytis cinerea during infection. PLoS One *10*.

Kooistra, S.M., and Helin, K. (2012). Molecular mechanisms and potential functions of histone demethylases. Nat. Rev. Mol. Cell Biol.

Kornberg, R.D. (1974). Chromatin Structure: A Repeating Unit of Histones and DNA. Science (80-.). *184*, 868–871.

Kornberg, R.D., and Lorch, Y. (1999). Twenty-five years of the nucleosome, fundamental particle of the eukaryote chromosome. Cell *98*, 285–294.

Kouzarides, T. (2007). Chromatin Modifications and Their Function. Cell *128*, 693–705.

Krogan, N.J., Keogh, M.C., Datta, N., Sawa, C., Ryan, O.W., Ding, H., Haw, R.A., Pootoolal, J., Tong, A., Canadien, V., et al. (2003). A Snf2 Family ATPase Complex Required for Recruitment of the Histone H2A Variant Htz1. Mol. Cell *12*, 1565–1576.

Krumm, T., Bandemer, K., and Boland, W. (1995). Induction of volatile biosynthesis in the Lima bean (Phaseolus lunatus) by leucine- and isoleucine conjugates of 1-oxo- and 1-hydroxyindan-4-carboxylic acid: evidence for amino acid conjugates of jasmonic acid as intermediates in the octadecanoid signalli. FEBS Lett. *377*, 523–529.

Kunze, G., Zipfel, C., Robatzek, S., Niehaus, K., Boller, T., and Felix, G. (2004). The N Terminus of Bacterial Elongation Factor Tu Elicits Innate Immunity in Arabidopsis Plants. Plant Cell *16*, 3496–3507.

Laemmli, U.K. (1970). Cleavage of structural proteins during the assembly of the head of bacteriophage T4. Nature *227*, 680–685.

Langham, R.J., Walsh, J., Dunn, M., Ko, C., Goff, S.A., and Freeling, M. (2004). Genomic Duplication, Fractionation and the Origin of Regulatory Novelty. Genetics *166*, 935–945.

Latrasse, D., Jégu, T., Li, H., de Zelicourt, A., Raynaud, C., Legras, S., Gust, A., Samajova, O., Veluchamy, A., Rayapuram, N., et al. (2017). MAPK-triggered chromatin reprogramming by histone deacetylase in plant innate immunity. Genome Biol. *18*, 131.

Lee, S.C., and Luan, S. (2012). ABA signal transduction at the crossroad of biotic and abiotic stress responses. Plant. Cell Environ. *35*, 53–60.

Lee, S., Seo, P.J., Lee, H.J., and Park, C.M. (2012). A NAC transcription factor NTL4 promotes reactive oxygen species production during drought-induced leaf senescence in Arabidopsis. Plant J. *70*, 831–844.

Lee, S., Fu, F., Xu, S., Lee, S.Y., Yun, D.-J., and Mengiste, T. (2016). Global regulation of plant immunity by histone lysine methyl transferases. Plant Cell tpc.00012.2016.

Lemarié, S., Robert-Seilaniantz, A., Lariagon, C., Lemoine, J., Marnet, N., Jubault, M., Manzanares-Dauleux, M.J., and Gravot, A. (2015). Both the Jasmonic Acid and the Salicylic Acid Pathways Contribute to Resistance to the Biotrophic Clubroot Agent Plasmodiophora brassicae in Arabidopsis. Plant Cell Physiol. *56*, 2158–2168.

Lewis, L.A., Polanski, K., de Torres-Zabala, M., Jayaraman, S., Bowden, L., Moore, J., Penfold, C.A., Jenkins, D.J., Hill, C., Baxter, L., et al. (2015). Transcriptional Dynamics Driving MAMP-Triggered Immunity and Pathogen Effector-Mediated Immunosuppression in Arabidopsis Leaves Following Infection with *Pseudomonas syringae* pv tomato DC3000. Plant Cell *27*, 3038–3064.

Li, B., Carey, M., and Workman, J.L. (2007). The Role of Chromatin during Transcription. Cell *128*, 707–719.

Li, C., Chen, C., Gao, L., Yang, S., Nguyen, V., Shi, X., Siminovitch, K., Kohalmi, S.E., Huang, S., Wu, K., et al. (2015a). The Arabidopsis SWI2/SNF2 Chromatin

Remodeler BRAHMA Regulates Polycomb Function during Vegetative Development and Directly Activates the Flowering Repressor Gene SVP. PLoS Genet. *11*.

Li, C., Gu, L., Gao, L., Chen, C., Wei, C.-Q., Qiu, Q., Chien, C.-W., Wang, S., Jiang, L., Ai, L.-F., et al. (2016). Concerted genomic targeting of H3K27 demethylase REF6 and chromatin-remodeling ATPase BRM in Arabidopsis. Nat. Genet. *48*, 687–693.

Li, F., Cheng, C., Cui, F., De Oliveira, M.V.V., Yu, X., Meng, X., Intorne, A.C., Babilonia, K., Li, M., Li, B., et al. (2014a). Modulation of RNA polymerase II phosphorylation downstream of pathogen perception orchestrates plant immunity. Cell Host Microbe *16*, 748–758.

Li, G., Zhang, J., Li, J., Yang, Z., Huang, H., and Xu, L. (2012). Imitation Switch chromatin remodeling factors and their interacting RINGLET proteins act together in controlling the plant vegetative phase in Arabidopsis. Plant J. *72*, 261–270.

Li, G., Liu, S., Wang, J., He, J., Huang, H., Zhang, Y., and Xu, L. (2014b). ISWI proteins participate in the genome-wide nucleosome distribution in Arabidopsis. Plant J. *78*, 706–714.

Li, J., Zhong, R., and Palva, E.T. (2017). WRKY70 and its homolog WRKY54 negatively modulate the cell wall-associated defenses to necrotrophic pathogens in Arabidopsis. PLoS One *12*, e0183731.

Li, R., Zhang, J., Li, J., Zhou, G., Wang, Q., Bian, W., Erb, M., and Lou, Y. (2015b). Prioritizing plant defence over growth through WRKY regulation facilitates infestation by non-target herbivores. Elife *4*.

Li, T., Chen, X., Zhong, X., Zhao, Y., Liu, X., Zhou, S., Cheng, S., and Zhou, D.-X. (2013). Jumonji C Domain Protein JMJ705-Mediated Removal of Histone H3 Lysine 27 Trimethylation Is Involved in Defense-Related Gene Activation in Rice. Plant Cell *25*, 4725–4736.

Li, X., Zhang, Y., Clarke, J.D., Li, Y., and Dong, X. (1999). Identification and cloning of a negative regulator of systemic acquired resistance, SNI1, through a screen for suppressors of npr1-1. Cell *98*, 329–339.

Li, X., Jiang, Y., Ji, Z., Liu, Y., and Zhang, Q. (2015c). BRHIS1 suppresses rice innate immunity through binding to monoubiquitinated H2A and H2B variants. EMBO Rep. *16*, 1192–1202.

Li, Y., Tessaro, M.J., Li, X., and Zhang, Y. (2010). Regulation of the Expression of Plant Resistance Gene SNC1 by a Protein with a Conserved BAT2 Domain. PLANT Physiol. *153*, 1425–1434.

Lieberman-Aiden, E., Van Berkum, N.L., Williams, L., Imakaev, M., Ragoczy, T., Telling, A., Amit, I., Lajoie, B.R., Sabo, P.J., Dorschner, M.O., et al. (2009). Comprehensive mapping of long-range interactions reveals folding principles of the human genome. Science (80-.). *326*, 289–293.

Lin, N.C., and Martin, G.B. (2005). An avrPto/avrPtoB mutant of Pseudomonas syringae pv. tomato DC3000 does not elicit Pto-mediated resistance and is less virulent on tomato. Mol Plant-Microbe Interact *18*, 43–51.

Liu, N., Fromm, M., and Avramova, Z. (2014). H3K27me3 and H3K4me3 chromatin environment at super-induced dehydration stress memory genes of arabidopsis thaliana. Mol. Plant *7*, 502–513.

Liu, X., Li, M., Xia, X., Li, X., and Chen, Z. (2017). Mechanism of chromatin remodelling revealed by the Snf2-nucleosome structure. Nature *544*, 440–445.

Liu, Y., Tian, T., Zhang, K., You, Q., Yan, H., Zhao, N., Yi, X., Xu, W., and Su, Z. (2018). PCSD: a plant chromatin state database. Nucleic Acids Res. *46*, D1157–D1167.

Livak, K.J., and Schmittgen, T.D. (2001). Analysis of relative gene expression data using real-time quantitative PCR and the 2(-Delta Delta C(T)) Method. Methods *25*, 402–408.

Lopez-Gonzalez, L., Mouriz, A., Narro-Diego, L., Bustos, R., Martinez-Zapater, J.M., Jarillo, J.A., and Pineiro, M. (2014). Chromatin-Dependent Repression of the Arabidopsis Floral Integrator Genes Involves Plant Specific PHD-Containing Proteins. Plant Cell *26*, 3922–3938.

Lou, Y.-R., Bor, M., Yan, J., Preuss, A.S., and Jander, G. (2016). Arabidopsis NATA1 acetylates putrescine and decreases defense-related hydrogen peroxide accumulation. Plant Physiol. pp.00446.2016.

Love, M.I., Huber, W., and Anders, S. (2014). Moderated estimation of fold change and dispersion for RNA-seq data with DESeq2. Genome Biol. *15*, 550.

Lozano-Durán, R., and Zipfel, C. (2015). Trade-off between growth and immunity: Role of brassinosteroids. Trends Plant Sci. *20*, 12–19.

Lu, D., Lin, W., Gao, X., Wu, S., Cheng, C., Avila, J., Heese, A., Devarenne, T.P., He, P., and Shan, L. (2011a). Direct Ubiquitination of Pattern Recognition Receptor FLS2 Attenuates Plant Innate Immunity. Science (80-.). *332*, 1439–1442.

Lu, F., Cui, X., Zhang, S., Jenuwein, T., and Cao, X. (2011b). Arabidopsis REF6 is a histone H3 lysine 27 demethylase. Nat. Genet. *43*, 715–719.

De Lucia, F., Crevillen, P., Jones, A.M.E., Greb, T., and Dean, C. (2008). A PHD-Polycomb Repressive Complex 2 triggers the epigenetic silencing of FLC during vernalization. Proc. Natl. Acad. Sci. *105*, 16831–16836.

Ludwig, A.A., Romeis, T., and Jones, J.D.G. (2004). CDPK-mediated signalling pathways: Specificity and cross-talk. In Journal of Experimental Botany, pp. 181–188.

Luger, K., Mäder, a W., Richmond, R.K., Sargent, D.F., and Richmond, T.J. (1997). Crystal structure of the nucleosome core particle at 2.8 A resolution. Nature *389*, 251–260.

Luna, E., Bruce, T.J.A., Roberts, M.R., Flors, V., and Ton, J. (2012). Next-Generation Systemic Acquired Resistance. Plant Physiol. *158*, 844–853.

Ma, K.-W., Flores, C., and Ma, W. (2011). Chromatin Configuration as a Battlefield in Plant-Bacteria Interactions. Plant Physiol. *157*, 535–543.

Macho, A.P., and Zipfel, C. (2014). Plant PRRs and the activation of innate immune signaling. Mol. Cell *54*, 263–272.

Maier, F., Zwicker, S., Hückelhoven, A., Meissner, M., Funk, J., Pfitzner, A.J.P., and Pfitzner, U.M. (2011). Nonexpressor Of Pathogenesis-Related Proteins1 (NPR1) and some NPR1-related proteins are sensitive to salicylic acid. Mol. Plant Pathol. *12*, 73–91.

March-Díaz, R., García-Domínguez, M., Lozano-Juste, J., León, J., Florencio, F.J.,

and Reyes, J.C. (2008). Histone H2A.Z and homologues of components of the SWR1 complex are required to control immunity in Arabidopsis. Plant J. *53*, 475–487.

Marino, D., Dunand, C., Puppo, A., and Pauly, N. (2012). A burst of plant NADPH oxidases. Trends Plant Sci. *17*, 9–15.

Mbengue, M., Navaud, O., Peyraud, R., Barascud, M., Badet, T., Vincent, R., Barbacci, A., and Raffaele, S. (2016). Emerging Trends in Molecular Interactions between Plants and the Broad Host Range Fungal Pathogens Botrytis cinerea and Sclerotinia sclerotiorum. Front. Plant Sci. *7*.

Mittler, R., Vanderauwera, S., Suzuki, N., Miller, G., Tognetti, V.B., Vandepoele, K., Gollery, M., Shulaev, V., and Van Breusegem, F. (2011). ROS signaling: The new wave? Trends Plant Sci. *16*, 300–309.

Miya, A., Albert, P., Shinya, T., Desaki, Y., Ichimura, K., Shirasu, K., Narusaka, Y., Kawakami, N., Kaku, H., and Shibuya, N. (2007). CERK1, a LysM receptor kinase, is essential for chitin elicitor signaling in Arabidopsis. Proc. Natl. Acad. Sci. U. S. A. *104*, 19613–19618.

Mozgová, I., Wildhaber, T., Liu, Q., Abou-Mansour, E., L'Haridon, F., Métraux, J.-P., Gruissem, W., Hofius, D., and Hennig, L. (2015). Chromatin assembly factor CAF-1 represses priming of plant defence response genes. Nat. Plants *1*, 15127.

Mur, L.A.J., Kenton, P., Lloyd, A.J., Ougham, H., and Prats, E. (2008). The hypersensitive response; The centenary is upon us but how much do we know? In Journal of Experimental Botany, pp. 501–520.

Narro-Diego, L., López-González, L., Jarillo, J.A., and Piñeiro, M. (2017). The PHD-containing protein EARLY BOLTING IN SHORT DAYS regulates seed dormancy in Arabidopsis. Plant. Cell Environ. 2393–2405.

Nasmyth, K., Stillman, D., and Kipling, D. (1987). Both positive and negative regulators of HO transcription are required for mother-cell-specific mating-type switching in yeast. Cell *48*, 579–587.

Navarro, L., Navarro, L., Zipfel, C., Zipfel, C., Rowland, O., Rowland, O., Keller, I., Keller, I., Robatzek, S., Robatzek, S., et al. (2004). The Transcriptional Innate Immune Response to g22. Interplay and Overlap with Avr Gene-Dependent

Defense Responses and Bacterial Pathogenesis. Plant Physiol. *135*, 1113–1128.

Nishizawa, A., Yabuta, Y., Yoshida, E., Maruta, T., Yoshimura, K., and Shigeoka, S. (2006). Arabidopsis heat shock transcription factor A2 as a key regulator in response to several types of environmental stress. Plant J. *48*, 535–547.

Noctor, G., Reichheld, J.P., and Foyer, C.H. (2017). ROS-related redox regulation and signaling in plants. Semin. Cell Dev. Biol.

Noh, B., Lee, S.-H., Kim, H.-J., Yi, G., Shin, E.-A., Lee, M., Jung, K.-J., Doyle, M.R., Amasino, R.M., and Noh, Y.-S. (2004). Divergent Roles of a Pair of Homologous Jumonji/Zinc-Finger-Class Transcription Factor Proteins in the Regulation of Arabidopsis Flowering Time. Plant Cell *16*, 2601–2613.

Ntoukakis, V., Mucyn, T.S., Gimenez-Ibanez, S., Chapman, H.C., Gutierrez, J.R., Balmuth, A.L., Jones, A.M.E., and Rathjen, J.P. (2009). Host Inhibition of a Bacterial Virulence Effector Triggers Immunity to Infection. Science (80-.). *324*, 784–787.

Oh, S., Park, S., and Van Nocker, S. (2008). Genic and global functions for Paf1C in chromatin modification and gene expression in arabidopsis. PLoS Genet. *4*.

Oliveros, J.C. (2007). VENNY. An interactive tool for comparing lists with Venn Diagrams. BioinfoGP of CNB-CSIC http://bioinfogp.cnnb.csic.es/tools/venny/index.ht.

Osakabe, K., Yoshioka, T., Ichikawa, H., and Toki, S. (2002). Molecular cloning and characterization of RAD51-like genes from Arabidopsis thaliana. Plant Mol. Biol. *50*, 71–81.

Osakabe, K., Abe, K., Yoshioka, T., Osakabe, Y., Todoriki, S., Ichikawa, H., Hohn, B., and Toki, S. (2006). Isolation and characterization of the *RAD54* gene from *Arabidopsis thaliana*. Plant J. *48*, 827–842.

Pagnussat, G.C., Yu, H.-J., Ngo, Q. a, Rajani, S., Mayalagu, S., Johnson, C.S., Capron, A., Xie, L.-F., Ye, D., and Sundaresan, V. (2005). Genetic and molecular identification of genes required for female gametophyte development and function in Arabidopsis. Development *132*, 603–614.

Pape, S., Thurow, C., and Gatz, C. (2010). The Arabidopsis PR-1 Promoter Contains Multiple Integration Sites for the Coactivator NPR1 and the Repressor SNI1.

PLANT Physiol. *154*, 1805–1818.

Park, J., Oh, D.-H., Dassanayake, M., Nguyen, K.T., Ogas, J., Choi, G., and Sun, T. (2017). Gibberellin Signaling Requires Chromatin Remodeler PICKLE to Promote Vegetative Growth and Phase Transitions. Plant Physiol. *173*, 1463–1474.

Pauwels, L., and Goossens, A. (2011). The JAZ Proteins: A Crucial Interface in the Jasmonate Signaling Cascade. Plant Cell *23*, 3089–3100.

Peirats-Llobet, M., Han, S.K., Gonzalez-Guzman, M., Jeong, C.W., Rodriguez, L., Belda-Palazon, B., Wagner, D., and Rodriguez, P.L. (2016). A Direct Link between Abscisic Acid Sensing and the Chromatin-Remodeling ATPase BRAHMA via Core ABA Signaling Pathway Components. Mol. Plant *9*, 136–147.

Penaloza-Vazquez, A., Preston, G.M., Collmer, A., and Bender, C.L. (2000). Regulatory interactions between the Hrp type III protein secretion system and coronatine biosynthesis in Pseudomonas syringae pv. tomato DC3000. Microbiology *146*, 2447–2456.

Pokholok, D.K., Zeitlinger, J., Hannett, N.M., Reynolds, D.B., and Young, R.A. (2006). Activated Signal Transduction Kinases Frequently Occupy Target Genes. Science (80-.). *313*, 533–536.

Qi, Y., Tsuda, K., Glazebrook, J., and Katagiri, F. (2011). Physical association of pattern-triggered immunity (PTI) and effector-triggered immunity (ETI) immune receptors in Arabidopsis. Mol. Plant Pathol. *12*, 702–708.

Qiu, J.-L., Fiil, B.K., Petersen, K., Nielsen, H.B., Botanga, C.J., Thorgrimsen, S., Palma, K., Suarez-Rodriguez, M.C., Sandbech-Clausen, S., Lichota, J., et al. (2008). Arabidopsis MAP kinase 4 regulates gene expression through transcription factor release in the nucleus. EMBO J. *27*, 2214–2221.

Rajjou, L., Duval, M., Gallardo, K., Catusse, J., Bally, J., Job, C., and Job, D. (2012). Seed Germination and Vigor. Annu. Rev. Plant Biol. *63*, 507–533.

Rando, O.J., and Chang, H.Y. (2009). Genome-Wide Views of Chromatin Structure. Annu. Rev. Biochem. *78*, 245–271.

Ranf, S., Gisch, N., Schäffer, M., Illig, T., Westphal, L., Knirel, Y.A., Sánchez-

Carballo, P.M., Zähringer, U., Hückelhoven, R., Lee, J., et al. (2015). A lectin S-domain receptor kinase mediates lipopolysaccharide sensing in Arabidopsis thaliana. Nat. Immunol. *16*, 426–433.

Richter, K.S., Ende, L., and Jeske, H. (2015). Rad54 is not essential for any geminiviral replication mode in planta. Plant Mol. Biol. *87*, 193–202.

Robert-Seilaniantz, A., Grant, M., and Jones, J.D.G. (2011). Hormone Crosstalk in Plant Disease and Defense: More Than Just JASMONATE-SALICYLATE Antagonism. Annu. Rev. Phytopathol. *49*, 317–343.

Rodriguez, E., El Ghoul, H., Mundy, J., and Petersen, M. (2016). Making sense of plant autoimmunity and "negative regulators." FEBS J. *283*, 1385–1391.

Rodriguez-Granados, N.Y., Ramirez-Prado, J.S., Veluchamy, A., Latrasse, D., Raynaud, C., Crespi, M., Ariel, F., and Benhamed, M. (2016). Put your 3D glasses on: Plant chromatin is on show. J. Exp. Bot. *67*, 3205–3221.

Roitinger, E., Hofer, M., Köcher, T., Pichler, P., Novatchkova, M., Yang, J., Schlögelhofer, P., and Mechtler, K. (2015). Quantitative Phosphoproteomics of the Ataxia Telangiectasia-Mutated (ATM) and Ataxia Telangiectasia-Mutated and Rad3-related (ATR) Dependent DNA Damage Response in *Arabidopsis thaliana*. Mol. Cell. Proteomics *14*, 556–571.

Rosa, S., and Shaw, P. (2013). Insights into Chromatin Structure and Dynamics in Plants. Biology (Basel). *2*, 1378–1410.

Rosa, S., Ntoukakis, V., Ohmido, N., Pendle, A., Abranches, R., and Shaw, P. (2014). Cell Differentiation and Development in Arabidopsis Are Associated with Changes in Histone Dynamics at the Single-Cell Level. Plant Cell *26*, 1–14.

Roudier, F., Ahmed, I., Bérard, C., Sarazin, A., Mary-Huard, T., Cortijo, S., Bouyer, D., Caillieux, E., Duvernois-Berthet, E., Al-Shikhley, L., et al. (2011). Integrative epigenomic mapping defines four main chromatin states in Arabidopsis. EMBO J. *30*, 1928–1938.

Sachs, M., Onodera, C., Blaschke, K., Ebata, K., Song, J., and Ramalho-Santos, M. (2013). Bivalent Chromatin Marks Developmental Regulatory Genes in the Mouse Embryonic Germline InVivo. Cell Rep. *3*, 1777–1784.

Sambrook, J., and Maniatis, T. (1989). Molecular Cloning: A Laboratory Manual.

Sang, Y., Silva-Ortega, C.O., Wu, S., Yamaguchi, N., Wu, M.F., Pfluger, J., Gillmor, C.S., Gallagher, K.L., and Wagner, D. (2012). Mutations in two non-canonical Arabidopsis SWI2/SNF2 chromatin remodeling ATPases cause embryogenesis and stem cell maintenance defects. Plant J. *72*, 1000–1014.

Schmid, M., Davison, T.S., Henz, S.R., Pape, U.J., Demar, M., Vingron, M., Schölkopf, B., Weigel, D., and Lohmann, J.U. (2005). A gene expression map of Arabidopsis thaliana development. Nat. Genet. *37*, 501–506.

Schurch, N.J., Schofield, P., Gierliński, M., Cole, C., Sherstnev, A., Singh, V., Wrobel, N., Gharbi, K., Simpson, G., Owen-Hughes, T., et al. (2016). How many biological replicates are needed in an RNA-seq\nexperiment and which differential expression tool should you use? RNA.

Sequeira-Mendes, J., Araguez, I., Peiro, R., Mendez-Giraldez, R., Zhang, X., Jacobsen, S.E., Bastolla, U., and Gutierrez, C. (2014). The Functional Topography of the Arabidopsis Genome Is Organized in a Reduced Number of Linear Motifs of Chromatin States. Plant Cell *26*, 2351–2366.

Sessions, A., Burke, E., Presting, G., Aux, G., McElver, J., Patton, D., Dietrich, B., Ho, P., Bacwaden, J., Ko, C., et al. (2002). A High-Throughput Arabidopsis Reverse Genetics System. Plant Cell *14*, 2985–2994.

Shaked, H., Avivi-Ragolsky, N., and Levy, A.A. (2006). Involvement of the arabidopsis SWI2/SNF2 chromatin remodeling gene family in DNA damage response and recombination. Genetics *173*, 985–994.

Shilatifard, A. (2012). The COMPASS Family of Histone H3K4 Methylases: Mechanisms of Regulation in Development and Disease Pathogenesis. Annu. Rev. Biochem. *81*, 65–95.

Shirasu, K., Nakajima, H., Rajasekhar, V.K., Dixon, R.A., and Lamb, C. (1997). Salicylic Acid Potentiates an Agonist-Dependent Gain Control That Amplifies Pathogen Signals in the Activation of Defense Mechanisms. Plant Cell *9*, 261.

Singh, P., Yekondi, S., Chen, P.-W., Tsai, C.-H., Yu, C.-W., Wu, K., and Zimmerli, L. (2014). Environmental History Modulates Arabidopsis Pattern-Triggered Immunity in a HISTONE ACETYLTRANSFERASE1-Dependent Manner. Plant Cell *26*, 2676–2688.

Singleton, M.R., Dillingham, M.S., and Wigley, D.B. (2007). Structure and Mechanism of Helicases and Nucleic Acid Translocases. Annu. Rev. Biochem. *76*, 23–50.

Sirinakis, G., Clapier, C.R., Gao, Y., Viswanathan, R., Cairns, B.R., and Zhang, Y. (2011). The RSC chromatin remodelling ATPase translocates DNA with high force and small step size. EMBO J. *30*, 2364–2372.

Sollars, E.S.A., Harper, A.L., Kelly, L.J., Sambles, C.M., Ramirez-Gonzalez, R.H., Swarbreck, D., Kaithakottil, G., Cooper, E.D., Uauy, C., Havlickova, L., et al. (2016). Genome sequence and genetic diversity of European ash trees. Nature *541*, 212–216.

Song, J., Durrant, W.E., Wang, S., Yan, S., Tan, E.H., and Dong, X. (2011). DNA repair proteins are directly involved in regulation of gene expression during plant immune response. Cell Host Microbe *9*, 115–124.

Spoel, S., Koornneef, A., Claessens, S., Korzelius, J., Van Pelt, J., Mueller, M., Buchala, A., Métraux, J., Brown, R., Kazan, K., et al. (2003). NPR1 Modulates Cross-Talk between Salicylate- and Jasmonate-Dependent Defense Pathways through a Novel Function in the Cytosol. Plant Cell *15*, 760–770.

Spoel, S.H., Mou, Z., Tada, Y., Spivey, N.W., Genschik, P., and Dong, X. (2009). Proteasome-Mediated Turnover of the Transcription Coactivator NPR1 Plays Dual Roles in Regulating Plant Immunity. Cell *137*, 860–872.

Stec, N., Banasiak, J., and Jasiński, M. (2016). Abscisic acid - an overlooked player in plant-microbe symbioses formation? Acta Biochim. Pol. *63*, 53–58.

Stern, M., Jensen, R., and Herskowitz, I. (1984). Five SWI genes are required for expression of the HO gene in yeast. J. Mol. Biol. *178*, 853–868.

Sundaresan, V., Springer, P., Volpe, T., Haward, S., Jones, J.D.G., Dean, C., Ma, H., and Martienssen, R. (1995). Patterns of gene action in plant development revealed by enhancer trap and gene trap transposable elements. Genes Dev. *9*, 1797–1810.

Sung, S., and Amasino, R.M. (2004). Vernalization in Arabidopsis thaliana is mediated by the PHD finger protein VIN3. Nature *427*, 159–164.

Swain, T., and Hillis, W.E. (1959). The phenolic constituents of Prunus domestica.

I.—The quantitative analysis of phenolic constituents. J. Sci. Food Agric. *10*, 63–68.

Tambini, C.E., Spink, K.G., Ross, C.J., Hill, M.A., and Thacker, J. (2010). The importance of XRCC2 in RAD51-related DNA damage repair. DNA Repair (Amst). *9*, 517–525.

Tang, L., Nogales, E., and Ciferri, C. (2010). Structure and function of SWI/SNF chromatin remodeling complexes and mechanistic implications for transcription. Prog. Biophys. Mol. Biol. *102*, 122–128.

Tao, Y., Xie, Z., Chen, W., Glazebrook, J., Chang, H.-S., Han, B., Zhu, T., Zou, G., and Katagiri, F. (2003). Quantitative nature of Arabidopsis responses during compatible and incompatible interactions with the bacterial pathogen Pseudomonas syringae. Plant Cell *15*, 317–330.

Tena, G., Boudsocq, M., and Sheen, J. (2011). Protein kinase signaling networks in plant innate immunity. Curr. Opin. Plant Biol. *14*, 519–529.

Thines, B., Katsir, L., Melotto, M., Niu, Y., Mandaokar, A., Liu, G., Nomura, K., He, S.Y., Howe, G.A., and Browse, J. (2007). JAZ repressor proteins are targets of the SCFCOI1 complex during jasmonate signalling. Nature *448*, 661–665.

Tian, D., Traw, M.B., Chen, J.Q., Kreitman, M., and Bergelson, J. (2003). Fitness costs of R-gene-mediated resistance in Arabidopsis thaliana. Nature *423*, 74–77.

Tian, S., Wang, X., Li, P., Wang, H., Ji, H., Xie, J., Qiu, Q., Shen, D., and Dong, H. (2016). Plant Aquaporin AtPIP1;4 Links Apoplastic H(2)O(2) Induction to Disease Immunity Pathways. Plant Physiol. *171*, 1635–1650.

Ton, J., Flors, V., and Mauch-Mani, B. (2009). The multifaceted role of ABA in disease resistance. Trends Plant Sci. *14*, 310–317.

Torres, M.A., Dangl, J.L., and Jones, J.D.G. (2002). Arabidopsis gp91phox homologues AtrbohD and AtrbohF are required for accumulation of reactive oxygen intermediates in the plant defense response. Proc. Natl. Acad. Sci. *99*, 517–522.

de Torres-Zabala, M., Truman, W., Bennett, M.H., Lafforgue, G., Mansfield, J.W., Rodriguez Egea, P., Bögre, L., and Grant, M. (2007). Pseudomonas syringae pv. tomato hijacks the Arabidopsis abscisic acid signalling pathway to cause

disease. EMBO J. *26*, 1434–1443.

de Torres Zabala, M., Littlejohn, G., Jayaraman, S., Studholme, D., Bailey, T., Lawson, T., Tillich, M., Licht, D., Bölter, B., Delfino, L., et al. (2015). Chloroplasts play a central role in plant defence and are targeted by pathogen effectors. Nat. Plants *1*, 15074.

Toufighi, K., Brady, S.M., Austin, R., Ly, E., and Provart, N.J. (2005). The botany array resource: e-Northerns, expression angling, and promoter analyses. Plant J. *43*, 153–163.

Tsuda, K., and Somssich, I.E. (2015). Transcriptional networks in plant immunity. New Phytol. *206*, 932–947.

Tsuda, K., Sato, M., Stoddard, T., Glazebrook, J., and Katagiri, F. (2009). Network properties of robust immunity in plants. PLoS Genet. *5*.

Tucker, H.G. (1959). A Generalization of the Glivenko-Cantelli Theorem. Ann. Math. Stat. *30*, 828–830.

Turck, F., Roudier, F., Farrona, S., Martin-Magniette, M.L., Guillaume, E., Buisine, N., Gagnot, S., Martienssen, R.A., Coupland, G., and Colot, V. (2007). Arabidopsis TFL2/LHP1 specifically associates with genes marked by trimethylation of histone H3 lysine 27. PLoS Genet. *3*, 0855–0866.

Vinatzer, B.A., Teitzel, G.M., Lee, M.W., Jelenska, J., Hotton, S., Fairfax, K., Jenrette, J., and Greenberg, J.T. (2006). The type III effector repertoire of Pseudomonas syringae pv. syringae B728a and its role in survival and disease on host and non-host plants. Mol. Microbiol. *62*, 26–44.

Vongs, a, Kakutani, T., Martienssen, R. a, and Richards, E.J. (1993). Arabidopsis thaliana DNA methylation mutants. Science *260*, 1926–1928.

Wagner, D., and Meyerowitz, E.M. (2002). SPLAYED, a novel SWI/SNF ATPase homolog, controls reproductive development in Arabidopsis. Curr. Biol. *12*, 85–94.

Walley, J.W., Rowe, H.C., Xiao, Y., Chehab, E.W., Kliebenstein, D.J., Wagner, D., and Dehesh, K. (2008). The chromatin remodeler SPLAYED regulates specific stress signaling pathways. PLoS Pathog. *4*, 1–8.

Wan, J., Zhang, X.-C., Neece, D., Ramonell, K.M., Clough, S., Kim, S. -y., Stacey, M.G., and Stacey, G. (2008). A LysM Receptor-Like Kinase Plays a Critical Role in Chitin Signaling and Fungal Resistance in Arabidopsis. Plant Cell *20*, 471–481.

Wang, Y., and Bouwmeester, K. (2017). L-type lectin receptor kinases: New forces in plant immunity. PLoS Pathog. *13*.

Wang, L., Wuerffel, R., Feldman, S., Khamlichi, A.A., and Kenter, A.L. (2009). S region sequence, RNA polymerase II, and histone modifications create chromatin accessibility during class switch recombination. J. Exp. Med. *206*, 1817–1830.

Wang, L., Tsuda, K., Truman, W., Sato, M., Nguyen, L. V., Katagiri, F., and Glazebrook, J. (2011). CBP60g and SARD1 play partially redundant critical roles in salicylic acid signaling. Plant J. *67*, 1029–1041.

Wang, L., Kim, J., and Somers, D.E. (2013). Transcriptional corepressor TOPLESS complexes with pseudoresponse regulator proteins and histone deacetylases to regulate circadian transcription. Proc. Natl. Acad. Sci. *110*, 761–766.

Wang, S., Durrant, W.E., Song, J., Spivey, N.W., and Dong, X. (2010). Arabidopsis BRCA2 and RAD51 proteins are specifically involved in defense gene transcription during plant immune responses. Proc. Natl. Acad. Sci. *107*, 22716–22721.

Wang, Y., Weide, R., Govers, F., and Bouwmeester, K. (2015a). L-type lectin receptor kinases in Nicotiana benthamiana and tomato and their role in Phytophthora resistance. J. Exp. Bot. *66*, 6731–6743.

Wang, Z., Casas-Mollano, J.A., Xu, J., Riethoven, J.-J.M., Zhang, C., and Cerutti, H. (2015b). Osmotic stress induces phosphorylation of histone H3 at threonine 3 in pericentromeric regions of Arabidopsis thaliana. Proc. Natl. Acad. Sci. U. S. A. *112*, 8487–8492.

Whalen, M.C., Innes, R.W., Bent, A.F., and Staskawicz, B.J. (1991). Identification of Pseudomonas syringae Pathogens of Arabidopsis and a Bacterial Locus Determining Avirulence on Both Arabidopsis and Soybean. Plant Cell *3*, 49–59.

Windram, O., Madhou, P., McHattie, S., Hill, C., Hickman, R., Cooke, E., Jenkins,

D.J., Penfold, C.A., Baxter, L., Breeze, E., et al. (2012). Arabidopsis Defense against Botrytis cinerea: Chronology and Regulation Deciphered by High-Resolution Temporal Transcriptomic Analysis. Plant Cell *24*, 3530–3557.

Woody, S.T., Austin-Phillips, S., Amasino, R.M., and Krysan, P.J. (2007). The WiscDsLox T-DNA collection: An arabidopsis community resource generated by using an improved high-throughput T-DNA sequencing pipeline. J. Plant Res. *120*, 157–165.

Wu, K., Zhang, L., Zhou, C., Yu, C.W., and Chaikam, V. (2008). HDA6 is required for jasmonate response, senescence and flowering in Arabidopsis. J. Exp. Bot. *59*, 225–234.

Wu, M., Sang, Y., Bezhani, S., Yamaguchi, N., Han, S., Li, Z., Su, Y., Slewinski, T.L., and Wagner, D. (2012a). SWI2/SNF2 chromatin remodeling ATPases overcome polycomb repression and control floral organ identity with the LEAFY and SEPALLATA3 transcription factors. Pnas *109*, 3576–3581.

Wu, S., Shan, L., and He, P. (2014). Microbial signature-triggered plant defense responses and early signaling mechanisms. Plant Sci. *228*, 118–126.

Wu, Y., Zhang, D., Chu, J.Y., Boyle, P., Wang, Y., Brindle, I.D., De Luca, V., and Després, C. (2012b). The Arabidopsis NPR1 Protein Is a Receptor for the Plant Defense Hormone Salicylic Acid. Cell Rep. *1*, 639–647.

Xie, D.X., Feys, B.F., James, S., Nieto-Rostro, M., and Turner, J.G. (1998). COI1: An Arabidopsis gene required for jasmonate-regulated defense and fertility. Science (80-.). *280*, 1091–1094.

Xin, X.-F., and He, S.Y. (2013). Pseudomonas syringae pv. tomato DC3000: a model pathogen for probing disease susceptibility and hormone signaling in plants. Annu. Rev. Phytopathol. *51*, 473–498.

Xu, E., Vaahtera, L., and Brosché, M. (2015). Roles of Defense Hormones in the Regulation of Ozone-Induced Changes in Gene Expression and Cell Death. Mol. Plant *8*, 1776–1794.

Xu, G., Yuan, M., Ai, C., Liu, L., Zhuang, E., Karapetyan, S., Wang, S., and Dong, X. (2017). UORF-mediated translation allows engineered plant disease resistance without fitness costs. Nature *545*, 491–494.

Xu, L., Liu, F., Lechner, E., Genschik, P., Crosby, W.L., Ma, H., Peng, W., Huang, D., and Xie, D. (2002). The SCFCOI1 Ubiquitin-Ligase Complexes Are Required for Jasmonate Response in Arabidopsis. Plant Cell *14*, 1919–1935.

Yan, Y., Stolz, S., Chetelat, A., Reymond, P., Pagni, M., Dubugnon, L., and Farmer, E.E. (2007). A Downstream Mediator in the Growth Repression Limb of the Jasmonate Pathway. Plant Cell *19*, 2470–2483.

Yang, R., Zheng, Z., Chen, Q., Yang, L., Huang, H., Miki, D., Wu, W., Zeng, L., Liu, J., Zhou, J.X., et al. (2017). The developmental regulator PKL is required to maintain correct DNA methylation patterns at RNA-directed DNA methylation loci. Genome Biol. *18*.

Yang, Y., Costa, A., Leonhardt, N., Siegel, R.S., and Schroeder, J.I. (2008). Isolation of a strong Arabidopsis guard cell promoter and its potential as a research tool. Plant Methods *4*, 6.

Yu, X., Li, L., Li, L., Guo, M., Chory, J., and Yin, Y. (2008). Modulation of brassinosteroid-regulated gene expression by jumonji domain-containing proteins ELF6 and REF6 in Arabidopsis. Proc. Natl. Acad. Sci. *105*, 7618–7623.

Zhang, T., Marand, A.P., and Jiang, J. (2016). PlantDHS: A database for DNase I hypersensitive sites in plants. Nucleic Acids Res. *44*, D1148–D1153.

Zhang, X., Clarenz, O., Cokus, S., Bernatavichute, Y. V., Pellegrini, M., Goodrich, J., and Jacobsen, S.E. (2007). Whole-genome analysis of histone H3 lysine 27 trimethylation in Arabidopsis. PLoS Biol. *5*, 1026–1035.

Zhang, X., Bernatavichute, Y. V, Cokus, S., Pellegrini, M., and Jacobsen, S.E. (2009). Genome-wide analysis of mono-, di- and trimethylation of histone H3 lysine 4 in Arabidopsis thaliana. Genome Biol. *10*, R62.

Zhou, C., Zhang, L., Duan, J., Miki, B., and Wu, K. (2005). HISTONE DEACETYLASE19 Is Involved in Jasmonic Acid and Ethylene Signaling of Pathogen Response in Arabidopsis. Plant Cell *17*, 1196–1204.

Zhu, Z., An, F., Feng, Y., Li, P., Xue, L., A, M., Jiang, Z., Kim, J.-M., To, T.K., Li, W., et al. (2011). Derepression of ethylene-stabilized transcription factors (EIN3/EIL1) mediates jasmonate and ethylene signaling synergy in Arabidopsis. Proc. Natl. Acad. Sci. *108*, 12539–12544.

Zilberman, D., Coleman-Derr, D., Ballinger, T., and Henikoff, S. (2008). Histone H2A.Z and DNA methylation are mutually antagonistic chromatin marks. Nature *456*, 125–129.

Zipfel, C., Robatzek, S., Navarro, L., Oakeley, E.J., Jones, J.D.G., Felix, G., and Boller, T. (2004). Bacterial disease resistance in Arabidopsis through flagellin perception. Nature *428*, 764–767.

Zipfel, C., Kunze, G., Chinchilla, D., Caniard, A., Jones, J.D.G., Boller, T., and Felix, G. (2006). Perception of the Bacterial PAMP EF-Tu by the Receptor EFR Restricts Agrobacterium-Mediated Transformation. Cell *125*, 749–760.

Supplementary figures and tables

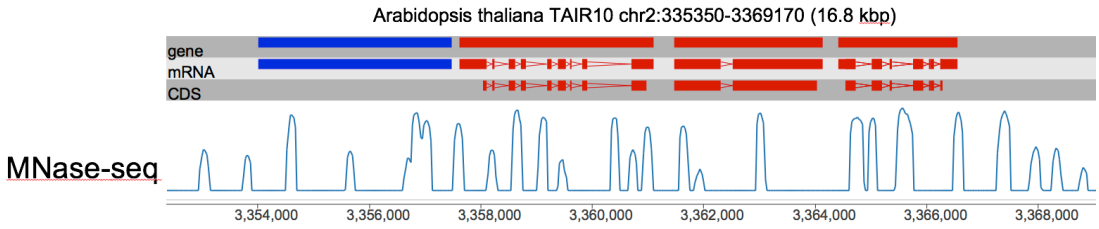

Supplementary figure **SI.1.** Pericentromeric highly structured chromatin. Micrococcal nuclease (MNase) digests histone-free DNA leaving nucleosomal DNA intact. Chromatin digestion followed by deep sequencing allows the visualisation of nucleosome distribution (single peaks of ~150 bp) on a highly structured region pericentromeric region of *Arabidopsis* chromosome 2. Genes, mRNA and CDS are represented on the top, red for sense transcription and blue for antisense transcription. The clear blue line represents average MNase-seq readings across samples (see Chapter 3 for further details).

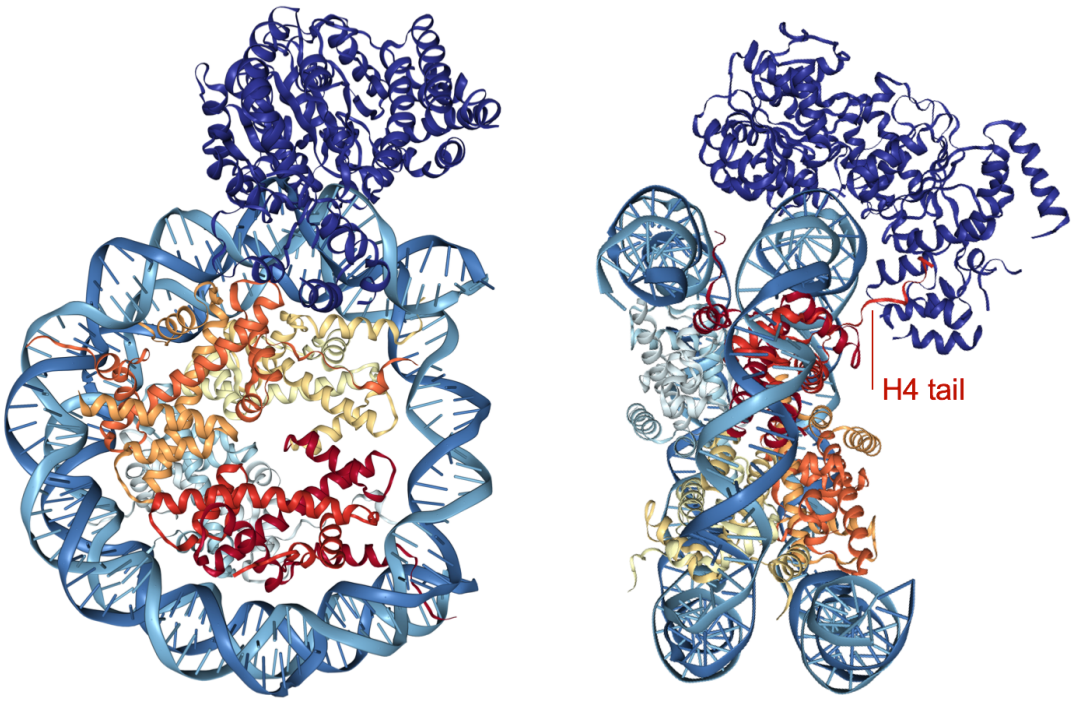

Supplementary figure **SI.2.** Nucleosome and chromatin remodelling ATPase SNF2 complex. Yeast SNF2 (in dark blue) interacting with a nucleosome in two different positions with SNF2 interacting with histone H4 tail (in red). 3D image generated with NGL viewer (http://nglviewer.org/ngl/; Rose and Hildebrand, 2015), from structures with PDB numbers X50X and X50Y (Liu et al., 2017).

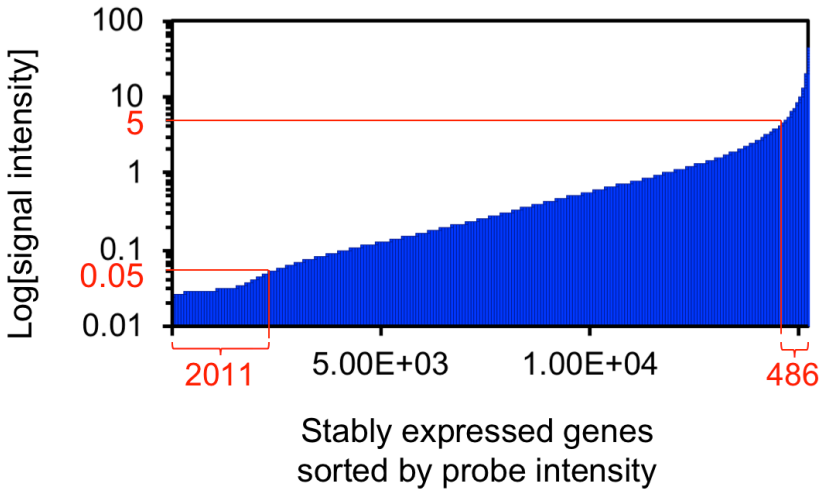

Supplementary figure **S1.1.** Stably expressed genes (14745 genes with less than 2-fold gene expression change between every replicate out of three, treatment; mock, flg22 and OG, and time point; 1 and 3 hours). Genes (on X axis) are sorted in ascendant order according to average signal intensity (Y axis). Selected lowly expressed genes (probes with less than 0.05 log intensity, bottom 2011), and highly expressed genes (probes with an intensity greater than 5 log, top 486 genes) for further analysis.

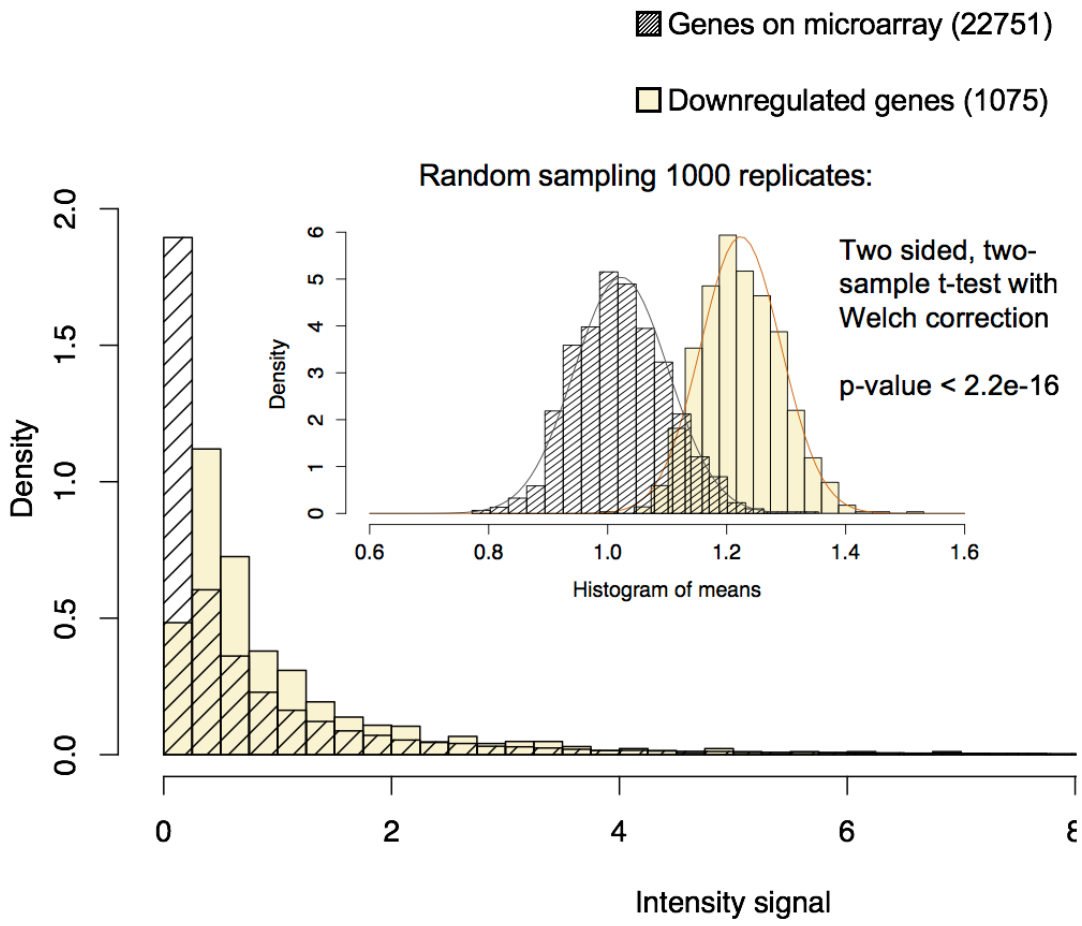

Supplementary Figure **S1.2**. Random sampling over all genes represented in the microarray data does not generate a set of genes similarly distributed to genes chosen on gene expression basis, in this example, being down-regulated upon flg22.

Supplementary Table **S1.1**. Genes identified as Calcium-dependent protein kinase (CPK) separated according to gene expression levels (bioinformatics analysis on Boudsocq et al., 2010 data).

CPK lowly expressed genes	CPK partially expressed genes
AT1G21110	AT1G01120 AT3G20510 AT5G53590
AT1G26380	AT1G03850 AT3G22600 AT5G54510
AT1G26410	AT1G05000 AT3G25900 AT5G57560
AT1G26420	AT1G12200 AT3G53260 AT5G57890
AT1G47890	AT1G21130 AT3G53720 AT5G61210
AT1G66690	AT1G22890 AT3G54400 AT5G67360
AT1G66830	AT1G26770 AT3G54640
AT1G74000	AT1G28240 AT3G57450
AT1G74080	AT1G35140 AT3G57550
AT2G26560	AT1G60740 AT3G59080
AT2G30750	AT1G61810 AT4G08770
AT2G30770	AT1G61820 AT4G20780
AT2G35730	AT1G68410 AT4G21410
AT3G13950	AT1G76930 AT4G22590
AT3G21070	AT2G17480 AT4G25030
AT3G48450	AT2G27080 AT4G25810
AT3G50770	AT2G31945 AT4G30210
AT3G53150	AT2G32660 AT4G33920
AT4G19370	AT2G34500 AT5G02230
AT4G19460	AT2G37940 AT5G03610
AT4G21390	AT2G39480 AT5G04870
AT4G23700	AT2G43290 AT5G05730
AT4G31970	AT2G44500 AT5G07440
AT4G33070	AT2G44790 AT5G14700
AT4G34210	AT2G46650 AT5G15470
AT4G37290	AT2G47550 AT5G15730
AT5G13080	AT3G03470 AT5G18150
AT5G57220	AT3G04000 AT5G37770
AT5G64890	AT3G09270 AT5G39580
AT5G64905	AT3G12700 AT5G44380
AT5G65600	AT3G16530 AT5G44480

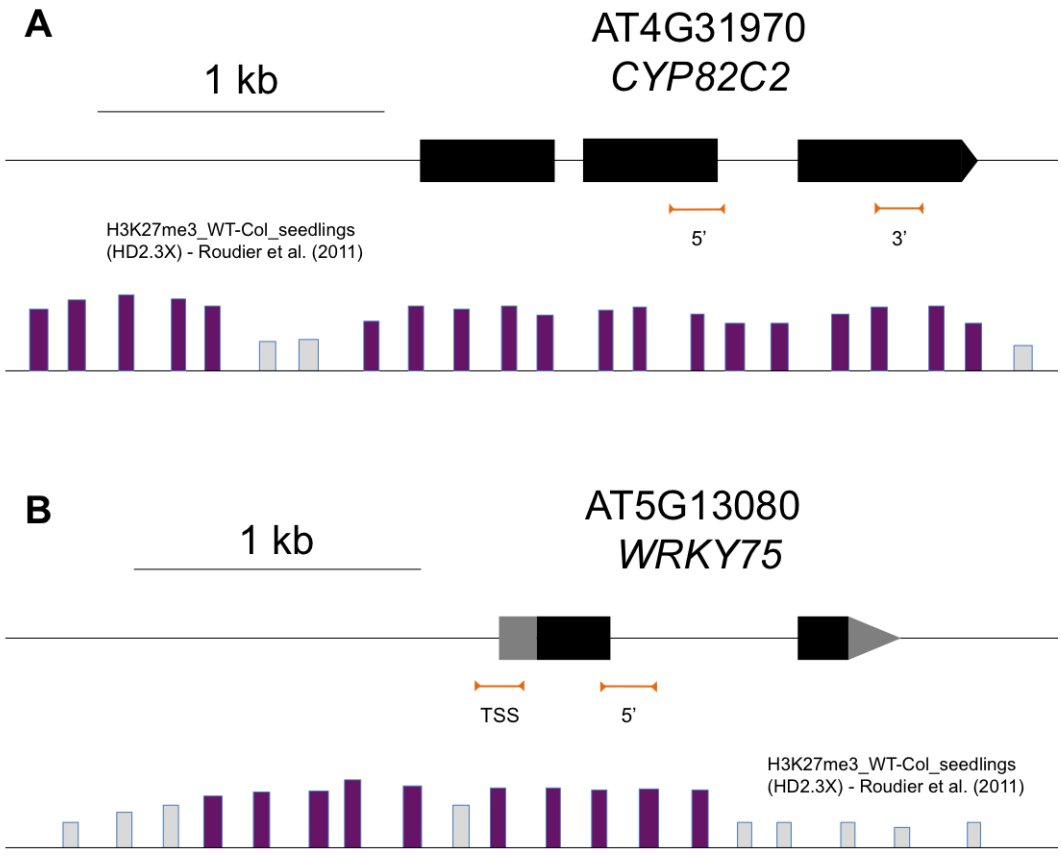

Supplementary figure **S1.3.** Probe localisation of CPK-dependent genes with low levels of expression chosen for ChIP assay. Primers for ChIP-qPCR were designed for optimal H3K27me3 enrichment according to available data from http://epigara.biologie.ens.fr/ (Roudier et al., 2011). (A) gene cartoon, primer amplification region (5' and 3') and H3K27me3 enrichment for *CYP82C2*. (B) gene cartoon, primer amplification region (5' and 3') and H3K27me3 enrichment for *WRKY75*.

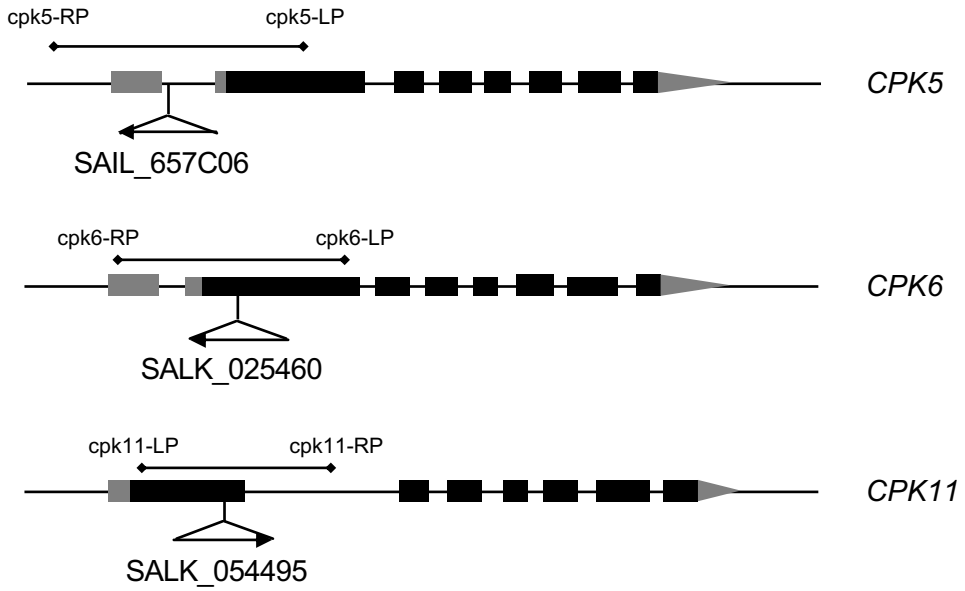

Supplementary figure **S1.4.** Gene cartoon, T-DNA location and direction, genotyping primers (sequence in Supplementary table A.2) for CPK genes *CPK5*, *CPK6* and *CPK11*, as described elsewhere (Boudsocq et al., 2010).

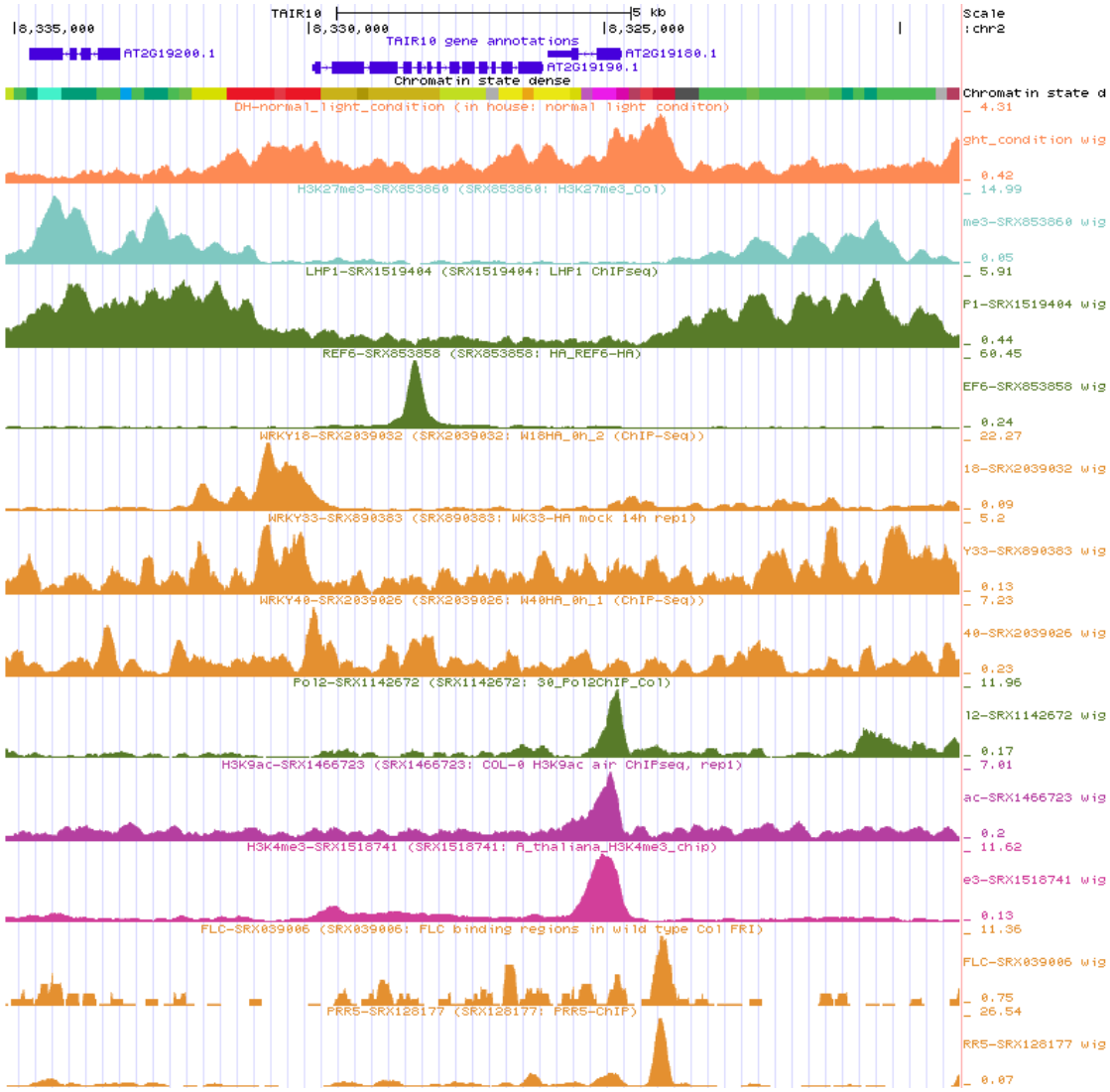

Supplementary figure **S1.5** Genome browser cartoon representing *FRK1* locus (transcript, top band, dark blue), chromatin state (line with colours. According to Liu et al., 2018 http://systemsbiology.cau.edu.cn/chromstates/) DNA hypersensitive sites (DHS) or accessible DNA (orange) and histone marks (H3K72me3 in dark green and H3K9ac, H3K4me3 in pink) and TF deposition (LHP1 in dark green, WRKY18, 33 and 40 in orange, RNA-polymerase II in dark green and FLC and PRR5 in orange).

Interestingly, 2 kb around the single REF6 peak there is barely any H3K27me3 (neither LHP1), and WRKY TF bind strongly at the *FRK1* promoter.

Supplementary Table **S2.1**. Phenotype for the different CRAs versus *Pst* DC3000 Δ*avrPto/avrPtoB*. Gene AGI, gene name, T-DNA insertion lines chosen, whether homozygous plants were obtained and bacterial phenotype (Roman numerals indicate experiment repeats).

Gene	Name	T-DNA line	hmz	Bacterial Growth
At1g08060	*MOM1*	SAIL_610_G01	Yes	No II
		SALK_141293 (*mom-2*)	Yes	No II
At3g16600		SALK_067458	Yes	No I
		SAIL_1254_D05	Yes	No I
At3g54460		SALK_008164	Yes	No VI
		SALK_065434	Yes	No VI
At1g05120		SAIL_757_C04	Yes	No II
		SAIL_451_E01	Yes	No II
At1g02670		SAIL_291_E03	Htz	-
		SALK_075484	Yes	-
At2g40770		SALK_075262	Yes	-
		SALK_025888	-	-
At5g05130		GT_5_89799	Yes	-
		SALK_113940	-	-
At5g22750	*RAD5*	SALK_092877	Yes	-
		SALK_124891	-	-
At5g43530		WiscDsLox421A7	Htz	-
At4g31900	*CHR7, PKR2*	SALK_118921	Yes	No II
		SALK_115303	Yes	**Susceptible II**
At2g25170	*CHR6, CHD3*	SAIL_878_E10	Yes	-
		GK-273E06	-	-
At5g44800	*CHR4, PKR1*	SALK_089483	-	-
		SAIL_783_C05	WT	-
At2g13370	*CHR5*	SALK_025939	Yes	No I
		SAIL_504_D01	Yes	No I
At2g46020	*CHR2, BRM*	SALK_038610	Yes	No II
		SALK_030046	Yes	No II
At2g28290	*CHR3, SYD*	SALK_127748	Yes	No I
		SALK_023209 (*syd-5*)	Htz	-
At5g18620	*CHR17*	SALK_139387	Yes	No II
		SALK_080144	Yes	**Resistant II**
At3g06400	*CHR11*	SALK_082046	Yes	-
		SALK_082028	-	-
At5g19310	*CHR23, MINU2*	SALK_057856	Yes	-
		SALK_139883	Yes	-
At3g06010	*CHR12, MINU1*	SALK_112468	WT	-
		SALK_105465	Yes	-
At5g66750	*CHR1, DDM1*	SALK_024844	Yes	No I
		WiscDsLox390D06	Yes	No I
At2g44980	*CHR10, ASG3*	SALK_084703	Yes	No II
		SALK_095969	Yes	No II
At2g02090	*CHR19, ETL1*	SALK_054130	Yes?	**Resistant I**
		SALK_069014	Yes	**Resistant I**
At3g12810	*CHR13, PIE1*	SALK_116597	Yes	No I
		SALK_096434 (*pie1-5*)	Htz	-
At3g57300	*INO80*	SALK_003909 (O)	Htz	-
		SAIL_261_E05	-	-
At3g54280		SALK_113141	-	-
At1g48310	*CHR18*	WiscDsLox435D8	Yes	No II
		SAIL_154_H02	Yes	No II
At5g07810		SALK_133371	Yes	No I
		SALK_113907	Yes	No I
At1g03750	*CHR9, SWI2*	SAIL_1265_E08 (*chr9-1*)	Yes	No II
		SALK_064383	Yes	No II
At3g19210	*CHR25, RAD54*	SALK_205160	Yes	**Susceptible I**
		SAIL_667_A08	Yes	**Susceptible I**
At1g08600	*CHR20, ATRX*	SALK_025687	Yes	No II
		SALK_024609	Yes	No II
At2g18760	*CHR8*	SALK_000799	Yes	No II
		SAIL_381_A07	Yes	No II
At5g63950	*CHR24*	SAIL_592_D03	Yes	-
		SALK_007071	WT	-
At2g21450	*CHR34*	SALK_014697	Yes	No I
		SALK_059100	Yes	No I
At5g20420	*CHR42*	WiscDsLoxHs041_03F	-	-
		SAIL_848_F03	Yes	-
At3g42670	*CHR38, CLSY1*	SALK_204860	Yes	-
		SAIL_1229_H10	Htz	-
At3g24340	*CHR40*	SALK_071275	Yes	-
		SALK_102252	Yes	-
At1g05490	*CHR31*	SAIL_739_F04	Yes	No II
		SALK_204501	Yes	No II
At3g20010	*CHR27, FRG1*	SAIL_1271_F06	Htz	-
		SALK_063135 (AX)	Yes	No VI
At1g50410	*CHR28, FRG2*	SALK_057016 (L) (S)	Yes	**Resistant VI**
		WiscDsLox324G06	Yes	**Resistant VI**
At1g61140	*EDA16*	SAIL_40_F09 (*eda16-1*)	Yes	**Susceptible VI**
		SALK_208691 (*eda16-3*)	Yes	**Resistant III**
		SAIL_735_G06 (*eda16-5*)	Yes	**Resistant III**
At1g11100		WiscDsLoxHs079_12B	-	-
		SALK_113298	Yes	No VI

etl1-1 *etl1-2*

Supplementary Figure **S2.1**. *etl1-1* plants (left hand side) show an invereted “u” shape leaf phenotype (curved leaf, or curly) that *etl1-2* (right hand side on the picture) does not show.

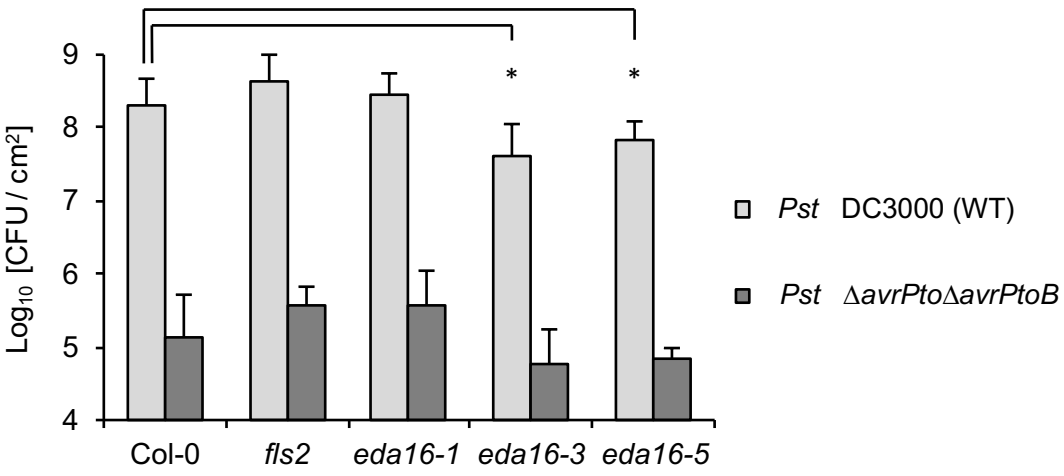

Supplementary Figure **S3.1.** Growth of *Pst* DC3000 (WT) and Δ*avrPto*Δ*avrPtoB* on Col-0 and eda16 mutants Arabidopsis plants 3 days after spray inoculation. Statistical significance determined by a two- sided T-test (on Log_{10}[colony forming units / cm^2]) assuming equal variances, n = 6, "*" indicates p-value < 0.01. Error bars represent standard deviation.

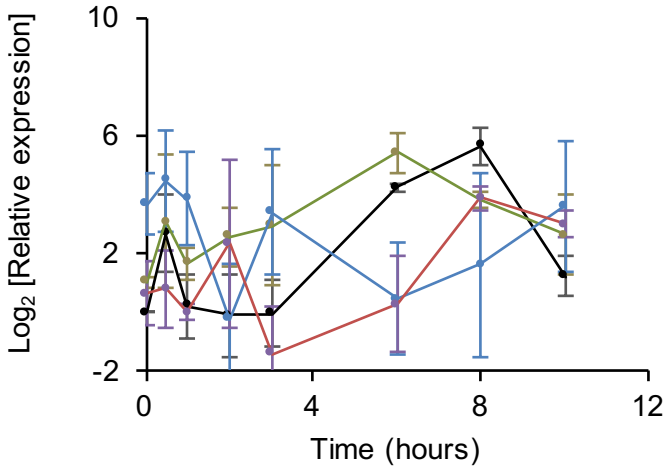

Supplementary Figure **S3.2.** Flg22-induced gene expression of SA marker gene *PR1* in *eda16* mutants. qPCR analysis on wild-type (Col-0) and mutants *eda16-1* (OE), *eda16-3* and *eda16-5* (KO) seedlings following elicitation with 100 nM flg22. Gene expression was referenced to α-TUB gene. Data shown are means of two biological replicates and error bars represent standard deviations.

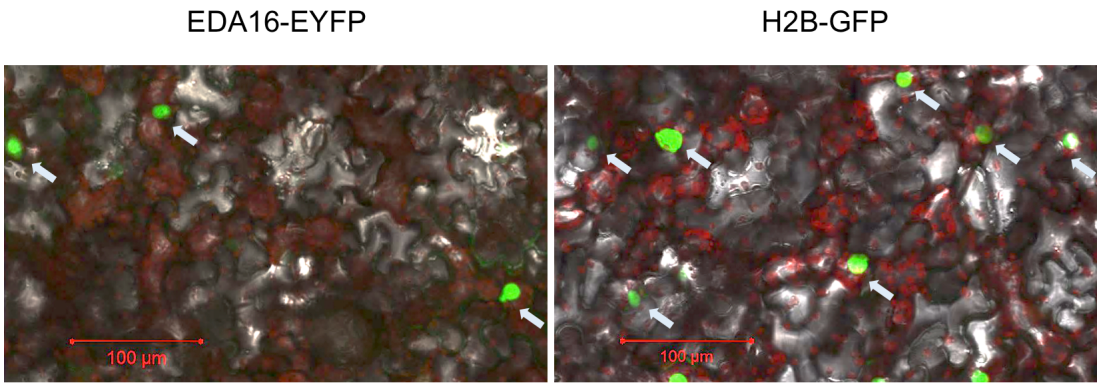

Supplementary Figure **S3.3.** Nuclear localization of EDA16. 35S:cEDA16-EYFP-HA (left) and 35S:H2B-GFP (right) constructs were transiently expressed in *N. benthamiana dcl2dcl3*. Subcellular localisation of these constructs was observed by confocal microscopy. Nuclei are indicated with white arrows. The average number of nuclei derived from 4 pictures was used to estimate that ~50% of the nuclei transiently express EDA16-EYFP compared to H2B-GFP, and that the intensity signal is ~20% compared with transient expression of H2B-GFP.

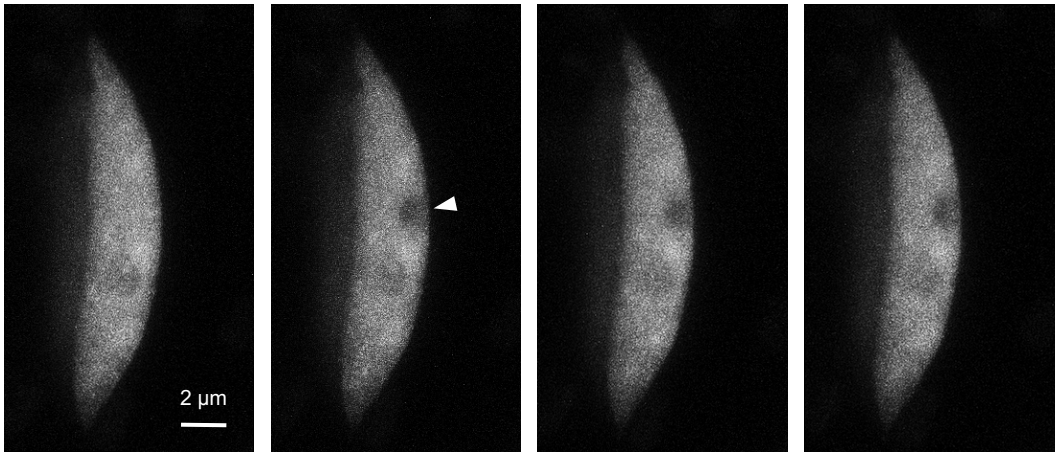

0 min 1 min 2 min 3 min

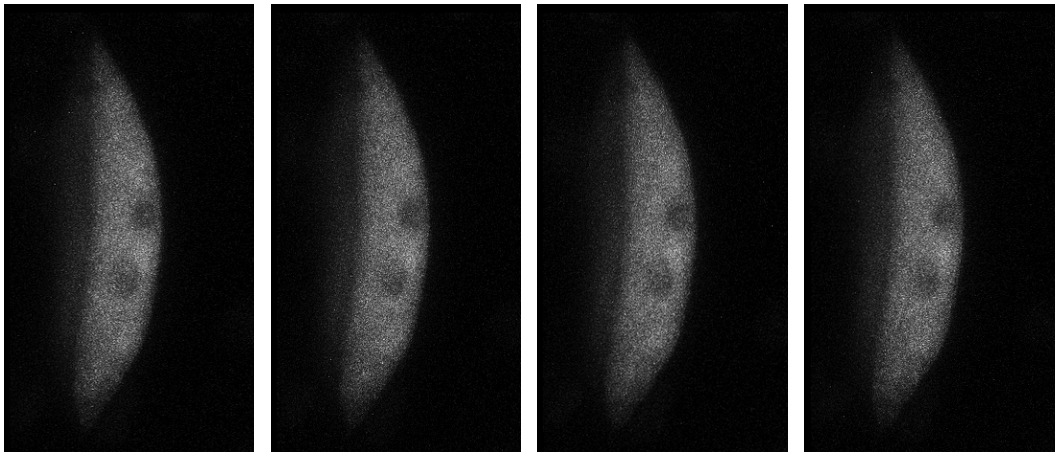

25 min 26 min 27 min 28 min

Supplementary Figure **S3.4.** FRAP data collected from Col-0 35S::H2B-GFP seedling leaf tissue, developmentally mature cell with a big, elongated nucleus. Frames 1 (not bleached) to 4 (first 3 bleached frames; white arrow) and last 4 bleached frames after 24 minutes. FRAP was performed with a Zeiss LSM 710 (Carl Zeiss Ltd; Cambridge, UK). An area of 1µm in radius was bleached in the centre section of the nucleus, avoiding the nucleolus, with a three-channel laser (458, 488 and 514 nm) 100% power, and 18 iterations. Subsequently, the nucleus was imaged (Frame size: 512 x 512) every minute for 28 minutes taking a Z-stack with 14 planes separated by 1 µm. Raw Z-stack images were stacked into one plane with ImageJ software (https://imagej.nih.gov/ij/). Using the "Z project" tool, projection type "Max intensity".

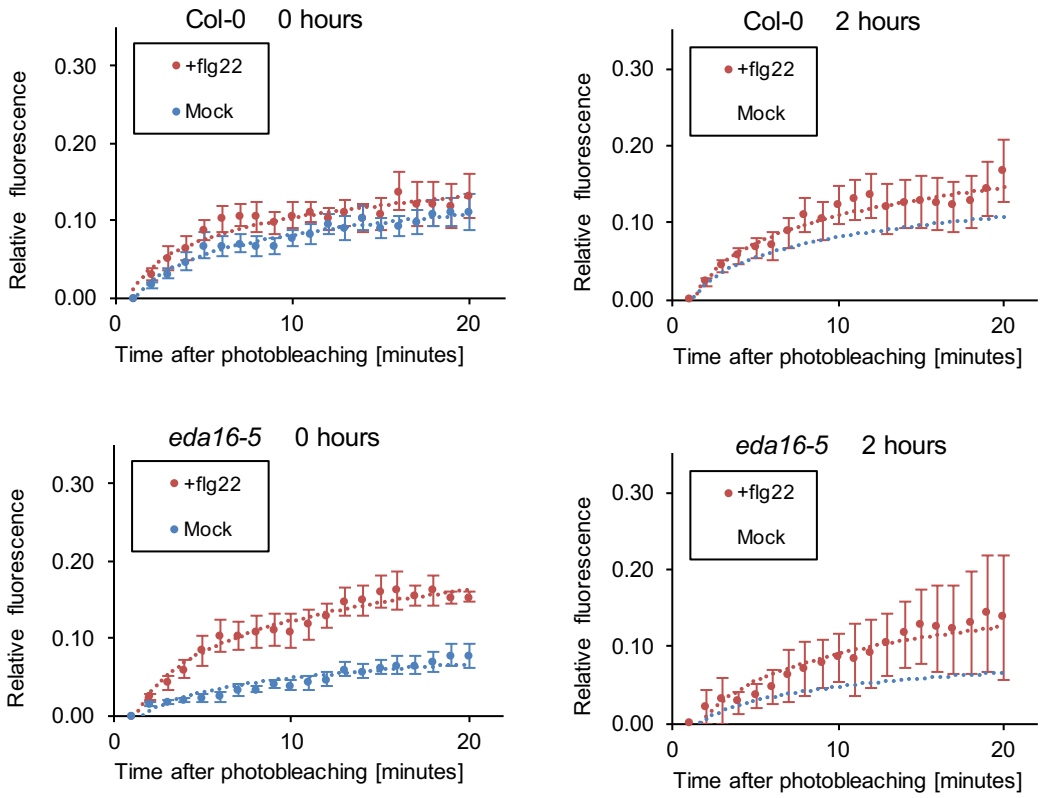

Supplementary Figure **S3.5**. Response to flg22 in Col-0 and *eda16-5*. FRAP data collected from seedling leaf tissue. H2B-GFP in Col-0 and *eda16-5*. The seedlings were exposed to water (A) or 100 nM flg22 for 10 minutes (B) or 2 hours (C). Data points are averages of at least 8 nuclei for each condition and genotype. Error bars represent standard errors.

Supplementary table **S3.1.** Half-time recovery after FRAP in minutes for Col-0 and *eda16-5* H2B-GFP lines before any treatment, 10 minutes and 2 hours after exposure to 100 nM flg22. Values represent means ± standard error of the mean. Half-life were calculated by individually fitting the FRAP recoveries of each nucleus to a single exponential function, and results were then averaged.

	Time 0	**10 min**	**2 hours**
Col-0 H2B-GFP	111.40 ± 15.81	82.71 ± 18.35	108.00 ± 26.37
eda16-5 H2B-GFP	128.59 ± 17.45	75.15 ± 9.28	119.86 ± 27.95

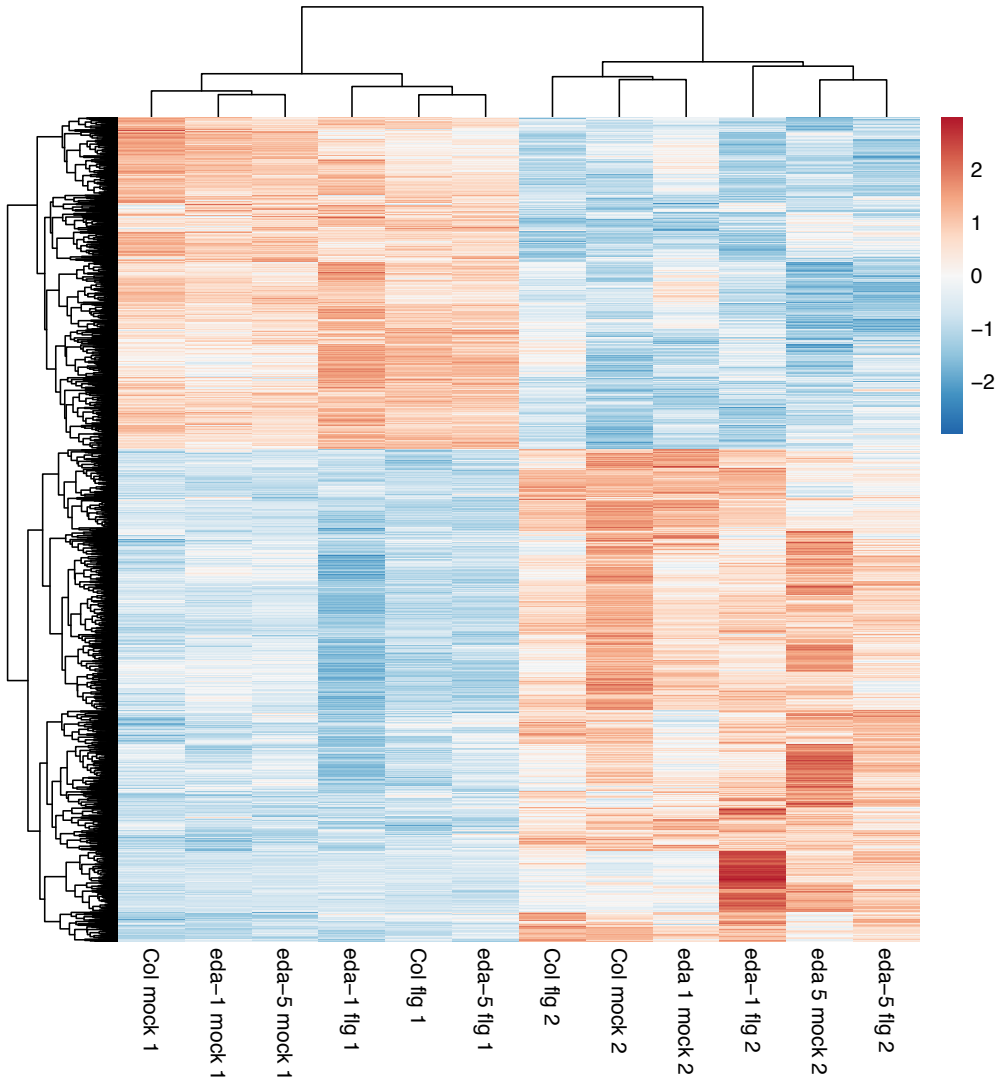

Supplementary Figure **S3.6.** Relative gene expression heat map for differentially expressed genes between replicates and hierarchical clustering. RNA-seq data analysis to find Genes changing with replicate: 1732 genes (p-value < 0.01, fold-change > square root of 2).

Supplementary Table **3.2** (next page). No GO terms with Virtual plant online (http://virtualplant.bio.nyu.edu/cgi-bin/vpweb/), only with TopGO, (see following table. Fisher's exact test with FDR correction, p-value < 0.01).

GO.ID	Term	Annotated	Significant	Expected	Fis
GO:0048451	petal formation	72	18	4.88	9.90E-07
GO:0048453	sepal formation	72	18	4.88	9.90E-07
GO:0000911	cytokinesis by cell plate formation	204	32	13.82	7.30E-06
GO:0010106	cellular response to iron ion starvation	116	21	7.86	3.10E-05
GO:0007043	cell-cell junction assembly	5	4	0.34	9.90E-05
GO:0006826	iron ion transport	121	20	8.2	0.00018
GO:0016572	histone phosphorylation	62	13	4.2	0.00022
GO:0080003	thalianol metabolic process	3	3	0.2	0.00031
GO:0010167	response to nitrate	197	27	13.35	0.00037
GO:0000226	microtubule cytoskeleton organization	243	31	16.46	0.00051
GO:0048767	root hair elongation	188	25	12.74	0.00093
GO:0015996	chlorophyll catabolic process	58	11	3.93	0.00157
GO:0015706	nitrate transport	209	26	14.16	0.00198
GO:0080170	hydrogen peroxide transmembrane transport	5	3	0.34	0.0028
GO:0005983	starch catabolic process	16	5	1.08	0.00329
GO:0006354	DNA-templated transcription, elongation	125	17	8.47	0.00456
GO:0019755	one-carbon compound transport	4	4	0.27	0.00457
GO:0035434	copper ion transmembrane transport	2	2	0.14	0.00459
GO:0015840	urea transport	2	2	0.14	0.00459

Continues…

Continues…

GO.ID	Term	Annotated	Significant	Expected	Fis
GO:0090316	positive regulation of intracellular protein transport	2	2	0.14	0.00459
GO:0000025	maltose catabolic process	2	2	0.14	0.00459
GO:0010501	RNA secondary structure unwinding	2	2	0.14	0.00459
GO:0009554	megasporogenesis	6	3	0.41	0.00531
GO:0009631	cold acclimation	33	7	2.24	0.00579
GO:0008283	cell proliferation	263	29	17.82	0.00663
GO:0010054	trichoblast differentiation	354	45	23.98	0.00786
GO:0009750	response to fructose	144	18	9.76	0.00863
GO:0044772	mitotic cell cycle phase transition	72	11	4.88	0.0088
GO:0080143	regulation of amino acid export	7	3	0.47	0.00883
GO:0032508	DNA duplex unwinding	13	4	0.88	0.00914
GO:0070925	organelle assembly	54	9	3.66	0.00979

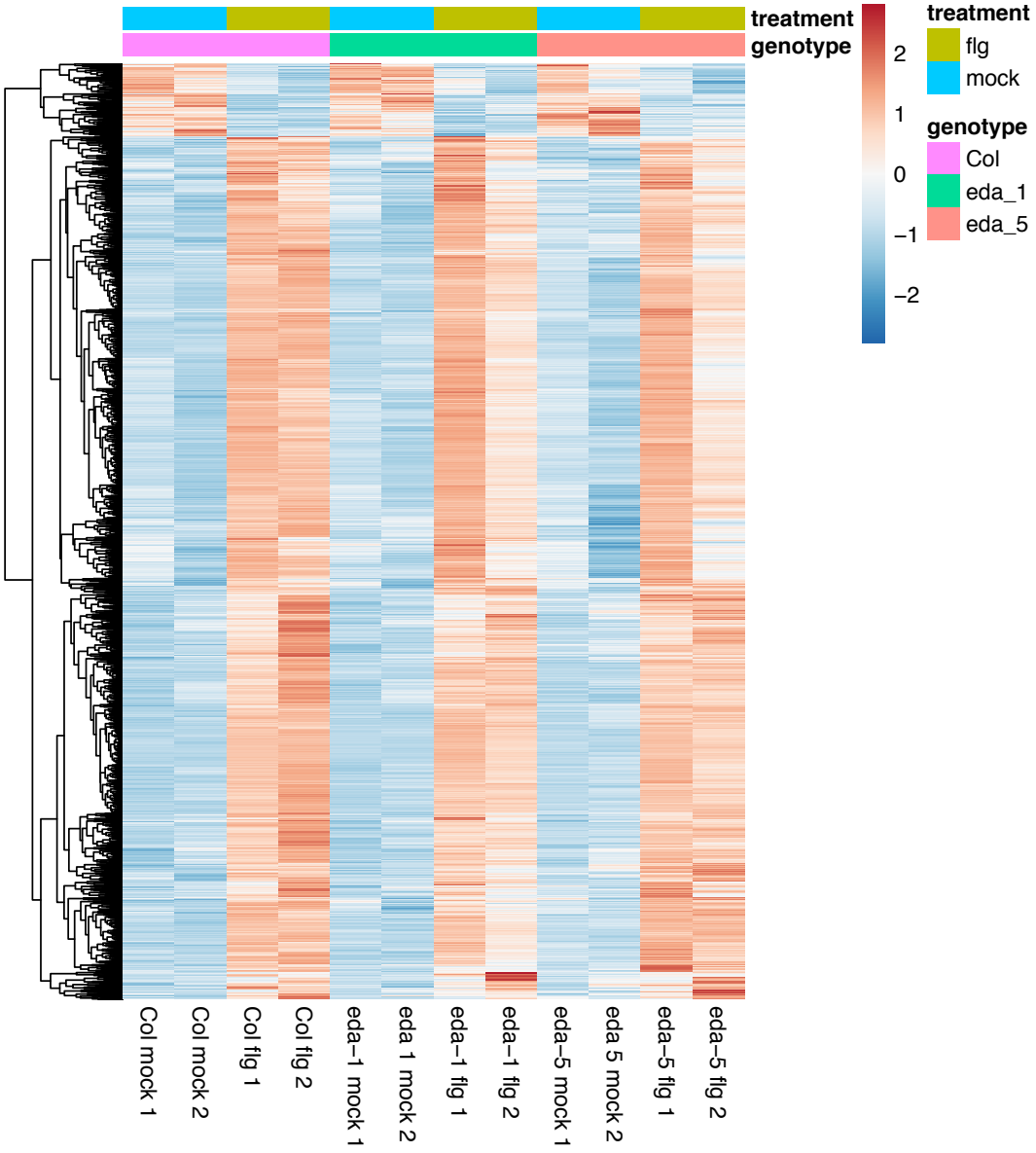

Supplementary Figure **S3.7.** Relative gene expression heat map for differentially expressed genes between treatments and hierarchical clustering. RNA-seq data analysis to find Genes changing with replicate: 1520 genes (p-value < 0.01, fold-change > 2).

Figure below. Venn diagram representing the minimum overlap between the genes differentially expressed by treatment (2 h flg22 100 µM) and replicate

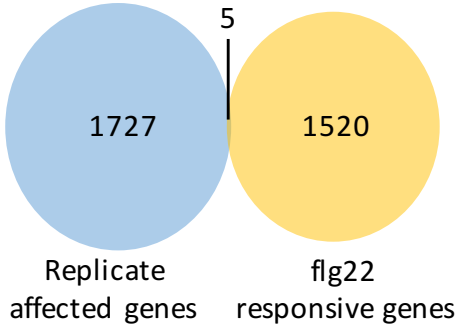

Supplementary Table **3.3**. GO terms, only with TopGO, (see following table. Fisher's exact test with FDR correction, p-value < 0.01).

Up-regulated:

GO.ID	Term	Annotated	Significant	Expected	Fis
GO:0010200	response to chitin	421	176	25.25	< 1e-30
GO:0050832	defense response to fungus	350	125	20.99	< 1e-30
GO:0002679	respiratory burst involved in defense response	121	75	7.26	< 1e-30
GO:0010363	regulation of plant-type hypersensitive response	371	119	22.25	< 1e-30
GO:0006612	protein targeting to membrane	376	119	22.55	< 1e-30
GO:0009697	salicylic acid biosynthetic process	209	87	12.53	< 1e-30
GO:0031348	negative regulation of defense response	277	99	16.61	< 1e-30
GO:0009723	response to ethylene	353	104	21.17	< 1e-30
GO:0000165	MAPK cascade	220	78	13.19	< 1e-30
GO:0043069	negative regulation of programmed cell death	168	68	10.07	< 1e-30
GO:0009862	systemic acquired resistance, salicylic acid	251	80	15.05	< 1e-30
GO:0009867	jasmonic acid mediated signaling pathway	285	81	17.09	< 1e-30
GO:0009627	systemic acquired resistance	446	143	26.75	< 1e-30
GO:0034976	response to endoplasmic reticulum stress	354	119	21.23	1.50E-30
GO:0009693	ethylene biosynthetic process	119	50	7.14	5.40E-30
GO:0042742	defense response to bacterium	401	99	24.05	1.00E-29
GO:0030968	endoplasmic reticulum unfolded protein response	182	60	10.91	7.20E-29

Continues…

Continues…

GO.ID	Term	Annotated	Significant	Expected	Fis
GO:0010310	regulation of hydrogen peroxide metabolism	186	60	11.15	2.80E-28
GO:0009738	abscisic acid-activated signaling pathway	247	65	14.81	6.50E-25
GO:0002237	response to molecule of bacterial origin	101	41	6.06	4.00E-24
GO:0009595	detection of biotic stimulus	104	46	6.24	1.00E-23
GO:0052542	defense response by callose deposition	63	36	3.78	8.50E-23
GO:0009407	toxin catabolic process	211	57	12.65	1.30E-22
GO:0009611	response to wounding	333	72	19.97	5.80E-22
GO:0042542	response to hydrogen peroxide	194	51	11.63	1.70E-18
GO:0009863	salicylic acid mediated signaling pathway	353	112	21.17	4.70E-16

Down-regulated:

GO.ID	Term	Annotated	Significant	Expected	Fis
GO:0006869	lipid transport	128	6	0.6	3.10E-05
GO:0030418	nicotianamine biosynthetic process	4	2	0.02	0.00013
GO:0009741	response to brassinosteroid	113	4	0.53	0.00199
GO:0010233	phloem transport	15	2	0.07	0.0022
GO:0060560	developmental growth involved in morphogenesis	546	8	2.57	0.00413
GO:0010597	green leaf volatile biosynthetic process	1	1	0	0.0047
GO:0009828	plant-type cell wall loosening	27	2	0.13	0.0071
GO:0071497	cellular response to freezing	2	1	0.01	0.00938

Supplementary table **S3.4**. Differentially expressed genes and p-values for the different pairwise comparisons between the three genotypes and the two treatments (Col-0 vs. *eda16-1* Col-0 vs. *eda16-1*, and *eda16-1* vs. *eda16-5*, treated and untreated). fold-change > 2 and p-value < 0.01.

		Col-0 vs *eda16-1*				**Col-0 vs *eda16-5***				***eda16-1* vs *eda16-5***			
		flagellin		**mock**		**flagellin**		**mock**		**flagellin**		**mock**	
	baseMean	**log_2FC**	**p-value**	**log_2FC**	**p-value**	**log_2FC**	**p-value**	**log_2FC**	**p-value**	**log_2FC**	**p-value**	**log_2FC**	**p-value**
AT1G53480	820.30	**5.47**	**6.10E-79**	**5.21**	**4.54E-74**	0.01	1.00E+00	-0.01	1.00E+00	**-5.46**	**5.72E-79**	**-5.22**	**1.61E-74**
AT1G53490	208.71	**2.68**	**2.63E-25**	**1.59**	**1.66E-07**	-0.04	1.00E+00	0.13	1.00E+00	**-2.73**	**3.27E-26**	**-1.46**	**3.40E-06**
AT1G24280	368.02	**1.29**	**5.16E-07**	**1.22**	**7.58E-06**	0.09	1.00E+00	-0.24	1.00E+00	**-1.20**	**7.86E-06**	**-1.46**	**1.93E-09**
AT2G39030	47.45	1.22	2.56E-01	-0.09	1.00E+00	-0.84	1.00E+00	-0.89	1.00E+00	**-2.06**	**6.64E-06**	-0.81	6.43E-01
AT3G29644	84.25	1.19	1.27E-01	0.89	1.00E+00	**-1.27**	**9.58E-02**	**-1.28**	**8.93E-02**	**-2.46**	**2.41E-12**	**-2.16**	**1.93E-09**
AT5G05340	74.99	1.07	2.04E-01	0.33	1.00E+00	-0.34	1.00E+00	-0.92	1.00E+00	**-1.42**	**2.44E-03**	**-1.25**	**8.59E-02**
AT4G39100	1217.96	**1.01**	**2.09E-07**	**1.05**	**4.29E-08**	0.11	1.00E+00	0.24	1.00E+00	-0.90	9.17E-06	-0.81	2.22E-04
AT2G26150	383.82	0.92	1.24E-01	0.50	1.00E+00	0.19	1.00E+00	-0.70	1.00E+00	-0.73	4.26E-01	**-1.20**	**9.35E-03**
AT5G35940	154.95	0.91	6.13E-01	**1.62**	**1.57E-04**	-0.36	1.00E+00	-0.36	1.00E+00	**-1.27**	**1.75E-02**	**-1.98**	**5.01E-08**
AT5G12030	567.75	0.89	4.60E-01	0.67	1.00E+00	0.35	1.00E+00	-0.82	1.00E+00	-0.54	8.96E-01	**-1.49**	**4.36E-04**
AT3G22231	117.68	0.74	1.00E+00	0.33	1.00E+00	-0.82	1.00E+00	-0.83	7.76E-01	**-1.57**	**8.65E-06**	**-1.16**	**1.13E-02**
AT1G73120	457.87	0.67	3.45E-01	0.95	3.03E-04	-0.38	1.00E+00	-0.25	1.00E+00	**-1.05**	**2.18E-04**	-1.20	4.06E-08
AT2G16005	69.74	0.52	1.00E+00	0.56	1.00E+00	-0.76	1.00E+00	-0.97	7.76E-01	**-1.29**	**2.10E-02**	**-1.52**	**8.11E-04**
AT2G43550	292.02	0.49	1.00E+00	-0.07	1.00E+00	-0.64	1.00E+00	-0.42	1.00E+00	**-1.13**	**2.95E-03**	-0.35	7.27E-01
AT5G23830	253.93	0.15	1.00E+00	0.60	1.00E+00	-0.41	1.00E+00	-0.59	1.00E+00	-0.56	6.07E-01	**-1.19**	**2.38E-05**
AT5G09315	160.95	-0.06	1.00E+00	-0.09	1.00E+00	0.67	1.00E+00	1.00	8.93E-02	0.73	3.12E-01	**1.08**	**1.56E-03**
AT2G01422	371.44	-0.23	1.00E+00	-0.33	1.00E+00	**-6.65**	**2.73E-109**	**-6.53**	**7.57E-106**	**-6.42**	**5.86E-101**	**-6.21**	**3.26E-99**
AT1G20350	59.03	-0.29	1.00E+00	-1.01	1.00E+00	0.23	1.00E+00	0.45	1.00E+00	0.53	9.18E-01	**1.46**	**3.37E-03**
AT1G61150	1515.33	**-1.35**	**2.13E-10**	-0.56	1.00E+00	0.02	1.00E+00	0.01	1.00E+00	**1.36**	**8.05E-11**	0.57	3.10E-01
AT1G61140	4349.40	**-2.69**	**2.60E-40**	**-1.75**	**1.74E-15**	-0.08	1.00E+00	-0.25	1.00E+00	**2.61**	**5.21E-38**	**1.51**	**5.36E-11**

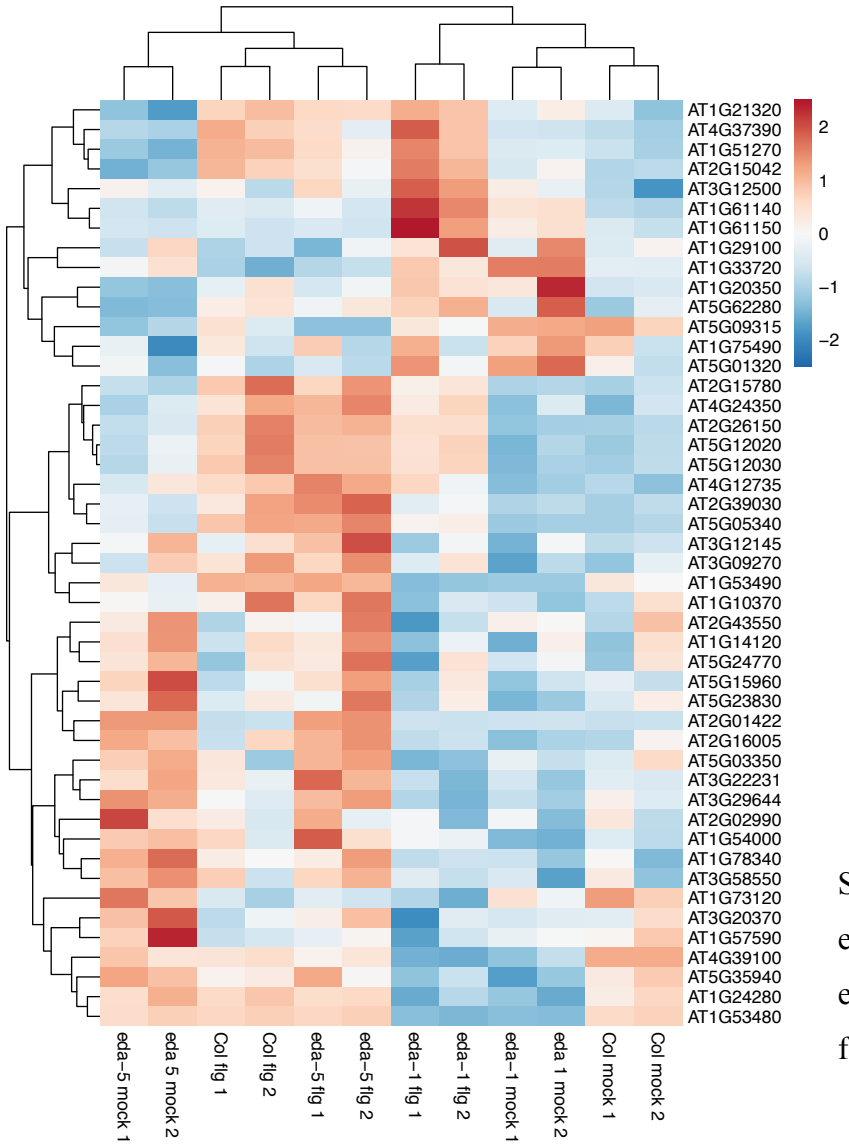

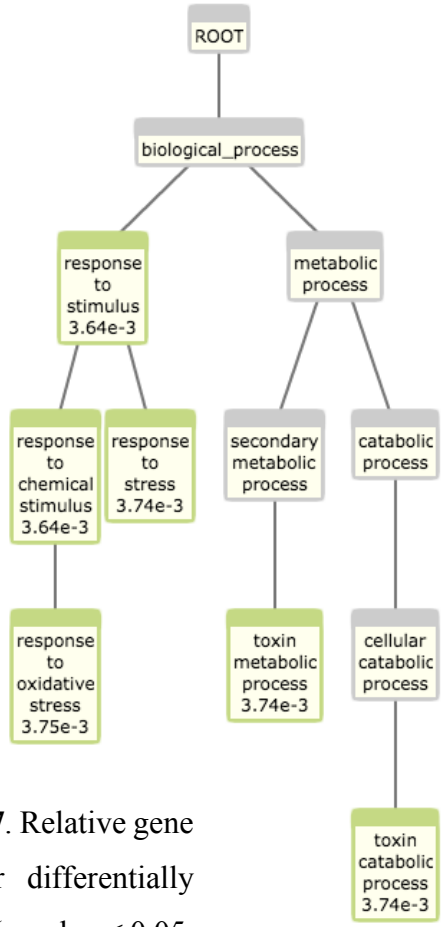

Supplementary Figure **S3.7**. Relative gene expression heat map for differentially expressed genes genotype (p-value < 0.05, fold-change > Square root of 2).

Table A1. CRA T-DNA insertion mutant lines and primers for genotyping (designed with T-DNA primer design, http://signal.salk.edu.tdnaprimers.2.html)

Gene AGI	Gene Name	T-DNA insertion line	Code	Sequence	Code	Sequence
				LP		RP
At1g02670		SAIL_291_E03	VN262	TCTCTGATGTGGAAATACCGG	VN263	CCACTGAGAAAGAGCAACAGG
		SALK_075484C	VN164	TCAACATCATTCTGGAGAGGG	VN165	GTTCTTAATCTTCGGGTTGCC
At1g03750	SWI2, CHR9	SAIL_1265_E08 (*chr9-1*)	VN284	ATCTTTCCGGAGCAGTAGCTC	VN285	GAAGCCCTGTGGTAGTTTTCC
		SALK_064383C	VN220	CAGAACGGAAAAACTTGTTTTTG	VN221	TCGGAATCTCTCCAATTGATG
At1g05120		SAIL_757_C04	VN276	AACAACCAAATCTCGTCATGG	VN277	ACAATGGGACGATTAGGGATC
		SAIL_451_E01	VN274	TTGCAGCAAGTCATTTTACCC	VN275	TTGGCTTGGCCACATACTAAC
At1g05490	CHR31	SAIL_739_F04	VN238	TTGAGCTTTGCAAATCCTCAC	VN239	AGAGAAGGGCATGAAGAAAGC
		SALK_204501C	VN228	CAGGTCTTGATGGCTCTTCAG	VN229	GGAGAAGAAATCAGGTCCCAG
At1g08060	MOM1	SAIL_610_G01	VN236	ACAATGCAGGAGCAAACACTC	VN237	GGAAAGGAGATACTTCACCGG
		SALK_141293 (*mom-2*)	VN282	ACGAGAATTCATGAATCACGC	VN283	CTGCTCACCAAGAATCTGGAG
At1g08600	CHR20, ATRX	SALK_025687C	VN194	GGAGGTAATGGAGGTGAAAGC	VN195	GTCAAGCTCAGATGTTCCAGC
		SALK_024609C	VN184	TGTAGGATGGCGTGATCTAGG	VN185	TGTTGCTGCTGAAATGATGAC
At1g11100		WiscDsLoxHs079_12B	VN280	ACACTTCAATTCCAGGCAGAG	VN281	TCTAATGTTTTTGGTCAAACCT
		SALK_113298C	VN188	ACGCTCACAAGGGAATATGTG	VN189	ATTTTCATGCAGACTTGCAGG
At1g48310	CHR18	WiscDsLox435D8	VN254	TTCCCCACAAAGACTTGTGAC	VN255	GATTGCAAGAAAAATGGCAAG
		SAIL_154_H02	VN258	TTCCCCACAAAGACTTGTGAC	VN259	CTCTCACATTACCTTCGTCGC
At1g50410	CHR28, FRG2	SALK_057016 (*frg2-1*)	VN124	CATAAGGGGAACCGAAAGAAG	VN125	GCTGAAGGTTGCATTTCTGAC
		WiscDsLox324G06 (*frg2-2*)	VN248	AAGCCATTTGACCATTCTGTG	VN249	TCTTCGGTTTGTGCATTTTTC
At1g61140	EDA16	SAIL_40_F09 (*eda16-1*)	VN234	CTTTGCACATGGTTGTTTGTG	VN235	CGAAATTCAGAAGTAGACGCG
		SALK_107256.28.05.x	VN150	TCGATCCACATGTCTAATTCC	VN151	GTGAATCCTTGAGCTCGTCAG
		SALK_208691C (*eda16-3*)	VN502	CGAGAAGAGGGTGATCACAAG	VN503	AACGCTTGTTGTATGTCCCAC
		SAIL_1156_D12C1	VN504	CGAAGCTCGTTCTCATGAATC	VN505	AACAGTGCATTTATGAACGCC
At2g02090	CHR19, ETL1	SAIL_735_G06 (*eda16-5*) (*fr*	VN506	AAAGTGTCCAAGCGAGAGACTC	VN507	ATGAGGGTATGAGCGTTGATG
		SALK_054130C	VN170	ACCATCCAACGAAACACACTC	VN171	AAAGCTCTTTTCGAAGATCCG
		SALK_069014C	VN186	CAAGTTGCTGCATGACATCAG	VN187	TTGAATCTGTGATGATCGCAG

At2g13370	CHR5	SALK_025939C	VN196	GCTTCAGGAGAATCTGGGTTC	VN197	AATTGAAAGCAGATCCACACG
		SAIL_504_D01	VN266	TCAGCATCCTCCTCTTCAATG	VN267	TCTCATCAGAGGATGACCCTG
At2g18760	CHR8	SALK_000799C	VN218	TACCGTTTCAACAAAACCAGC	VN219	TCTTTGACGAAACCAGTTTCG
		SAIL_381_A07	VN264	TGGGTACCATTTCTGTGCTTC	VN265	CTGATTCCTGTGGGATTATGC
At2g21450	CHR34	SALK_014697	VN134	TTTGCCAAAACAATTTCAAAAC	VN135	AAATCATGCAAAACCCATTTG
		SALK_059100C	VN176	TTATGGGAAACAAAAAGACGC	VN177	CTGGACAGAGAAGCAGACACC
At2g25170	CHR6, CHD3	SAIL_878_E10	VN242	TAGCCCCACAAGTGTTAGTGG	VN243	GAAGACGAACCTTTGAAATGG
		GK-273E06	VN128	GCAAGTCGAGGCTATTGTCAG	VN129	GACAAGATATTCCAGCTCCCC
At2g28290	CHR3, SYD	SALK_127748C	VN202	GTTTCCCTTTAGAGACACGCC	VN203	CAGAGGTCCACAATTCATGTG
		syd-5	VN136	CTGCGAAGTTAGCTGTTTTGG	VN137	CTTCTCACGGTGAAGTCGTTC
At2g40770		SALK_075262C	VN198	ATCCACATGCTCTCACGAAAC	VN199	ATCAAAGTTCTGCTGCTGCTC
		SALK_025888.34.20.x	VN140	TTCATACCAGCAAGGATACCG	VN141	ATAGAAATCAATTACCCGGCG
At2g44980	CHR10, ASG3	SALK_084703C	VN214	TGGAGTTGGCAGTTATGAACC	VN215	GAAGCTCAATAAACGACGTCG
		SALK_095969C	VN178	TTCATACAGCCAGGACACGTAC	VN179	CTCGAAACGGTAGCGTATGAC
At2g46020	CHR2, BRM	SALK_038610	VN142	CCTGCTGGTTCAAAACTGTTC	VN143	AATTAAACCCAATGCACAACG
		SALK_030046C	VN174	AATATACGCTTGCTGCATTGG	VN175	AGTTTATACCGTTGCATCCCC
At3g06010	CHR12, MINU1	SALK_112468C	VN200	AAACGAACAAACACAGTCATGG	VN201	TTCACCGTTTTCGATTTCAAC
		SALK_105465C	VN216	CCAATCACGAAGATTGAAAGC	VN217	CGCCTGTAATTCACTCTCGAG
At3g06400	CHR11	SALK_082046C	VN208	TCCCAGTAGCATGACCACTTC	VN209	CCGAATCCATTGCATTAAATG
		SALK_082028.29.55.x	VN144	TCCCAGTAGCATGACCACTTC	VN145	CCGAATCCATTGCATTAAATG
At3g12810	CHR13, PIE1	SALK_116597C	VN212	TGCAGAATGATCCAAATAGCC	VN213	AAAATAAAAGGAGCCAGTCGC
		SALK_096434.48.95.x	VN148	TTCATTATCTGCTTTCGCCAG	VN149	GGAGGATGAAAAACACTTCAC
At3g16600		SALK_067458C	VN192	CAGGAGGTAGATCCTTTTCGG	VN193	CATGACTGATCTTCTAGCCCG
		SAIL_1254_D05	VN272	ATTTCTCTGTCCAAGCCAACC	VN273	CGTCGAGATCGTTTTACCAAG
At3g19210	CHR25, RAD54	SALK_205160C	VN232	AAACAATGGAATACGCGTTTG	VN233	AGTCATAGGAAGAGGAAGCGC
		SAIL_667_A08	VN268	CTTTTAAGCTGCATGCAGAGG	VN269	GGAGTTTAGGTGATGCTGCAC
At3g20010	CHR27, FRG1	SAIL_1271_F06	VN246	AGATCGATTCAAACGGTGTTG	VN247	TGAAACCCACTACAAAGCCAC
		SALK_063135 (*frg1-2*)	VN126	ATTTTTCTGAGGTGCATGGTG	VN127	TCATCGTTCTCATCCTCATCC

At3g24340	CHR40	SALK_071275C	VN168	TGACACTTCGATTTGGTAGGC	VN169	CCCACACTGCTCAGAGATCTC
		SALK_102252C	VN172	CTCCATCACAGAGTTTTTCGC	VN173	TGATGCTTGTTCACCTTCTCC
At3g42670	CHR38, CLSY1	SALK_204860C	VN230	ATGGCATCATCCTTACCCATC	VN231	CCATCCATTTAATCCATGTCG
		SAIL_1229_H10	VN244	CTCTGAAGTCTCGCCATCATC	VN245	ATTGTGACGGATGAAGATTGC
At3g54280		SALK_113141.39.50.x	VN286	CGAGGTCTTTGTTTTAACAATTTT	VN287	TCAACCACAGCCCTGTATCTC
At3g54460		SALK_008164	VN132	ACGGTTGATCACAATTTCTGG	VN133	TGTTCCGGAATTCTCAACATC
		SALK_065434C	VN204	CATCATGATTTCCTGGACTGG	VN205	TCGGACTCGAAACAGAAGAAG
At3g57300	INO80	salk_003909 (O)	VN130	TTTTTGTACATGCTCCCCAAG	VN131	AACACCAAGTGTCTGTCCAGG
		SAIL_261_E05	VN260	TACGAGGTTTGGATTCTGTGG	VN261	CTTCTGCTTAGACACCGCATC
At4g31900	CHR7, PKR2	SALK_118921C	VN190	CAAACTGTTTGAATTCCTCTCG	VN191	CATCTTGTACGCTCCTCCTTG
		SALK_115303C	VN166	TTCTGATTTTTCAACCGATGG	VN167	GGGGAGGAGTATCTGGTGAAG
At5g05130		GT_5_89799	VN122	ATCACAGAAGGTGGACAAACG	VN123	TTGTTCTGACTTTGGGGTGTC
		SALK_113940.36.30.x	VN154	CGTCGCAGTAAAGATCCAAAG	VN155	CTCAATTCAGGAAGATGCTGC
At5g07810		SALK_133371.43.40.x	VN158	AGGTGTTGGGAAGATTAACGG	VN159	TTTCTCAATTGACGAAGGCAC
		SALK_113907.31.15.x	VN152	ATGCTATGGCAAGTCATCTGC	VN153	TGGCAAAAATATAATGCCTCG
At5g18620	CHR17	SALK_139387C	VN160	TGCCATTAACTTACCGCAGAG	VN161	TATAACGGAACGGCCTTATCC
		SALK_080144C	VN206	ACCTGCGTTTGTTACAAGGTG	VN207	TTACCTGCATGAGTACAGGGG
At5g19310	CHR23, MINU2	SALK_057856C	VN210	TGAAAACAATTTGTGAATTTCATT	VN211	ATTGGCTCCATAGGCTTTTTC
		SALK_139883.42.25.x	VN162	GGATCTTAGTTCCCCACCTTG	VN163	ATACTGGCTGCGTTTGAATTG
At5g20420	CHR42	WiscDsLoxHs041_03F	VN278	TCCTCATTGTTATCGTCCTCG	VN279	GTTCTTCTGCTCGGGTACATG
		SAIL_848_F03	VN240	ACCTCGTTGTCATCGAGAATG	VN241	GAACAGTGCAAACCAAGATGG
At5g22750	RAD5	SALK_092877.43.15.x	VN146	CCCATTGCGTCTGCTAATATC	VN147	CTGAAGCTTTGAGCATCATGG
		SALK_124891.47.95.x	VN156	CTCGGTTTGATCCCCTTTAAG	VN157	TAGAAACCCAGTTGATGCAGC
At5g43530		WiscDsLox421A7	VN252	TCGTCACAGATTCGATAAGCC	VN253	TGGTAGACTTCCGATGGAGTG
At5g44800	CHR4, PKR1	SALK_089483C	VN180	GAGCCGATAAGAGCAGATCAC	VN181	CAATGATCCATGACTGATCCC
		SAIL_783_C05	VN270	CGAGCATCAACTTCTTCTTGG	VN271	TGAAATGGTTCTGGCTGACTC
At5g63950	CHR24	SAIL_592_D03	VN256	TGTCGGATGACCAATGTTTAAG	VN257	CATCAGCTTCGTCTTCCTTTG
		SALK_007071C	VN182	CGAAAAGAAAAGTGCAGGTTG	VN183	TCTGGTGTTTGATTTTCGGTC
At5g66750	CHR1, DDM1	SALK_024844	VN138	AGCTTTCTCTTCATCTTCCCG	VN139	AATCATCGGAGACAGATGACG
		WiscDsLox390D06	VN250	TCACAAAGCAACCACACTACG	VN251	AATCATCGGAGACAGATGACG

Other genotyping primers

Name	Sequence (5' to 3')	Use	Comments	Tm; %GC; primer length
LBb1.3	ATTTTGCCGATTTCGGAAC		genotyping SALK lines	
LB3	TAGCATCTGAATTTCATAACCAATCTCGATACAC		genotyping SAIL lines	
RB1.2	CTCCTTCAACGTTGCGGTTCTG		genotyping SALK lines	
p745_WiscDsLox	AACGTCCGCAATGTGTTATTAAGTTGTC		T-DNA specific primer to genotype Wisconsin Ds Lox lines (LB) (Woody et al., 2007)	
N698685_LP	CGAGAAGAGGGTGATCACAAG		genotyping ATP-dependent chromatin remodeller genes	
N698685_RP	AACGCTTGTTGTATGTCCCAC		genotyping ATP-dependent chromatin remodeller genes	
N867339_LP	CGAAGCTCGTTCTCATGAATC		genotyping ATP-dependent chromatin remodeller genes	
N867339_RP	AACAGTGCATTTATGAACGCC		genotyping ATP-dependent chromatin remodeller genes	
N862993_LP	AAAGTGTCCAAGCGAGAGACTC		genotyping ATP-dependent chromatin remodeller genes	
N862993_RP	ATGAGGGTATGAGCGTTGATG		genotyping ATP-dependent chromatin remodeller genes	
N24754_LP	GTTTAAAGGGACGGGCTGTAG		genotyping ATP-dependent chromatin remodeller genes	
N24754_RP	ATCGTTTCACAAAACGTTTGG		genotyping ATP-dependent chromatin remodeller genes	
N655353_LP	CCACAGAGAGATGCGATTCTC		genotyping ATP-dependent chromatin remodeller genes	
N655353_RP	TGCTGTTGTTTCACTCTGTGG		genotyping ATP-dependent chromatin remodeller genes	
N659762_LP	GAATTCTTTAACCGCCCTGTC		genotyping ATP-dependent chromatin remodeller genes	
N659762_RP	GCTTGAAGCTGATTCACGTTC		genotyping ATP-dependent chromatin remodeller genes	
cpk5-LP	TCGTTCCAAATTGACCTTGAC		for genotyping *cpk5* mutant (At4g35310, SAIL_657C06) - from Boudsocq et al. Nature 2010	
cpk5-RP	GAGGAAACAGCGGAGAGAGAC		for genotyping *cpk5* mutant (At4g35310, SAIL_657C06) - from Boudsocq et al. Nature 2010	
cpk6-LP	CTCGCAACTAACGCTTACCTG		for genotyping *cpk6* mutant (At2g17290, SALK_025460) - from Boudsocq et al. Nature 2010	
cpk6-RP	TTTTGGGATCTATAATGATCGATG		for genotyping *cpk6* mutant (At2g17290, SALK_025460) - from Boudsocq et al. Nature 2010	
cpk11-LP	AAATGATGGTGTTTTTATTTATGTAAAG		for genotyping *cpk11* mutant (At1g35670, SALK_054495) - from Boudsocq et al. Nature 2010	
cpk11-RP	AAACCAATTAGGCGATGAACC		for genotyping *cpk11* mutant (At1g35670, SALK_054495) - from Boudsocq et al. Nature 2010	
N654864_LP	CGTTAAACCAATGGCTCATTC		Genotyping jumogy histone demethylase AT3G48430, line ref6-2, SALK_001018	Len 21 TM 59.47 GC 42.86
N654864_RP	TTATCCACAGTGGCTCTCCAG		Genotyping jumogy histone demethylase AT3G48430, line ref6-2, SALK_001018	Len 21 TM 60.26 GC 52.38
N654971_LP	TCATATACAAGGCGTTCGGTC		Genotyping jumogy histone demethylase AT3G48430, line ref6-1, SALK_001018	Len 21 TM 59.97 GC 47.62
N654971_RP	CAGTTGCAACTCTGGAGAAGG		Genotyping jumogy histone demethylase AT3G48430, line ref6-1, SALK_001018	Len 21 TM 60.04 GC 52.38
N666435_LP	ACGTCAATGCGGTAATCATTC		Genotyping jumogy histone demethylases AT5G04240, line elf6-3, SALK_074694	Len 21 TM 59.84 GC 42.86
N666435_RP	TTTGCAGATCCCATTGCTTAC		Genotyping jumogy histone demethylases AT5G04240, line elf6-3, SALK_074694	Len 21 TM 60.09 GC 42.86
N866227_LP	TGAAATGGAACTGCATAAGGC		Genotyping jumogy histone demethylases T-DNA insertion primer design	
N866227_RP	CGATTCCAATCAAAACCAAAC		Genotyping jumogy histone demethylases T-DNA insertion primer design	
N65609_LP	TCAGAAAAGGAAGCATCAACG		Genotyping jumogy histone demethylases T-DNA insertion primer design	
N65609_RP	ATCACTGGCGATTTTTGTTTG		Genotyping jumogy histone demethylases T-DNA insertion primer design	
N852055_LP	TTCGAAAATAATCGATGGCTC		Genotyping jumogy histone demethylases T-DNA insertion primer design	
N852055_RP	TTCTGGTGAAATTGGATGGTC		Genotyping jumogy histone demethylases T-DNA insertion primer design	
N874635_LP	TTCAAAAAGGTCAGGCAAATG		Genotyping jumogy histone demethylases T-DNA insertion primer design	
N874635_RP	TTGAGACGTTTGGGTTTGAAC		Genotyping jumogy histone demethylases T-DNA insertion primer design	
N661982_LP	AGGCGACATATGAACGAACAC		Genotyping jumogy histone demethylases T-DNA insertion primer design	
N661982_RP	GATGCAATTTCTTCTGGCAAG		Genotyping jumogy histone demethylases T-DNA insertion primer design	
N654864_b_LP	agtcagtaggtagaggcaac		Genotyping jumogy histone demethylases T-DNA insertion primer design	
N654864_b_RP	ACTCAGAGGGATAAAAGCCG		Genotyping jumogy histone demethylases T-DNA insertion primer design	

Primers for cloning				
Name	Sequence (5' to 3')	Use	Comments	Tm; %GC; primer length
attB1	GGGGACAAGTTTGTACAAAAAAGCAGGCT			
attB2	GGGGACCACTTTGTACAAGAAAGCTGGGT			
EDA16_cDNA_F1	AAAAAGCAGGCTCCACCGGTGAGGAAGGTTCAAT			
EDA16_cDNA_F2	AAAAAGCAGGCTCCACCGGTGAGGAAGGTTCAATG			
EDA16_cDNA_R1	AGAAAGCTGGGTCTCATGAATCAGCCATAAAC			
EDA16_cDNA_R2	AGAAAGCTGGGTCTCATGAATCAGCCATAAACA			
EDA16_g_F2	AAAAAGCAGGCTCCACCGGTGAGGAAGGTTCAATG			
EDA16_g_R1	AGAAAGCTGGGTCagttttgcgctctaca			
EDA16_g_R2	AGAAAGCTGGGTCagcaagctctttctcat			
EDA16-F	AAAAAGCAGGCTCCACCGGTGAGGAAGGTTCA	attB1	clone Eda16 in pDONR-Zeo, from Start (no ATG included)	
EDA16-prom-F	AAAAAGCAGGCTCCACCaacggaattgttgatc	attB1	clone Eda16 in pDONR-Zeo, from promoter (996 bp upstream ATG)	
EDA16-RC	AGAAAGCTGGGTCTCATGAATCAGCCATA	attB2	clone Eda16 in pDONR-Zeo, from Stop (with Stop codon)	
EDA16-RO	AGAAAGCTGGGTCTGAATCAGCCATAAACA	attB2	clone Eda16 in pDONR-Zeo, from Stop (no Stop codon)	
M13-F	GTTGTAAAACGACGGCCAGT			
M13-R	CACAGGAAACAGCTATGACC			
oligodT19	TTTTTTTTTTTTTTTTTTVN		for RT-PCR	
pDONR207-F	TCGCGTTAACGCTAGCATGGATCTC		for sequencing clones in pDONR207, forward primer, 106 nt from cloned ORF	Tm 57C
pDONR207-R	GTAACATCAGAGGATTTTGAGACAC		for sequencing clones in pDONR207, reverse primer, 123 nt from cloned ORF	Tm 57C
Primers for qPCR				
Name	Sequence (5' to 3')	Use	Comments	Tm; %GC; primer length
ACT8-F	CCAGTGGTCGTACAACCGGTA	qPCR	AT1G49240, ACT8, primers from Solano's group, see Gimenez-Ibanez et al., plos	Tm: 61.76, %57.14, 289bp, size: 21
ACT8-R	TAGTTCTTTTCGATGGAGGAGCTG	qPCR	AT1G49240, ACT8, primers from Solano's group, see Gimenez-Ibanez et al., plos	Tm: 60.38, %45.83, 289bp, size: 24
BRM-F	CCTCCTCGTGATGATGCTGGT	qPCR	At2g46020	239 57.14/57.14 61.91/61.86 21/21
BRM-R	TCCCCTTCATCACGGTCATGG	qPCR		239 57.14/57.14 61.91/61.86 21/21
CBP60g-F	AAGAAGAATTGTCCGAGAGGAG	qPCR	From Ruth Schäfer	
CBP60g-R	GGCGAGTTTATGAAGCACAG	qPCR	From Ruth Schäfer	
CR01-F	GCTGTGTTCAACTGGTGGGAA	qPCR	Forward primer for qPCR At1g02670, RAD5 family ATP chromatin remodeller	165bp, Tm 61.02, %GC 52.38, 21
CR01-R	ACCACGGGTCCATCATGAACA	qPCR	Reverse primer for qPCR At1g02670, RAD5 family ATP chromatin remodeller	165bp, Tm 61.73, %GC 52.38, 21
CR02-F	AACTGGTGGGAAGCATGACCA	qPCR	Forward primer for qPCR At1g05120 RAD5 family ATP chromatin remodeller	186bp, Tm 61.95, %GC 52.38, 21
CR02-R	CTTGTGCTTGCCTCTCAACCG	qPCR	Reverse primer for qPCR At1g05120 RAD5 family ATP chromatin remodeller	186bp, Tm 62.06, %GC 57.14, 21
CR03-F	ATCTGGTTCGGGCGAGAAGAG	qPCR	Forward primer for qPCR At5g43530 RAD5 family ATP chromatin remodeller	208bp, Tm 61.90, %GC 57.14, 21
CR03-R	ACCGACTCCTCCAGCTTTCAG	qPCR	Reverse primer for qPCR At5g43530 RAD5 family ATP chromatin remodeller	208bp, Tm 61.77, %GC 57.14, 21
CR04-F	GATGGAGTTCGAGTAGCCCCT	qPCR	At3g16600	182 57.14/57.14 61.03/61.14 21/21
CR04-R	GGGCACGTATTGTTATCCCCG	qPCR		182 57.14/57.14 61.03/61.14 21/21
EDA16-F	TCTCGGACTGAACATGGTGGC	qPCR	At1g61140	241 57.14/57.14 62.38/62.04 21/21
EDA16-mid F	AGGCGCACATTCTCCAGTCT	qPCR	qPCR for EDA16 (including potential splicing variants)	20 61.55 55.00 PRODUCT SIZE: 202
EDA16-mid R	CGCATTGTCATGGATGGCCC	qPCR	qPCR for EDA16 (including potential splicing variants)	20 62.08 60.00 PRODUCT SIZE: 202
EDA16-R	GTGAGACTGTCGGCTTCCCTT	qPCR		241 57.14/57.14 62.38/62.04 21/21
FRG1-F	GGAAAGTCGTGGTGGGTGCTA	qPCR	Forward primer for qPCR At3g20010, FRG1, similar to rice BRHIS1, RAD5 family A	213bp, Tm 62.32, %GC 57.14, 21
FRG1-R	TTCCAGACAAGCACCACCTCC	qPCR	Reverse primer for qPCR At3g20010, FRG1, similar to rice BRHIS1, RAD5 family A	213bp, Tm 62.27, %GC 57.14, 21

FRG2-F	TGTGTCTGCCATGATCCACCA	qPCR	At1g50410	192bp, Tm 61.73, %GC 52.38, 21
FRG2-R	ACCCAAATCATCAGCAACGCA	qPCR		192bp, Tm 61.16, %GC 47.62, 21
PIE1-F	ACAGGCAGCAAGTGGAAGTCT	qPCR	At3g12810	201 52.38/52.38 61.93/62.14 21/21
PIE1-R	ATTCGGCAGCCAGTGATCCTT	qPCR		201 52.38/52.38 61.93/62.14 21/21
qaTUB_F	TACACCAACCTCAACCGCCT	qPCR	apha tubuline 4 AT1G04820	Length: 20, Tm: 61.41, GC%: 55.00, Amplicon size: 153
qaTUB_R	TGGGGCATAGGAGGAAAGCA	qPCR	apha tubuline 4 AT1G04820	Length: 20, Tm: 60.92, GC%: 55.00, Amplicon size: 153
qCPK11-F	GCATTACGGGTAATTGCTGAG	qPCR	for checking the expression of *cpk11* (At1g35670) - from Boudsocq et al. Nature 2010	
qCPK11-R	GTTCCGCTGTTGTCTGTGTC	qPCR	for checking the expression of *cpk11* (At1g35670) - from Boudsocq et al. Nature 2010	
qCPK5-F	TATGGATGCGGCTGATGTAG	qPCR	for checking the expression of *cpk5* (At4g35310) - from Boudsocq et al. Nature 2010	
qCPK5-R	GCTCTTCCCGCTCTAGTTTG	qPCR	for checking the expression of *cpk5* (At4g35310) - from Boudsocq et al. Nature 2010	
qCPK6-F	AGACAACGATGGACGGATTG	qPCR	for checking the expression of *cpk6* (At2g17290) - from Boudsocq et al. Nature 2010	
qCPK6-R	CTCCCTACACCAGCATTTCC	qPCR	for checking the expression of *cpk6* (At2g17290) - from Boudsocq et al. Nature 2010	
qCYP82C2_F	CTGTTTTCGGGTTTGCGCCT	qPCR	qPCR for CYP82C2, At4g31970	
qCYP82C2_R	GCTTTCCGGCCACCATTCTC	qPCR	qPCR for CYP82C2, At4g31970	
qCYP82C2-F	AATCTACCTGCCTGGCACTG	qPCR	for qPCR, Zipfel lab primer	
qCYP82C2-R	GAGAAATGGCCCATGTAAGG	qPCR	for qPCR, Zipfel lab primer	Size: 20, Tm: 59.75,GC%: 55.00, Amplicon size 72 bp
qFRK1_A-F	TCTTGAGCTGGGAAGAGAGGT	qPCR	Extra pair for detecting FRK1 expression	192bp Tm 60.20, %GC 52.38, 21
qFRK1_A-R	GACCGCTTCCTTCAACAGAGA	qPCR	Extra pair for detecting FRK1 expression	192bp Tm 60.00, %GC 52.38, 21
qFRK1-F	ATCTTCGCTTGGAGCTTCTC	qPCR	for qPCR, At2g19190, Zipfel lab primer, 108bp fragment	
qFRK1-R	TGCAGCGCAAGGACTAGAG	qPCR	for qPCR, At2g19190, Zipfel lab primer, 108bp fragment	
qMYB122_F	GTCAGGATCATCATCAGCTCGGT	qPCR	AT1G74080 Encodes a putative transcription factor, member of the R2R3 factor g	Length: 23, Tm: 62.12, GC%: 52.17, Amplicon size: 256
qMYB122_R	GGGGGAGTCAGAGAACGTGG	qPCR	AT1G74080 Encodes a putative transcription factor, member of the R2R3 factor g	Length: 20, Tm: 61.89, GC%: 65.00, Amplicon size: 256
qMYB22_F	TCAGGATCATCATCAGCTCGGT	qPCR	for qPCR AT1G74080 length = 255	
qMYB22_R	GGGGGAGTCAGAGAACGTGG	qPCR	for qPCR AT1G74080 length = 255	
qNLH10-F	TTCCTGTCCGTAACCCAAAC	qPCR	for qPCR, Zipfel lab primer	Size: 20, Tm: 56.16,GC%: 50.00, Amplicon size 72 bp
qNLH10-R	CCCTCGTAGTAGGCATGAGC	qPCR	for qPCR, Zipfel lab primer	
qPHI1-F	TTGGTTTAGACGGGATGGTG	qPCR	for qPCR, Zipfel lab primer	Size: 20, Tm: 57.52, GC% 50.00, Amplicon size: 130 bp
qPHI1-R	ACTCCAGTACAAGCCGATCC	qPCR	for qPCR, Zipfel lab primer	Size: 20, Tm: 59.18, GC%: 55.00, Amplicon size: 130 bp
qTIP41	GTTGGTGCCTCATCTTCGCC	qPCR	TIP41 AT4G34270	Length: 20, Tm: 61.65, GC%: 60.00, Amplicon size: 161
qTIP41_F	GAACTGGCTGACAATGGAGTGT	qPCR	TIP41 AT4G34270	Length: 22, Tm: 60.81, GC%: 50.00, Amplicon size: 161
qUBox_A_F	GCCACAACATTGCCGAGCTT	qPCR	U-BOX At5g15400	Length: 20, Tm: 62.15, GC%: 55.00, Amplicon size: 223
qUBox_A_R	GGTCTCTGCTCCCACTCTGC	qPCR	U-BOX At5g15400	Length: 20, Tm: 62.24, GC%: 65.00, Amplicon size: 223
qUbox-F	TGCGCTGCCAGATAATACACTATT	qPCR	for qPCR, At5g15400, Zipfel lab primer, 51bp fragment	
qUbox-R	TGCTGCCCAACATCAGGTT	qPCR	for qPCR, At5g15400, Zipfel lab primer, 51bp fragment	
qWRKY75_F	GTGGATTTCTCGATGGGATGCG	qPCR	for qPCR AT5G13080 length = 222	
qWRKY75_R	TGCGTTTCAAACAAGGAGCCAA	qPCR	for qPCR AT5G13080 length = 222	
RAD5-F	ACTCATCACAGCACCAACCGA	qPCR	Forward primer for qPCR At5g22750, RAD5 RAD5 family ATP chromatin remodell	218bp, Tm 61.98, %GC 52.38, 21
RAD5-R	TTAGCGTGCCATCAAGACGGA	qPCR	Reverse primer for qPCR At5g22750, RAD5 RAD5 family ATP chromatin remodell	218bp, Tm 62.10, %GC 52.38, 21
SEDA-F	ATGCCCCATGTGATCGTACCA	qPCR	At1g11100	242 52.38/57.14 61.59/62/04 21/21
SEDA-R	ACCACCCACACTACTCTTCGC	qPCR		242 52.38/57.14 61.59/62/04 21/21
SYD-F	TGCAACCGTCGCCTAAGTACA	qPCR	At2g28290	241 52.38/52.38 62.03/62.04 21/21
SYD-R	TCACTCCTCAATCGCCGTTGT	qPCR		241 52.38/52.38 62.03/62.04 21/21

Primers for ChIP

Name	Sequence (5' to 3')	Use	Comments	Tm (for Phusion, Thermo-Scientific); %GC; primer length
cFLT_F	GTTGCGACGTTTGGAGAAGG	ChIP PCR	LEFT PRIMER for AT5G10140	20 59.77 55.00 PRODUCT SIZE: 138
cFLT_R	gcgacttgaacccaaacctg	ChIP PCR	RIGHT PRIMER for AT5G10140	20 59.69 55.00 PRODUCT SIZE: 138
cFTM_F	GGGAACTACTTTGTTGGTGGTG	ChIP PCR	LEFT PRIMER for AT1G62360. Questa et al., science 2016	22 59.38 50.00 PRODUCT SIZE: 104
cFTM_R	GCCCATCATGACATCACATCAA	ChIP PCR	RIGHT PRIMER for AT1G62360. Questa et al., science 2016	22 59.05 45.45 PRODUCT SIZE: 104
cMYB122_3_F	CATCCACGTTCTCTGACTCCC	ChIP PCR	3'_F for AT1G74080	21 60.13 57.14 PRODUCT SIZE: 233
cMYB122_3_R	CGGCGTCACGTAGCTATCAT	ChIP PCR	3'_R for AT1G74080	20 60.04 55.00 PRODUCT SIZE: 233
cMYB122_5_a_F	CCTTCCGGACAAAGCTGgta	ChIP PCR	5_a_F for AT1G74080	20 59.68 55.00 PRODUCT SIZE: 174
cMYB122_5_a_R	GCCCATCTCAATCTGCAGCT	ChIP PCR	5_a_R for AT1G74080	20 60.47 55.00 PRODUCT SIZE: 174
cMYB122_5_b_F	TCCATCATCAACCTCCACGC	ChIP PCR	5_b_F for AT1G74080	20 60.11 55.00 PRODUCT SIZE: 80
cMYB122_5_b_R	gtccttaggcctgtcgatgg	ChIP PCR	5_b_R for AT1G74080	20 59.89 60.00 PRODUCT SIZE: 80
cMYB122_mid_F	AGGTATTGATCCGTTGACCCAC	ChIP PCR	mid_F for AT1G74080	22 60.09 50.00 PRODUCT SIZE: 88
cMYB122_mid_R	AACGCTGCTTTTCTCGGGAT	ChIP PCR	mid_R for AT1G74080	20 60.32 50.00 PRODUCT SIZE: 88
cMYB122_Prmtr_F	cacacgagccatgccaaatc	ChIP PCR	Prmtr_F for AT1G74080	20 60.18 55.00 PRODUCT SIZE: 180
cMYB122_Prmtr_R	gatactcgactttgctagcttttcg	ChIP PCR	Prmtr_R for AT1G74080	25 60.28 44.00 PRODUCT SIZE: 180
cMYB122_Trmt_F	tgtgtgtagtgtgtttcgaccg	ChIP PCR	Trmt_F for AT1G74080	22 61.05 50.00 PRODUCT SIZE: 224
cMYB122_Trmt_R	cttgtccactcgtgagccatc	ChIP PCR	Trmt_R for AT1G74080	21 61.00 57.14 PRODUCT SIZE: 224
cMYB122_TSS_1_F	tcgatccatcacaagcccac	ChIP PCR	TSS_1_F for AT1G74080	20 60.11 55.00 PRODUCT SIZE: 100
cMYB122_TSS_1_R	GGCGTCCGTACCATtcttga	ChIP PCR	TSS_1_R for AT1G74080	20 60.11 55.00 PRODUCT SIZE: 100
cMYB122_TSS_2_F	tcaagaATGGTACGGACGCC	ChIP PCR	TSS_2_F for AT1G74080	20 60.11 55.00 PRODUCT SIZE: 112
cMYB122_TSS_2_R	CGCCTTCACCATGTCGTTG	ChIP PCR	TSS_2_R for AT1G74080	19 59.50 57.89 PRODUCT SIZE: 112
cPHI-1_3p_F	CGACGTTGGTTTAGACGGGA	ChIP PCR		20 60.04 55.00 PRODUCT SIZE: 205
cPHI-1_3p_R	ATAACTCCCACCGGTCGTTG	ChIP PCR		20 59.75 55.00 PRODUCT SIZE: 205
cPHI-1_5p_F	AAGTTTAAACCGTCGCAGCG	ChIP PCR		20 59.77 50.00 PRODUCT SIZE: 120
cPHI-1_5p_R	CTTCTCCACCGTCTTCCACC	ChIP PCR		20 60.04 60.00 PRODUCT SIZE: 120
cPHI-1_mid_F	TCGTGTTGACCTCAGCTGAC	ChIP PCR		20 59.97 55.00 PRODUCT SIZE: 93
cPHI-1_mid_R	ATCCTTTCTTGCCTGACCCG	ChIP PCR		20 60.04 55.00 PRODUCT SIZE: 93
cPHI-1_Prmtr_F	aattaactcccactgccgca	ChIP PCR		20 59.96 50.00 PRODUCT SIZE: 180
cPHI-1_Prmtr_R	gcgcgtttggatgttacagt	ChIP PCR		20 59.48 50.00 PRODUCT SIZE: 180
cPHI-1_Trmtr_R	caaagtcatcagaagcacccag	ChIP PCR		22 59.51 50.00 PRODUCT SIZE: 98
cPHI-1_Trmtr_R	cgtagccaaactctcttctcagt	ChIP PCR		23 60.06 47.83 PRODUCT SIZE: 98
cPHI-1_TSS_F	acacaaactcatacaggcatcac	ChIP PCR		23 59.25 43.48 PRODUCT SIZE: 154
cPHI-1_TSS_R	ACATGAAAGCAACAGCGAACA	ChIP PCR		21 59.32 42.86 PRODUCT SIZE: 154
CYP82C2_3p_F	CACAGGAGAAGCAAAAGAGTTCG	ChIP PCR		
CYP82C2_3p_R	TGAAGGAAACGAGCAAGACCTAA	ChIP PCR		
CYP82C2_5p_F	CACCGTGTCCGATGCTTTTC	ChIP PCR		
CYP82C2_5p_R	tgtgtagttaaagatgtacCAGGCA	ChIP PCR		
CYP82C2_5p2_F	gttaattttgttatgatgcgatattgac	ChIP PCR		
CYP82C2_5p2_R	CAGGGGATAACGAGCCG	ChIP PCR		

CYP82C2_5p3_F	TGATGGTGAGAATGGTGGCC	ChIP PCR					
CYP82C2_5p3_R	AATTTGCGACGCCCTTTCTG	ChIP PCR					
CYP82C2_pmtr_F	tgttcatactctcatgcttggt	ChIP PCR					
CYP82C2_pmtr_R	tgggagctctgagttatggg	ChIP PCR					
CYP82C2_TSS_F	acacacatctcttttgcacgc	ChIP PCR					
CYP82C2_TSS_R	AAGCTGTTCCTTGCCACTGA	ChIP PCR					
FRK1_3_F	ACGCTGATCCACGATTCCTC	ChIP PCR	3' for AT2G19190	20	59.90	55.00	PRODUCT SIZE: 174
FRK1_3_R	TCGACTCGCCAAATGAACGA	ChIP PCR	3' for AT2G19190	20	60.04	50.00	PRODUCT SIZE: 174
FRK1_5_a_F	CGTCGGAACATCGTAACAGC	ChIP PCR	5_a for AT2G19190	20	59.36	55.00	PRODUCT SIZE: 134
FRK1_5_a_R	CGGATTCGGCGTTTGTTGAT	ChIP PCR	5_a for AT2G19190	20	59.55	50.00	PRODUCT SIZE: 134
FRK1_5_b_F	TCGGGCGGTCTGAAACTAAG	ChIP PCR	5_b for AT2G19190	20	59.75	55.00	PRODUCT SIZE: 174
FRK1_5_b_R	TGACCGTATATGGACACCGC	ChIP PCR	5_b for AT2G19190	20	59.61	55.00	PRODUCT SIZE: 174
FRK1_mid_F	TTCAACGGCCCATTCCTCTC	ChIP PCR	mid for AT2G19190	20	60.04	55.00	PRODUCT SIZE: 128
FRK1_mid_R	GCTTTGTTCCGGCGTTTCAA	ChIP PCR	mid for AT2G19190	20	60.25	50.00	PRODUCT SIZE: 128
FRK1_Prmtr_F	gcgaggaagaggaagtgagg	ChIP PCR	Prmtr for AT2G19190	20	59.83	60.00	PRODUCT SIZE: 89
FRK1_Prmtr_R	gttgtagaagccgcggtagt	ChIP PCR	Prmtr for AT2G19190	20	60.11	55.00	PRODUCT SIZE: 89
FRK1_Trmt_F	gcttcttccacttgccagagt	ChIP PCR	Trmt for AT2G19190	21	60.54	52.38	PRODUCT SIZE: 248
FRK1_Trmt_R	CGAGATGGTTCCTCGAGCAA	ChIP PCR	Trmt for AT2G19190	20	59.83	55.00	PRODUCT SIZE: 248
FRK1_TSS_1_F	gctgctttctctgggctaga	ChIP PCR	TSS_1 for AT2G19190	20	59.46	55.00	PRODUCT SIZE: 146
FRK1_TSS_1_R	acgtcctggtccgaacattc	ChIP PCR	TSS_1 for AT2G19190	20	60.04	55.00	PRODUCT SIZE: 146
FRK1_TSS_2_F	CACTTGATTGAAACTGAGCTGCA	ChIP PCR	TSS_2 for AT2G19190	23	60.00	43.48	PRODUCT SIZE: 112
FRK1_TSS_2_R	CCGGATGATTCTAGCTACAACGA	ChIP PCR	TSS_2 for AT2G19190	23	60.00	47.83	PRODUCT SIZE: 112
oACT7_F	CGTTTCGCTTTCCTTAGTGTTAGCT	ChIP PCR	AT5G09810; ACT7; Primers for ChIP from Julia Engelhorn; H3K27me3 negative cc	Size: 24, Tm: 61.81, GC%: 44.00, Ampliconsize: 134			
oACT7_R	AGCGAACGGATCTAGAGACTCACCTT	ChIP PCR	AT5G09810; ACT7; Primers for ChIP from Julia Engelhorn; H3K27me3 negative cc	Size: 24, Tm: 64.92, GC%: 50.00, Ampliconsize: 134			
oSEP3i1_F	GATATTGTTTCCACGACAATCC	ChIP PCR	AT1G24260; AGAMOUS-LIKE 9, AGL9, SEP3, SEPALLATA3; Primers for ChIP from J	Size: 22, Tm: 55.53, GC%: 40.91, Amplicon size: 250			
oSEP3i1_R	CCATTAATCTTACTCATCAAGTTC	ChIP PCR	AT1G24260; AGAMOUS-LIKE 9, AGL9, SEP3, SEPALLATA3; Primers for ChIP from J	Size: 22, Tm: 53.55, GC%: 33.33, Amplicon size: 250			
SEP3_3p_F	acattagcgtcaattcaaaaccca	ChIP PCR	AT1G24260 AGAMOUS-LIKE 9, AGL9, SEP3, SEPALLATA3	Size: 24, Tm: 59.72, GC%: 37.50, Amplicon size: 159			
SEP3_3p_R	gtttccacctttttgattctgggg	ChIP PCR	AT1G24260 AGAMOUS-LIKE 9, AGL9, SEP3, SEPALLATA3	Size: 23, Tm: 59.99, GC%: 47.83, Amplicon size: 159			
SEP3_5p_F	CTTGAGATACTCCTGCTGGCTAC	ChIP PCR	AT1G24260 AGAMOUS-LIKE 9, AGL9, SEP3, SEPALLATA3	Size: 23, Tm: 60.24, GC%: 52.17, Amplicon size: 180			
SEP3_5p_R	CACCAGAACCCAATGTGCCT	ChIP PCR	AT1G24260 AGAMOUS-LIKE 9, AGL9, SEP3, SEPALLATA3	Size: 20, Tm: 60.54, GC%: 55.00, Amplicon size: 180			
WRKY75_3p_F	TGCTTCTTCACATTGCATCC	ChIP PCR	For qPCR AT5G13080 (WRKY75)	20	59.81	45.00	PRODUCT SIZE: 177
WRKY75_3p_R	ttataatttggattcgggaaca	ChIP PCR	For qPCR AT5G13080 (WRKY75)	22	58.37	31.82	PRODUCT SIZE: 177
WRKY75_5p_F	tctagggccgatgtgaatga	ChIP PCR	For qPCR AT5G13080 (WRKY75)	20	58.21	50.00	PRODUCT SIZE: 194
WRKY75_5p_R	GGCCGTCAAGAACAACAAGT	ChIP PCR	For qPCR AT5G13080 (WRKY75)	20	58.98	50.00	PRODUCT SIZE: 194
WRKY75_Prmter_F	tcgttgtggtgagatacggt	ChIP PCR	For qPCR AT5G13080 (WRKY75)	20	58.75	50.00	PRODUCT SIZE: 162
WRKY75_Prmter_R	gtttgcgtctgtggtgatca	ChIP PCR	For qPCR AT5G13080 (WRKY75)	20	58.77	50.00	PRODUCT SIZE: 162
WRKY75_TSS_1_F	gacagaccgatccacctgaa	ChIP PCR	For qPCR AT5G13080 (WRKY75)	20	59.10	55.00	PRODUCT SIZE: 168
WRKY75_TSS_1_R	cgcctcttcgtctttgactt	ChIP PCR	For qPCR AT5G13080 (WRKY75)	20	58.22	50.00	PRODUCT SIZE: 168
WRKY75_TSS_2_F	AGCTCTCTTCTTCGCCTTGA	ChIP PCR	For qPCR AT5G13080 (WRKY75)	20	58.74	50.00	PRODUCT SIZE: 152
WRKY75_TSS_2_R	ttcaggtggatcggtctgtc	ChIP PCR	For qPCR AT5G13080 (WRKY75)	20	59.10	55.00	PRODUCT SIZE: 152

Gene Abbreviations

Gene	Full name	AGI number
ACT7	*ACTIN7*	AT5G09810
ATM	*ATAXIA-TELANGIECTASIA MUTATED*	AT3G48190
ATR	*ATAXIA TELANGIECTASIA-MUTATED AND RAD3-RELATED*	AT5G40820
BAK1	*BRI1-ASSOCIATED RECEPTOR KINASE*	AT4G33430
BIK1	*BOTRYTIS-INDUCED KINASE1*	AT2G39660
BSK1	*BRASSINOSTEROID-SIGNALING KINASE 1*	AT4G35230
CERK1	*CHITIN ELICITOR RECEPTOR KINASE 1*	AT3G21630
CHR11	*CHROMATIN-REMODELING PROTEIN 11*	AT3G06400
CHR17	*CHROMATIN-REMODELING PROTEIN 17*	AT5G18620
DDM1	*DECREASED DNA METHYLATION 1*	AT5G66750
EDS1	*ENHANCED DISEASE SUSCEPTIBILITY 1*	AT3G48090
EFR	*EF-TU RECEPTOR*	AT5G20480
EIL1	*ETHYLENE-INSENSITIVE3-LIKE 1*	AT2G27050
EIN3	*ETHYLENE-INSENSITIVE3*	AT3G20770
ELF6	*EARLY FLOWERING 6*	AT5G04240
ERF1	*ETHYLENE RESPONSE FACTOR 1*	AT3G23240
ERF104	*ETHYLENE RESPONSE FACTOR 104*	AT5G61600
ETL1	*CHROMATIN REMODELING 19*	AT2G02090
FLC	*FLOWERING LOCUS C*	AT5G10140
GCN5	*GENERAL CONTROL NONDEREPRESSIBLE 5*	AT3G54610
HAC1	*HISTONE ACETYLTRANSFERASE OF THE CBP FAMILY 1*	AT1G79000
HDA19	*HISTONE DEACETYLASE 1*	AT4G38130
HDA6	*HISTONE DEACETYLASE 6*	AT5G63110
MKS1	*MAP KINASE SUBSTRATE 1*	AT3G18690
MOM1	*ATP-dependent helicase family protein*	AT1G08060
NPR1	*NONEXPRESSER OF PR GENES 1*	AT1G64280
PAD3	*PHYTOALEXIN DEFICIENT 3*	AT3G26830
RAD54	*DNA repair/recombination protein*	AT3G19210
RIN4	*RPM1 INTERACTING PROTEIN 4*	AT3G25070
RPD3	*DNA-directed RNA polymerase family protein*	AT2G15430
RPM1	*RESISTANCE TO P. SYRINGAE PV MACULICOLA 1*	AT3G07040
RPS4	*RESISTANT TO P. SYRINGAE 4*	AT5G45250
SDG13	*SET DOMAIN PROTEIN 13*	AT1G02580
SFA2	*Heat shock transcription factor A2*	AT2G26150
SNC1	*SUPPRESSOR OF NPR1-1*	AT4G16890

SNI1	*SUPPRESSOR OF NPR1-1, INDUCIBLE 1*	AT4G18470
SSN2	*SUPPRESSOR OF SNI1 2*	AT4G33925
SUMO1	*SMALL UBIQUITIN-LIKE MODIFIER 1*	AT4G26840
SUVR2	*SET DOMAIN PROTEIN 18*	AT5G43990
TUB	*ALPHA-1 TUBULIN*	AT1G64740
UBOX	*SNC1 -ENHANCING 3*	AT5G15400
VSP2	*VEGETATIVE STORAGE PROTEIN 2*	AT5G24770